Renewable Energy Sources & Energy Storage

Md. Rabiul Islam
Naruttam Kumar Roy
Saifur Rahman *Editors*

Renewable Energy and the Environment

Springer

Renewable Energy Sources & Energy Storage

Series editor

Xiangjun Li, China Electric Power Research Institute, Beijing, China

The book series Renewable Energy Sources & Energy Storage publishes monographs, professional books and textbooks on the latest advances and developments in the field of renewable energy sources (RES; incl. wind, solar, hydrogen, biomass, etc.), energy storage (ES), conversion and applications from micro-grid to macro-grid level. Topics covered in the series are the key technologies and practices involved in RES and ES systems; solving problems in equipment manufacture; system integration; installation & debugging; SCADA; control; power prediction; status estimation; safety assessment; energy management; economic evaluation; experimental methods; establishment of standards and grid application.

More information about this series at http://www.springer.com/series/15433

Md. Rabiul Islam · Naruttam Kumar Roy
Saifur Rahman
Editors

Renewable Energy and the Environment

Springer

Editors
Md. Rabiul Islam
Department of Electrical and Electronic Engineering
Rajshahi University of Engineering & Technology
Rajshahi
Bangladesh

Naruttam Kumar Roy
Department of Electrical and Electronic Engineering
Khulna University of Engineering & Technology
Khulna
Bangladesh

Saifur Rahman
Virginia Tech Advanced Research Institute
Arlington, VA
USA

ISSN 2509-9698 ISSN 2509-9701 (electronic)
Renewable Energy Sources & Energy Storage
ISBN 978-981-10-7286-4 ISBN 978-981-10-7287-1 (eBook)
https://doi.org/10.1007/978-981-10-7287-1

Library of Congress Control Number: 2017960907

Printed on acid-free paper

This Springer imprint is published by Springer Nature
The registered company is Springer Nature Singapore Pte Ltd.
The registered company address is: 152 Beach Road, #21-01/04 Gateway East, Singapore 189721, Singapore

Preface

This book is intended to discuss a variety of recent and vital technical and non-technical issues related to the global energy, environment, and socioeconomic developments for professionals and students who are directly and indirectly involved in the relevant fields. The impetus for this book comes from our view that there is lack of a clear vision in the development of technology and policy on how to reach the mandatory renewable energy targets of the world to reduce greenhouse gas emission and exhilarate socioeconomic development. The chapters of this book have been structured in such a way that it provides a consistent compilation of fundamental theories, a compendium of current research and development activities as well as new directions to overcome critical limitations. This book will be of benefit to researchers, planners, policy makers, and manufacturers.

Chapter 1 aims to present the importance of renewable energy, its sources, present situation, and future prospects. In the modern and fast-growing civilization, the growth of energy consumption is the measuring parameter of social and economic growth. To meet this high energy demand, suggestions are also made to make the renewable energy more popular among investors. Implementation of these suggestions will help to increase the smooth penetration of renewable energy sources in electrical power systems to preserve economy and environment.

It has been becoming obvious that renewable energy can overcome the challenges thrown by conventional fossil fuel-based power plants. Among renewable energy sources, the solar photovoltaic (PV) has been gaining a significant popularity since last decade, and nowadays, the cost of electricity generation from solar PV system is comparable with those from traditional generation systems. By the end of 2016, the cumulative installed capacity reached around 300 GW, whereas it was only 17.06 GW in 2010. About 15,000 tons of carbon dioxide emission can be reduced every year by a 10 MW solar PV plants. The comparative technical specifications of different components of large-scale solar PV plant, e.g., solar module, inverter, tracker, and transformer, are presented in Chap. 2. In addition, necessary factors that influence the selection of a site for a solar PV plant are also discussed.

Existing power transmission infrastructures are not robust and less efficient due to the power loss over long distance. High-temperature superconducting (HTS) materials and technologies have become available to design and build power cables. Chapter 3 aims to present basic theoretical background knowledge of HTS cables. The necessary improvements required have been comprehensively identified to reach the goal of industrial and board application of HTS cables and transmission technologies which are potential critical elements for future power system renewables.

The oceanic wave, also known as a wind wave, has the high-power density compared to the other popular renewable energy sources. The conventional machineries are not suitable for the energy conversion from the sea wave. To extract maximum power, scientists around the world proposed a wide variety of new electrical machines. Some of such electrical machines with their properties and the prospects of a high-power density linear generator are discussed in Chap. 4.

A converter is an essential part of a wind energy system. The conventional rectifier–inverter arrangement contains a giant capacitor and produces harmonics distortion in its output. A matrix converter is now popular as it does not contain capacitor which has a bulky size. It can be provided in a simple construction to provide a wide range of output frequency. Chapter 5 introduces a modified algorithm for space vector modulation that reduces total harmonic distortion of the output voltage. Moreover, a modified open-loop control of matrix converter with indirect space vector modulation is introduced to provide constant frequency and output voltage even if the wind speed changed.

Recent trends of connecting small-scale generator lead to the concept of micro-grid. In smart grid environment, several micro-grids will work parallel to support the load demand. It is essential to keep the nodal voltage of grid-connected renewable energy systems within an acceptable limit. The major advantage that attracts the matrix converter for grid-interactive applications is its inherent capability of bidirectional power flow. It can be used as voltage regulators in the low-voltage (LV) distribution network by adding a series compensation voltage with a transformer. However, to achieve these functionalities, a proper switching scheme and commutation process are necessary. The major focus of Chap. 6 is to discuss different types of switching and commutation strategies for matrix converter that considers silicon carbide (SiC)-based junction field-effect transistors (JFETs), MOSFETs, and SiC-based MOSFETs. The experimental results reveal that the SiC-based MOSFET devices are the best for designing the matrix converter for micro-grid applications.

In the near future, multiple energy sources having diverse characteristics will come into play in power systems. When a large number of renewable energy sources are interconnected with traditional power systems, it arises several critical challenges for the operation of the system. Intermittent nature of renewable energy and variable load demand on power systems make the control tasks more challenging. These challenges might cause the interruption of steady-state operation of the system and interrupt power supply to consumers. Chapter 7 attempts to present technical challenges related to the operation and protection that arise due to

the large-scale interconnection of renewable energy. A detailed discussion on the necessity of implementation of control techniques is highlighted to ensure the continuity of service.

Rajshahi, Bangladesh — Md. Rabiul Islam
Khulna, Bangladesh — Naruttam Kumar Roy
Arlington, USA — Saifur Rahman

Contents

About the Editors

Dr. Md. Rabiul Islam (M' 14, SM' 16, IEEE) received the **B.Sc.** and **M.Sc.** degrees from Rajshahi University of Engineering & Technology (RUET), in 2003 and 2009, respectively, both in Electrical and Electronic Engineering (EEE), and the **Ph.D.** degree from the University of Technology Sydney (UTS), Sydney, Australia, in 2014, in Electrical Engineering.

In 2005, he was appointed a Lecturer in the Department of EEE, RUET, where he was an Assistant Professor and Associate Professor from June 2008 to June 2015 and July 2015 to March 2017, respectively, and was promoted to a **Professor** in April 2017. He has authored and co-authored **more than 70 technical papers** (IEEE, IET, AIP, Elsevier, and Hindawi), **two books** (Springer), and **three book chapters** (Springer, IET). **Three more books** have already been accepted by Springer. His research interests are in the fields of renewable energy technologies, power electronic converters, electrical machines, and smart grid.

Dr. Rabiul is a **Senior Member** of the **IEEE** (USA), and a Member of IEB (Bangladesh) and the AIE (Australia). He received the University Gold Medal and Joynal Memorial Award from RUET for his outstanding academic performance while pursuing B.Sc. engineering degree. He also awarded some prestigious international scholarships, such as **Australian Government** International Postgraduate Research Scholarship (**IPRS**), University of Technology Sydney President Scholarship (UTSP), Asian Development Bank (**ADB**) Scholarship, and **Japanese Government Monbukagakusho** scholarship. He received Best Paper

Awards at IEEE PECon-2012, ICEEE 2015, ICCIE 2015, ICECTE 2016, and ICEMS 2017.

As a Lead Guest Editor, Dr. Rabiul has been invited to organize special issues in peer review high-quality Journals and Chair the sessions of some international conferences, e.g., ECCE 2017, IEEE ICIT 2016, ICECTE 2016, and ICEEE 2015. He has organized many IEEE technical sponsored international conferences such as ICEEE 2017 (Technical Secretary), IEEE ICIT 2016 (Special Session Organizer), ICECTE 2016 (Technical Secretary), ICEEE 2015 (Chair, Registration Committee), ICCIE 2015 (Organizing Committee Member), and IEEE COMPUMAG 2011 (Local Organizing Committee Member).

Dr. Naruttam Kumar Roy (M'10 IEEE) received his Ph.D. degree in Electrical Engineering from the University of New South Wales (UNSW), Australia, in 2013. As part of his Ph.D. research, he worked with the CSIRO Energy Technology, Newcastle, Australia. He is currently an Associate Professor in the Department of Electrical and Electronic Engineering at Khulna University of Engineering & Technology (KUET), Bangladesh. He previously worked as a Lecturer in the School of Engineering at Deakin University, Australia, and as a Research Publication Fellow at UNSW, Australia. He has also held a visiting appointment at CIITECH-METEC, Addis Ababa, Ethiopia.

Dr. Roy has published more than 50 peer-reviewed papers in reputed international journals and conferences as well as several book chapters through well-regarded publishers. His research interests include distributed generation, renewable energy, smart grids, FACTS devices, electrical machines, artificial intelligence, power electronics, and control applications. He received the **Best Paper Award** from the IEEE Conference on Industrial Electronics and Applications (ICIEA 2013) and **High Impact Journal Publications Award 2013** from UNSW. He also received a **University Gold Medal** from KUET recognizing his outstanding performance throughout his undergraduate studies. He has served as an Assistant Secretary, Member of Technical Program Committee, Track Co-Chair and Session Chair of a number of international conferences and

workshops. He is an Associate Editor of Technology and Economics of Smart Grids and Sustainable Energy which is a Springer Journal. He is a member of the Institution of Engineers, Bangladesh (IEB), and the Institute of Electrical and Electronics Engineers (IEEE), USA.

Prof. Saifur Rahman is the Founding Director of the Advanced Research Institute (www.ari.vt.edu) at Virginia Tech where he is the Joseph R. Loring Professor of Electrical and Computer Engineering. He also directs the Center for Energy and the Global Environment (www.ceage.vt.edu). He is a Fellow of the IEEE and an IEEE Millennium Medal winner. He is the President of the IEEE Power and Energy Society (PES) for 2018–2019. He was the Vice President for publications of IEEE and a member of the governing board in 2006. He was the Founding Editor-in-Chief of the IEEE Electrifications Magazine and the IEEE Transactions on Sustainable Energy. He served as the Chair of the US National Science Foundation Advisory Committee for International Science and Engineering from 2010 to 2013. He is a Distinguished Lecturer for the IEEE PES and has lectured on smart grid, smart cities, energy-efficient buildings, renewable energy, demand response, distributed generation, and critical infrastructure protection topics in over 30 countries on all six continents.

He received his B.Sc. degree from Bangladesh University of Engineering and Technology, in 1972, M.S. degree from Stony Brook University, New York, in 1975, and Ph.D. degree from Virginia Tech in 1978, all in Electrical Engineering. His industry and government experience includes work with the Tokyo Electric Power Company in Japan, the Brookhaven National Laboratory in New York, Duke Energy in North Carolina, Consultancy for the World Bank in the United Nations, US Agency for the International Development, and the Asian Development Bank.

Acronyms

AC	Alternating current
ARENA	Australian Renewable Energy Agency
a-Si	Amorphous silicon cell
a-Si/μc-Si	Amorphous and micro-morph silicon multi-junction
AWS	Archimedes wave swing
BESS	Battery energy storage system
BS GPP	Binary cycle geothermal power plant
CC	Copper conductor
CdTe	Cadmium telluride
CE	Common emitter
CFC	Chlorofluorocarbon
CI[G]S	Copper-indium-[gallium]-[di]-sulfide
CO	Carbon monoxide
CO2	Carbon dioxide
c-Si	Crystalline silicon
CSP	Concentrating solar power
DC	Direct current
DDS	Direct drive system
DG	Distributed generator
DHI	Diffuse horizontal irradiance
DNI	Direct normal irradiance
DNO	Distribution network operator
DS GPP	Dry steam geothermal power plant
DSC	Dye-sensitized cell
DSM	Demand-side management
DSP	Digital Signal Processing
EJ	Exajoule = 1018 Joule
EPRI	Electric Power Research Institute
EU	European Union
EV	Electric vehicle

FS GPP	Flash steam geothermal power plant
FSPMLG	Flux-switching permanent magnet linear generator
GHG	Greenhouse gas
GHI	Global horizontal irradiance
GIS	Geographic information system
GSM	Global system for mobile communication
GW	Gigawatts
HAWT	Horizontal-axis wind turbine
HE	Hall effect
HFO	Heavy fuel oil
HPDPMLG	High-power density permanent magnet linear generator
HPP	Hydropower plant
IAEA	International Atomic Energy Agency
IEA	International Energy Agency
IGBTs	Insulated-gate bipolar transistors
IPCC	Intergovernmental Panel on Climate Change
IRENA	International Renewable Energy Agency
IRP	Instantaneous reactive power
ISVM	Indirect space vector modulation
JFET	Junction field-effect transistors
kWh/m2/year	Kilowatt-hour per meter square per year
LFO	Light fuel oil
LG	Linear generator
LV	Low voltage
MAS	Multi-agent system
MC	Matrix converter
MGCC	Micro-grid central controller
MOSFET	Metal oxide semiconductor field-effect transistor
MOSFETs	Metal oxide semiconductor field-effect transistors
MPPT	Maximum power point tracker
MW	Megawatts
NO2	Nitrogen oxide
OLTC	On-load tap changer
OTC	Ocean thermal energy conversion
OWE	Oceanic wave energy
PCC	Point of common coupling
PCSs	Power-conditioning systems
PM	Permanent magnet
PMLG	Permanent magnet linear generator
PMSM	Permanent magnet synchronous motor
PMx	Particulate matter
PTO	Power take-off
PV	Photovoltaic cell
RES	Renewable energy source
RMC	Reverse matrix converter

rms	Root mean square
RoR	Run over river
rpm	Revolution per minute
SC	Switched capacitor
SCADA	A supervisory control and data acquisition
SCIG	Squirrel-cage induction generator
SCR	Silicon-controlled rectifier
SDG	Sustainable development goal
SEIG	Self-excited induction generator
SHPP	Storage Hydropower plant
Si	Silicon
SiC	Silicon carbide
SM	Superconducting magnet
SMLG	Superconducting magnetic linear generator
SOC	State of charge
SOx	Sulfur oxide
SVM	Space vector modulation
SVR	Step voltage regulator
THD	Total harmonic distortion
TREIA	Texas Renewable Energy Industries Alliance
TWh	Trillions of watt-hour
TWh	Terawatt-hour
UC	Unit commitment
UK	United Kingdom
UN	United Nations
UNDP	United Nations Development Program
UNFCCC	United Nations Framework Convention on Climate Change
UNGA	United Nations General Assembly
USD	United States Dollar
UV	Ultraviolet
VAWT	Vertical-axis wind turbine
VSC	Voltage source converter
W	Watts
WBG	Wide band gap
WECS	Wind energy conversion system
WSN	Wireless sensor network
WT	Wind turbine

Symbols

E	Kinetic energy (J)
M	Mass (Kg)
V	Velocity (m/s)
P	Power (W)
ρ	Density (kg/m^3)
A	Swept area (m^2)
C_p	Power coefficient
r	Radius (m)
$x,\ s$	Distance (m)
t	Time (s)
$\frac{dm}{dt}$	Mass flow rate (kg/s)
$\frac{dE}{dt}$	Energy flow rate (J/s)
F	Force (N)
a	Acceleration (m^2/s)
P_r	Pressure in mm of Hg
VP	Vapor pressure of water vapor
T	Temperature in degree Kelvin
C_p	Coefficient of performance
P_e	Power output
η_m	Efficiency (mechanical transmission)
η_g	Efficiency (electrical conversion)
Z	Sun of the zenith angle
I_s	Cell saturation of dark current
V_T	Thermal voltage
K	Boatman's constant
T_c	Cell's working temperature
q	Electron charge
n	Identity factor
g	Gravitational acceleration
Q	Flow rate in cubic meters per second

H	Height of waterfall in meter
η	Efficiency
$p(t)$	Vertical position of the oceanic wave
$v(t)$	Vertical displacement of the oceanic wave
H_m	Height of the oceanic wave
θ_i	Initial phase angle of the oceanic wave
T_w	Period of the oceanic wave
v_t	Translator velocity
P_τ	Pole pitch of the PMLG
f_g	Generated frequency
Φ_{ag}	Air gap flux
E_p	Induced emf/phase
k_w	Winding factor
N	Turn number
m	Mass of an object
ρ	Density of the object
h	Height of the object
E_p	Potential energy of the object
E_{pw}	Potential energy of the oceanic wave
P_w	Wave power per unit of wave crest length
a,b,c	Input phase voltages
A,B,C	Output phase voltages
C_p	Power coefficient of the turbine
λ	Tip speed ratio
β	Rotor blade pitch angle
P	Mechanical power
ρ	Air density in g/m^3
A_r	Turbine rotor area in m^2
R_r	Rotor blade radius
v_w	Wind speed in m/s
I^*_{IN}	Reference input current
I_γ	Second vector of the current source rectifier
I_δ	First vector of the current source rectifier
d_γ	Duty cycle of the second vector of the current source rectifier
d_δ	Duty cycle of the first vector of the current source rectifier
m_c	Current modulation index of rectifier
θ_c	Angle between reference input current and first vector
d_{0c}	Zero vector duty cycle of current source rectifier
V_β	Second vector of the voltage source inverter
V_α	First vector of the voltage source inverter
d_β	Duty cycle of the second vector of the voltage source inverter

d_z	Duty cycle of the first vector of the voltage source inverter
m_v	Voltage modulation index of inverter
θ_v	Angle between reference output voltage and first vector
d_Z	Zero vector duty cycle of voltage source inverter
V_s^{abc}	Voltage vector of stator's winding
V_r^{abc}	Voltage vector of rotor's winding
i_s^{abc}	Current vector of stator's winding
i_r^{abc}	Current vector of rotor's winding
λ_s^{abc}	Stator's winding flux linkage vector
λ_r^{abc}	Rotor's winding flux linkage vector
r_s^{abc}	Resistance vector of stator's winding
r_r^{abc}	Resistance vector of rotor's winding
L_{SS}	Self-inductance of the stator winding
L_{sm}	Mutual inductance between stator winding
L_{rr}	Self-inductance of the rotor winding
L_{rm}	Mutual inductance between rotor winding
L_{sr}	Maximum value of Mutual inductance between stator and rotor winding
L_{ls}	Leakage inductance of stator winding
L_{lr}	Leakage inductance of rotor winding
q	Ratio between output voltage and input voltage
Saa, Sbb, Scc, Sdd, Snn	Main switching states for two-, three-, and four-step commutation
S0, S1, S2, S3, S4…Sn	Intermediate switching states (from S0 to Sn) for four-step commutation
D1, D2, D3…DN	Body diodes for different switches
S1d, S2d, S3d…Snd	Direct switches for two-, three-, and four-step commutation
S1r, S2r, S3r…Snr	Reverse switches for two-, three-, and four-step commutation
SW1, SW2	Bidirectional switches
Sz1, Sz2	Zero switching loss switches
Sb1	Bride rectifier bidirectional switch
SJ1, SJ2	SiC-JFET switches
V1, V2	Generalized supply voltages
V_{GS}	Switch gate to source voltage
V_{DS}	Switch drain to source voltage
I_{DS}	Switch drain to source current
G, D, S	Switch symbolized as gate, drain, and source
SG1, SG2	GaN device cascade switches
V_G	Grid side voltage
V_{PCC}	Voltage at point of common coupling (PCC)
R	Resistance of the distribution feeder

X	Reactance of the distribution feeder
$OLTC$	On-load tap changing transformer
P_L	Active power consumed by the load
Q_L	Reactive power consumed by the load
P	Active power flowing through the feeder
Q	Reactive power flowing through the feeder
P_{DG}	Active power generated by the renewable DG
Q_{DG}	Reactive power generated by the renewable DG
$\widehat{V_{\mathrm{PCC}}}$	Phasor quantity of DG bus voltage (PCC voltage)
$\widehat{V_G}$	Phasor quantity of grid voltage
$\hat{I}$	Phasor quantity of current flowing through distribution network
$E\angle\delta$	Converter output voltage
$Z\angle\theta$	Line impedance
ω	Angular frequency
D_P, D_Q	Droop coefficient
δ	Phase deviation
$K_{PP}^{Tertiary}$	Proportional gain for tertiary control of active power
$K_{IP}^{Tertiary}$	Integral gain for tertiary control of active power
$K_{PQ}^{Tertiary}$	Proportional gain for tertiary control of reactive power
$K_{IQ}^{Tertiary}$	Integral gain for tertiary control of reactive power

List of Figures

List of Tables

Chapter 1
Prospects of Renewable Energy Sources

Naruttam Kumar Roy and Aparupa Das

1.1 Introduction

The power sector has turned the whole world into a global village. With time, the primary energy usage of the world has risen by 1.8% [1]. To meet this extended demand, we must find other resources to generate more power, especially electric power. Again, another important concern is to preserve our environment. The power generation from fossil fuel emits tons and tons of carbon-di-oxide (CO_2). It also causes environmental damages and risks to public health. We must not forget that the fossil fuel is finite resource and leaves hazards for our posterity. World's scientists are looking forward to making sustainable development that is to generate power for social development, preserve the resources for future generations and hamper the environment as less as possible.

In the year 2015, the global people have witnessed the first effective initiative to boost up access to technology, related to renewable energy by global communities like G20 and G7. The United Nations General Assembly (UNGA) has also adopted a Sustainable Development Goal (SDG) that describes "Sustainable energy for all" (SDG-07). The largest annual increment ever took place in that year and it was estimated about 147 Gigawatts (GW), where renewable energy contributed about 19.2% of global energy consumption [2]. To understand the discussion more deeply, we must learn more about "Renewable or Green Energy".

N. K. Roy · A. Das (✉)
Department of Electrical and Electronic Engineering,
Khulna University of Engineering & Technology, Khulna 9203, Bangladesh
e-mail: aparupa.das92@gmail.com

N. K. Roy
e-mail: nkroy@eee.kuet.ac.bd

M. R. Islam et al. (eds.), *Renewable Energy and the Environment*, Renewable Energy Sources & Energy Storage, https://doi.org/10.1007/978-981-10-7287-1_1

The New Webster's Dictionary defines [3], "Renewable" as "Replaceable naturally or by human activity. Renewable resources are replenished by the environment over relatively short period of time. Examples of renewable resources include trees and other plants, animal populations, ground water, solar energy, wind energy, etc.".

According to the Texas Renewable Energy Industries Alliance (TREIA) [4], the definition of "Renewable energy" is "Any energy resource that is naturally regenerated over a short time scale and derived directly from the sun (such as thermal, photochemical, photoelectric), indirectly from the sun (such as wind, hydro power and photosynthetic energy stored in bio-mass) or from other natural movements and mechanisms of the environment (such as geothermal and tidal energy). Renewable energy does not include energy resources derived from fossil fuels, waste products from fossil sources or waste products from inorganic sources".

Australian Renewable Energy Agency (ARENA) defines [5], "Renewable energy" as "Renewable energy is energy which can be obtained from natural resources that can be constantly replenished".

1.2 Types of Renewable Energy

In this world, there are different kinds of renewable energy sources (RESs) from where we can avail renewable or green energy. However, we are commonly well known with six types of RESs as given in Fig. 1.1. These RESs give us the ways to generate power not only by alternative means but also in traditional ways. By using these sources properly, we can move towards a safe and sound environment. These help us to minimize carbon footprint from the environment. Most of the renewable energies rely on the sunlight directly or indirectly. The wind power is the effect of solar radiation. The differential heating of the sun on the earth-surface makes the air move and this movement of air in known as "Wind". Hydro-cycle is a result of solar energy. Hydro-cycle and gravitational flow of water are the fundamental aspects that establish the system to gain hydro-energy. The solar power is directly

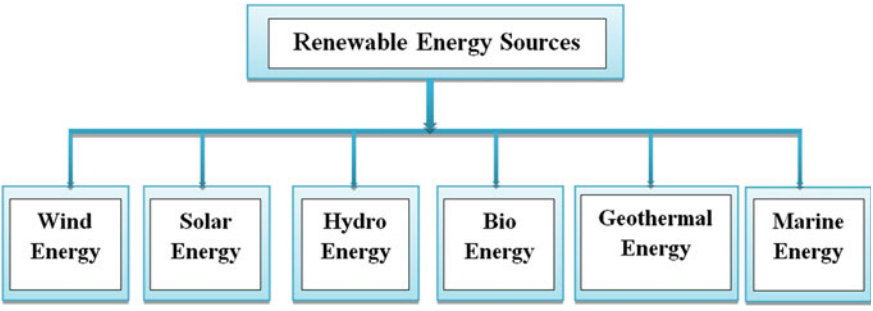

Fig. 1.1 Classification of renewable energy

converted from sunlight. Collectors or photovoltaic cells convert the sunlight into electricity. Again, plants collect solar power and these plants are converted to "Bio-mass". There are some RESs that do not rely on the solar power such as geo-thermal and marine energy. In the case of geo-thermal energy, the heat from the radioactive decay is pulled out from the crust of the earth for power generation. And when it is the turn of marine energy, conversion of wave, gravitational and potential energy of water mass, differential salinity are the basic concepts to generate power from this resource. RESs quickly and effectively replenish themselves and can be used again and again. For this reason, renewable energies are sometimes termed as "infinity energy resources".

1.2.1 Wind Energy

Since 1990 wind energy has been one of the rapidly growing sectors in the globe. Wind power is generated by the conversion of the kinetic energy of moving air to mechanical energy and afterwards the mechanical energy is converted to gain electric power. The working principle of a wind turbine is opposite of a fan. Like a fan, it does not use electricity to produce wind, rather the wind turbine uses wind to generate electricity. When air flows, it turns the blades which rotate a shaft and the connecting generator produces electricity. It captures the wind's energy by means of sophisticated blade design or air-foils to gather mechanical energy and then converts the mechanical energy to electric power. However, the most difficult task involves in this conversion is to design cost-effective turbines with aeronautic blades. Current available turbines with shafts can capture only 40–50% of the total available energy. These wind power plants generally can produce 5–300 MW, though plants of higher and lower capacity are also seen [6, 7].

According to Global Wind Statistics 2016, the world's total capacity of wind energy was 486,749 MW. In comparison with other countries of the world, China generates the maximum amount of wind energy, whereas Pacific Islands generate lowest, only 13 MW electricity from wind turbines. In 2016, China installed 23,328 MW (cumulatively) wind based power stations. From the given graph in Fig. 1.2, we can predict the current generation of power from wind energy around the world [8].

The generation capacity varies from place to place due to their environmental condition. Asia has the maximum proportion in this sector as there is a plenty of availability of wind in Asian sub-continent as shown in Fig. 1.3 [8].

Commonly, there are two types of wind turbines [9]:

- Horizontal axis wind turbine
- Vertical axis wind turbine.

The most easily found wind turbine is horizontal axis. In horizontal axis wind turbine, there is a tower. The tower holds three airplane propellers blades. Blades

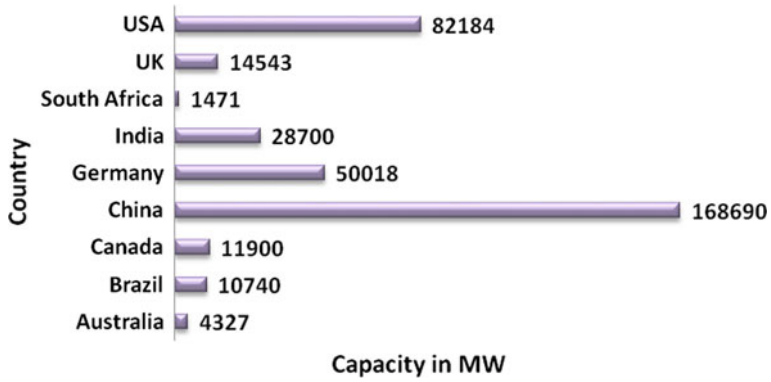

Fig. 1.2 World leaders in wind power capacity (in MW)

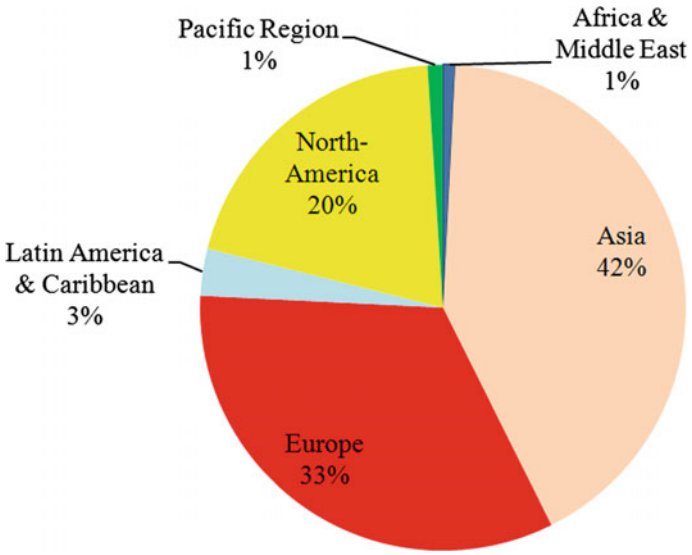

Fig. 1.3 Percentage of wind capacity around the world

are connected to the shaft. The shaft is mounted horizontally, parallel to the ground. When wind hits the blades, the shaft also rotates. The shaft has a gear and it turns a generator and produces electricity. The real view of horizontal axis wind turbine is shown in Fig. 1.4 [10].

In vertical axis wind turbine, the shaft is mounted vertically to the ground like an eggbeater. The Darrieus wind turbine is the most common vertical axis turbine. In 1931, French engineer Georges Darrieus designed this model [9]. It cannot start itself and needs additional electrical mechanism for star up. Nowadays, vertical axis

Fig. 1.4 Horizontal axis wind turbine [10]

wind turbines are not popular like horizontal-axis turbines for their lower performance. The real view of vertical axis wind turbine is shown in Fig. 1.5 [10].

1.2.1.1 Parts of Wind Turbine

Wind turbines have three important parts as shown in Fig. 1.6.

- Nacelle
- Rotor
- Tower.

The nacelle is the main mechanical compartment of the wind turbine. It has gear box, brake or controlling mechanism and generator. The controlling mechanism increases energy collection and conversion. A shaft connects nacelle with the rotor hub. There are three (usually) wing-shaped blades known as rotor. The rotor is connected with the central hub. The wind strikes the rotor and then it starts moving. Therefore, the wind's kinetic energy is captured by the rotor and is turned into rotational energy. The total system is established on a strong foundation and it is made enough high so that the blades can gain necessary wind resources. This system requires a conduit to transfer electricity generated from the wind turbine to the collection system. Generally, the whole amount of the electricity is transferred to the national grid. According to the location, wind farm can be classified into two types: one is on-shore and another is off-shore.

Fig. 1.5 Vertical axis wind turbine [10]

When the wind turbine is located on land, it is called on-shore whereas, off-shore wind farm is constructed off-shore (sea or freshwater). Off-shore wind farms get stronger wind speed compared to the land based on-shore wind farms. Therefore, off-shore wind farm can produce more electricity than on-shore. But the on-shore wind farm is cost-effective and easier to maintain, on the contrary, the off-shore wind farm has higher construction cost and its maintenance is also very tough. In general, the maintenance cost of off-shore wind turbine is 20% higher than the on-shore one [11]. The main disadvantage of on-shore wind farm is, it needs a back up supply in the time of insufficient wind strength. In 1991, the first off-shore wind farm was constructed in Denmark [12]. From on-shore wind farm, UK generated 7 TWh electricity in 2010 [13]. According to the estimations, this can save the emission of 6 million tons of CO_2 gases. The on-shore wind generation will be 30 TWh by 2020 in UK. This phenomenon will contribute greatly in preventing the emission of greenhouse gases (GHGs) of UK [13].

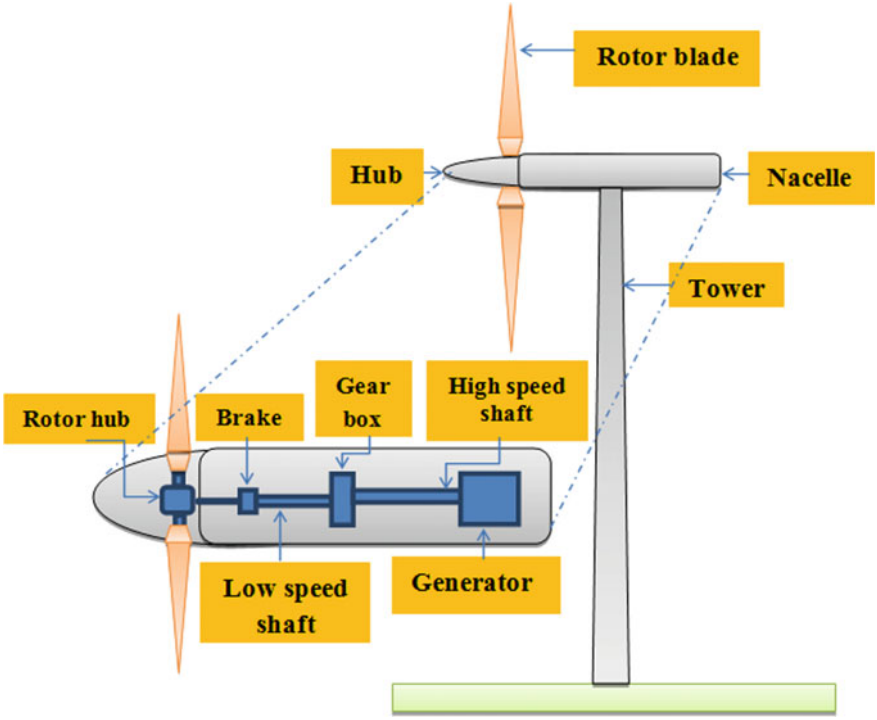

Fig. 1.6 Energy conversion in a typical wind turbine

1.2.1.2 Mathematical Model

The notations that used in the mathematical model are given below [14, 15].

E = Kinetic energy (J)
m = Mass (kg)
v = Wind speed (m/s)
P = Power (W)
$\frac{dm}{dt}$ = Mass flow rate (kg/s)
$\frac{dE}{dt}$ = Energy flow rate (J/s)
ρ = Density (kg/m^3)
A = Swept area (m^2)
C_p = Power coefficient
r = Radius (m)
t = Time (s)
x = Distance (m)

Under constant acceleration, the kinetic energy "E" is equal to the work-done "w". Here, an object has mass "m" and velocity "v", is displaced and covered a distance "s" with a force "F", that is

$$E = W = Fs$$

According to Newton's law, we know,

$$F = ma$$

Thus,

$$E = mas \tag{1.1}$$

According to the third equation of motion,

$$v^2 = u^2 + 2as$$

Now we get,

$$a = \frac{v^2 - u^2}{2s}$$

Since the initial velocity of the object is zero, i.e., $u = 0$, so, we get,

$$a = \frac{v^2}{2s}$$

Substituting it in Eq. (1.1) we get that, the kinetic energy of a mass is:

$$E = \frac{1}{2}mv^2 \tag{1.2}$$

The power in the wind is given by the rate of change in energy:

$$P = \frac{dE}{dt} = \frac{1}{2}v^2\frac{dm}{dt} \tag{1.3}$$

Hence, mass flow rate is given by

$$\frac{dm}{dt} = \rho A\frac{dx}{dt}$$

And the rate of change of distance is given by $\frac{dx}{dt} = v$,

Therefore, from the Eq. (1.3) the power can be defined as,

$$P = \rho A v^3$$

The density function, ρ, is given by [14],

$$\rho = 1.2925 \frac{(P_r - VP)}{760} \frac{273}{T} \quad \text{kg/m}^3 \tag{1.4}$$

here,

P_r = Pressure in mm of Hg
VP = Vapor pressure of water vapor
T = Temperature in degree Kelvin.

The vapor pressure can be found if the dew point is known. However, the vapor pressure correction affects the density by less than 1%. Hence, it is usually dropped from the calculation.

The power in the wind is converted to mechanical power which is transmitted to the generator. The electrical power output (P_e) is given by,

$$P_e = C_p \eta_m \eta_g P \tag{1.5}$$

where,

C_p = Coefficient of performance
η_m = Mechanical efficiency
η_g = Electrical efficiency.

1.2.2 Solar Energy

The solar energy is generated from the power of sun. It can be done in two ways [16]:

- Using photovoltaic (PV) cell
- Generating electric power through concentrating solar power (CSP) method.

These techniques are well known around the world and installed in numerous parts of the world to generate electricity in the last decade [17]. Location is the main factor for the solar power generation. Direct and diffuse are the two components of solar radiation. When solar radiation comes to the earth then two things happen—absorbtion and scattering. In the case of direct radiation, the sun ray directly comes in a line whereas in diffuse radiation, it is scattered out by different things like clouds. The total global irradiation of sun is the sum of direct, diffuse as well as reflected beams. Here,

$$GHI = DNI \cos Z + DHI \tag{1.6}$$

where,

GHI = Global Horizontal Irradiance (important aspects for PV)
DNI = Direct Normal Irradiance(important aspects for CSP)
DHI = Diffuse Horizontal Irradiance
Z = The sun zenith angle.

The amount of GHI and DNI differs from place to place. In Africa, the GHI value lies between 1600–2700 (kWh/m^2/year); where the lowest value in Congo Basin and highest value in Sahara and Namib. The DNI value lie between 900–3200 (kWh/m^2/year); lowest in Congo Basin and highest in Southern Namibia and North-Western South Africa Deserts [18]. The solar radiation in Bangladesh is approximately 1700 kWh/m^2/year [19].

1.2.2.1 Solar PV Cell

Solar PV is a semiconductor device which directly converts sunlight into electricity. PV cells are interconnected with each other and the amalgamation of the cells are called PV module. Generally, a PV module has the capacity of 50–200 W. There are different kinds of components in a PV module that are inverter, battery, electrical components and mounting system. By connecting PV modules, it is possible to generate few watts to tens of megawatts. The PV cells with mono-crystalline silicon have conversion efficiency up to 23% [20]. From the given graph (Fig. 1.7), it is possible to have a glace of the development of PV solar capacities during 2010–2015 [21].

The global competition is increased in solar PV market. More than thousand vendors and organizations are working worldwide to supply PV cells and their modules. The large segments of vendors are from US, Japan, Europe and China [22]. Many countries invest huge amount of money for increasing their PV capacity. Among them China is the market leader with generating capacity 43,050 MW in 2015 [21]. Figure 1.8 shows the scenario of worldwide percentage of PV capacity.

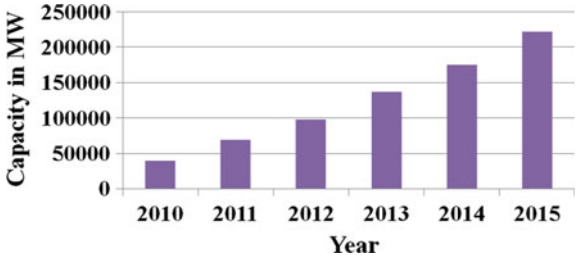

Fig. 1.7 Annual installed PV capacities in MW projection from 2010 to 2015

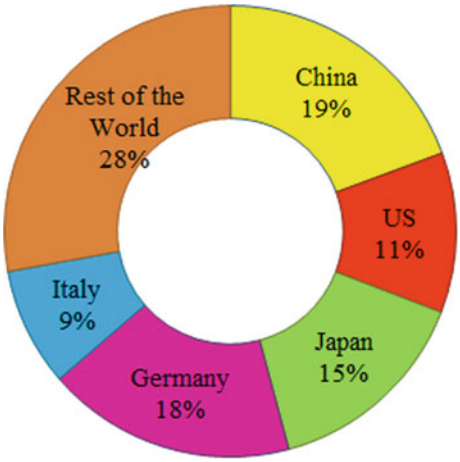

Fig. 1.8 Worldwide percentage of PV capacity in the year of 2015

Solar panels are installed at heights. It could be installed at every individual house. For commercial uses, the modules are installed for establishing a strong network within the panels. When sun rays fall on the panels, electrons are emitted. The flow of electron is controlled with a charge controller. The charges are stored in a battery. Then the inverter converts the dc current into ac current and thus the electricity is provided directly to consumers or to the grid as shown in Fig. 1.9.

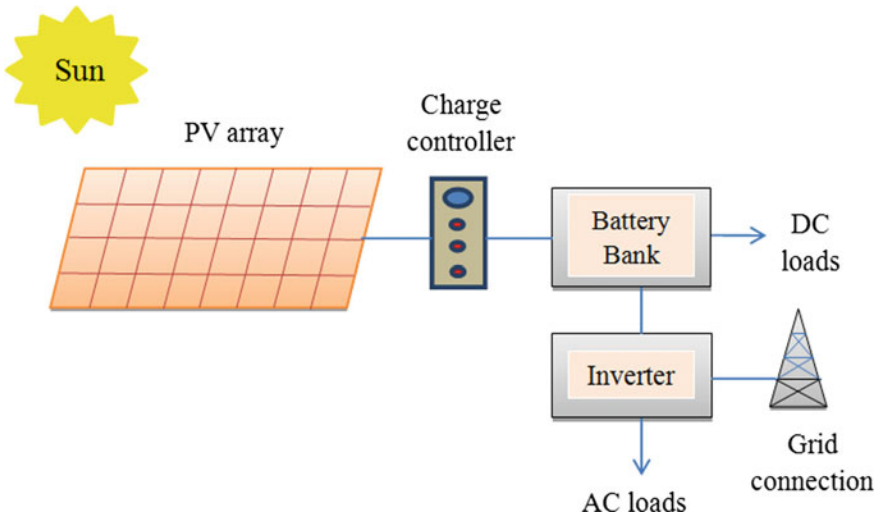

Fig. 1.9 Schematic diagram of PV system

The solar PV has two major advantages:

1. The PV modules can be used to produce massive amount of power which gives the benefit of economies of scale (Economies of scale mean if the production is in a large scale then its cost can be minimized).
2. Rather than CSP and solar thermal system, a PV is a very modular system that uses direct sunlight as well as diffuse component of sunlight. It can work even under unclear sky.

The output current "I" of an ideal PV cell, which consists of a single diode connection in parallel with a light generated current source "I_{ph}", can be written as [23]:

$$I = I_{ph} - I_s\left[\exp\left(\frac{V}{nV_T}\right) - 1\right] \tag{1.7}$$

where,

I_s = Cell saturation of dark current
V_T = Thermal voltage = KT_c/q
K = Boltzmann's constant = 1.38×10^{-23} J/K
T_c = Cell's working temperature
q = Electron charge = 1.6×10^{-19} C
n = Identity factor.

1.2.2.2 CSP Plants

In early stage, commercial CSP plants were generating 354 MW in California that continued to operate commercially till now [24, 25]. In the year 2009, 700 MW CSP plants were installed and 1500 MW CSP plants were under construction around the world [26].

In Asian region, India topped in CSP generation. Around the world Spain leads the CSP market. From the following graphical representation (Fig. 1.10), we can analyze the facts concerning the power generation using CSP [18].

The CSP is a type of solar thermal technology [16]. It consists of two parts: one is collector part and another is converter. This type of plant requires large area for collecting solar radiation. Power tower systems, trough systems, and dish/engine systems-approaches are used in CSP plants [27].

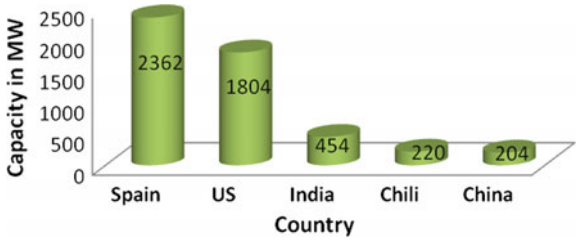

Fig. 1.10 Installed capacity of CSP of the top 5 countries

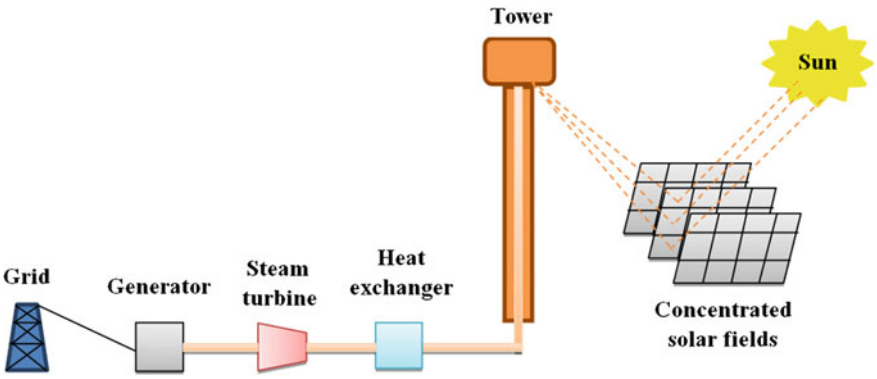

Fig. 1.11 Schematic diagram of CSP generation

In tower based CSP plants, the tower is the central receiver. Solar beams are directly concentrated by lenses or flat heliostats mirrors using the principle of light reflection to accrue heat in liquid and to turn them into steam, which is then used for electricity generation. A CSP has mirror (or lenses) converted dishes that are focused to boil water in a conventional steam generator to produce electricity as shown in Fig. 1.11.

Trough system CSP plants generally have large U-shaped or parabolic focusing mirrors. Some pipes are going along with the focal points of the focusing mirrors which are filled with oil. The mirrors collect the sun rays so that the oil becomes hot and this hot oil then boils the water. Afterwards, the boiling of water produces steam which runs the steam turbine and generator and produces electricity [27].

Mirror dishes, which are nearly 10 times larger than a backyard satellite dish, are set in dish engine system to concentrate solar power onto a receiver. This receiver is placed at the center of the dish. The receiver moves along the sun throughout day to capture the highest possible amount of solar power. The receiver has an external engine which contains helium or hydrogen gases to operate four piston cylinders. By using the expansion and contraction of helium or hydrogen gas, the heat energy is converted to mechanical energy and a crankshaft is made to rotate which runs a generator and thus, the generation of electricity takes place [27].

1.2.3 Hydro Energy

Hydro power is one of the most commonly used renewable energy, which generates around 16% of the global electricity in 2008 [28]. According to the International Energy Agency (IEA) in 2008, the world's hydro power production was 3288 TWh [29]. In 2015, in the whole world, there has been newly installed 33.7 GW of hydro power. Therefore, the hydro power has surely become friendlier to the countries, authorities. And that is why, 16.4% of global energy and 71% energy from RESs,

Table 1.1 Global position and installed capacity of top 3 countries in hydro power generation

Position	Country	Globally installed capacity (Word Market Share) (%)
1st	China	26%
2nd	USA	8.4
3rd	Brazil	7.6

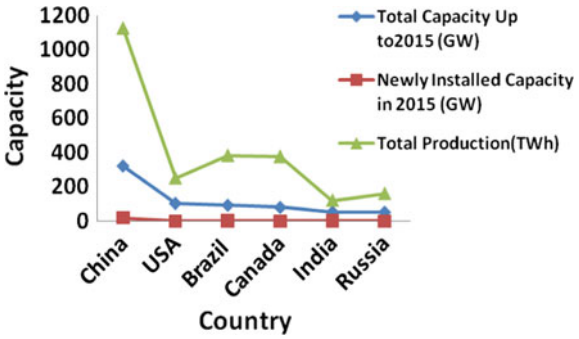

Fig. 1.12 Top 6 countries of hydro power generation in 2015

are generated from hydro. In this sector, the market leaders are shown in Table 1.1 [30].

If the statistics are analyzed, between the years 2005–2015, the upsurge taken place is 39% and per year this development is 4% on an average. In the year of 2015, the total generation from the hydro power has been found maximum in China, followed by USA as shown in Fig. 1.12 [30].

The three portions of the world are water. Among them only some portions of hydro potential are used where maximum potential are in unutilized condition as shown in Fig. 1.13 [30]. By using this huge potential in future, we can mitigate the power crisis with a clean environment.

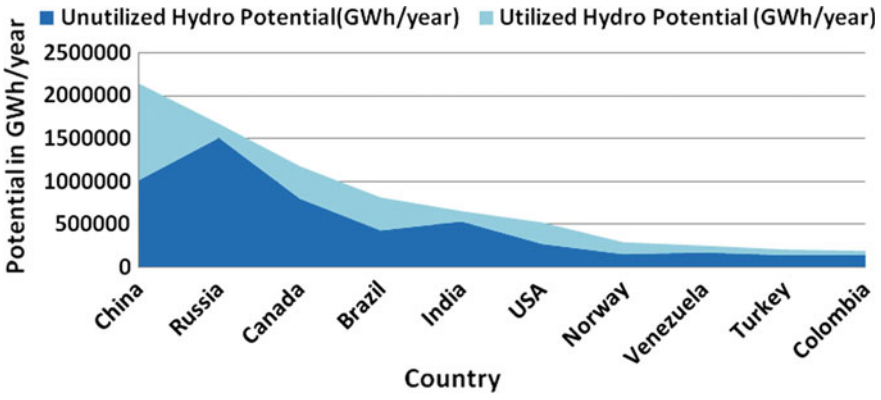

Fig. 1.13 Top 10 countries of hydro power potential

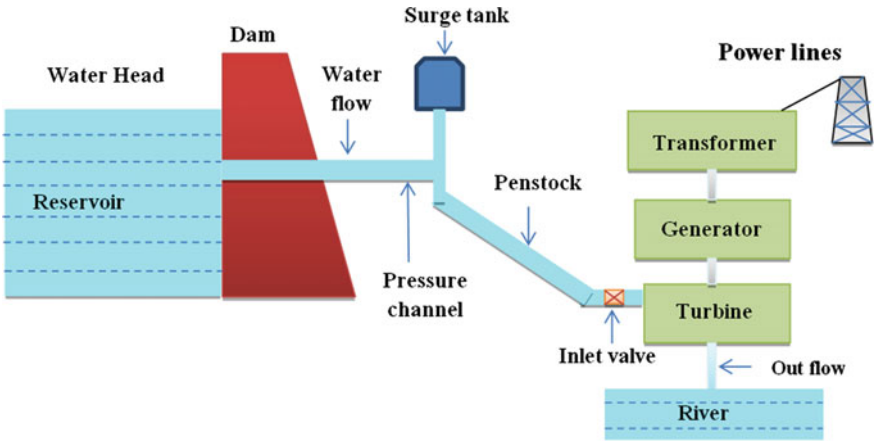

Fig. 1.14 Schematic diagram of HPP

Hydro power is the energy that is generated from the potential energy of water at high level. The solar radiation causes hydrological movement and from the movement of water the hydro power is generated. We consider the hydro power as a renewable energy because the water always returns in the plant in cyclic order from the nature.

In hydro power plant (HPP), the water head is made by constructing a dam across the river or lake. From the dam water moves towards the turbine through penstock and the energy of falling water is converted from hydraulic energy to mechanical energy, where the alternator works to convert the mechanical energy to electrical energy as shown in Fig. 1.14.

HPPs are classified into three types, based on their operation and water flow:

- Run of River (RoR) HPP
- Storage HPP
- Pumped Storage HPP.

In RoR hydro-plant, water is drawn from the main river flow to generate power. In this system, the generation is mostly dependent on the river flow, though sometimes it stores water for short term to maintain demand. Therefore, in RoR HPP, hydrological cycle of water is the determinant function for power generation.

The plant that has a reservoir is termed as the storage HPP and this stored water is used for later consumption. Downstream generation stations are connected with the reservoir by the pipe line. The type and design of reservoir is based on the landscape.

Pumped storage HPPs are with storage devices where water is pumped from a lower reservoir to higher reservoir and generally used in off-peak hour. The working principle is nearly same as the storage HPP. In this system, though it consumes the net energy generated for pumping water to reservoir, but

it is very much effective as it provides a wide range of energy storage benefits. A pumped storage HPP provides the largest share of power in the grid available worldwide [1].

The physics of hydro power is straight forward. The power carried by the water mass is given by [31],

$$P\,(kW) = g\,Q\,H \tag{1.8}$$

Here,

g = gravitational acceleration = 9.81 m/s^2
Q = flow rate in cubic meters per second
H = height of water fall in meter.

Because 2% error is insignificant in the engineering community [31], it always takes g = 10 m/s^2

Hence in terms of kilowatt,

$$P = 10QH \tag{1.9}$$

With the "Francis Turbine", invented by American Engineer James B. Francis in 1848 [31], the efficiency (η) for converting hydraulic power to mechanical power is greater than 90%, which makes it one of the most efficient machines. The electric power generated by the hydraulic system is

$$P = 10\eta QH. \tag{1.10}$$

1.2.4 Bio Energy

The latest data depict that "Bio energy" supplies 10% of global energy. From the forests, woody bio-mass and wastes supply 56 *EJ* (1 *EJ* = Exajoule = 10^{18} J). Latin American and Caribbean zones are using bio energy mostly [32].

The bio-energy comes from all organic materials originated from plants, trees, crops and animals. The term bio-energy covers both bio-mass and bio-fuels. Bio-mass and bio-fuels are the collection of sun's energy through photosynthesis as shown in Fig. 1.15.

The bio-mass can be found from different sources as shown in Fig. 1.16. It is mainly generated from forest woods and wastes. Agricultural crops are also an important source of bio-mass. Though the waste from urban areas can be a good source, but still it is not the dominant sector for supplying of bio-mass [33].

The worldwide bio-mass plant capacity is increased from 66 to 72 GW in 2012. The average growth rate of it in 2012 was 5%. In long run, the bio-mass generation as well as waste power generation could be 270 GW by the end of 2030 [34].

Though bio-energy is sustainable and renewable, but it has many characteristics like fossil resources. Bio-fuels can be stored as well as transported and provide a

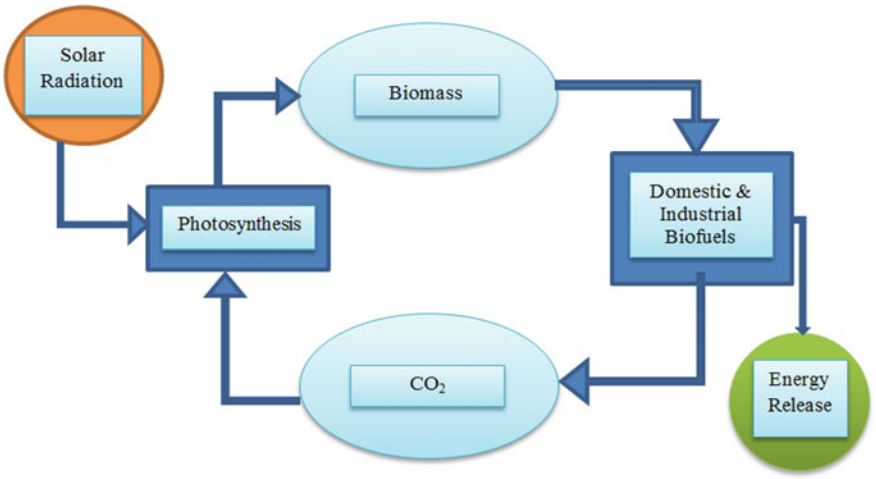

Fig. 1.15 Formation of bio-mass and fuel

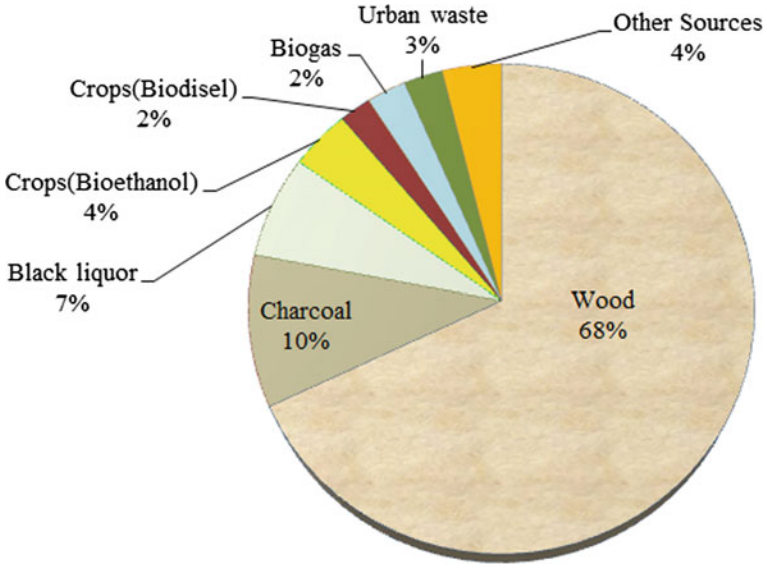

Fig. 1.16 Share of sources in bio-mass production

solution to intermittence of the renewable energy. Bio-fuels or bio-mass feedstock can be converted to bio energy by thermo-chemical or bio-chemical conversion process which can be sub-divided in various groups like combustion, pyrolysis, gasification and anaerobic digestion as shown in Fig. 1.17. Not only bio-energy can minimize the present energy crisis but also provides security for energy worldwide.

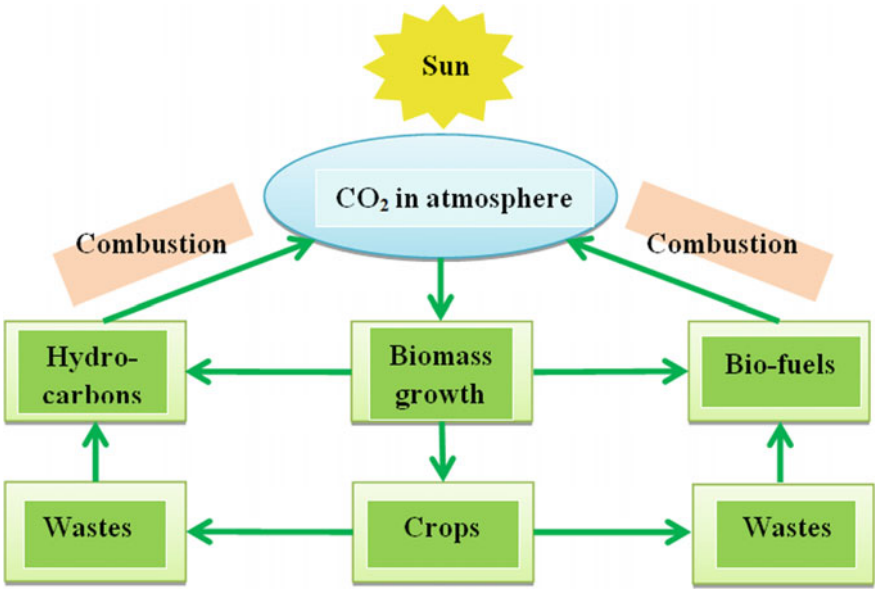

Fig. 1.17 A typical diagram of bio-mass energy synthesis

1.2.5 Geothermal Energy

The geothermal energy is one of the most effective, cost beneficial and environment friendly energy resources. In this process, the renewable energy of the earth is pulled out to generate power. For this, one mile or more is drilled beneath the surface level and steam and hot water from the underground is taken out to use in geothermal power plants. To drive a conventional steam turbine, an underground vertical pipeline is constructed to make a flow of water and steam. Through one pipeline water is injected and another supplies steam. The hot vapor or steam powers an electric generator. The cyclic movement of water in the process helps to recharge the reservoir. Thus, the whole cycle of renewable energy takes place as shown in Fig. 1.18.

The geothermal energy is used for various purposes. In many ways, direct or indirect, this energy is used mostly in heat pumps and green house and space heating. The usage of geothermal energy is shown in Table 1.2 [35].

Usually we can find three different sorts of geothermal power plants (GPPs) [36]:

- Dry steam GPP (DS GPP)
- Flash steam GPP (FS GPP)
- Binary cycle GPP (BC GPP).

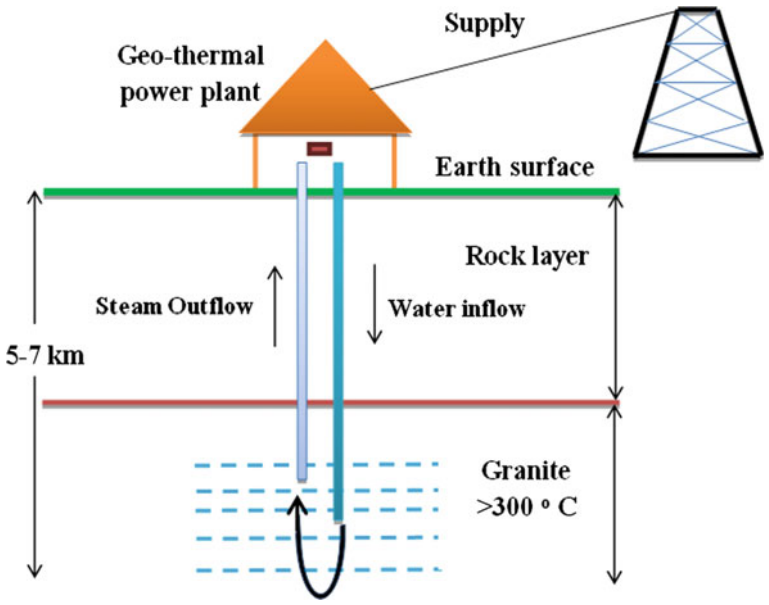

Fig. 1.18 Schematic diagram of geothermal system

Table 1.2 Usage of geothermal energy for various purposes

Purpose	Utilization (in %)
Geothermal heat pumps	55.30
Space heating	15.01
Green house heating	4.54
Agricultural pond heating	2.03
Industrial uses	1.78
Bathing and swimming	20.31
Others	1.03

The DS GPP draws vapor from the steam reservoir. But both FS GPP and BC GPP draw from hot water reservoir. The flash steam plants generally use water at temperature >360 °F. The binary cycle plant can operate at 225–260 °F.

Geothermal energy can be classified on the basis of their origin [1] as

- Shallow geothermal energy
- Deep geothermal energy.

The stored solar energy in the earth surface is "shallow geothermal energy". The main feature of it is to ameliorate the effectiveness of the electric heaters. The vapor compressed heat pumps or refrigerators basically increase the workability of electric heaters.

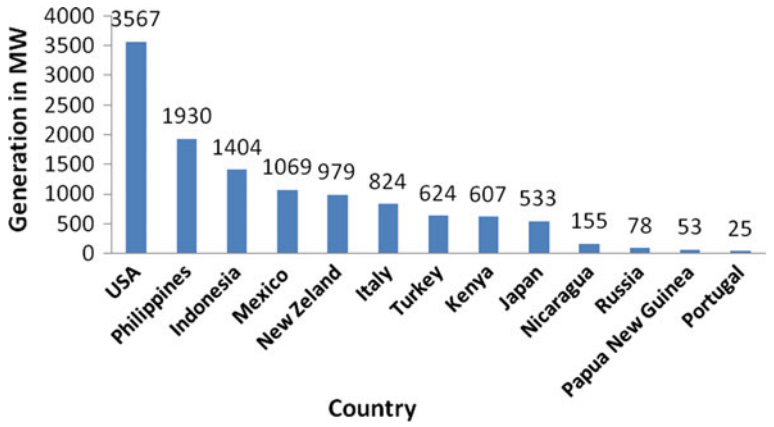

Fig. 1.19 Country wise generation of electricity from geothermal energy in 2015

The stored heat in the center of the earth is known as "deep geothermal energy". The temperature of this section might be hundreds of degrees. Various countries nowadays use this technology to generate electricity. Sometimes the space heating is also done by deep geothermal energy.

Though geothermal is one of the most efficient ways of power generation, only a small amount of power is generated as compared with the fundamental energy consumption of the world. In 2015, the geothermal power capacity was raised to 13.2 GW by adding new 315 MW. The USA has contributed the maximum amount of power by geothermal process and in this race, Philippines has stood 2nd and Indonesia in the 3rd position as shown in Fig. 1.19 [35].

1.2.6 Marine/Ocean Energy

We can avail marine or ocean energy by six distinct systems as

- Waves
- Tidal ranges
- Tidal currents
- Ocean currents
- Ocean thermal energy conversion (O.T.C)
- Salinity gradients.

The technology to draw power from the ocean is still not that much developed. From the experts, it is predicted that the total ocean wave energy in the open sea is about 10 TW [37]. If we can generate this much energy from the ocean, it will play a significant role in the total power consumption in the world. Moreover, solar, wind or other traditional RESs are uncertain as per their availability and to set up

them, we really need a very large land area. However, the oceanic energy does not need excessive area in comparison with other RESs. Again, oceanic wave energy has potential compared to other RESs and we can have an easy prediction about the energy availability. Therefore, the power generation from the oceanic wave energy has become the target area of investment and it will provide comparative advantages over the other forms of renewable sources [38]. But at present, without tidal ranges, other ocean energies are not improved that it can be used for commercial purposes. There are many researches undergoing on the technologies to draw power from oceans. It might be the most extensive source of energy in the future. Theoretically, it is estimated that the ocean could be an energy source of nearly 7400 EJ/year [39]. This quantity of energy could easily meet future demands and needs. However, scientists have not been able to draw power effectively from marine energy resources.

In recent years, marine generates only 0.5 and 1.7 GW is under construction. The lion portion comes from tidal ranges and that is 99% of marine power. If the researches remain on the right path at the right speed, then by 2050, it is possible to generate 748 GW by creating 160,000 jobs. Figures 1.20 and 1.21 show the wave power and tidal range power capacity, respectively [40].

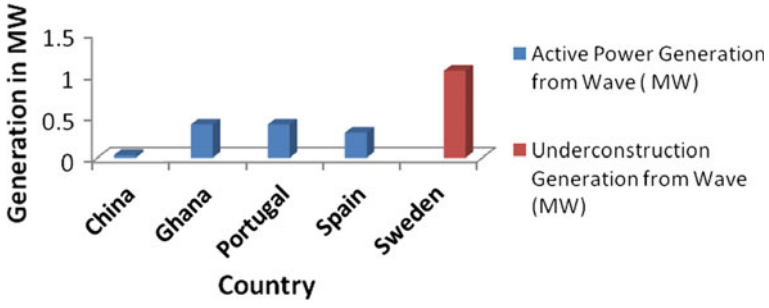

Fig. 1.20 Wave power installed capacity in 2016

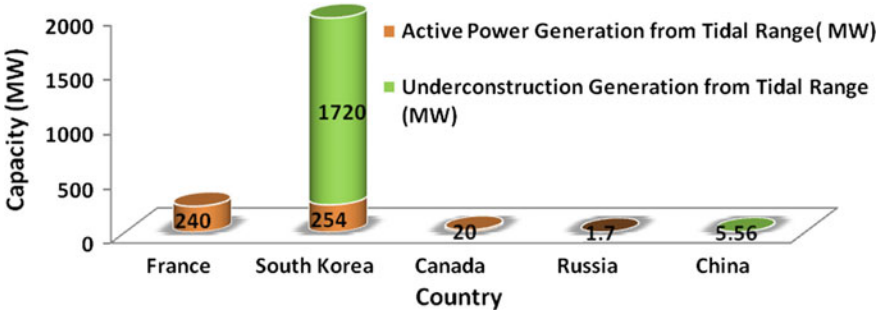

Fig. 1.21 Tidal range power installed capacity in 2016

1.3 Needs for Renewable Energy

The major need for renewable energy is the sustainability of the resources. It means it will never run out. The renewable energy facilities generally need less maintenance than traditional generator. The availability of the natural resources makes them attractive.

The important benefits that we can achieve from RESs can be discussed under four correlated parameters as shown in Fig. 1.22 [41].

- **Energy Security for Future**: There is no hard and fast definition of "Energy Security". However, it is defined as "the continuous and uninterrupted supply of energy which is primarily essential for running an economy" [29]. The growth of economy and energy consumption and supply is inter-related. The access to energy is the most fundamental aspect in the political as well as technical world. The development of economy is very much dependent on it. To reduce the economic gap between developed and developing countries, it is necessary to ensure the access to stable and continuous energy. If the generation of power is hampered, the series of economic and basic functionality difficulties arise in most of the society. The renewable energy is well distributed around the globe as compared to fossil fuel, so it can be a solution to reduce expenditures on

Fig. 1.22 Co-relations factors for analyzing the need of renewable energy

imports. The diversification of the supply also ensures energy security. It also can minimize the economic risks of sustaining the volatility of price. If the renewable energy is introduced everywhere it can make contribution to increase the reliability and services can reach the remote areas where there is an insufficient energy access. Good management and strong system design can create a diverse portfolio of renewable resources to enhance the energy security.

- **Socio-economic Development**: It is always seen that there has been a deep relation between social and economic development with the energy consumption. Therefore, no society can develop until there is a development in the power sector as it runs all the production and industrial activities. Any positive change in per capita energy consumption will bring a positive change in per capita income. It can be surely said that the growth of energy consumption is the measuring parameter of social and economic growth. When an economic development takes place, we can also find a social revolution in every aspect. It creates employment, improves lifestyle and a sustainable growth in the economy that brings peace and harmony in the society.

The renewable study 2008 has proven that this sector has created a large job market [41]. Around 2.3 million people were involved in this sector. Gender equality, reduction in economic disparity, improvement of education, health, sanitation sector and moreover, the development of environment have taken place with the increment of job market and quality of jobs.

- **Accessibility of Energy**: The United Nation has adopted SDG and according to its goal 7 the UN urges all the countries to ensure an affordable and clean energy by 2030 [42]. Not only this, UN tries to create a bond among the countries to provide cheap, clean, sustainable, accessible and available energies for all. And this goal can only be fulfilled by using and spreading renewable energy. Renewable sources are distributed across the globe and this makes it easily accessible to all. Access concerns are hard to be analyzed in the global context rather in local aspects. It is a common fact that there is a wide difference in electrification between cities and villages. This problem is very much acute in Sub-Saharan African countries like Ethiopia, Somalia, and Eritrea and in South Asian countries like Bangladesh, India, Nepal, etc. If renewable energy is installed we can easily diminish the difference of electrifications in urban-rural and develop-developing countries.
- **Environmental and Health Impacts**: The GHGs like SO_2, CO_2, etc. could be reduced, if we ensure renewable sources for the purpose of energy generation. By adopting RESs, we can make a safe and clean environment. It will reduce carbon footprint. Again, reducing GHG from our environment, we can also reduce health hazards as most of the diseases are involved with these harmful gases.

The bar chart (Fig. 1.23) below describes the most vulnerable countries affected by environmental changes and deaths due to environmental hazards [43].

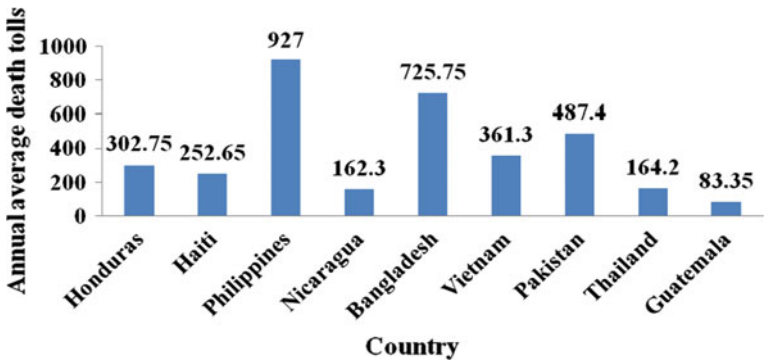

Fig. 1.23 Annual average death for climate changes in most affected countries

1.4 Advantages and Disadvantages of Renewable Energy

There are some benefits which we can easily avail from RESs. Some common features of renewable energy beneficial to us are listed here:

- Renewable energy is environment friendly. It does not emit GHG. Again, it does not pollute water and air as fossil fuels do.
- It has limited or low operation cost, as the resources to operate such plant is regenerated. Though startup cost may be high, but once a plant is constructed we can have energy throughout the year without expending much.
- Renewable energy is the agenda of United Nations Development Programme (UNDP), World Bank and many other international organizations. They want to push renewable resources. Therefore, to lessen initial investment, government and various Non-Governmental Organizations (NGOs) and international organizations provide interest free loan and technical support to this project.
- Fossil fuel is limited and its price is always moving up-down. Whereas, RESs are infinite and all the countries have access to it. Therefore, all the people around the world can use this power.
- Renewable energy sector occupies a good number of employees. It helps people to grow financially maintaining their environment.
- Like fossil fuel extraction, it does not damage land. Not only this, the renewable energy-based plant is aesthetic in both visual and environmental aspect.
- It can bring development in rural areas. Where the grid connection is nearly impossible, there renewable energy is the most effective solution.
- It helps to develop local people.
- It ensures sustainable development as renewable energy enables to preserve energy for the future. Reducing dependency on fossil fuel has economic and social benefits.

- It is resilient and more reliable in terms of large scale failure. Renewable resources are modular. Therefore, if any part is any how damaged, we can expect clean and uninterrupted power from other modules.

The modern world is very much conscious about the renewable energy. Each of the resources of renewable energy has different types of cost benefits, economic, social and environmental value. And researchers have worked really hard to minimize the cost of the accessories for the renewable energy. The Table 1.3 summarizes different types of advantages and disadvantages of various RESs.

Table 1.3 Advantages and disadvantages of renewable energies

Type of energy	Advantages	Disadvantages
Wind Energy	• No air or water pollution • Free source of energy • Wind farms are relatively inexpensive • The land of the wind farms can be used for other purposes	• Requires constant and significant amount of air • Requires significant amount of space • Have visual impact on landscapes
Solar Energy	• Infinite source of energy supply • No air and water pollution	• Manufacture and implementation of solar panels are costly • Storage and back up is mandatory • Workability depends on the availability of sun light
Hydro Power	• Sources are abundant, clear and safe • No standby losses • Relatively inexpensive	• Costly to build • Can causes flood • Uncertainty of availability of water
Bio Energy	• Cheap to construct • Burns waste products	• When burns it gives of atmospheric pollution including GHGs • Bio-mass is only renewable if the crops are replanted
Geothermal Energy	• Potentially infinitive energy supply • Produce no air and water pollution	• Set up and development cost can be expensive • Maintenance cost can be tough due to corrosion
Marine Energy	• Ideal for Island countries • Captures energy that would otherwise not be collected	• Construction can be costly • Opposes by some environmental groups or locals as it has a negative impact on marine eco system • Needs large space that causes difficulties to move ships or water vehicles

1.5 The Economics of Renewable Energy

It has become a key component to use RESs throughout the world to combat climate change, reduce hazards and pave a way towards sustainable developments. In the past, the fossil fuel was more cost-effective than renewable energy. However, nowadays it is a matter of hope that cost benefits of fossil fuel over renewable energy is being minimized day by day. From the following comparative analysis given in Fig. 1.24 the facts can be understood [44].

Already RESs are competing fossil fuel in financial terms. The US Department of Energy portrays this fact with authentic data. Like, from 1998 to 2011, the cost of installation of solar PV system fell by 5–7% per year on average. Again, there was another decline in installation by 11–14% between 2010 and 2011 [45]. Analyzing this trend of fall of price of the PV cells, it can be said that in future the price may decrease again and the technology will be updated as researchers and scientists are working day and night for the improvement of this technology [45]. This phenomenon will attract the businessman to invest in this sector. Figure 1.25 shows the trend in the investment of solar power [18].

From a study we have come to know that only the wind, hydro, and solar power are capable of providing all new energy by 2030, and by 2050 all the non-renewable energy sources commonly fossil fuels will be market out as this place will be captured by renewable resources [46].

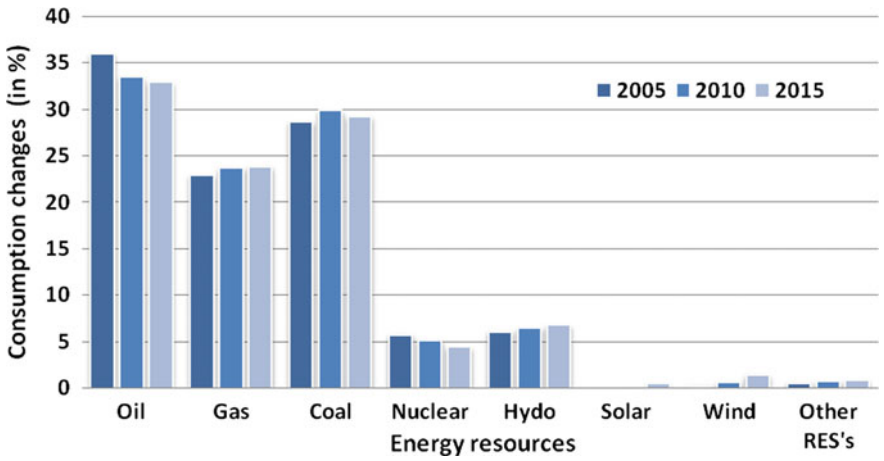

Fig. 1.24 Analysis of consumption changes (in percentage) in energy market of fossil fuel and renewable from 2005 to 2015

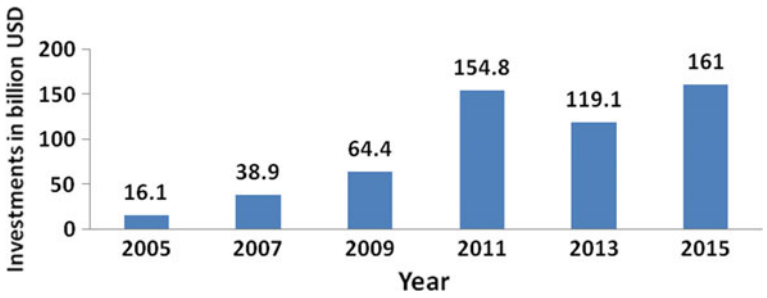

Fig. 1.25 Investments in billion USD in solar sector

1.5.1 Cost Challenges

We can certainly hope that in future renewable energy will take over the market. To make this happen renewable resources have to take "Cost Challenges" that include, net energy of renewable resources, challenges for unavailability of renewable resources, and dependency on intensive capital.

- **Net Energy Analysis and Estimation**

Fossil fuels like oil, gas, coal reserve a certain amount of energy. For example, a gallon of gasoline has a potential energy of about 37 kWh [29]. A typical solar panel of 3 × 6 ft with 1 hour of bright sunlight can generate about 0.2 kWh [29]. Therefore, it can be easily understood that the energy gain from renewable resources is too low.

The definition of net energy is given below [29, 47]:

"Net energy is the physical attribute of an energy source, which is the ratio of energy available for final consumption and energy required to produce it".

$$\text{Net Energy Ratio} = \frac{\text{Available Energy for Final Consumption}}{\text{Energy Required for Production}} \tag{1.11}$$

The net energy ratio depends on the parameters like the technology of production and condition of the energy resource. From the Table 1.4, we can have a glace of net energy of various forms of resources.

- **Challenges for Unavailability of RESs**

Renewable energy cannot provide sufficient energy supply as per the requirement as like the fossil fuel. We know that RESs are intermittent. The availability of the resources is not constant rather they vary during various periods of day, month and year. For example, on cloudy days the sun might not be available and it may interrupt the production of solar energy. In case of wind and hydro power, the

Table 1.4 Net energy ratios of various energy sources [29,47]

Energy sources	Net energy ratio
Oil (Global)	35
Natural gas	10
Coal	80
Shale oil	5
Nuclear	5–15
Hydropower	>100
Wind	18
Photovoltaic cell	6.8
Ethanol (Sugar cane)	0.8–10
Ethanol (Corn based)	0.8–1.6
Biodiesel	1.3
Farmed willow chips	55

availability of wind and water may vary. At the time of drought, water is unavailable. If there is a crops failure, we will not have the supply of feedstock and the production of bio-mass will be stopped. Because of the low capacity of the renewable energy, the cost of energy from this sources becomes expensive.

In the electricity sector, the supply and demand must be the same all the time. If the supply becomes less, then load shedding takes place and if the supply is more than the demand, then it won't be cost-effective. Along the day, the demand of electricity varies from time to time. We can control the generation of power according to the demand by controlling the supply of fossil fuel. However, this benefit is unavailable for the RESs because they dependent on the nature and we do not have any control over the supply of them.

To get rid of this intermittency, the energy diversity is an effective solution. To diverse the energy, the combination of solar and wind energy is an appropriate way, as in summer solar energy is the strongest source and in winter, the wind energy is the strongest source. Not only this, the storage of energy is another significant solution for intermittency.

- **Dependency on Intensive Capital**

Renewable resources require large investment to start up rather than fossil fuel. And high investments need high borrowing from money market and this will cost high interest. When the authorities have to pay high amount of interest, they become inactive to establish such huge project. Not only this, high investments are involved with high risks if the project does not work properly.

On the other hand, the operating and maintenance cost of the plants running by solar and wind energy is comparatively low. After constructing the plant, we can generate power without spending anything for the resource and the maintenance cost is too low. When it comes to fossil fuel, it requires a large expenditure to operate the plant. And if the authority reduces interest rate on renewable resources, it will become more attractive to the investors.

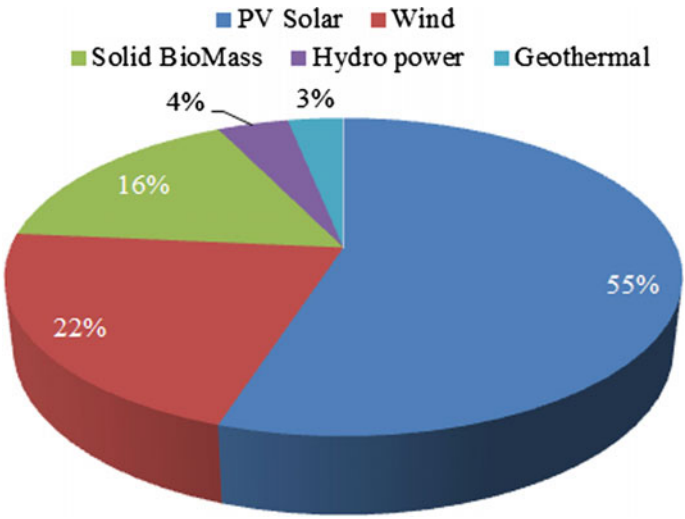

Fig. 1.26 Employment in renewable sector around the world

1.5.2 Impacts on Job Market

With the growing trend of using renewable energy, a new job sector is also created. The sector of solar technology provides the highest amount of employment and it is nearly of 2.5 million in the whole world [48]. As the production and establishment cost of wind plants are falling, many people are now willing to invest and create new opportunities. From the last count [49], we have come to know that 834,000 people were directly and indirectly involved in this field. China covers nearly half of the total employees working in the wind industry. IRENA predicts that by the year of 2030, 16 million people will be engaged with renewable sector [49], 1.3 million people were involved in large scale hydro power plants in the year of 2015. Figure 1.26 and Table 1.5 depict the world employment status of renewable energy [2].

1.6 Roles of RESs in Environment Protection

Throughout the world "climate change" has become the burning question. There is no path to protect the climate without adopting the renewable energy in the place of extensive use of fossil fuels because by adopting the renewable resources we can reduce the amount of carbon emission from power plants and thus it will help to build a better environment for us as well as for our future generation. The United

Table 1.5 Statistics of employment around the world in renewable sector in 2015

Industry	Total employment in the world
PV Solar	27,72,000
Wind	10,81,000
Solid Bio-mass	8,22,000
Hydro power (Small Scale)	2,04,000
Geothermal	1,60,000

Nations Framework Convention on Climate Change (UNFCCC) defines climate change as follows [50]:

> When the climate is being attributed directly or indirectly by human activities that alter the composition of the global atmosphere and which in turn exhibits variability in natural climate observed over comparable time periods.

Renewable sources are the ultimate solution to preserve our environment. It causes no harm to our environment. It does not produce secondary or harmful wastage. Again from the bio-fuel or bio-mass, we can generate compost fertilizers. By using resources from renewables, the stress on grid can largely be reduced. Thus, the customer can be relieved from the pressure of high electricity bill. Another important thing is, it decreases the demand of non-renewables, and so huge amount of wealth can be saved by adopting such technologies in our daily life.

Non-renewables create high risk for our environment. When fossil fuels are burnt, a high level of CO_2 releases. This gas can absorb temperature and as a result, the global temperature is rising. This incident is coined as "Global Warming". From a report [51], it is found that the electricity production plants are the reason for 29% of total US GHG emissions. Another fact is, the CO_2 emission by the US power sector is mostly taking place due to the burning of coal in power plants which is 68% of the total share whereas gas based power plants contribute to 30% [52]. The carbon emission from fossil fuel is shown in Fig. 1.27 [53].

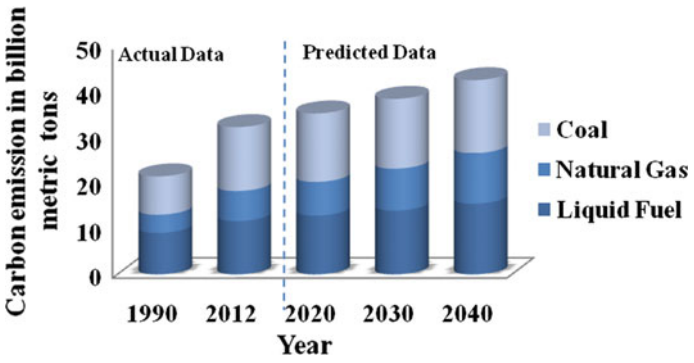

Fig. 1.27 Carbon emission from fossil fuel around the globe

The rise in the temperature makes the weather condition very whimsical. We have to face extreme hot weather at the time of summer and less cold in winter. The periods of seasons are also altered by this change. As the average global temperature is rising, the ice of the North Pole is being melted. This is causing a rise in the sea level. It is estimated that low lying areas of the world may go under water in the future. Island countries like Myanmar, Solomon Islands, etc. are at the high risk of going under the sea.

Our ozone layer is being attacked every moment by CO_2, chloro-fluoro-carbon (CFC) and other gaseous particles. This is destroying the ozone layer. The ozone layer is the protector of us from ultraviolet (UV) rays of sun and other cosmic rays. If the ozone layer is damaged, we will be exposed to UV and cosmic rays. This will increase patients of cancer and other dangerous diseases.

Not only this, fossil fuels exploration pollutes the ground water. At the time of coal mining and drilling for natural gas various harmful chemicals and heavy metal particles get mixed with water. If we drink such water, it may take our lives. All fossil fuel power plants drained the waste and hot water to the river or sea which damage the ecosystem of water. This not only damages our environment but also destroys the marine life and the quality of water.

If we adopt and promote the renewables, then the carbon emission will be slowed down. From a study of "Union of Concerned Scientists" it is estimated that by 2025 renewable power plants can minimize carbon emission by 277 million metric tons [54]. In addition, according to the US National Renewable Energy Laboratory, there is a scope to generate 80% of US electricity from renewable sources by 2050 and the global warming due to carbon emission can be mitigated up to 81% [55]. The carbon emission associated with the production, installation, maintenance, dismantling and discharge of wastage is minimal in case of renewable energy [26,56].

There are some impacts on environment by RESs. Different types of sources affect the environment with different factors.

1.6.1 Environmental Impacts of Wind Power

The wind turbine has low environment impacts. It takes a little amount of land for its construction. It may emit a very tiny amount of GHG at the time of installation but there is no emission of harmful gas at the time of its operation. It reduces the net amount of pollution. Recent technologies have made the blade rotation of the turbine slow and silent. It does not hamper free movement of birds [57]. Nowadays, the blades are located in upwind rather lower wind. As a result, the level of infrasound is minimized. Scientists and authorities prove that there is no risk due to low infrasound [58].

1.6.2 Environmental Impacts of Solar Power

Unlike other typical power generation station, PV cells are safe. At the time of operation PV cells do not emit harmful particles. Generally PV module of 100 W can decrease 2 tons of CO_2 emission [59]. However, from PV cells different kinds of chemicals are disposed to air and water, which sometimes create many problems in the environment [59]. According to the report of "Toxics Release Inventory System" of USA, there are 6, among all the other PV cells producing companies, whose used chemical are not released in reportable quantities [60].

1.6.3 Environmental Impacts of Hydroelectric Power

The hydropower plant is known as a clean source of energy because it does not produce any kind of pollution. However, in the construction and operation phase, the dam creates some effects on the eco-system of water. The environmental impact of a specific hydro power facility requires point to point reviews. We have to develop new technologies for modeling the hydro power plant so that this problem can be avoided.

1.6.4 Environmental Impacts of Bio-Mass

In general, we think bio-mass is free from carbon emission as bio-mass gathers carbon from the environment. However, recent studies have proven that it is not true at all. Bio-mass emits CO_2 and it has little effect on the environment. Again some people promote harvesting bio-fuels rather food crops. This may lead us towards insecurity of food production. We also can get bio-mass from the municipal wastage. This can be a solution if the waste management is properly carried out [61].

1.6.5 Environmental Impacts of Geothermal Energy

If we use a 1 kilowatt-hour (kWh) of geothermal energy in the place of same amount of non-renewables, then the global warming will be reduced up to 95% declares by International Atomic Energy Agency (IAEA) [62]. However, the development of geothermal energy has some negative impacts. Large-scale construction and drilling operations have inverse effects on local area and ecology. In drilling phase, the important activity is the protection of ground water. During the construction phase, the main visual impact is the exaggeration of high technological and powerful machineries. After the construction phase is over, then it is the most

effective way to generate power with nearly nil emission of GHG. This technology leaves no carbon footprint and the surrounding atmosphere has the cleanest air. Geothermal plants emission typically falls below the threshold [63].

1.6.6 Environmental Impacts of Marine Energy

As we all know, the ocean wave energy is free from pollution and very much promising for the environment. Therefore, we can certainly say that it will reduce carbon and other harmful gas emission and create a milestone towards saving bio-chemical resources [64]. Though marine or ocean power plants do not emit CO_2 or other GHGs, they cause damages to marine wildlife. Animals living in the sea are very much disturbed by the large apparatus for generating power. Again, fishes, marine mammals may collide with the instruments of the power generating plants.

1.7 Smart Grid Technology

Renewable resources are costly to establish and intermittent in nature. Uncertainty of the renewable sources makes the output hard to be controlled [65,66]. To improve such barriers, it needs advanced and upgraded technology which can be met by the "Smart Grid Technology". At present, we avail power from the national grid after generation from the plants. However, in future, if we can adopt smart grid technology, then every house (smart house) will be a generation point as well as a consumer of that electricity with RESs. The national power grid will not only supply electricity to house-holds but also buy electricity from them. Therefore, every entity, like households and grids will become both buyer as well as seller of electricity as shown in Fig. 1.28.

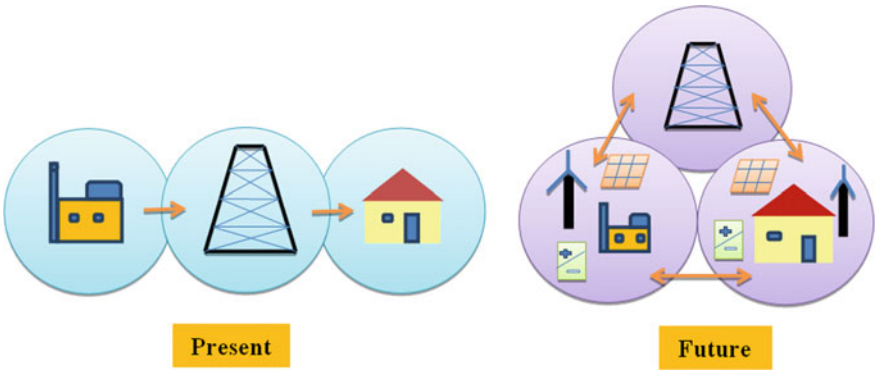

Fig. 1.28 Smart grid technology: present and future

Charles F. Brush designed the first automatically operating wind turbine in 1887 to generate 12 kW power, which was installed in Cleveland, Ohio [67]. This automatically run wind turbine worked for 20 years. At the speed of 6.6 rpm, it worked most effectively. The output voltage was always kept 70–80 V by the smart technology. Palmer Putnam developed another wind turbine with a capability of 1.25 MW [68].

The EU's smart grids technology platform delineates the advantages of smart grid technology. They are as follows [67,69].

- Gives various easy technology for the connection and operation of generators of different powers and sizes
- Beneficial to consumers as they can control power consumption
- Give consumers information and knowledge regarding supply which they can use
- Minimize the atmospheric impacts of the supply system
- Enhance the reliability, quality and security of supply
- Accelerate market integration.

Smart grid technologies can be categorized into four functional portfolios shown in Fig. 1.29 [70].

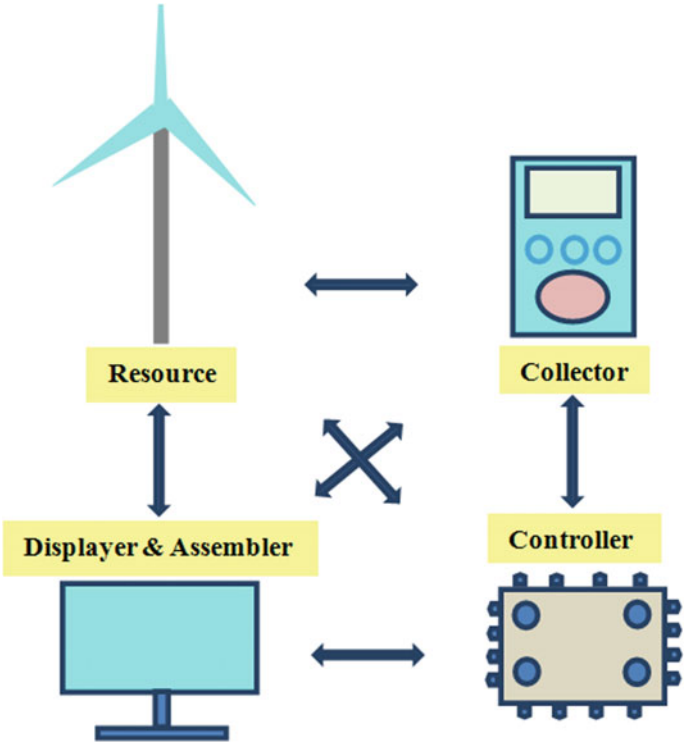

Fig. 1.29 The four functions of smart grid technology [70]

- **Collector**: In smart grids, various kinds of sensors are used for various purposes. One of them is collecting data. Again, sensors are used for measuring performance characteristics of different electrical machineries. For instance, voltage or current meter, temperature, vibration tracking sensors, etc.
- **Controller**: These components get data. Afterwards, it processes them and takes necessary steps for controlling the behavior of other devices. The main purpose of this is to achieve specific targets, like controlling the flow of current and voltage.
- **Displayer and Assembler**: This subclass consists of devices which show as well as analyze information.
- **Resource**: Technologies associated with generation, storing of energy or minimizing the demand for electricity are included here.

1.8 Recommendations for Future Use of Renewable Energy

Our present energy market is dominated by the coal based power generation. Though it is cost-effective to startup but the operation cost is high. And, the GHG emission from the plant costs a significant deterioration to the environment. On the other hand, a nuclear power plant does not emit GHG, but its startup cost and maintenance is very high and any accident in the plant would destroy the surrounding area with radiation. Considering all the available facts, renewable energy is the source that we can use to make sustainable energy and build a better future for all.

Still investors and authorities are unwilling to invest on the renewable sector. To make it more popular among the authorities, following suggestions can be effective:

- The energy generation from RESs should be diversified. If we construct hybrid power plants with solar, wind, and hydro energy, we can create a perfect mix to achieve continuous and uninterrupted power supply.
- Various incentive programs for the renewable resources should be entertained and be promoted in developed and developing countries simultaneously. If the developed and developing countries produce power from renewable sources, then this will balance the world's total power generation.
- In developing countries of South Asian and Sub Saharan area, where the grid connection is not available everywhere, renewable power plants on small scale can be an ultimate solution. For example, by installing rooftop solar panels and community based bio-gas plants, we can supply electricity in the remotest corner of a country.
- Law and Treaties to promote renewable energy should be made and launched in every country.
- We have to broaden the sectors of using renewable energy. Though it is highly appreciated in power sector, but in transportation and industrial purposes, it is

not that much popular. Therefore, vehicles and industrial apparatus should be designed to run by RESs.

- Carbon tax should be imposed properly. Highly industrialized countries should pay carbon tax. This money can be used for launching renewable energies and settling the environmental vulnerable countries and people throughout the world.
- Authorities should make a detailed plan for introducing renewable sources. There must be a smooth integration of current technology and future expected renewable based advanced technology.
- Governments and international organizations should invest as much as possible in research and development sector to improve the current technology and invent new and highly efficient technology to generate power from renewable sources.
- It is essential to incorporate smart grid technologies for an effective supply of renewable energy. The advanced storage and effective transmission can make renewable energy more popular. Researchers and scientists should focus to introduce smart grid transmission and storage technology for renewable energy.

1.9 Conclusions

From the above discussion and analysis, it is true that we cannot expect to sustain in this planet without introducing renewable energy. Fossil fuels would run out and the nuclear power is risky. Only the renewable energy gives us a complete solution for sustainable development. Various economic institutions, agencies, organizations and governments of various countries like Norway, Germany put emphasis on the use of RESs and invest and give subsidy to inspire the use of these resources. GHGs capture heat and increase the global temperature. An increment in the global temperature causes the ice pole melt which, in turn, rises the sea level. Extreme emissions of CO_2, NO_2, NO_3, SO_3, SO_4 and other gases cause air pollution and acid rain, which are dangerous for all creatures living in this planet. Our total ecosystem is disturbed by the excess use of fossil fuels. On the other hand, the renewable energy is very much eco-friendly and cost-effective. It just needs launching boast; afterwards with a minimal operation cost, it will supply energy for a long time. People around the world believe that renewable energy technology will bring a positive change in the environment and current practice of power generation. Investors, users and supply providers shall also be benefitted if the renewable energy takes over the fossil fuel. However, still we have a long way to go. All the parties like academics, technologists and others should focus on renewable sources. To build a better world, the renewable energy should be promoted and installed by all. Governments and different agencies should come forward to develop and inspire this green technology for a peaceful world with birds chirping and blooming flowers.

References

1. Ellabban O, Abu-Rub H, Blaabjerg F (2014) Renewable energy resources: current status, future, prospects and their enabling technology. Renew Sustain Energy Rev 39:748–764
2. REN 21, Global Status Report 2016. Available at: http://www.ren21.net/status-of-renewables/global-status-report/. Accessed 8 June 2016
3. Merriam-Webster, Renewable. Available at: https://www.merriam-webster.com/dictionary/renewable. Accessed 5 Mar 2017
4. TREIA, Definition of Renewable Energy. Available at: http://www.treia.org/renewable-energy-defined/. Accessed 5 Mar 2017
5. Arena, What is renewable energy? Available http://arena.gov.au/about-renewable-energy/. Accessed 11 Mar 2017
6. Islam MR, Mekhilef S, Saidur R (2013) Progress and recent trends of wind energy technology. Renew Sustain Energy Rev 21:456–468
7. Eltamaly AM (2013) Design and implementation of wind energy in Saudi Arabia. Renew Energy 60:42–52
8. Fried Lauha (2017) Global wind statistics 2016. GWEC, Brussels, Belgium
9. EIA, Types of Wind Turbines (2017). Available at: https://www.eia.gov/energyexplained/index.cfm?page=wind_types_of_turbines . Accessed 20 May 2017
10. Governor's School for Agriculture, Wind turbines. Available at: https://govschoolagriculture.com/tag/wind-turbines/. Accessed 14 May 2017
11. Islam MR, Guo YG, Zhu JG (2014) A review of offshore wind turbine nacelle: technical challenges, and research and development trends. Renew Sustain Energy Rev 33:161–176
12. BOEM, Offshore Wind Energy. Available at: https://www.boem.gov/Renewable-Energy-Program/Renewable-Energy-Guide/Offshore-Wind-Energy.aspx. Accessed 25 May 2017
13. The guardian, onshore wind energy. Available at: https://www.theguardian.com/environment/2012/sep/25/climate-change.windpower. Accessed 18 May 2017
14. Johnson GL (1978) Economic design of wind electric systems. IEEE Transactions on Power Apparatus and Systems, PAS-97(2), pp 554–562
15. The Royal Academy of Engineering, Wind Turbine Power Calculations. Available at: http://www.Raeng.org.uk/publications/other/23-wind-turbine. Accessed 22 Mar 2017
16. Solar Energy Development programmatic EIS, Utility-Scale Solar Energy. Available at: http://solareis.anl.gov/guide/solar/index.cfm. Accessed 14 May 2017
17. Byrne J, Kurbgelashvili L, Mathai MV, Kumar A, Yu J, Zhang X, Tain J, Rickerson W, Timilsina GR (2010) World solar energy review: technology, market and policies. Report of Centre for Energy and Environmental Policy, University of Delaware, USA
18. World Energy Resources Solar 2016, 24th Edn, WEC, UK, October, 2016
19. Islam MR, Islam MR, Beg MRA (2008) Renewable energy resources and technologies practice in Bangladesh. Renew Sustain Energy Rev 12(2):299–343
20. Andrei H, Nicolaescu G, Radulescu S, Andrei PC (2013) New approach of PV cell efficiency. In: Proceedings of 12th international conference on environment and electrical engineering, Wroclaw. pp 106–111, 5–8 May 2013
21. Whiteman A, Rinke T, Esparrago J, Elsayed S (2016) Renewable capacity statistics 2016. IRENA Report, UAE
22. Islam MR, Rahman MF, Xu W (eds) (2016) Advances in solar photovoltaic power plants. Green energy and technology series. Springer-Verlag GmbH, Heidelberg, Germany. ISBN 978-3-662-50519-9
23. El-Basit W, El-Maksood AM, Soliman F (2013) Mathematical model for photovoltaic cells. Leonardo J Sci 23:13–28
24. Sioshansi R, Denholm P (2010) The value of concentrating solar power and thermal energy storage. IEEE Trans Sustain Energy 1(3):173–183

25. Machinda GT, Chowdhury SP, Chowdhury S, Kibaara S, Arscott R (2011) Concentrating solar thermal power technologies: are view. In: Annual IEEE India conference (INDICON), 16–18 Dec 2011
26. Edenhofer O, Pichs-Madruga R, Sokona Y, Seyboth K, Matschoss P, Kadner S, Zwickel T, Eickemeier P, Hansen G, Schlömer S, Stechow CV (eds) (2011) IPCC special report on renewable energy sources and climate change mitigation. Cambridge University Press, Cambridge, United Kingdom and New York, NY, USA
27. Solar Energy Development programmatic EIS, Concentrating Solar Power (CSP) Technologies. Available at: http://solareis.anl.gov/guide/solar/csp/index.cfm. Accessed 12 May 2017
28. IEA, Renewable Energy Essentials: Hydropower. Available at: https://www.iea.org/. Accessed 11 March 2017
29. Timmons D, Harris JM, Roach B (2014) The economics of renewable energy, GDAE teaching module. Tuffs University, Medford, MA, USA
30. World Energy Resources Hydropower 2016, 24th Edn, WEC, UK, October, 2016
31. Chen CJ (2011) Introduction, in Physics of Solar Energy. Wiley, Hoboken, New Jersey, pp 9–10
32. IRENA working paper, Biomas for power generation, vol 1(1/5), June, 2012
33. Kummamuru B (2016) WBA global bio-energy statistics report 2016. WBA, Stockholm
34. World Energy Resources Bioenergy 2016, 24th Edn, WEC, UK, October, 2016
35. World Energy Resources Geothermal 2016, 24th Edn, WEC, UK, October, 2016
36. California Energy Commission, Types of Geothermal Power Plants. Available at: http://www.energy.ca.gov/almanac/renewables_data/geothermal/types.html. Accessed 20 Mar 2017
37. Wu F, Zhang XP, Ju P, Sterling MJH (2008) Modeling and control of AWS-based wave energy conversion system integrated into power grid. IEEE Trans Power Syst 23(3):1196–1204
38. Watanabe R, Shin JS, Koseki T, Kim HJ (2014) Optimal design for high output power of transverse-flux-type cylindrical linear synchronous generator. IEEE Trans Magn 50(11):1–4
39. Kayagusuz K (2012) Energy for sustainable development: a case of developing countries. Renew Sustain Energy Rev 16:1116–1126
40. World Energy Resources Marine Energy 2016, 24th Edn, WEC, UK, October, 2016
41. Owusu PA, Asumadu-Sarkodie S (2016) A review of renewable energy sources, sustainability issues and climate change mitigation. Cogent Eng 3(1):1–14
42. UNDP, GOAL 7 TARGETS. Available at: http://www.undp.org/content/undp/en/home/sustainable-development-goals/goal-7-affordable-and-clean-energy/targets/. Accessed 11 May 2017
43. Kreft S, Eckstein D, Dorsch L, Fischer L (2015) Global climate risk index 2016. Briefing Paper of Germanwatch, Berlin, Germany
44. World Energy Resources 2016, 24th Edn, WEC, UK, October, 2016
45. Feldman D, Barbose G, Margolis R, Wiser R, Darghouth N, Goodrich A (2012) Photovoltaic (PV) pricing trends: historical, recent, and near-term projections, SunShot US Department of Energy, DOE/GO-102012-3839
46. Jacobson MZ, Delucchi MA (2011) Providing all global energy with wind, water, and solar power, part I: technologies, energy resources, quantities and areas of infrastructure, and materials. Energy Policy 39(3):1154–1169
47. Murphy DJ, Hall CAS (2010) Year in review—EROI or energy return on (energy) invested. Ann N Y Acad Sci 1185:102–118
48. IRENA Report (2015) Renewable energy and jobs—annual review 2015
49. Amin AZ (2017) HUFFPOST, The economics of renewable energy: falling costs and rising employment. Available at: http://www.huffingtonpost.com/adnan-z-amin/the-economics-of-renewabl_b_7452996.html. Accessed 14 Mar 2017
50. UNFCCC (2011) Fact sheet: climate change science—the status of climate change science today. Available at: https://unfccc.int/files/press/backgrounders/application/pdf/press_factsh_science.pdf. Accessed 5 Mar 2017

51. Environmental Protection Agency (2015) Inventory of US greenhouse gas emissions and sinks: 1990–2015
52. US Energy Information Administration (EIA) (2017) How much of the US carbon dioxide emissions are associated with electricity generation? 2016. Available at: https://www.eia.gov/tools/faqs/faq.php?id=77&t=11. Accessed 19 Sept 2017
53. International Energy Outlook (2016) US EIA, Washington DC, May, 2016
54. Union of Concerned Scientists (UCS) (2009) Clean power green jobs. Available at: http://www.ucsusa.org/clean_energy/smart-energy-solutions/increase-renewables/clean-energy-green-jobs.html#.Whlv-TRLfIV. Accessed 20 Sept 2017
55. National Renewable Energy Laboratory (NREL) (2012) Renewable electricity futures study, vol 1, p 210
56. Nurunnabi M, Roy NK (2015) Renewable energy based hybrid power system: the best way to keep the world pollution free from GHG. In: Proceedings of 2nd international conference on electrical information and communication technologies (EICT), Bangladesh, pp 539–544, 10–12 Dec 2015
57. Macintosh A, Downie C (2006) Wind farms the facts and the fallacies. Discussion paper number 91, The Australia Institute
58. Levanthall G (2006) Infrasound from wind turbines—fact, fiction or deception. Can Acoust 34(2):29–36
59. Klugmann-Radziemska E (2014) Environmental impacts of renewable energy technologies. Int Conf Environ Sci Technol. IPCBEE, Singapore, pp 104–109
60. PIER final project report (2003) Potential health and environmental impacts associated with the manufacture and use of photovoltaic cells, Public interest energy research program. California Energy Commission, California
61. Spath PL, Mann MK (2004) Biomass power and conventional fossil systems with and without CO2 sequestration—comparing the energy balance, greenhouse gas emissions and economics. Technical Report of National Renewable Energy Laboratory
62. Hunt TM (2001) Five lectures on environmental effects of geothermal utilization, geothermal training programme. Institute of Geological and Nuclear Sciences, Taupo, New Zealand
63. Dumas P, Serdjuk M, Kutschick R, Fraser S, Reith S, Koelbel T (2013) Report presenting proposals for improving the regulatory framework for geothermal electricity, GEOELEC
64. Farrok O, Islam MR, Sheikh MRI (2016) Analysis of the oceanic wave dynamics for generation of electrical energy using a linear generator. J Energy 2016:1–14
65. Roy NK, Pota HR (2015) Investigating the controller interactions of distribution systems with distributed generation. IFAC-Papers Online 48(30):19–24
66. Roy NK, Pota HR (2015) Current status and issues of concern for the integration of distributed generation into electricity networks. IEEE Syst J 9(3):933–944
67. Camacho EF, Samad T, Garcia-Sanz M, Hiskens I (2011) Control for renewable energy and smart grids; In: Samad T, Annaswamy A (eds) The impact of control technology. Report of IEEE Control Systems Society. Available at: http://ieeecss.org/main/IoCT-report. Accessed 20 Sept 2017
68. Putnam PC (1948) Power from the wind. Van Nostrand Reinhold Inc, New York
69. European commission community research report (2006) European smart grids technology platform, Belgium
70. Kempener R, Komor P, Hoke A (2013) Smart grid and renewables: a guide for effective deployment, IRENA working paper

Chapter 2
Solar Photovoltaic Power Plants: Necessity and Techno-Economical Development

Pejush Chandra Sarker, Md. Rabiul Islam, Alok Kumar Paul and Subarto Kumar Ghosh

2.1 Introduction

The demand of energy is increasing remarkably with the fast growth of population and economy in the world [1, 2]. Figure 2.1 shows the total population between 1950 and 2013 [3]. It is observed from the Fig. 2.1 that the number of population increases with a constant growth rate. It is predicted that this rate will continue in future. At the same time, the economical growth creates large number of industries, higher electricity demand and larger transportation requirement. These factors affect the environment by increasing carbon dioxide (CO_2) known as greenhouse gas due to consuming huge amount of fossil fuel. In 2012, power generation sector was significantly emitting CO_2 which is about 44% of total emission due to fossil fuel burning [3]. Transportation and industrial sectors represent the second and third contributors of CO_2 emission. In 2012, their shares were about 20.6 and 17.8% respectively [3].

In 2014, 10,000 million tons of CO_2 was emitted from 12,928.4 million ton of oil equivalent fossil fuel [2]. The amount of CO_2 increases significantly every year which increases global temperature. Figure 2.1 shows the global CO_2 emission from fossil fuels. Figure 2.2 shows the average global temperature and atmospheric CO_2 concentration between 1950 and 2013 [3]. It is observed that up to 1970, the

P. C. Sarker (✉) · M. R. Islam · A. K. Paul · S. K. Ghosh
Rajshahi University of Engineering and Technology, Rajshahi 6204, Bangladesh
e-mail: pejush01@yahoo.com

M. R. Islam
e-mail: rabiulbd@hotmail.com

A. K. Paul
e-mail: alokeee10b@gmail.com

S. K. Ghosh
e-mail: subartoeee07@gmail.com

M. R. Islam et al. (eds.), *Renewable Energy and the Environment*, Renewable Energy Sources & Energy Storage, https://doi.org/10.1007/978-981-10-7287-1_2

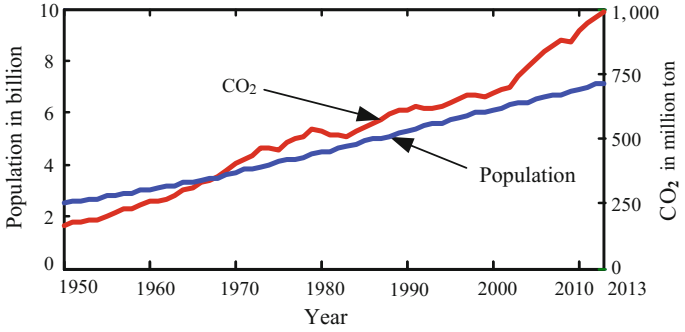

Fig. 2.1 Population and CO_2 emission from fossil fuel burning [3]

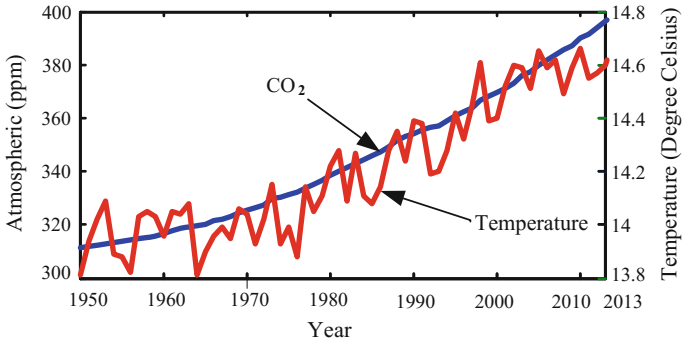

Fig. 2.2 Global temperature and atmospheric CO_2 concentration [3]

average temperature was about 14 °C but next four decades, it rose to 14.6 °C. At the same time, the concentration of CO_2 increased at constant rate. The concentration was about 325 ppm in 1970 whereas by 2013, it was increased to 398.55 ppm [3]. In addition, fossil fuel power plants generate some other greenhouse gases, e.g., carbon monoxide (CO), particulate matter (PM_x), nitrogen oxide (NO_2) and sulphur oxide (SO_x) which also affect the environment. Solid and liquid disposals of power plants affect surrounding water and soil. Nuclear power plant does not emit any green house gases but its radioactive operation, fuel and disposal make the environment radioactive near to the plant and mines.

On the other hand, the increasing energy demand is diminishing the reserve of fossil fuel. To solve these two major challenges, i.e., energy and environment, scientists all over the world are looking for alternative energy sources [4, 5]. Renewable energy may become one of the main alternative source which is richly available almost everywhere. Many countries have set targets for electricity generation from renewable sources, e.g., solar PV, concentrating solar power (CSP), wind power, biofuel and geothermal so that a significant amount of total electricity demand is fulfilled by nonconventional resources. Figure 2.3 shows the renewable

electricity generation targets taken by various countries. Costa Rica and Iceland have set their electricity generation targets in such a value that they will not require any fossil fuel or other fuel based power generation system, i.e., 100% electricity demand will be obtained from renewable energy by 2021 [6]. Similarly, Brazil and Fiji also have taken initiatives so that they can generate 80 and 75% of their total electricity from renewable sources by 2021 and 2025, respectively [6]. Germany, UK, India, China, Italy, Japan, Philippines have also set their own targets for different periods as shown in Fig. 2.3.

Due to substantial decline in PV module cost, the annual growth rate of solar PV plant becoming higher than other electric power generation systems. Now, it is becoming feasible to install a solar PV power plant with a capacity of more than 500 MWp. Gujarat solar park shown in Fig. 2.4 is one of the biggest solar PV power plants in the world which is generating more than 856 MWp. In near future, 1000 MWp in capacity solar PV power plant will have thereby become a reality. Up to 2014, about 1600 PV power plants were already installed all over the world [2]. It is reported that 4.9–9.1% and 17–21% of global electricity demand will be met with solar PV power by 2030 and 2050, respectively [2].

This chapter reviews development, construction, and operation of large scale solar PV power plant technologies which give a brief understanding of its necessity and techno-economical development. The module cost, tilt angle, inverter, module arrangement, mounting and tracking system are also discussed which are essential elements of a solar PV power plant. Atmospheric conditions highly affect the performance of a solar PV power plant. Therefore, proper monitoring and appropriate site selection are really critical issues for a solar PV power plant. This chapter also covers latest monitoring systems and site selection techniques which help to design a modern solar PV power plant.

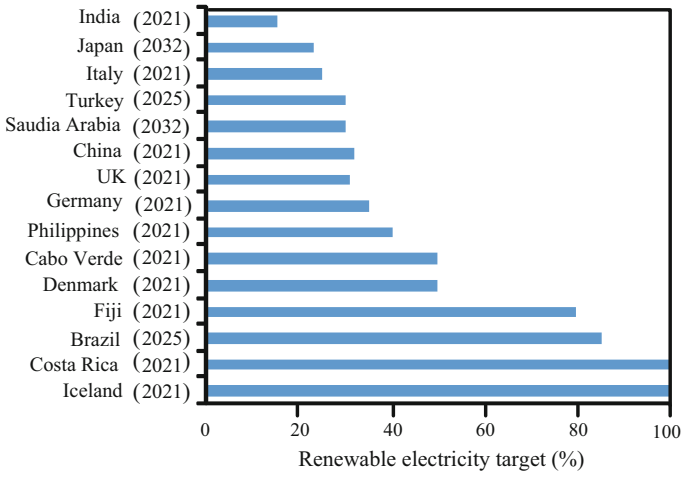

Fig. 2.3 Renewable energy targets by different countries [6]

Fig. 2.4 A photograph of Gujrat solar park [7]

2.2 The Use of Conventional Fuel

The present world still mainly depends on fossil fuel (coal, natural gas and oil) as most of the power plants are now using fossil fuel as source of energy. Moreover, many countries, e.g., France, Slovakia, Ukraine, Belgium and Hungary depend on nuclear energy as main energy source. Still coal, natural gas, oil and nuclear are the dominating conventional sources in the world.

2.2.1 Coal

Coal plays a very important role for the generation of electricity all over the world. Coal fired power is considered as a cheapest source of energy compared to other conventional energy sources, e.g., oil and natural gas [8]. Due to the lower generation cost, coal fired power plants generate 41% of the global electricity [9, 10]. Figure 2.5 expresses the consumption of coal for the generation of electricity from 1965 to 2013.

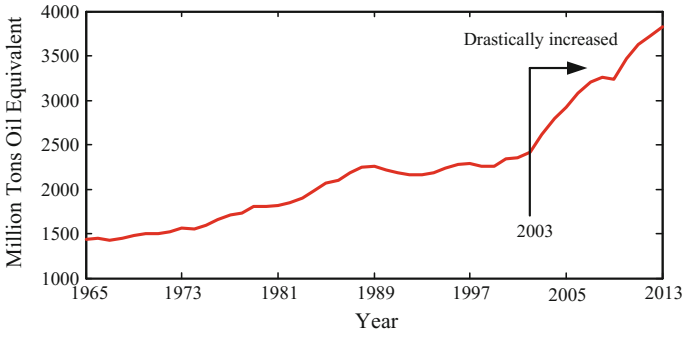

Fig. 2.5 Consumption of coal in the World [3]

Figure 2.5 also depicts that during 1965–1989, the consumption of coal was increased with almost a linear rate. After 1989, the coal consumption remained almost constant until 2003. Since 2003, the coal consumption has been drastically increasing to meet the rapid demand of electricity. In 2013, the amount of coal consumption for electricity generation was almost 4000 Million Tons Oil Equivalent.

2.2.2 Natural Gas

Due to the clean burning nature of natural gas compared to coal, it has become a very popular fuel for the generation of electricity. Figure 2.6 shows the worldwide natural gas consumption from 1965 to 2013. Figure 2.6 also depicts that the consumption of natural gas for electricity generation is increasing with a constant rate.

In 2012, about 22% of the global electricity was generated from natural gas. Literature shows that more than 28% of the global electricity will be generated from natural gas in 2040, i.e., about 2.7% annual growth rate until 2040 [11]. Natural gas is the least carbon-intensive fossil fuel which generates almost 50% less CO_2 than that of coal. In addition, natural gas based power generation technologies are more efficient than coal power generation.

2.2.3 Oil

To meet the growing demand of electricity, oil is the alternative option for producing electricity. In 2014, global oil consumption grew by 1.9 million barrels per day [12]. In 2012, about 5% of the global electricity generation was produced from liquid fuel. It is predicted that the share of the world electricity generation from

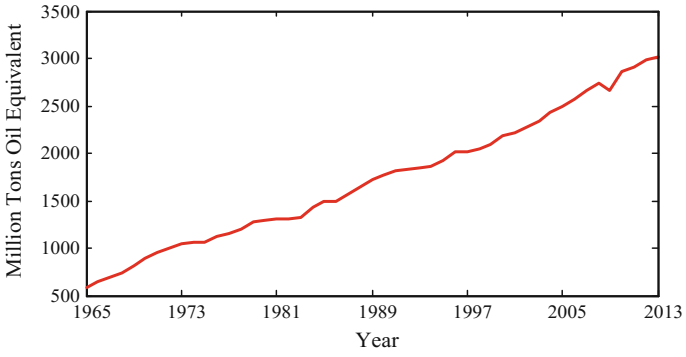

Fig. 2.6 Consumption of natural gas in the World [3]

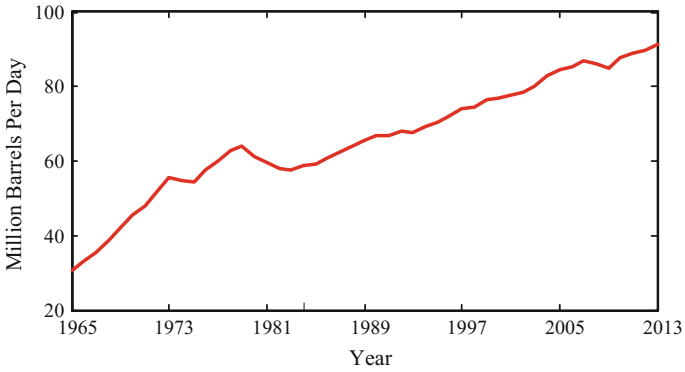

Fig. 2.7 Consumption of oil in the World [3]

liquid fuels will fall to 2% by 2040 as the prices of oil is getting higher [11]. Figure 2.7 demonstrates the oil consumption all over the world from 1965 to 2013.

2.2.4 Nuclear Power

In 2014, about 11% of the global electricity generation throughout the world was generated from nuclear power plants [13]. In France, 72.3% of the total electricity was produced by using nuclear energy in 2016. In 2016, about half of the total electricity demand in Slovakia, Ukraine, Belgium and Hungary was met using nuclear energy [13]. Figure 2.8 demonstrates the global electricity generation by nuclear power plants from 1970 to 2013.

Figure 2.8 also depicts that electricity generation from nuclear power grew until 2005 with almost a constant rate. In recent years, several nuclear power plants have

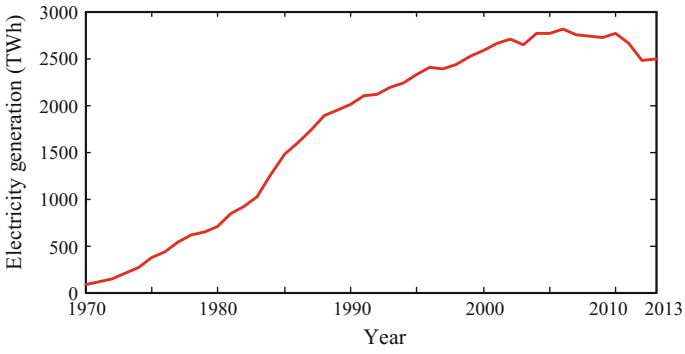

Fig. 2.8 Electricity generation using nuclear energy in the World [3]

been shut down permanently due to some natural disasters, e.g., earthquake and tsunami. In 2011, Fukushima Daiichi nuclear power plant was disabled due to earthquake and tsunami.

2.3 The Environmental Effects of Conventional Fuel Based Power Plants

The conventional power plants affect the environment by the various ways. The conventional fossil fuel based power plants emit greenhouse gases during fossil fuel burning. Moreover, during mining and transportation of fossil fuel, the environment is also affected. Nuclear power plant does not emit greenhouse gases as like fossil fuel based power plants. But, radioactive fuel and wastages of nuclear plants are dangerous for the environment. However, the toxic emission emitted from fossil fuel based power plants and nuclear power plants can deteriorate the ecosystem of the area near to the plants.

2.3.1 The Detrimental Effects of Fossil Fuel Based Power Plants

2.3.1.1 Air Pollution

During the operation of coal based plants, a huge amount of nitrogen oxide (NO_X), sulphur dioxides (SO_2), carbon monoxide (CO), carbon dioxide (CO_2) are produced which pollute air and are responsible for acid rain [8, 14–17]. Coal power plants also produce mercury and some unburned carbon which affects the environment [8, 14–17]. The natural gas based power plants also affect the environment by emitting carbon monoxide (CO), particulate matter (PM_x), nitrogen oxide (NO_2) and sulphur oxide (SO_x). Although, the amount of these pollutants is less compared to the coal based plants, the higher methane leakage during transportation and extraction of natural gas from mines jeopardize the climate benefits. Similarly, fossil oil, e.g., diesel, heavy fuel oil (HFO) and light fuel oil (LFO) based power plants emit CO, CO_2, NO_X, SO_X which pollute the environment.

2.3.1.2 Health Hazards

Due to the toxic emissions or pollutants from fossil fuel based power plants, people are suffering from many difficult diseases like as respiratory, cardiovascular, and cerebrovascular and so on [8, 16]. Mercury is also very toxic element emitted from the coal fired power plants available in both organic and inorganic forms.

The mixture of methyl-mercury (MeHg) with water is harmful for fish and rice as well. When people are having of that fish and rice, they are at health risk due to its bio-magnification property of toxic element [18].

2.3.1.3 Global Warming

The greenhouse gases (CO, CO_2, NO_X, SO_X, methane) emission from fossil fuel increases the global temperature. Scientists and researchers believe that continuous increase of greenhouse gases create rising sea level, altered ocean current, melting of glaciers and polar ice caps, climate alternation and severe storms, which significantly change the ecosystem [19].

2.3.1.4 Water Pollution

From coal fired power plants, a lot of wastage like as arsenic, selenium, boron, cadmium and mercury is disposed to waterways. As a result, water is being polluted. These pollutants lead to the negative impacts on nature and environment. Due to spills and leaks of chemical additives, diesel or other liquids from equipment and different storages appear as a risk of surface water. Moreover, huge amount water is used in condenser of a thermal power plant and is finally returned to the river at warmer temperature. This water affects the water plants, fish, and microbial activities. Moreover, ground water becomes contaminated with fracking fluid and gas near the oil and gas wells.

2.3.2 The Detrimental Effects of Nuclear Power Plants

Though nuclear power plants do not produce fly ash or a toxic or harmful gas, the radioactivity [20] that is released from the nuclear fission seriously affects the public health and environment [21]. The input of nuclear power plant is uranium oxide fuel prepared in few steps such as mining and milling of uranium, transport and reprocessing of irradiated fuel called nuclear fuel cycle. Huge amount of wastage is produced in each step. The serious impact on land, water and occupational health hazards during uranium mining and likely to increase cancer incidence on miners due to radon produced from radioactivity [21].

Moreover, health hazards are occurred due to use of toxic hydrogen fluoride and fluorine in fuel fabrication process. In addition, the gamma ray is emitted from fuel fabrication and nuclear fission process. Again, during serious accident, the cask walls are being ruptured while transporting radioactive materials leads to serious impact on health and environment [21, 22]. Radioactivity has its long term reaction on public health. Due to the thermal discharges from nuclear plant, normal life of biota is affected by hampering reproduction, growth, survival of larval forms,

juveniles and adults. Similarly, all fisheries are obstructed to lead normal life due to increase temperature of water by thermal discharge [20, 22].

2.4 Prospect of Renewable Energy

Solar energy is the one of the largest source of renewable energy. In the last decade, a remarkably change has been observed in solar PV market. In 2007, the total global installed capacity of solar PV was only 7.6 GW and it exceeded 100 GW in 2012 [23]. In 2013, the growth rate of solar PV was 28%. Up to 2013, roughly 58% of total capacity of solar PV plants has been installed in Europe. Now China's market is growing rapidly. By 2013, the installed capacity in China increased to 13 GW, whereas it was only 0.3 GW in 2009. In Italy, more than 7.8% of total electricity is generated from solar PV [23]. CSP is a solar thermal power generation technology that uses solar energy to generate electricity. Up to 2013, the global cumulative installed capacity of CSP was 3.4 GW [23]. About two-third of this capacity was installed in Spain. In total 5 MW projects of CSP are currently under construction in Australia, India, China, Chile, South Africa, Middle East and North African region. Wind energy is also dominating renewable source. Up to 2013, total cumulative installed capacity of wind power was 318 GW, whereas it was only 94 GW in 2007. Significant amount of wind power comes from Demark, Germany and US. At present, more than 240,000 wind turbines are operating in all over the world [23]. China, India, Brazil, Mexico and South Africa are becoming big markets for wind power development. Other renewable sources, e.g., biomass and geothermal are attracted less attention and getting smaller growth rate. In 2013, geothermal resources contributed only 76 TWh electricity with an installed capacity of 12 GW [23]. In recent years, the growth rate of geothermal power utilization remains almost constant at about 3%. The use of biomass in power sector is increasing every year. The total installed capacity of biomass power increased from 45 GW in 2007 to 88 GW in 2013 [23]. In 2013, the growth rate of biomass power was 12%. Total installed capacity of different renewable energy is shown in Table 2.1.

Table 2.1 Total installed capacity in GW [22]

Year	2007	2008	2009	2010	2011	2012	2013
Solar photovoltaic	7.6	13.5	21	40	71	100	139
Concentrating solar power	0.4	0.5	0.7	1.1	1.6	2.5	3.4
Wind power	94	121	159	198	238	283	318
Biomass	45	46	51	70	74	78	88
Geothermal power	10.4	10.7	11	11.2	11.4	11.7	12
Hydro power	920	950	380	935	960	990	1000

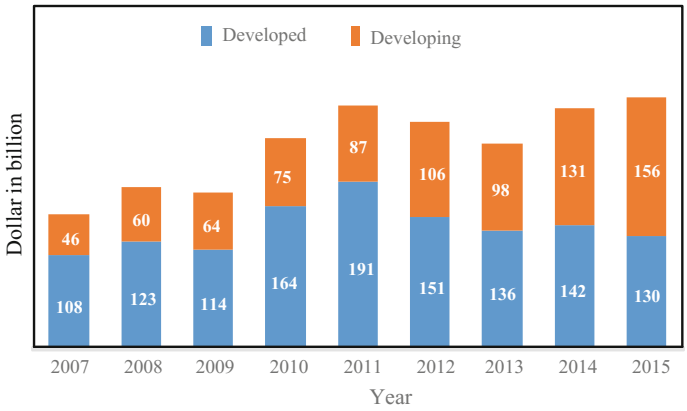

Fig. 2.9 Global new investment in renewable energy (billion dollar) [24]

Total investment in renewable sector increases continuously with some variation. The investment in developing countries also increases every year. In 2015, the investment in developing countries was USD 156 billion, whereas in 2007, it was only USD 46 billion [24]. On the other hand, up to 2011, the investment in developed countries had an increase trend and reached at USD 191 billion. After that, the investment is decreasing continuously. In 2015, the investment was decreased to USD 130 billion. Figure 2.9 shows the global new investment in renewable energy sector. However, solar and wind dominate in the total investment.

2.5 Historical Development of Solar PV Power Plants

A significant growth in solar PV power occurs all over the world in recent decades. Due to its versatility and advances in solar cell technologies, a substantial decline in the installation cost of solar PV power plants has been observed. About 80% of solar cell cost has been reduced in recent decades [25]. Because of huge cost reduction, it reduces the need for subsidies and helps to compete with other power generation systems. As a result, the number of PV power plants is continuously increasing every year in the world.

In recent years, the solar photovoltaic power plants have been gaining significant attention and show a dramatic growth in its cumulative installations. Figure 2.10 shows the cumulative installed capacity of solar PV power [23]. Till now, developed countries generate significant amount of total solar power generation. Day by day, solar PV power is getting popular in developing countries.

Figure 2.11 shows solar-generated electricity in leading countries from 2000 to 2013. Germany is the leading country for the generation of electricity from solar PV. Every year, in total, 30,000 GWh electricity has been generated from solar PV

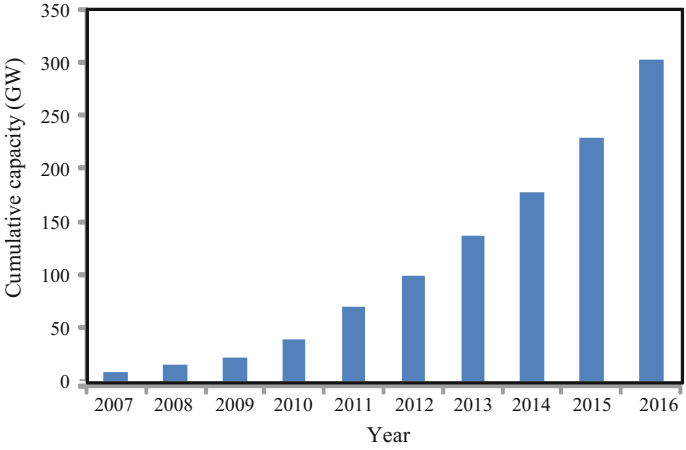

Fig. 2.10 Installed PV capacity worldwide [23]

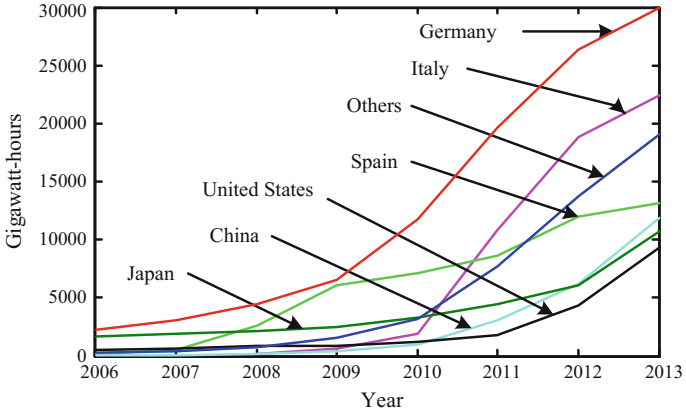

Fig. 2.11 Solar-generated electricity in leading countries [3]

systems, which accounts almost 24% of total global generation [3]. In 2013, Italy also generated significant amount of electricity from solar PV, which was the second largest contributor of global solar PV power and accounts for 18%. At the same time, Spain, China, Japan, US and France generated 10.5, 9.5, 8.6, 7.5 and 3.7% of the global generation, respectively.

Hi-Ren Scenario roadmap reported that future solar PV capacity will see a dramatic change. By 2030, the total cumulative installed capacity will be 1722 GW [26]. The report also shows that by 2050, solar PV sector will share about 16% of the world total power generation. It is expected that by 2050, the total installed capacity of solar PV system will reach at 4674 GW [26]. At present, Europe is the largest market of solar PV system. But, by 2030, China will be the leading country

Table 2.2 Solar PV power in different regions by 2030 and 2050 (GW) [26]

Year	US	EU	China	India	Africa	Middle east	Others	World
2030	246	192	634	142	85	94	329	1722
2050	599	229	1738	575	169	268	1096	4674

Table 2.3 Successful large scale PV plants by ABB [27]

Country	Location	Capacity (MW_p)	Structure	Year of installation
Italy	La Sugarella	24.2	Tracker	2010
Spain	Leon	13.3	Tracker	2010
Italy	Sicilia	6	Fixed	2011
India	Rajasthan	5	Fixed	2011
Italy	Puglia	5	Tracker	2011
Bulgaria	Poveda	50	Fixed	2012
USA	Nevada	24.8	Tracker	2012
Thailand	Lopburi	55	Fixed	2013
USA	Arizona	146	Fixed	2013

for generation of electricity from solar PV power plants and will share 36.84% of total global solar PV power. At the same time, US will be the second leading country for solar PV power plant installation, which will account for 14.3%, followed by EU (11.2%). The prediction shows that China and US will hold their position in future. The total installed capacity will be reached at 4674 GW in 2050. A significant change will be observed in India in solar PV power generation. By 2050, India will share about 12.3% of total global solar PV power which will be the third largest in the solar PV market. Similarly, Africa, Middle East and other developing countries will generate large amount of power from solar PV power plants. The future solar PV capacities are tabulated in Table 2.2 [26].

There are many companies that develop the components of large scale solar PV plants. ASEA Brown Boveri (ABB), Fuji Electric and Siemens are the main leading companies in the world. Currently, a large number of solar PV plants are in operation. Some successful projects installed by ABB are listed in Table 2.3.

2.6 Solar PV Modules in Solar PV Power Plant

The solar photovoltaic means producing electricity from sunlight. A PV cell consists of a positive semiconductor layer and a negative semiconductor layer [6]. When photon of sunlight is absorbed by semiconductor layer, electrons form negative layer are released. If an external circuit is used to interconnect these two layers, a current is established in it. PV cell technology can be categorized into three groups: (i) first generation, (ii) second generation and (iii) third generation.

Crystalline silicon (c-Si) cells are the first generation cells and thin film cells are the second generation cells. Concentrated PV, dye-sensitized cells (DSC) and organic cells are third generation solar cells. Third generation solar cells are not commercially available. First and second generation solar cells mainly dominate in solar cell market. Currently, c-Si cell technology dominates about 85% of the total PV market share [28–30]. It has two types, e.g., mono crystalline (Mono-c-Si) and multi crystalline (Multi-c-Si) cells. Both types are based on silicon wafer. A large silicon crystal ingot is sliced in a process to make mono-c-Si wafer. Multi-c-Si is fabricated over a large area and plasma processing is used to absorb larger light. Multi-c-Si is not as efficient as mono-c-Si.

On the other hand, thin film cells are made of a thin film deposition of a semiconductor on low cost substrate. One of the advantages of thin film technology is that it is cheaper than the crystalline silicon. But, the commercial efficiency is still lower which varies from 7.1 to 11.2%, hence it requires larger area than that of crystalline silicon [2]. There are mainly four types of thin film cell technologies, e.g., amorphous silicon (a-Si) cell, amorphous and micromorph silicon multi-junction (a-Si/µc-Si), copper-indium-[gallium]-[di]-sulfide (CI[G]S), and cadmium telluride (CdTe) [2]. Because of lower efficiency, solar PV plants based on thin film modules require larger space compared to plants based on c-Si modules. It is predicted that the commercial efficiency will achieve to 16% by 2020. It is surveyed that the life time of all types of solar cell is about 25 years. Performance of different types solar PV technologies are shown in Table 2.4.

The production of solar PV modules is increasing day by day. It was about 4028 MW in 2007 and increased to 39,987 MW in 2013. China dominates the production of PV modules. In 2010, China shared 53% of total market. The production capacity of PV modules is continuously increased. In 2013, Chinese PV module shared 64% of the global generation. Annual solar photovoltaic's module production by different countries is shown in Figs. 2.12 and 2.13.

The market price of PV modules is decreasing day by day due to the technical advancement of solar PV technologies. In 2009, the price of high efficiency c-Si was USD 2.45 per watt whereas in 2012, it was only USD 1.94 [31]. The price of Japanese c-Si decreased from USD 1.98 in 2010 to USD 1.22 per watt in 2012. Market price of PV module in Europe is tabulated in Table 2.5.

Table 2.4 Performance of commercial solar PV technologies [2]

PV technology		Efficiency (%)			Area/kW (m^2/kW)
		Module	Lab	Commercial	
c-Si	Mono-c-Si	13–19	24.7	22	7
	Multi-c-Si	11–15	–	20.3	8
TF	a-Si	4–8	10.4	7.1	15
	a-Si/µc-Si	7–9	13.2	10	12
	CI[G]S	7–12	20.3	12.1	10
	CdTe	10–11	16.5	11.2	10

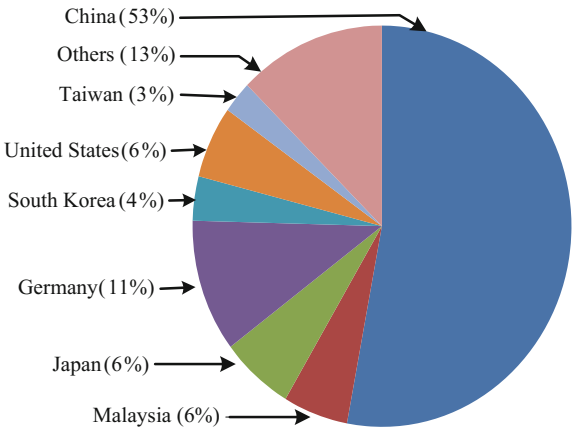

Fig. 2.12 Annual solar photovoltaics' module production in 2010 by different countries [3]

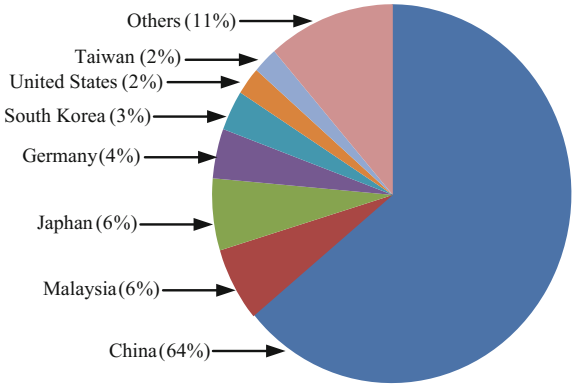

Fig. 2.13 Annual solar photovoltaics' module production in 2013 by different countries [3]

Table 2.5 Market price of PV module in Europe (USD/Watt) [31]

Year	2009	2010	2011	2012
High efficiency c-Si	2.45	2.21	2.00	1.94
Japanese/western c-Si	1.98	1.66	1.22	1.22
Chinese major c-Si	1.51	1.45	1.39	1.24
Emerging economies c-Si	1.45	1.43	1.02	1.02
High efficiency thin-film	1.26	1.27	0.93	0.93

2.7 Inverters in Solar PV Power Plant

Solar PV cell actually generate DC voltage which is variable in magnitude. This variable magnitude DC voltage requires converting into fixed magnitude AC voltage before supplying to the grid. That's why; a power electronic circuit called inverter is commonly used. In addition, to extract maximum power from PV array,

maximum power point tracker (MPPT) is also necessary [32–36]. Inverter can be classified based on the number of power stages such as single stage inverter, dual stage inverter and multi stage inverter [37–39]. In single stage inverter system, the inverter performs both inversion and MPPT operation. In dual stage inverter system, the DC-DC converter section performs the MPPT operation and DC-AC converter section performs the inversion. In large scale PV plant, a high value of stray capacitance exists which creates dangerous leakage current. This leakage current may affect system efficiency and output power quality. To overcome these problems, high frequency isolation transformer based multi-stage inverter is commonly used. In multistage inverter, DC power from PV array is first converted to high frequency AC and then passed through a high frequency transformer. After high frequency transformer, the high frequency power is converted to DC and line frequency AC through rectifier and inverter, respectively. Central and string inverters are two most commonly used inverter topologies especially for large scale solar applications [5]. In centralized PV inverter technology, a large number of solar PV modules are connected in series known as string to meet the voltage requirements. To obtain larger AC power, multiple numbers of strings are connected in parallel to an inverter (DC-AC) circuit. Both single stage and double stage topologies can be implemented in this inverter system. For large scale solar PV plant, central inverter topology is normally used. A centralized inverter system is shown in Fig. 2.14.

In DC-DC converter based inverter, many stings of PV modules are used and each string is connected with an individual DC-DC converter as shown in Fig. 2.15. The output of all DC-DC converters delivers power into a DC link. The common DC link voltage performs the input of the inverter circuit (DC-AC) and then the output of inverter is fed into the utility grid. The efficiency of these technologies is lower due to much more losses in DC-DC converter which also increases the component cost that makes system costlier. Only multistage topology is used in this converter.

There are many vendors who supply a sort of inverters for various power rating. ABB offers PVS 800 version inverter for power range 100–1000 kW. Central inverter is used in these types of inverter. Some specifications for a few PVS 800 inverters are tabulated in Table 2.6.

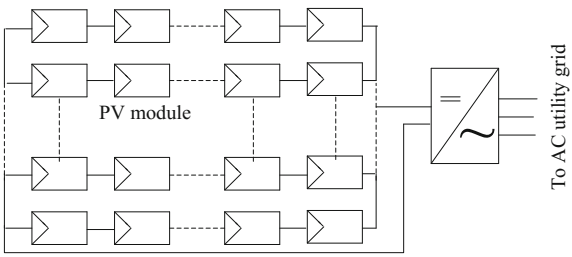

Fig. 2.14 A centralized inverter topology [39]

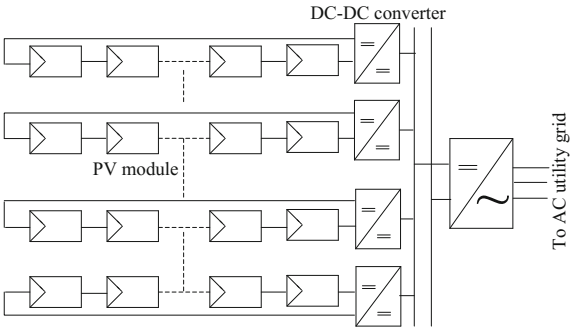

Fig. 2.15 A string inverter topology with DC-DC converter [39]

ABB also provides the ultra utility scale central inverter range from 700 to 1400 kW. It can operate under wide range of operating conditions. High speed MPPT leads it to obtain maximum efficiency. Ultra-1400-TL is the largest power inverter among ABB's inverter product with efficiency up to 98.7%. Some technical data are listed in Table 2.7.

Siemens is another leading inverter supplier in the PV market. Siemens offers central inverters SIVERT PVS 600 series with the power capacity range 500–2520 kW for medium and large scale solar PV plants. The maximum efficiency of these types of inverter is 98.7%. They provide five years' warranty as standard. These types of inverters are operated according to the master slave principle. In this concept, PVS inverters are integrated in an inverter station having a rotating master. It connects or disconnects the inverter subunit depending on the solar irradiance. Some technical data of SIVERT PVS 600 series central inverter is depicted in Table 2.8.

Fuji Electric offers a sort of inverters known as power conditioning systems (PCSs). Some are outdoor self-standing type PCS (PVI1000-3/1000 and PVI750-3/750) and some are indoor self standing type PCS (PVI500-3/500). Some specifications of Fuji PCSs are depicted in Table 2.9.

2.7.1 Substations in Solar PV Power Plant

Substation includes all the electrical components connected in between inverter output and medium voltage utility grid. Step-up power transformer, switchgear, monitoring system, and metering are basic elements of solar PV substations. Both power and distribution transformers are used in substation. Power transformer steps up the inverter output voltage to medium voltage level whereas distribution transformer is required to meet internal power demand. Transformer for solar PV

Table 2.6 Specifications of ABB's PVS 800 central inverters [40]

Type Code	Features	PVS 800-57-0500 kW-A	PVS 800-57-0630 kW-B	PVS 800-57-0875 kW-B	PVS 800-57-1000 kW-C
Input DC	Maximum input power	600 kWp	756 kWp	1050 kWp	1200 kWp
	DC voltage range	450–825 V	525–825 V	525–825 V	600–850 V
	Maximum DC voltage	1000 V	1000 V	1100 V	1100 V
	Maximum DC current	1145 A	1230 A	1710 V	1710 V
Output AC	Nominal AC output power	500 kW	630 kW	875 kW	1000 kW
	Maximum AC output power	500 kW	700 kW	1050 kW	1200 V
	Nominal AC current	965 A	1040 A	1445 A	1445 A
	Nominal output voltage	300 V	350 V	350 V	400 V
	Output frequency	50/60 Hz	50/60 Hz	50/60 Hz	50/60 Hz
	Harmonic distortion (Current)	<3%	<3%	<3%	<3%
	Maximum Efficiency	98.6%	98.6%	98.7%	98.8%

Table 2.7 Specification of Ultra utility scale central inverters [40]

Type code	Features	Ultra-700-TL	Ultra-1050.0-TL	Ultra-1400-TL
Input DC	MPPT DC voltage range at P_{acr} and V_{acr}	585–850 V, 750 kW 645–850 V, 780 kW	585–850 V, 1050 kW 645–850 V, 1170 kW	585–850 V, 1400 kW 645–850 V, 1560 kW
	Maximum DC voltage	1000 V	1000 V	1000 V
	Maximum DC current	1388 A	2082 A	2776 V
	Number of MPPT multi-master	2	3	4
Output AC	Nominal AC output power	780 kW	1170 kW	1560 kW
	Maximum AC output power	780 kVA	1170 kVA	1560 kVA
	Nominal AC current	650 A	975 A	1300 A
	Nominal output voltage	690 V	690 V	690 V
	Output frequency	50/60 Hz	50/60 Hz	50/60 Hz
	Harmonic distortion (Current)	<3%	<3%	<3%
	Maximum Efficiency	98.7%	98.6%	98.7%

Table 2.8 Specification of inverters SINVERT PVS 600 [41]

Type code	Features	PVS 600	PVS 1200	PVS 1800	PVS 2400
Input DC	Rated input power	613 kWp	1226 kWp	1839 kWp	12,452 kWp
	DC voltage range	570–820 V	570–820 V	570–820 V	570–820 V
	Number of DC inputs	3	6	9	12
	Maximum DC current	1104 A	2208 A	3212 V	4416 V
Output AC	Rated output power	600 kW	1200 kW	1800 kW	2400 kW
	Nominal AC current	936 A	1872 A	2808 A	3744 A
	Nominal output voltage	370 V	370 V	370 V	370 V
	Output frequency	50/60 Hz	50/60 Hz	50/60 Hz	50/60 Hz
	Maximum Efficiency	98.7%	98.7%	98.7%	98.7%

plant is specially designed to reduce size, weight and losses. There are many vendors, e.g., ABB, Fuji Electric and Siemens manufactures various transformers for solar PV plants. ABB supplies both liquid-filled and dry type transformers. They are designed so that transformers become compact, reliable and high efficient. Siemens also offers a special transformer, e.g., GEAFOL cast-resin for solar PV applications. However, there are varieties types of switchgear and protection system

Table 2.9 Specification of some PCSs supplied by Fuji Electric [42]

Type code	Features	PVI1000-3/1000	PVI750-3/750	PVI500-3/500
Input DC	DC voltage MPPT range	460–950 V	320–750 V	320–700 V
	DC voltage range	1000 V	750 V	750 V
Output AC	Rated output power	1000 kW	750 kW	500 kW
	Rated AC current	2138 A	2165 A	1444 A
	Rated output voltage	270 V	200 V	200 V
	Output frequency	50/60 Hz	50/60 Hz	50/60 Hz
	Maximum Efficiency	98.5%	97.8%	97.7%
	Output current distortion factor	<5%	<5%	<5%
Step-up transformer	Capacity	1000 kVA	750 kVA	500 kVA
	Number of phase	Three-phase	Three-phase	Three-phase
	Cooling system	Oil immersed self cooling	Oil immersed self cooling	Oil immersed self cooling

used to provide disconnection, isolation, earthing and protection during maintenance and in case of fault conditions. Up to 33 kV, SF_6 and vacuum circuit breakers are normally used. For over-current protection, string fuse or miniature circuit breakers are normally used. Different types of transformer protection systems are used such as Buchholz relay, pressure relieve device, over temperature protection, and oil level monitoring. All switchgear should be recognized by relevant international electro technical commission standards and national codes. ABB provides different range of medium voltage switchgear including air insulated and gas insulated switchgear [40]. A high level of reliability and personnel safety are ensured by a sealed string with constant atmospheric conditions.

ABB offers megawatt station PVS 800 which includes two inverters, transformer, switchgear, monitoring system and DC connection from solar array. Its capacity varies from 1 to 1.25 MW. Some technical specifications of megawatt stations PVS 800 are tabulated in Table 2.10. In addition, ABB provides inverter station PVS 800 with capability of 1.25–2 MW. For both PVS 800 MWS and PVS 800-IS, central inverter topology is commonly used to convert DC to AC voltage for medium voltage station. The schematic diagram of an inverter station PVS 800-IS is given in Fig. 2.16.

Auxiliary transformer can be used in case of unavailability of external energy supply. Some technical data of inverter stations PVS 800-IS are tabulated in Table 2.11.

Table 2.10 Specification of ABB's megawatt stations PVS 800-MWS [40]

Type code	Features	PVS 800-MWS-1000 kW-20 1 MW	PVS 800-MWS-1250 kW-20 1.25 MW
Input DC	Maximum input power	2 × 600 kW	2 × 760 kW
	Dc voltage range	450–825 V	525–825 V
	Maximum DC voltage	1000 V	1000 V
	Maximum DC current	2 × 1145 A	2 × 1145 A
	Number of MPP trackers	2	2
Output AC	Nominal AC output power	1000 kW	1250 kW
	Nominal AC current	28.9 A	36.1 A
	Nominal output voltage	20 kV	20 kV
	Output frequency	50/60 Hz	50/60 Hz
	Harmonic distortion (Current)	<3%	<3%
	Maximum Efficiency	98.7%	98.6%
	Inverter type (2 × ABB central inverter)	PVS 800-57-0500 kW-A	PVS 800-57-0630 kW-B
	Transformer type	ABB Vacuum cast coil dry type	

Due to the demand of the society, ABB and other vendors are trying to develop high power devices for large scale solar PV power plants. Recently ABB has developed multi-megawatt system PVS 980 MWS whose capacity varies from 3.6 to 4.6 MW. The electrical connection diagram of PVS 980 MWS is shown in Fig. 2.17.

2.7.2 Monitoring Systems in Solar PV Power Plant

A monitoring system offers the details information on systems performance, measurement of voltage, current and power. It also provides information for identifying the different types of faults and control mechanism depending on the weather condition and plant performance. In addition, monitoring system offers clear instruction on how to conduct and analyze the measurement and how to determine

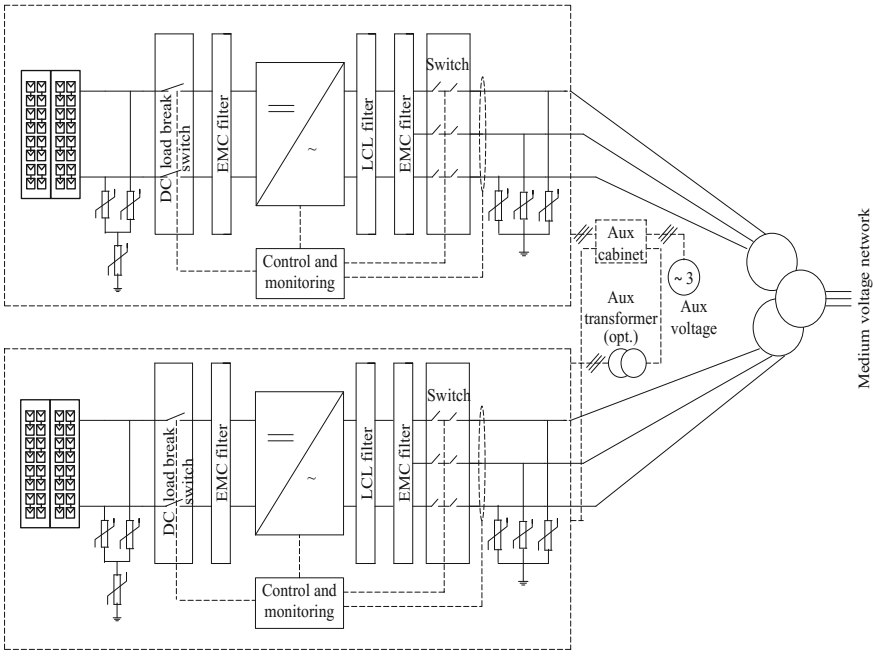

Fig. 2.16 ABB Inverter station design and power network connection [40]

Table 2.11 Specification of ABB's inverter stations PVS 800-IS [40]

Type code	Features	PVS 800-IS-1750 kW-B 1.75 MW	PVS 800-IS-2000 kW-C 2 MW
Input DC	Maximum input power	2 × 1050 kW	2 × 1200 kW
	Dc voltage range	525–825 V	600–850 V
	Maximum DC voltage	1100 V	1100 V
	Maximum DC current	2 × 1710 A	2 × 1710 A
	Number of MPP trackers	2	2
Output AC	Nominal AC output power	2 × 875 kW	2 × 1000 kW
	Maximum AC output power	2 × 1050 kW	2 × 1200 kW
	Nominal AC current	2 × 1445 A	2 × 1445 A
	Nominal output voltage	350	350
	Output frequency	50/60 Hz	50/60 Hz
	Harmonic distortion (Current)	<3%	<3%
	Maximum Efficiency	98.7%	98.6%

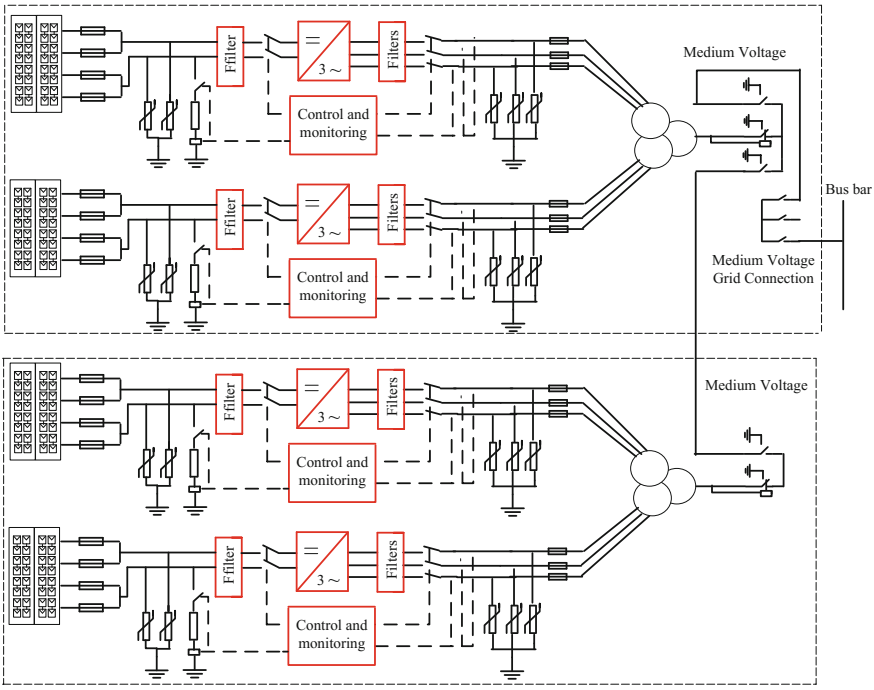

Fig. 2.17 ABB megawatt station design and grid connection [40]

whether the system is performing as expected. A schematic diagram of a monitoring system is shown in Fig. 2.18.

The measurement of DC and AC voltage, current and power in a PV power plant are done by different types of sensors and transducers, e.g., the Hall Effect transducer LEM LV25-P is used to sense the DC and AC voltages [43]. The transducers LA 305-S and LF305-S are used to measure DC and AC current, respectively. Different types of conditioning circuits are used to regulate the points of the data acquisition condition. Sometimes, wire sensor network is also used in PV power plant such as; a wireless sensor network (WSN) is used to record the atmospheric conditions and power generation related to inverters. A weather station is also installed for recording rain index, wind speed and direction, pressure and temperature of plant environment. The weather station also includes the wireless remote sensor incorporated into a computer. To visualize the plant information especially weather condition, Cumulus software is commonly used. The synchronization system synchronizes all subsystems and maintains a universal time reference with high precision for all wireless measurement. A robust communication network is required for real time monitoring system to ensure the reliability and continuity of the plant. A supervisory control and data acquisition (SCADA) system is used for real-time monitoring of the status of the data acquisition equipment and the collected measurements which is called PV–on time system.

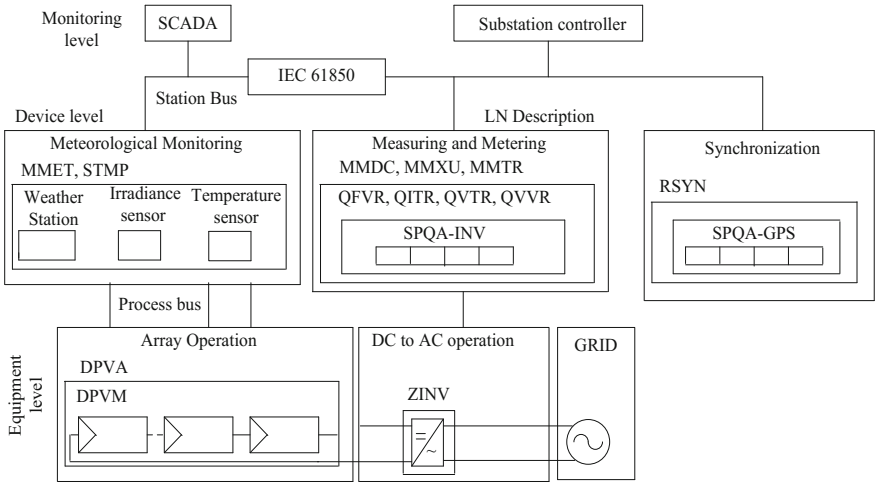

Fig. 2.18 A schematic diagram of a monitoring system [43]

ABB offers different types monitoring and communication devices, e.g., data logger VSN 700, Wi-Fi logger cards VSN 300 and the remote monitor PVI-AEC-EVO [40]. Data logger VSN 700 records data and events from inverters, energy meters, weather stations, and from other devices. It provides an internet gateway to transmit data securely and reliably for monitoring and recording data. There are three types of data loggers VSN 700, e.g., VSN 700-01, VSN 700-03, and VSN 700-05 data loggers. Among them, only VSN 700-05 is used for utility PV operation and SCADA integration. On the other hand, logger card VSN 300 is an advance monitoring and controlling system. Both remote and local monitoring system is achieved by the Wi-Fi logger card VSN 300. In addition, it offers the ability to use a standard web browser to access inverter data. The remote monitor PVI-AEC-EVO is also used for remote monitoring for PV plant with all ABB devices. The modular and expendable architecture is combined with din rail mountain system that makes PVI-AEC-EVO suitable for any kind of installation in PV plant. A proprietary Aurora Protocol is used for communication between remote monitor PVI-AEC-EVO and ABB devices. To store data for back up, 2 gigabyte secure digital card flush memory is used. In case of absent of local area network Ethernet, global system for mobile communication (GSM) can be used in remote monitoring PVI-AEC-EVO system. A block diagram of remote monitor PVI-AEC-EVO is shown Fig. 2.19.

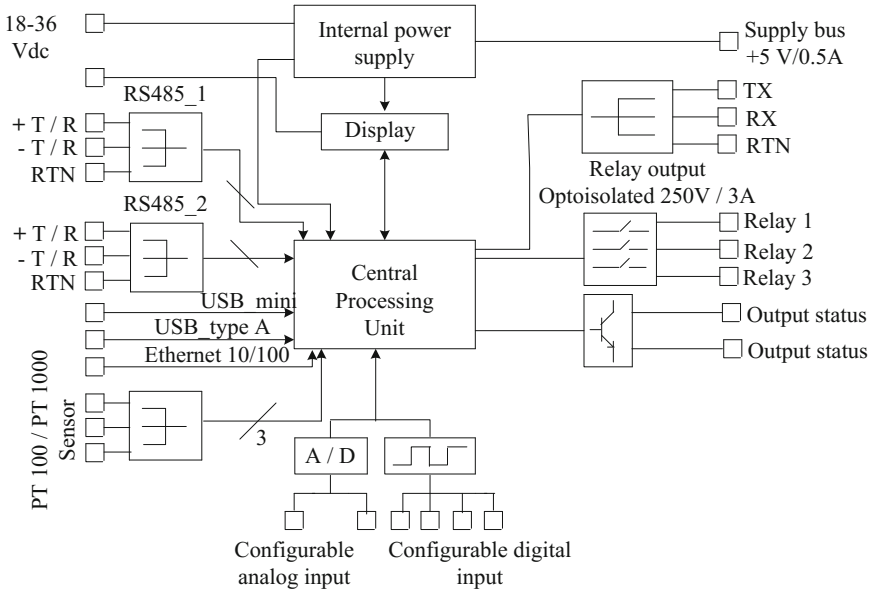

Fig. 2.19 Block diagram of the remote monitor PVI-AEC-EVO [40]

2.8 Mounting and Tracking Systems in Solar PV Power Plant

PV modules are usually set on a structure with supports and tracking systems. The tracking system helps to keep their orientation in the right direction. In fixed position system, PV modules are tilted away from horizontal plane with an optimum angle to get maximum annual irradiance. The fixed system requires less installation and maintenance cost than that of tracking based system. Tracking system can extract 30–50% additional energy depending on geographical location and day time [44]. Tracking system consumes a small amount of power to derive their motors. There are two types of tracking systems, e.g., single axis and double axis [45]. Double axis tracking system is more efficient than single axis tracking system as double axis tracking system can control both orientation and tilt angle [46, 47]. On the other hand, single axis tracking system can control either orientation or tilt angle. Single axis tracking system is cheaper and higher reliability than double axis tracker [46, 47]. However, tracking system is normally used for c-Si modules because of its higher efficiency. A number of vendors have been manufacturing controllers especially for tracking systems. Siemens provides tracking system based on controller SIMATIC S7-1200. Both single axis and double axis tracker systems can be controlled by this controller. KIPP & ZONEN offers two types of tracking systems or sun trackers, e.g., sun tracker SOLYS 2 and sun tracker 2AP [48]. Global positioning system is integrated in SOLYS 2 that locates the position of the sun. The sun tracker SOLYS 2 does not need any additional

Table 2.12 Specifications of trackers SOLYS 2 and 2AP [48]

Specifications	SOLYS 2	2AP
Pointing accuracy	<0.10° passive tracker <0.02° active tracking	<0.10° passive tracker <0.02° active tracking
Torque	>23 Nm (when sun tracking)	>40 Nm (when sun tracking)
Angular velocity	Up to 5°/s	Up to 1.8°/s
Payload (balance)	20 kg	65 kg
Supply voltage	18–30 VDC 90–264 VAC, 50/60 Hz	24 VDC 115–230 VAC, 50/60 Hz
Power sun tracker	21 W	50 W
Operating temperature	−20–+50 °C (DC power) −40–+50 °C (AC power)	0–+50 °C −20–+50 °C (DC power) (cold cover) −50–+50 °C (AC power) (Cold and heater cover)
Dimension (W × D × H)	50 × 34 × 38 cm	42 × 26 × 38 cm

computer or software. The sun tracker 2AP is normally used in the worst environment, e.g., high speed wind and snow fall. Pre- programmed movement of tracker can be achieved by software Win2AP. Some specifications of sun trackers SOLYS 2 and 2AP are given in Table 2.12.

2.9 Site Selection Criteria for Solar PV Power Plant

Site selection is one of the vital works for installing a solar PV plant which is a multi objectives problem. Many factors have to be considered during the selection of a site. These factors are classified into two classes, e.g., analysis criteria and exclusion criteria [49]. The selection criteria include solar radiation, availability of land, accessibility, and distance from the utility grid. Since the output of PV cells mostly depends on solar radiation, the availability of proper solar irradiance is an important factor to select a site. Land should be low price to reduce investment. There should be kept a possibility for further extension. Similarly, the exclusive criteria include local climate, module soling and topography of site, geotechnical issue. Climate affects the construction of plant. Flood, high speed wind and snow may affect the support of PV plant [25]. In addition, the efficiency of PV cell declines with increase of temperature. Efficient output is obtained from solar cells if they operate in between 25 and 45 °C [49]. In case of topography of site, south facing slope is preferable for projects in the northern hemisphere. Geotechnical factors, e.g., resistivity of soil, ground water level, soil pH and load bearing properties also affects during selection of site [46]. Software geographic information system (GIS) is mostly used to select a site for solar PV plant [50, 51]. This software helps to manage, analyse and to visualize the geographical data. There are many vendors, e.g., MapInfo, Autodesk, Bentley systems, Eredas Imagine, ESRI, IGIS, who dominates in supplying software GIS [49].

Table 2.13 Capital expenditure for installing a 100 MW solar PV plant [52]

Category	Description	USD/ W_{DC}	Total cost (USD)
Hard cost	Module	0.75	75,000,000
	Inverter	0.218	21,800,000
	BOS	0.1	10,000,000
Soft cost	Mounting Racks	0.083	8,300,000
	Civil works	0.06	6,000,000
	EC contract	0.0336	3,363,889
	Contingency	0.0673	6,727,778
	Pre-operative cost	0.0202	2,018,333
	Financial cost	0.0135	1,345,556
Total		1.3456	134,555,556

2.9.1 Capital Expenditure

Capital expenditure is an important issue for the installation of solar PV power plants. Although, the cost of PV module decreases substantially, still per unit cost is higher than the average cost of generation of electricity. The capital cost varies region to region because of many reasons, e.g., labor cost, the subsidy, taxes and incentives. The capital cost can be classified into two major categories, e.g., hard cost and soft cost. Hard cost is the main cost of a PV plant accounting for about 79.3% [52]. It includes the cost of solar module, inverter and balancing of system (BOS). The cost of BOS covers the cost of transformer, monitoring system, switchgear, cabling. The PV module cost is the main cost that covers about 55.7% which is much larger than cost of inverter and BOS accounting for 16.2 and 7.4%, respectively. On the other hand, soft cost includes the cost of civil cost, engineering and commissioning (EC), mounting rocks and project management. The share of soft cost is about 20.7%. In [52], the capital cost of a 100 MW solar PV plant in Ghana was analyzed. The costs of PV module, inverter and BOS have been assumed as USD 0.75 per W_{DC}, USD 0.75 per W_{DC} and USD 0.75 per W_{DC}, respectively. Table 2.13 shows the capital expenditure of a typical 100 MW solar PV plant. However, different software, e.g., RET Screen modeling software is used to analyze cost of PV power plant [53].

2.10 Conclusion

This chapter demonstrates the prospect and technical advancement of large scale solar PV power plants. Solar PV power plant is dramatically getting a platform of generating electricity all over the world. Till now, it is facing problems due to its

higher installed cost. But, due to technical advancement, cost reduction and renewable energy policy, solar PV power will be the one of the leading source of electricity in near future. International collaboration on research and development can enhance the success of large scale solar PV plant by reducing module cost, sharing planning, financing and grid integration. Governments can make policy to ensure a stable, predictable financial environment as well as to cut the soft cost. This system not only mitigates the carbon emission or improves the energy security but also plays an important factor in economy of a country by reducing dependence on imported fuel. In addition, solar PV plant becomes a field of investment and job sector. This analysis can play a part of research in the field of large scale solar PV plant as a de-carbonized energy system.

References

1. Islam MR, Islam MR, Beg MRA (2008) Renewable energy resources and technologies practice in Bangladesh. Renew Sustain Energy Rev 12:299–343
2. Islam MR, Rahman F, Xu W (2016) Introduction, advances in solar photovoltaic power plant. Springer-Verlag, Berlin Heidelberg, pp 1–6
3. Earth Policy Institute, "Climate, energy and transportation," Available online: http://www.earth-policy.org. Accessed 13 Oct 2016
4. Islam MR, Guo YG, Zhu JG (2014) A review of offshore wind turbine nacelle: technical challenges, and research and development trends. Renew Sustain Energy Rev 33:161–176
5. Islam MR, Guo YG, Zhu JG (2014) Power converters for medium voltage networks. Springer-Verlag, Berlin Heidelberg, pp 1–49
6. International Renewable Energy Agency (IRENA). Renewable energy target setting. Available at: http://www.irena.org. Accessed 10 Oct 2016
7. Gujrat Power Corporation LTD, Gujrat Solar Park. Available at: https://gpcl.gujarat.gov.in. Accessed: 05 Aug 2017
8. Physicians for social responsibility, Coal-fired power plants: understanding the health cost of a dirty energy sources. Available at: www.psr.org. Accessed 13 Mar 2017
9. International energy agency, coal. Available at: www.iea.org. Accessed 14 July 2017
10. World coal association, coal world, why is coal important? Available at: www.info.com. Accessed 14 July 2017
11. Independent statistic and analysis, International Energy Outlook 2016, US energy information administration. Available at: www.eia.gov. Accessed 04 July 2017
12. British Petroleum, BP statistical review of world energy June 2016. Available at: www.bp.com. Accesed 03 July 2017
13. Nuclear Energy Institute, world statistics, nuclear energy around the world. Available at: www.nei.org. Accessed 02 July 2017
14. Xu Y, Hu J, Hao H, Wang D, Zhang H (2017) Current and future emissions of primary pollutants from coal fired power plants in Shaanxi China. Sci Total Environ 595:505–514
15. Arora JV, Cai Y, Jones A (2016) The national and international impacts of coal-to-gas switching in China power sector. Energy Econ 60:416–426
16. Rachel's Democracy and Health News (2008) Green coal. Available at: www.precaution.org. Accessed 04 May 2017
17. Cohen BL (1990) T nuclear energy option, environmental problems with coal, oil, and gas: Penum press, Available at: www.phyast.pitt.edu. Accessed 30 Mar 2017

18. Xu X, Meng B, Zhang C, Feng X, Gu C, Guo J, Bishop K, Xu Z, Zhang S, Qiu G (2016) The impact of coal fired power plants on inorganic mercury and methyl-mercury distribution in rice (Oryza sativa L.). Environ Pollut 223:11–18
19. Public Service Commission of Wisconsin, Environmental impacts of power plants. Available online: Accessed 02 June 2017
20. Paschoa AS (2004) Interactions energy/environment-Environmental effects of nuclear power generation: Encyclopedia of life support systems
21. El-Hinnawi HE Review of the environmental impact of nuclear energy. IAEA BULLETIN 20 (2):32–42. Available at: https://www.iaea.org. Accessed 15 May 2017
22. Kivi R (2017) How does nuclear energy affect the environment? Sciencing. Available at: www.sciencing.com. Accessed 20 May 2017
23. Renewable Energy Policy Network for the 21st Century. The first decade: 2004–2014. Available at: http://www.ren21.net. Accessed 15 Oct 2016
24. FS-UNEP collaborating centre for climate and sustainable energy finance, Frankfurt School. Global trends in renewable energy investment 2016. Available at: http://www.fs-unep-centre.org. Accessed 21 Sept 2016
25. International Finance Corporation (IFC), World Bank Group. Utility- scale solar photovoltaic power plants. A project developer's guide. Available at: http://www.ifc.org. Accessed 15 Sept 2016
26. International Energy Agency (IEA). Technological roadmap: solar photovoltaic energy. Available at: http://www.iea.org. Accessed 16 Sept 2016
27. ASEA Brown Boveri. State of the art and experiences on efficient technologies for solar applications. Available at: http://www.new.abb.com. Accessed 11 Oct 2016
28. Energy technology systems analysis programme (2013) Solar photovoltaics: technology brief. International Renewable Energy Agency, Abu Dhabi
29. Li CT, Hsieh F, Yan S et al (2014) Crystalline silicon solar cells with thin silicon passivation film deposited prior to phosphorous diffusion. Int J Photoenergy 2014(491475): 1–8
30. Opwis K, Gutmann JS, Alonso ARL (2016) Preparation of a textile-based dye-sensitized solar cell. Int J Photoenergy 3796074:1–11
31. Renewable energy technologies: cost analysis series. International Renewable Energy Agency (2012):1(4/5). Available online: Accessed 02 June 2017
32. Lyden S, Haque ME (2015) Maximum power point tracking techniques for photovoltaic systems: a comprehensive review and comparative analysis. Renew Sustain Energy Rev 52:1504–1518
33. Liu L, Meng X, Liu C (2016) A review of maximum power point tracking methods of PV power system at uniform and partial shading. Renew Sustain Energy Rev 53:1500–1507
34. Rizzo SA, Scelba G (2015) ANN based MPPT method for rapidly variable shading conditions. Appl Energy 145:124–132
35. Verma D, Nema S, Shandilya AM, Dash SK (2014) Maximum power point tracking (MPPT) techniques: recapitulation in solar photovoltaic systems. Renew Sustain Energy Rev 54:1018–1034
36. Hlaili M, Mechergui H (2016) Comparison of different MPPT algorithms with a proposed one using a power estimator for grid connected PV systems. Int J Photoenergy 1728398:1–10
37. Carrasco JM, Franquelo LG, Bialasiewicz JT et al (2006) Power electronic systems for the grid integration of renewable energy sources: a survey. IEEE Trans Industr Electron 53 (4):1002–1016
38. Casaro MM, Martins DC (2010) Electronic processing of the photovoltaic solar energy in grid connected systems. Controley Automacao 21(2):159–172
39. Martins DC (2013) Analysis of a three-phase grid-connected PV power system using a modified dual-stage inverter. ISRN Renew Energy 2013(406312):1–18
40. ASEA Brown Boveri. ABB solar inverters for photovoltaic systems helping you get more energy out of every day. Available at: http://www.libray.e.abb.com. Accessed 11 Sept 2016
41. Siemens. SINVERT PVS 600 series central inverters and components for photovoltaic power plants. Available at: http://www.siemens.com. Accessed 11 Sept 2016

42. Fuji Electric. Large-scale photovoltaic power generation systems. Available at: http://www.fujielectric.com. Accessed 11 Sept 2016
43. Garcia IMM, Garcia EJP, Lopez VP et al (2016) Real-time monitoring system for a utility-scale photovoltaic power plant. Sensors 16(770):01–25
44. Eke R, Senturk A (2012) Performance comparison of a double-axis sun tracking versus fixed PV system. Sol Energy 86:2665–2672
45. Yao Y, Hu Y, Gao S et al (2014) A multipurpose dual axis solar tracker with two tracking strategies. Renew Energy 72:88–98
46. Rahimi M, Banybayat M, Tagheie Y et al (2015) An insight on advantage of hybrid sun-wind-tracking over sun-tracking PV system. Energy Convers Manag 105:294–302
47. Khader MMA, Badran OO, Abdallah S (2008) Evaluating multi-axes sun-tracking system at different modes of operation in Jordan. Renew Sustain Energy Rev 12:864–873
48. KIPP & ZONEN. Sun trackers for solar-tracking and PC-based positioning operations. Available at: http://www.kippzonen.com. Accessed 11 Sept 2016
49. Khan G, Rathi S (2014) Optimal site selection for solar PV power plant in an Indian state using geographical information system (GIS). Int J Emerg Eng Res Technol 2(7):260–266
50. Mondino EB, Fabrizio E, Chiabrando R (2015) Site selection of large ground-mounted photovoltaic plants: a GIS decision support system and an application to Italy. Int J Green Energy 12:515–525
51. Krpan L, Šteko V, Koren Z (2012) Model for selecting locations for construction of solar power plants. Gradevinar 64(9):741–748
52. Aguilar LA (2015) Feasibility study of developing large scale solar PV project in Ghana: an economical analysis. Master's Thesis, Chalmers University of Technology
53. Sarkodie SA, Owusu PA (2016) The potential and economic viability of solar photovoltaic power in Ghana. Energy Sour Part A Recovery, Utilizat Environ Eff 38(5):709–716

Chapter 3
Development of HTS Cable-Based Transmission Systems for Renewables

Jian Xun Jin, Md. Rabiul Islam and Abdul Goffar Khan

3.1 Introduction

With the economic development and growth of society, the power utility industry with an ever increasing global demand for electricity is growing, which requires the increase of capacity, quality, distance and space for electric power transmission systems. Currently, the traditional power cables are made of copper or aluminum having resistance and limited current carrying capacity, leading up to 10% power loss during transmission and also considerable land or space occupied. The annual electricity energy loss during transmission process is more than hundreds billion kWh, this invokes an effective technological option. With an estimated hundred thousand kilometers of underground cables throughout the world, superconducting cables can potentially provide an immense benefit to the utility industry and consumers with advantages to save energy. The use of superconducting cables also has striking economics over conventional above ground and below ground transmission cables, such as near zero environmental impact and higher operating efficiency.

Superconducting cables can offer the advantages of lower loss, higher capacity, lighter weight, and more compact dimensions as compared with the conventional cables, consequently they are leading the innovation in future power systems.

J. X. Jin (✉)
School of Electrical and Information Engineering, Tianjin University, 300072 Tianjin, China
e-mail: jxjin@tju.edu.cn

M. R. Islam · A. G. Khan
Rajshahi University of Engineering & Technology, 6204 Rajshahi, Bangladesh
e-mail: Rabiulbd@hotmail.com

A. G. Khan
e-mail: agmagk@gmail.com

M. R. Islam et al. (eds.), *Renewable Energy and the Environment*, Renewable Energy Sources & Energy Storage, https://doi.org/10.1007/978-981-10-7287-1_3

Superconducting materials and technologies developed to date, especially high temperature superconducting (HTS) materials, have technically made the superconducting power cables and transmissions applicable [1–6].

A comprehensive technical description of the HTS power cables is presented systemically including: (i) HTS cable structure and classification, (ii) HTS characteristics for cables, (iii) HTS cable design, (iv) HTS AC power transmission system, (v) HTS DC power transmission system, (vi) HTS smart grid, and (vii) Current development status of HTS cable systems and application prospect.

3.2 Basic HTS Cable Structure and Classification

The basic structure of HTS cables is shown in Fig. 3.1 as an example, where Fig. 3.1 from inside to outside includes (i) inner support core, (ii) HTS tape layers, (iii) thermal insulation, (iv) electrical insulation, and (v) shield and protection layer in general. Figure 3.1a shows a sample HTS cable [7], meanwhile Fig. 3.2 shows more structural and technical details of HTS cables.

HTS cables can be classified based on various criteria:

(a) By the method of transmission, they are classified as AC cables and DC cables;
(b) By the electrical insulation, they are classified as warm-dielectric (normal temperature) insulation and cold-dielectric (low temperature) insulation;
(c) By the phase connection and structure, they are classified as single phase HTS cable, three-phase parallel axis HTS cable and three-phase coaxial HTS cable;
(d) By the superconducting materials, they are classified as LTS wire cables, HTS first generation 1G Ag clad $(Bi,Pb)_2Sr_2Ca_2Cu_3O_{10+x}$ wire cables, HTS second generation 2G $Y_1Ba_2Cu_3O_{6+x}$ wire cables, and MgB_2 cables; further by the structure of the HTS conductors or layers;
(e) Others include by coolants and cooling methods, etc.

Based on the electrical insulation, for example, HTS cables can be classified into two categories: warm-dielectric (WD) cable and cold-dielectric (CD) cable. The WD HTS cable system can use the conventional electrical insulation which is placed at the outside of thermal insulation. However, it is difficult to reduce the cable volume. The CD HTS cable is a type of liquid nitrogen (LN_2) impregnated cable, where LN_2 on one hand provides electric insulation and in the meantime provides an effective cooling. Basically the CD HTS cable is similar to the normal oil-filled (OF) insulation cable. With this arrangement the required cable volume can be reduced significantly and thus a single cooling pipe can accommodate a three phase CD HTS cable. Additionally, the power capacity is able to be increased. A HTS cable can be one of single-core, 2-core or 3-core structures, and its design has commonly a concentric structure. Figure 3.3 is the summary to classify the HTS cables.

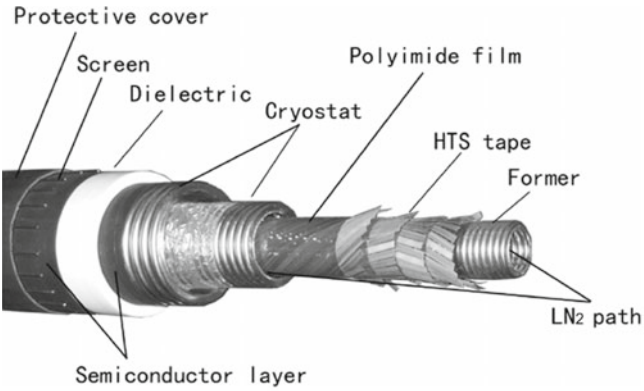

(a) A sample of HTS cables

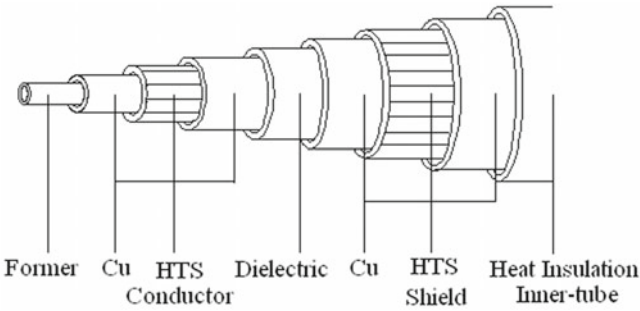

(b) HTS DC cable physical model

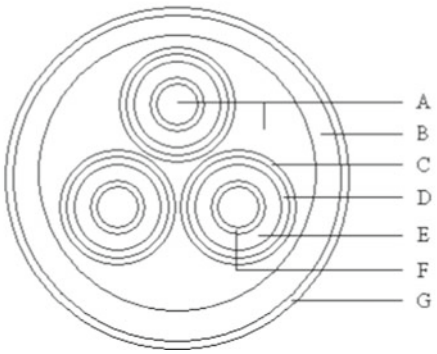

A – Liquid nitrogen path, B – Corrugate pipe cryostat, C – Protection layer, D – HTS shielding layer, E – Electrical insulation, F – HTS conductor layer with former, G – Protection jacket

(c) Multi-core and cold dielectric type cable

Fig. 3.1 Basic HTS cable structure

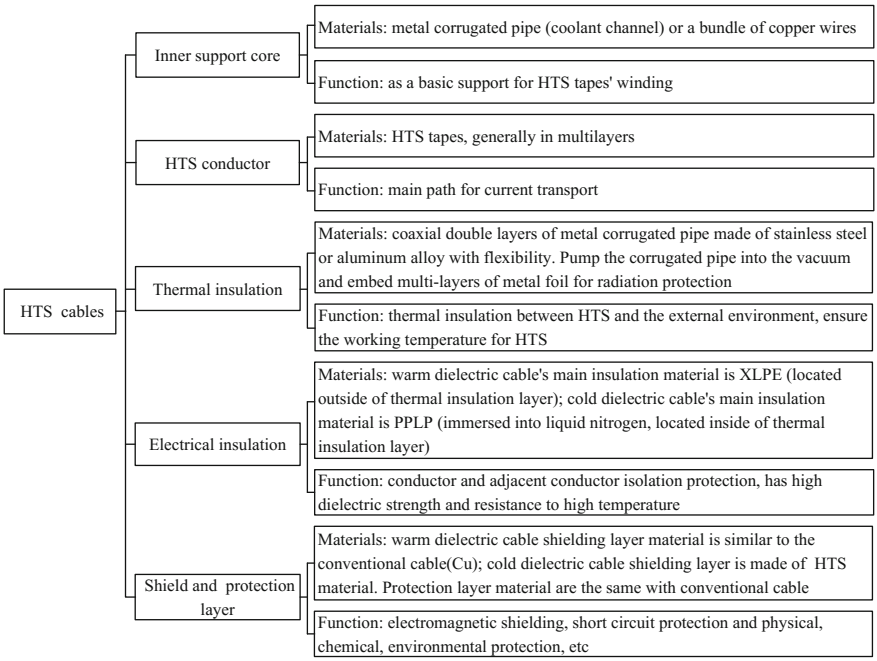

Fig. 3.2 Summary of the basic structures of HTS power cables

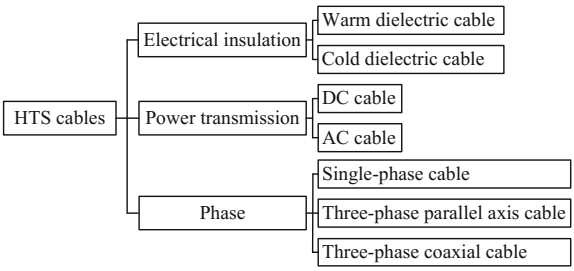

Fig. 3.3 Classifications of HTS cables according to different criteria

3.3 Basic Characteristics and Designs

Electrical power transmission and distribution system using traditional cables incurs large energy losses, up to 10% of total electricity generation in general. To reduce line losses and improve the energy efficiency in modern power systems and future smart grids, HTS materials having very high transport current density and nearly zero resistance are very attractive for designing electrical transmission and distribution cables. To date, both the AC and the DC cables fabricated from HTS tapes have made great progress. A number of in-grid HTS cable demonstrations have laid

a very firm basis for their use in high-capacity, high-efficiency power transmission and distribution in the near future.

The core technology of HTS cables is the conductor design and construction. Because of the conductor characteristics, electrical property, mechanical property and also geometry are different among various cable conductors. The superconducting cable conductor design is more difficult than the conventional one. Combined with the structural characteristics and the basic design method of a superconducting cable conductor, the design process of a HTS cable conductor generally follows: (i) cable structure, (ii) HTS layers, (iii) amount of HTS tapes, and (iv) detailed parameters including self inductance and mutual inductance models to obtain equal current distribution and also voltage drops.

3.3.1 Rated Current

The 1G HTS wire has achieved high critical current density $J_c \sim 10^5$ A/cm^2 at 77 K in self field and with 1 μV/cm criterion, even though the 2G HTS wires come with much better applicable properties, e.g. $J_c \sim 10^6$ A/cm^2. Both 1G and 2G HTS wires now can be commercially produced having high J_c under low applied magnetic fields H with long lengths up to several kilo-meters and mechanical flexibility, which are commonly required for electrical applications. The HTS wires have been verified for use in various electrical applications with various prototype devices produced [1, 2].

The practical J_c of the HTS wire is given by $J_c = I_c/CS_{HTS}$, where CS_{HTS} is the HTS material cross-section. The HTS wire as a conductor has potential to achieve engineering critical current density $J_e = I_c/CS \sim 10^4$ A/cm^2 for self field at 77 K operation, where CS is the HTS conductor total cross-section. The J_e is hundred times higher than that of the traditionally used resistive Cu conductors having $J_{Cu} = 3\times10^2$ A/cm^2 as the limit for normal applications. The J_c can be defined simply using $V = 1$ μV criterion. To decide the HTS cable rated DC current based on the HTS tape critical current, the $d^2V/dI^2 = 0$ criterion can be considered.

The HTS tape's DC *I-V* characteristic is essential to the DC cable application, and can be usually approached by the empirical power-law

$$V = V_0(I_{HTS} / I_0)^n \tag{3.1}$$

where I_{HTS} is the current flowing through the HTS core.
I_0 is a reference current when the voltage is V_0.
n reflects the general shape of the HTS *I-V* curve and the HTS conductor quality.

Value of n varies between 1 to 100 in general, and such as typical values of 20 for 1G and 30 for 2G HTS wires.

The value of n can be calculated by using criterion points $E_{c1} = 0.1$ μV and $E_c = 1$ μV, and the corresponding critical currents I_{c1} and I_c, so n can be described as

$$n = (\log E_c - \log E_{c1})/(\log I_c - \log I_{c1}) \tag{3.2}$$

For DC applications of the metal sheathed composite Bi-2223/Ag HTS wire, i.e. the case of a sinusoidal current frequency $f \to 0$, the current shearing between the HTS core and the metal sheath follows the equation

$$I = I_0(V/V_0)^{1/n} + V/R_s \tag{3.3}$$

where I is the total current of the HTS wire,
R_s is the resistance of the HTS metal sheath.

It can be fitted to the data of the HTS DC characteristic curves to determine the parameters including n value. Using these parameters with a sinusoidal current, the rms value of the resistive voltage can also be calculated. If AC ingredient in a DC system is taken into account, and considering the HTS worked under the critical magnetic field B_{c1}, the flux would penetrate to the superconductor, and produce AC losses. Based on Bean model, when the environment field less than the penetrate field B_p, the AC loss can be expressed as

$$P = [(4\sqrt{2})/3]\mu_0(I/P_e)3P_e f/J_c \tag{3.4}$$

where P_e is the superconductor perimeter, f is the AC current frequency.

The basic HTS DC cable configuration includes: (i) a protection shell, (ii) a thermal shield, (iii) an insulation layer, (iv) a HTS layer, and (v) a cooling pipe. The J_e in the level of 10^4 A/cm^2 at 77 K allows the HTS cable with a very high capability for highly rated transport currents, e.g. this gives 10 kA with cross-section area $S = 2$ cm^2 and filling factor λ ($= S_{HTS}/S_{HTSLayer}$) = 0.5, and with surface field constant $\sim$40 mT/kA. The rated HTS layer current is generally given by

$$I = [1 - k(J_c)]J_c\, S_{HTSLayer}\, \lambda \tag{3.5}$$

where $k(J_c)$ is a coefficient related to (i) self field, (ii) strain, (iii) thermal loss, (iv) process procedure, and (v) structure.

The HTS DC cable can also combine the power transmission with fault current limiting functions. In this case, the required S_{HTS} section is determined by the J_c and I_l—the starting point of the current limiting function, i.e. the HTS quench current; and $S_{HTS} = I_l/J_c$, and $S_{HTSLayer} = I_l/J_e$. In order to effectively limit the current below a maximum value I_m, the minimum cable length L is

$$L = V \cdot S_{HTSlayer}(\rho \cdot I_m)^{-1} = V \times I_l \times (r \times J_e \times I_m)^{-1} \tag{3.6}$$

where V is the system voltage, $\rho(T)$ is the resistivity of the HTS cable during its quenching, I_m is the maximum fault current allowed, and the rated current $I_1 = J_e$ $S_{HTSlayer}$.

3.3.2 Basic Cable Structure

In order to increase the transmission capacity of a HTS cable, the cable conductor layer has a multilayer structure, and the conductive layer is rounded by a certain number of superconducting tapes. For the helical structure conductor layer, to eliminate the axial magnetic field, a conductive layer which between the layers of tape, reverses coiling the tapes in adjacent layer with the equal pitch. To reduce the coupling loss, the skeleton and the conductor layers can round with insulation tape. The schematic view of the 4-layer conductors HTS cable is given in Fig. 3.4. Shielding layers can be added to the cable outside.

3.3.3 Number of HTS Tapes

If the average critical current of superconducting tapes is I_{ca} at operating temperature and self field, the rated current of HTS cable is I_R, and the design margin is m, which is generally larger than 20%, the number of superconducting tapes N on the conductor cross section should satisfy Eq. (3.7) as below [8].

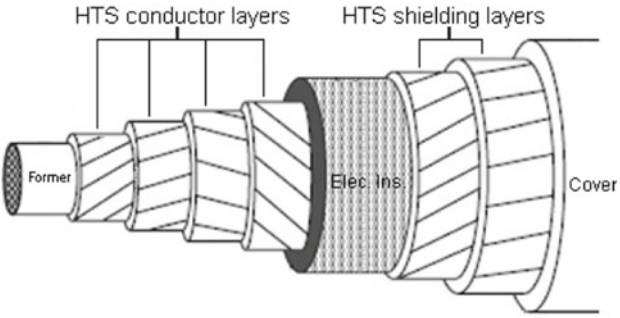

(a) Schematic diagram of a cold dielectric type multilayer structure of a common AC HTS cable

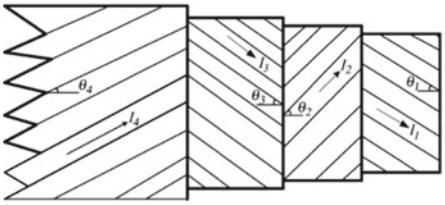

(b) A multilayer structure

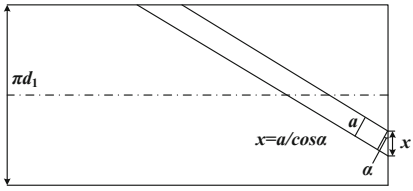

(c) A single tape in the layer

Fig. 3.4 Schematic diagram of a cold dielectric type multilayer structure of a common AC HTS cable

$$N \geq (1+m) \times I_R / I_{ca} \tag{3.7}$$

For AC cable, due to the given rated current in rms, the I_R should be $I_R\sqrt{2}$ instead.

3.3.4 Number of Layers

Figure 3.4 shows the relation among different physical parameters of a HTS cable, here d_1 is the diameter of the support tube including the electrical insulation layer and net, a is the width of the tape, and α is the winding angle. The maximum number n_1 of the tapes wound on the layers is expressed as follows

$$n_1 \leq \pi d_1 \cos \alpha_1 / a \tag{3.8}$$

The base diameter of the second layer is

$$d_2 = d_1 + 2(t_s + t_i) \tag{3.9}$$

where t_s is the thickness of the superconducting tape, t_i is the layer space, including the thickness of insulation film and interspace. If the winding angle of the second layer is α_2, the maximum number n_2 of the tapes of this layer is

$$n_2 \leq \pi d_2 \cos \alpha_2 / a \tag{3.10}$$

According to Eqs. (3.8) and (3.10), when the serial number of layers is larger than 2, Eqs. (3.9) and (3.10) can be modified as follows

$$d_k = d_{k-1} + 2(t_s + t_i) \tag{3.11}$$

$$n_k \leq \pi d_2 \cos \alpha_k / a \quad k = 3, 4 \ldots \tag{3.12}$$

3.3.5 Winding Design Parameters

After the number of HTS tapes and layers are determined, the most important design factor is to ensure that the current in each superconducting tapes is equal to be ideal.

DC superconducting cable conductor design is relatively easier. For AC superconducting cable conductor design, although the resistance is zero in HTS tape, the inductance in each layers should be kept the same in order to obtain the same layer current. The inductance of each layer includes two parts, one is self inductance, and the other is mutual inductance.

The conductor layer is regarded as a tightly wound long solenoid. The self-inductance of the conductor layer can be expressed as follows

$$L_{\mathrm{k}} = \mu_0 \frac{\pi d_{\mathrm{k}}^2}{l_{\mathrm{pk}}^2} + \mu_0 \frac{\ln\left(\frac{D}{d_{\mathrm{k}}}\right)}{2\pi} \tag{3.13}$$

where μ_0 is the vacuum permeability, l_{pk} is the winding intercept determined by winding angle of superconducting tape, D is the inner diameter of the shield layer, and d_{k} is the winding diameter.

The mutual inductance between ith layer and jth layer can be calculated according to Ampere's law. The mutual inductance per unit length can be expressed as follows

$$M_{\mathrm{ij}} = M_{\mathrm{ji}} = \frac{a_{\mathrm{i}}\, a_{\mathrm{j}}\, \mu_0}{l_{\mathrm{pi}} l_{\mathrm{pj}}} \pi d_{\mathrm{i}}^2 + \frac{\mu_0}{2\pi} \ln\left(\frac{D}{d_{\mathrm{j}}}\right) \tag{3.14}$$

where a_{i} and a_{j} are constant, which stand for the winding direction respect to each other, l_{pi} and l_{pj} is the intercept of ith layer and jth, d_{i} and d_{j} is winding diameter of ith and jth layer, respectively.

Based on the above analysis, if each conductor layer is regarded as a circuit branch, multilayer superconducting cable can be expressed as an equivalent circuit consisting of resistance, self inductance and mutual inductance as shown in Fig. 3.5.

The current distribution and voltage drop (e_{i}) in each layer at steady transmission state can be expressed as

$$\begin{bmatrix} e_1 \\ e_2 \\ \vdots \\ e_{\mathrm{n}} \end{bmatrix} = \begin{bmatrix} L_1 + \frac{R_1}{j\omega} & M_{21} & \cdots & M_{\mathrm{n1}} \\ M_{12} & L_2 + \frac{R_2}{j\omega} & \cdots & M_{(\mathrm{n}+1)2} \\ \vdots & \vdots & \ddots & \vdots \\ M_{1\mathrm{n}} & M_{2\mathrm{n}} & \cdots & L_{\mathrm{n}} + \frac{R_{\mathrm{n}}}{j\omega} \end{bmatrix} \cdot \begin{bmatrix} I_1 \\ I_2 \\ \vdots \\ I_{\mathrm{n}} \end{bmatrix} \tag{3.15}$$

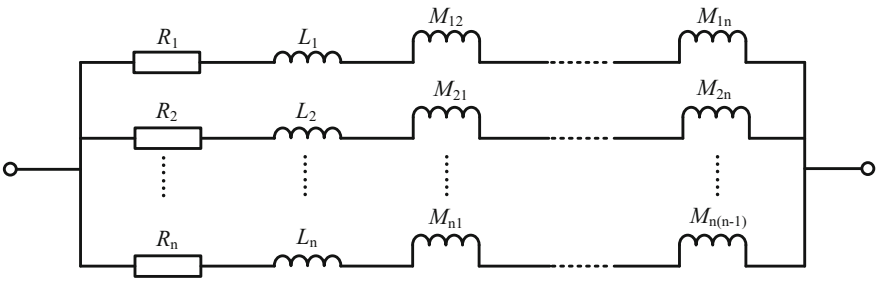

Fig. 3.5 Equivalent circuit of a multilayer HTS cable

where R_n is the resistance of conductor joint, ω is the angular frequency, j is the imaginary unit, I_n is the current in layer n.

In a parallel circuit, the voltage drop in each branch is equal, that is, $e_1 = e_2 = \ldots = e_n$. Therefore, in order to obtain equal current in each branch, the impedance of each branch should be kept equal. The factors affecting impedance of each branch are: (i) self inductance, (ii) mutual inductance, and (iii) joint resistance. After the parameters, including the number of HTS tapes and layers, the diameter of winding and the thickness of insulation, are determined, the only factor affecting the self and mutual inductance of conductor layer is the wound intercept l_p. However, after the winding diameter d is determined, the winding intercept l_p is determined by winding angle α. Therefore, the winding angle α is the key parameter to determine the current distribution in the conductor layers.

3.3.6 AC Losses of a HTS Cable

AC losses of a HTS cable mainly include: (i) hysteresis loss, (ii) eddy current loss, and (iii) coupling loss.

(a) Hysteresis loss. Related to the nature of the superconductivity, power loss will occur whenever there is a change of magnetic field including both applied magnetic field and self field by conductor current. Expression for the total AC loss Q_{tot} includes the transport current loss Q_t plus the magnetization loss Q_m. Basically the model describes an 'infinite' slab fed with a transport current with amplitude I_t, in a parallel applied magnetic field with amplitude B_a and a constant critical current density J_c. The loss for the normalized magnetic field, $\beta = B_a/B_p$, and the normalized transport current, $i = I_t/I_c$, can be formulated. The penetration field for a typical BSCCO/Ag tape with fully coupled filaments is around 10 mT, and in most applications $\beta \gg 1$.

(b) Eddy current loss. Eddy current loss mainly comes from the HTS cable metal support tube, the adiabatic thermostat, and the metal matrix of HTS tapes. (i) Eddy current loss of the metal support tube: Assume that the cable is composed of N layers of conductors, the total magnetic field intensity produced at the support tube is sum of all the layers. The cable support tube eddy current loss is proportional to the radius of the cube and the thickness of support tube, but inversely proportional to the resistivity ρ. (ii) Eddy current loss of the adiabatic thermostat: A diabatic thermostat generally consists of two coaxial metal tubes, and the adiabatic thermostat is vacuum. Because adiabatic tube is outside of the conductor, a magnetic field along the circumferential tangential direction is produced. A closed-loop current in opposite direction is induced near the inner side of the metal tube of the adiabatic thermostat. The power loss of eddy current per unit length of the inner metal tube of the adiabatic thermostat can be calculated. The eddy current loss is inversely proportional to the resistivity, that is the reason why adiabatic use stainless steel ($\rho = 70\ \mu\Omega$),

instead of copper (ρ = 0.21 μΩ) or aluminum (ρ = 0.25 μΩ). (iii) Eddy current loss in substrate of the superconducting tape: The eddy current loss of substrate mainly depends on the structure and winding way of HTS tape. Theoretical analysis and experimental data shows that the eddy current loss of the 1G HTS wire, BSCCO, is small. For a single phase HTS power cable with rated current 2000 A, the eddy current loss of BSCCO can be reduced to 10^{-4}–10^{-3} W/m. For the 2G HTS wire, YBCO, the eddy current loss and hysteresis loss is large than the 1G HTS wire's. Because the size of metal substrate is larger, and the Ni alloy brings in hysteresis loss. Except the affect from the material of support tube and adiabatic thermostat, and the geometric dimension, the following method can reduce the eddy current loss: (i) Use insulated HTS tape; (ii) Don't overlap the uninsulated HTS tapes at the same layer, and ensure the insulation between the conductor layers; and (iii) Use HTS tape with higher I_c, which can reduce the amount used and the eddy current loss of HTS tape.

(c) Coupling loss. Coupling loss happens when coupling currents in the pairs of adjacent HTS tapes, i.e. between HTS tapes or between HTS tapes and metal base. The coupling loss is proportional to the applied field frequency and the square of the applied field amplitude. The coupling loss can be reduced by twisting the HTS tapes to a pitch as small as possible.

3.3.7 Hurdles for Design and Application

On top of the HTS material J_c, hurdles in the HTS cable design do exist to build practical HTS cables and systematically applications. Some issues as examples are summarized as follows:

(a) Critical current. Apart from the HTS intrinsic property, how to design and optimize the structure of the cable is a major effort to maintain a higher I_c.
(b) AC losses. How to design and optimize the cable structure in order to reduce AC losses.
(c) Refrigeration. How to operate in a low cost for a long distance HTS cable line.
(d) Insulation. Apart from electrical insulation, materials and techniques are necessary to be developed to reduce the heat leak between low temperature section and normal temperature section.
(e) Reliability. Operational reliability of superconducting cable, monitoring and protection from fault operation conditions, recovery from over or short circuit current, and system overvoltage.
(f) Uniform distribution of I_c.

Taking the (f) for example, the current distribution in the parallel HTS tapes is determined by the resistance and inductance in general. When the HTS cable in normal state, each the HTS layer has a certain conductor resistance. When the HTS cable in superconducting state, the DC resistance in each HTS layer is zero, which has no influence on the current distribution. Inductance is closely related to

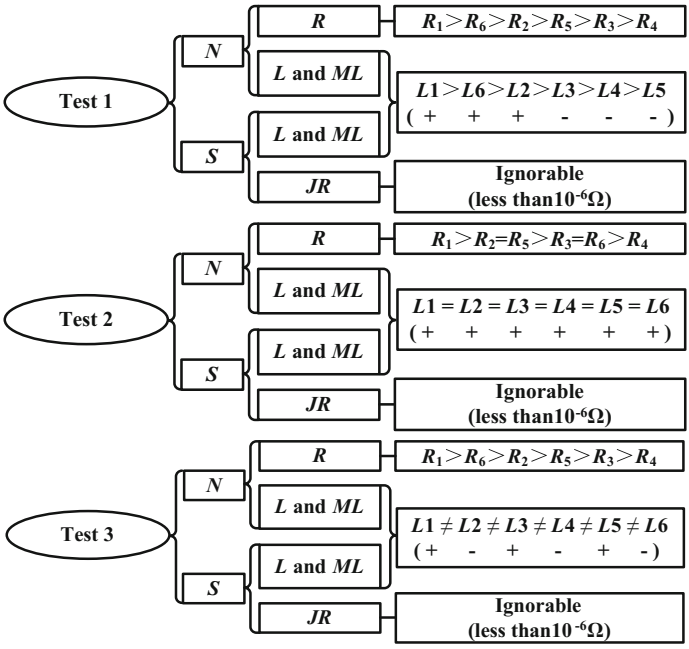

Fig. 3.6 Current distribution among the 6 layers of a multilayer HTS conductor

conductor structure. Generally, for a HTS cable, the larger the winding angle is, the larger the self inductance will be. The mutual inductance is not only related to the winding angle, but also related to the winding direction. Therefore, theoretically, the current distribution is determined only by self inductance and mutual inductance in superconducting state. In order to verify the conclusion, a series experiments were conducted and experimental current distribution results of the HTS samples are shown in Fig. 3.6.

The experimental sample is a 3 m long cable having 6 layers HTS cable, and three different experiments have been made, which is shown in Fig. 3.6. *N* stands for normal state, *S* stands for superconducting state, *R* stands for resistance, *L* stands for inductance, *ML* stands for mutual inductance, and *JR* stands for joint resistance.

In the experiment Test 1, the inductance can be regarded the same among different layers. Theoretically, in superconducting state, the current should be uniformly distributed amongst all the layers. However, the experiment result is $I_6 > I_1 > I_5 > I_2 > I_4 > I_3$, where 1–6 stands for the layer number, i.e. 1st layer is the innermost layer, and the 6th is outmost layer. From the result, it can be found that, the current in the outermost and inner most layer is relatively larger, while the middle layers 3rd and 4th have smaller values. This result disagrees the assumption "the inductance influences the current distribution among different layers in superconducting state".

In the experiment Test 2, the inductance in each layer is different. Theoretical, in superconducting state, the current values in the 1st and 6th layer are smaller than other layers, and the middle layers, such as 4th and 5th layer should have larger values. However, the experiment result of $I_6 > I_5 > I_1 > I_2 > I_3 > I_4$, is almost the same as the Test 1 result. This result disagrees the assumption "the inductance influences the current distribution among different layers in superconducting state" again.

Experiments of Test 1 and Test 2 have excluded the decisive function of inductance in determining the current distribution among conductor layers. The third experiment is made to verify the function of winding direction to determine the current distribution. The conductor number in each layer and winding angle of Test 3 is the same as Test 1, but the conductor winding direction is different to the Test 1. However, the Test 3 result is almost the same as Test 1, which is $I_6 > I_1 > I_5 > I_3 > I_2 > I_4$. From Test 3 result, the "winding direction" can be excluded.

From the above three experiments, although the inductance, winding angle and winding direction are different among the three tests, the same trend occurs in superconducting state. It can be concluded that the current in the outermost or innermost layer is larger than the other layers, i.e. the current in the middle layers is smaller. This phenomenon is the so called proximity effect. Usually, the inductance of each layer is first considered in uniform current distribution among HTS layers. However, experiment results show that the proximity effect is the most important factor affecting the current distribution. A filament conductor carrying AC current and generating magnetic field will affect the current distribution of its neighbor filament conductor, i.e. proximity effect.

Another example is the AC loss reduction. AC loss reduction of HTS power transmission cables is important to apply the HTS cables in power grid applications. Methods to insulate the individual HTS filament core or twist the HTS filaments or tapes, and also other efforts have been presented with applicable techniques developed. Various variable parameters, such as number of layers, lateral J_c distributions of coated conductors, and load rate have influences on the AC losses of the designed cables. For example, a method was proposed to reduce the AC loss by tailoring the normal HTS tape (4 mm wide) with narrow ones (2 mm wide), and the reduction is verified experimentally for both monolayer and multilayer cases.

3.4 Power Transmission Systems with HTS Cables

3.4.1 HTS AC Transmission System

Figure 3.7 shows a typical HTS AC cable system. The three-phase AC cables are normally divided into the three-core parallel-axis cable type and the three-in-one concentric cable type. Each phase in the three-core parallel-axis cable type has an independent HTS layer, an electrical insulating layer, and a HTS shield, and all three phases are installed inside a common warm dielectric layer and a cable sheath.

Three phase HTS layers and their matched electrically insulating layers are coaxially placed in one core, and installed inside a common conventional shield, warm dielectric layer, and cable sheath.

In additional to the existing flux flow loss, the AC cable also suffers from more serious hysteresis loss caused by the AC current and field. If the ratio between the AC current amplitude and the critical current as a factor i, thus the hysteresis loss P_{hys} can be expressed by the following W. Norris's AC loss equation

$$P_{\text{hys}}(t) = S_{\text{HTS}} \times \frac{\mu_0 I_c^2 f}{\pi} \times \left[\begin{array}{l} (1-i)\ln(1-i) + \\ (1+i)\ln(1+i) - i^2 \end{array} \right] \tag{3.16}$$

where f is the operational frequency, typically 50 or 60 Hz.

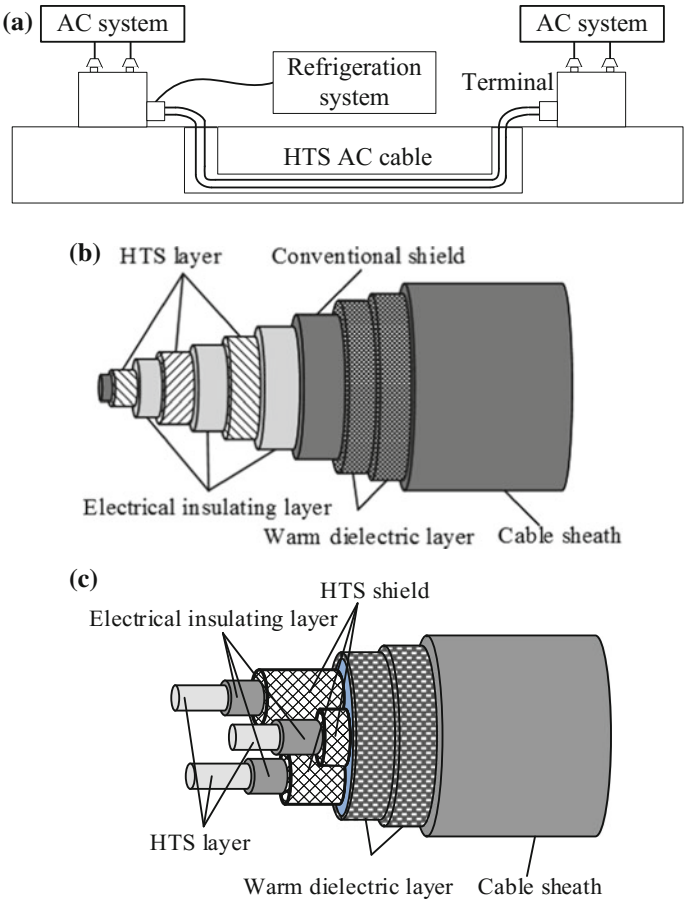

Fig. 3.7 **a** HTS AC cables and system, **b** three-core parallel-axis cable type, **c** three-in-one concentric cable type

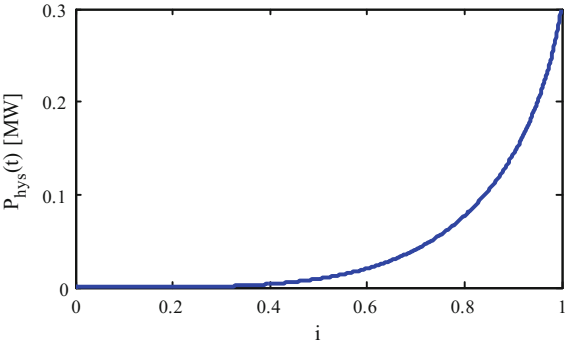

Fig. 3.8 Hysteresis loss curve of a superconducting cable (S_{HTS} = 10 km, f = 50 Hz, I_c = 2 kA)

Figure 3.8 shows a typical hysteresis loss curve of a HTS cable. The hysteresis loss increases exponentially as the ratio i between the AC current amplitude and the critical current becomes larger. In contrast to the flux flow loss data from Ref. [1], the hysteresis loss accounts for the vast majority of the AC loss contributions under AC condition. For instance, when i = 0.5, the hysteresis loss from the Fig. 3.8 is about 9.3 kW, whereas the flux flow loss is only 0.93 μW. Therefore, HTS DC cables are more favored for long-distance high-capacity power transmission in future power systems.

Figures 3.9 and 3.10 show the HTS cable and its demonstration system at Puji substation in Kunming, Yunnan Province, China, which Bi-2223/Ag HTS cable and system's main parameters are: The rated is voltage 35 kV, rated current is 2000 A, cooling power is 2000 W, conductor AC loss is 1.0 W/m, minimum cable bending diameter is less than 3 m, total loss of a single terminal is 108 W, and HTS conductor current uniformity is 81%. The loss of the 33.5 m long demonstration system is much less than conventional cable, saving 110,000 Chinese Yuan each year, and for a 110 kV HTS transmission system can save 3.4 million Chinese Yuan per kilometer each year [7].

After its installation, field tests were carried out including DC resistance, electrical insulation, thermal insulation, AC voltage withstanding, and current carrying capacity tests. For the cable's current carrying capacity test, the three ends of the cables on one side were shorted and powered each phase of the three phases on the other side. The current source was from boost converters that were connected to the grid through voltage-regulating transformers. Six boost converters and four voltage-regulating transformers were used for each phase.

In the test, the initial current was 100 A. Then the current was increased by an increment of 200 A for each step up to 1500 A. The current was held at 1500 A for two hours and then raised to and held at 2000 A for 35 min. At each step, the voltage and the phase angle of each phase were measured. The test results showed that the system was able to carry AC 2000 A without any signs of quench.

Some field test results are summarized in Table 3.1.

On 19th April 2004, the system was activated in the 35 kV live-grid at a transmission current of about 600 A. Since the maximum current of the

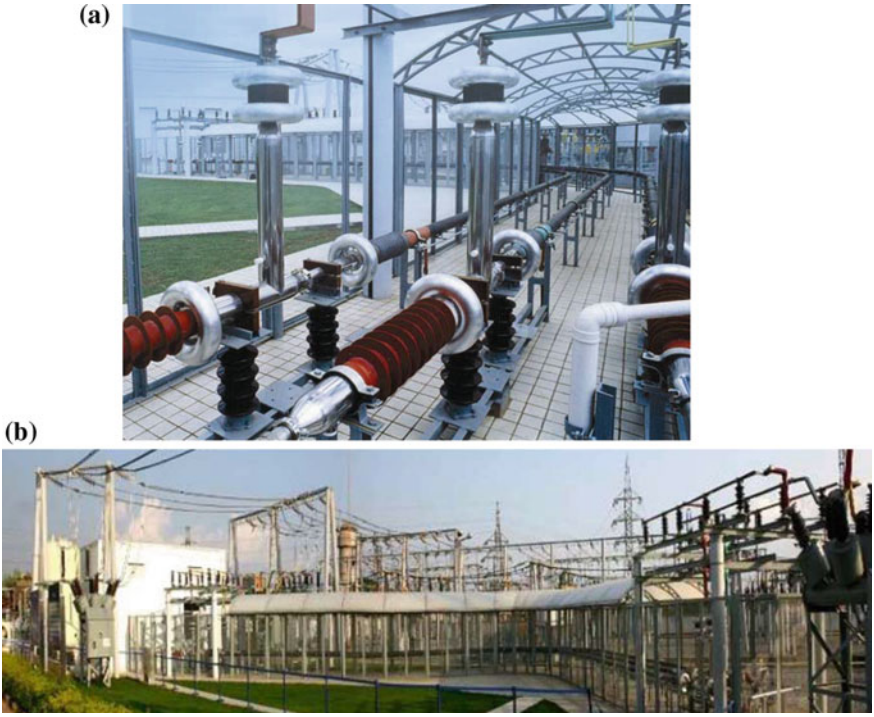

Fig. 3.9 HTS cable site at Puji substation in China

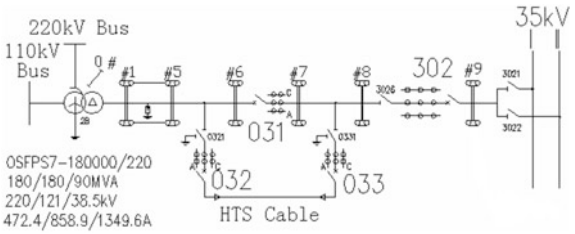

Fig. 3.10 Puji HTS AC transmission scheme

transformer's 35 kV outlet was 1350 A, in order to test the actual operating performance of the cable system at the level close to the rated capacity, the substation central control diverted more power through the bus from another transformer of the station to go through our cables. The total load of the two transformers at the 35 kV outlets was in the range from 1600 to 1700 A during the 90 min test period. The superconducting cable system operated faultlessly in the full load test run. After the full load test, the central of the substation returned 35 kV lines to normal operation mode. The superconducting cable system formally started its live-grid operation.

Operation and maintenance includes issues of: operation instructions and regulations; protection strategy; routine operation; system performance; improvement,

Table 3.1 The field test results

DC resistance (cable + terminations, at ambient temperature before system cooling down)	Phase A 10.6 mΩ Phase B 10.1 mΩ Phase C 10.2 mΩ
DC resistance (cable + terminations, at 74 K of cable conductor after system cooling down)	Phase A 85 μΩ Phase B 84 μΩ Phase C 84 μΩ
DC resistance of a termination (at 77 K, factory)	40 μΩ
Phase shift between I and V (at 50 Hz, 1500 A, 74 K)	Phase A 83.0° Phase B 84.6° Phase C 85.1°
AC loss (at 50 Hz, 1500 A, 74 K)	26–30 W/phase

Table 3.2 The parameters of cables and terminations

Rated voltage	35 kV
Rated current	2 kA
Operation temperature	74–78 K
Operation pressure	40–100 kPa
Operation current	450–950 A
AC loss	<1.0 W/single phase
Heat load of electrical lead	<45 W/kA
Operation thermoelectric of termination electrical lead	70–310 K
Loss of one termination	<120 W

scheduled maintenance and repair. Those did ensure the HTS cable practically operated continuously to ten years.

Tables 3.2 and 3.3 list the key specifications and operation parameters of the cable system [9].

3.4.2 HTS DC Transmission System

AC electric power transmission is currently the main way of power delivery and the most commonly used, which somehow results to HTS DC cable investigation lagged to HTS AC cables. The HTS zero resistance is observed only in DC currents, therefore a HTS DC cable and its DC transmission has better performance than for the AC case in which HTS AC loss exists. With the use of HTS DC cables, the transmission line voltages can be lower than conventional cables when the same power is transmitted because of the greater transmitting current capability.

Table 3.3 The parameters of cryogenic system

Refrigeration power	2000 W/70 K
Temperature of LN_2 entry	74–77 K
Temperature of LN_2 exit	75–78 K
Working pressure of heat exchange cryostat (gauge pressure)	−0.06–0.14 MPa
Flow rate of LN_2 (L/h)	Phase A 800–1000, Phase B/C 400–500
Working pressure of LN_2 pump box (gauge pressure)	0.14 MPa
Temperature of cooling water	15–37 °C
Operation thermoelectric of termination electrical lead	70–310 K
Loss of one termination	<120 W

The AC/DC convertors on the termination of the DC transmission cable become simple and low cost consequently.

HTS cables cannot completely avoid transmission resistive loss in any AC case. Moreover it is necessary to take measures to solve the problems inherited to HTS AC cables, such as protecting against short circuit current and solution to avoid unbalanced AC current in each HTS conductor tape. The HTS DC cable, on the other hand, utilizes the advantages of superconductivity most effectively, and shows no such problems inherited to HTS AC cables.

Power transmission cables based on HTS have been designed to replace the normal conductor cables with advantages of high transport current capability and low resistive loss in AC power transmission systems. It is expected that the new type of HTS cables can also provide similar advantages in DC power transmission, such as much higher current carrying capability, lower energy loss, and more compact systems. With the development of HTS technology, HTS wires have achieved the required performances in LN_2 temperature region, which not only benefit the normal AC transmission systems, but also make DC transmission systems become more practicable, and viable technically and economically. The DC application of HTS cables can be expected to expand greatly in the future, with the advancement of AC/DC converters.

To identify the suitability of HTS cable structures, in addition to the commonly used WD HTS cable, a CD HTS cable system has been developed by SECRI and installed in Baosteel in 2013 as the first CD HTS cable demonstration project in China, consisted of three 50 m CD HTS cables, with rated capacity 120 MVA/rated voltage 35 kV/rated current 2000 A, as shown in Fig. 3.11.

DC electric power transmission has well achieved recently. A ± 1100 kV UHVDC transmission Changji-Guquan line has been started to construct on 11th May 2016 in Xinjiang, China. This is currently the highest voltage level with 1.2×10^4 MW transport capacity. It will be used to send power to central and east China each year about 66 billion kWh, reducing coal transport 30 million 240 thousand tons, 24 thousand tons emission reduction of smoke and dust, 149 thousand tons sulfur dioxide, 157 thousand tons nitrogen oxides.

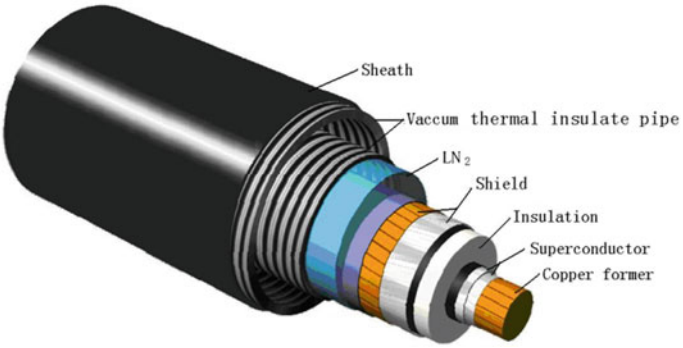

Fig. 3.11 Schematic of a 35 kV 2000 A CD HTS cable

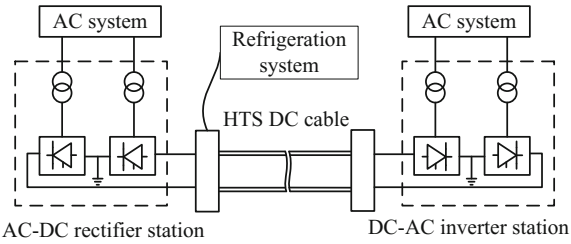

Fig. 3.12 A typical HTS DC cable system

Figure 3.12 shows a typical HTS DC cable system, while Fig. 3.13 shows typical HTS DC cable structures. The typical HTS DC cable system consists mainly of an AC/DC rectifier station, DC cable, a DC/AC inverter station, and a refrigeration system. The HTS cables are normally divided into warm-dielectric type and cold-dielectric type. The coaxial components in the warm-dielectric cable from inner to outer are the LN_2 channel, supporting tube, HTS layer, warm dielectric layer, electrical insulation layer and cable sheath, respectively. The coaxial components in a cold-dielectric cable from inner to outer are the LN_2 channel, supporting tube, HTS layer, electrical insulation layer, HTS shield, LN_2 return channel, cold dielectric layer, and cable sheath, respectively.

The total operation losses of a HTS DC cable system mainly include power electronic devices' losses from rectifier and inverter stations, heat leakage loss from the DC cable pipe and flux flow loss from the DC cable itself. According to the *E-J* power law, the flux flow loss $P_{\text{flux}}(t)$ can be expressed by [10]

$$P_{\text{flux}}(t) = S_{\text{HTS}} \times E_{\text{c}} \times \frac{I_{\text{op}}^{n+1}(t)}{I_{\text{c}}^{n}} \tag{3.17}$$

A currently used conventional DC electrical power transmission system is selected for analysis with replacement by a HTS cable as shown in Fig. 3.14. The HTS technology brings a resistance-less cable to the DC power transmission system, as

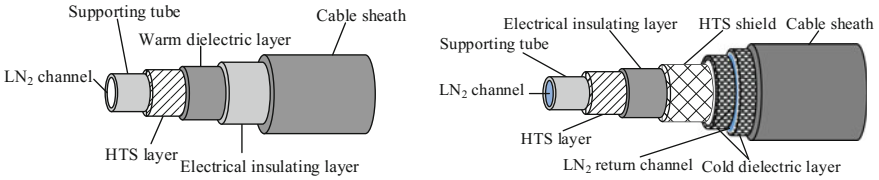

Fig. 3.13 HTS DC cable structures: (left) warm-dielectric type; (right) cold-dielectric type

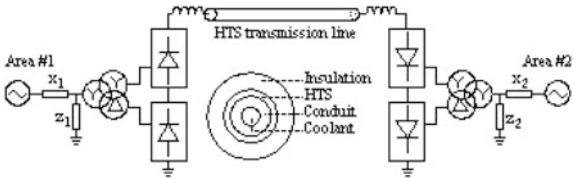

Fig. 3.14 HTS DC electrical power transmission model

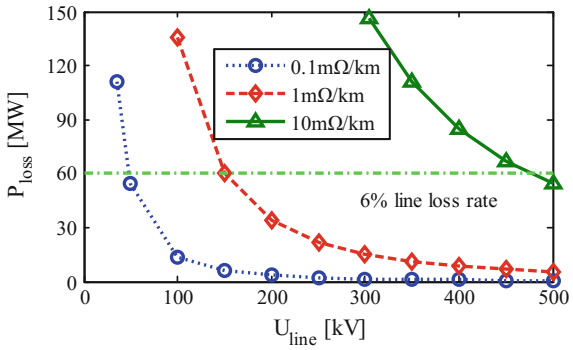

Fig. 3.15 HTS transmission system loss at various voltage levels

well as consequent changes of the conventional DC transmission system. In the CIGRE model, the transmission cable inductance L and capacitance C per unit length are given by $L = \mu_0/\pi\ [1/4 + \ln(D/a)]$ and $C = \pi\varepsilon_0\ [\ln(D/a)]^{-1}$, where a is the conductor radius; D is the distance between cables in the two line system or two times the distance between the cable and ground in the single line system. For analysis, the diameter of the HTS cable is selected to be 1/2–1/4 of the conventional cable (i.e. $\ln D/a = 0.693 - 1.386$).

In a CIGRE standard DC transmission model (1 GW/500 kV/2 kA/1360 km), HTS DC cables with very high J_c and nearly zero resistance have significant potential to replace conventional copper transmission lines [6]. Figure 3.15 shows the HTS transmission system loss at various voltage levels. Considering a typical transmission line loss rate of about 6%, the practically allowable transmission voltage levels are 50 kV, 150 and 500 kV when the equivalent line resistances per km are set as 0.1, 1 and 10 mΩ, respectively. The currently mature HTS DC cable technology can achieve a reduction of 10 or 1% in the total line resistance even

considering the practical thermal leakage from the long-distance cable pipeline. Therefore, it can be definitely expected that high-voltage power transmission levels can be reduced from the present 500–1000 kV to 110–220 kV in future smart girds.

3.4.3 *Specification of HTS Cable System*

Figure 3.16 shows a practically developed CD HTS cable transmission system [9]. HTS AC loss of the cable and termination was tested by measuring the evaporation of LN_2. The thermal loss of the flexible cryostat is about 2 W/m, and the AC loss of the HTS cable under 2000 A current is about 1.2 W/m. The thermal loss of one HTS cable termination is about 200 W.

The 35 kV/2000 A HTS cables system is mainly comprised of 3 cables, 6 terminations and cryogenic system, and Table 3.4 shows its key specifications [9].

Cryogenic system is a mandatory requirement in order to provide the appropriate low temperature operating conditions for HTS cable. Figure 3.17 presents the schematic of refrigeration system for 35 kV/2000 A HTS cables.

The refrigeration system consists of cryocooler, circulation pump, Dewar vessel, heat exchanger, LN_2 tank and vacuum pump. As shown in Fig. 3.17, the subcooled LN_2 that provided from cryogenic system is divided into two equal parts, then parallelly flows through the phase B and C cables, and last return to cryogenic system from phase A cable. During the process, the LN_2 absorbs the energy into the circuit and returns it to the cryogenic refrigeration, which removes the absorbed heat and cools downs to initial temperature. The cryogenic system was designed combination of open and closed refrigeration. The G-M cryocooler was selected as closed refrigeration, and would have long-time running, meanwhile the open

Fig. 3.16 35 kV 2000 A CD HTS cable terminal

Table 3.4 35 kV 2000 A CD HTS cable specifications

Items	Design value
Rated voltage (kV)	35
Rated current (A)	2000
Rated transmission capacity (MVA)	120
Length (m)	50
Total cooling power (W)	4000
Cable inlet temperature (K)	70–73
Cable outlet temperature (K)	73–76
LN_2 flow rate (m^3/h)	2.4

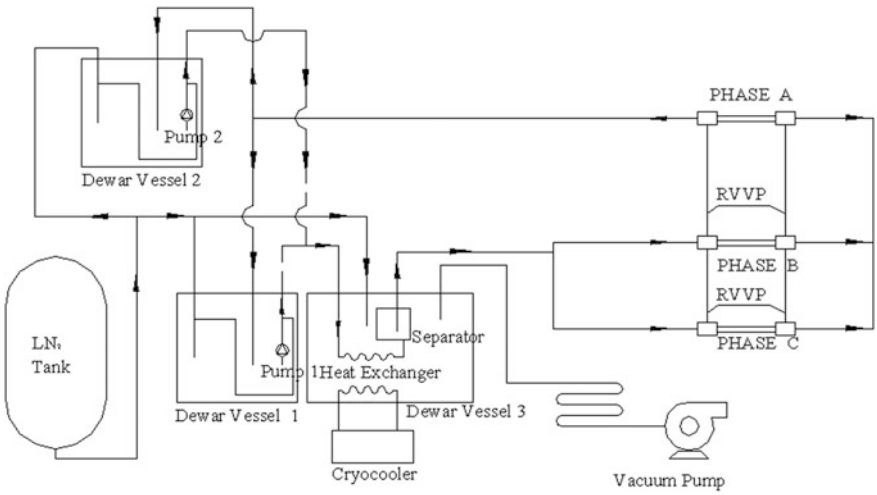

Fig. 3.17 Schematic diagram of the cryogenic system

system was back-up refrigeration and would be used while the G-M cryocooler need maintenance or has a failure. Two circulation pumps are designed in parallel, one is used to circulate the LN_2 flowing along the cables and the other for redundancy.

The heat load of system is the basis for design of cryogenic system. Usually, it comes in two forms: heat leaks from the surroundings and the heat generation in the device. Firstly, the heat generation includes AC loss of HTS cable, and joule loss generated in resistive components in cable system. Secondly, the head leak consists of 4 parts: the current lead loss, the conduction heat loss, the radiation heat loss and residual gas conduction loss.

Current lead loss: the current lead connects the superconducting cable and conventional cable, and operates between the room temperature and LN_2 temperature. The current lead loss can be calculated by an approximate equation.

$$Q_1 = (k(T)A\frac{dT}{dz} + \rho(T)I^2\frac{dTdz}{A})\Big|_{z=l} \tag{3.18}$$

where T and A are the temperature and the cross-section at $z = l$, while $k(T)$ and $\rho(T)$ are the thermal conductivity and electrical resistivity of material at T temperature, and I is the operation current.

Conduction heat loss: the conduction heat loss means that the heat leaks from the surroundings to interface of LN_2 along the solid material. It appears in the termination, cold box, pump box and joint of LN_2 channel in the system.

$$Q_2 = \frac{\lambda A \Delta T}{L} \tag{3.19}$$

where λ is the thermal conductivity of the material, A is the cross-section, ΔT is the temperature difference between room temperature and LN_2 temperature, L is the heat transfer distance.

The HTS cable can only be run under an appropriate low temperature condition, the total loss of the HTS cable system need to be taken away by the circulation of LN_2 which flows through the cable. Therefore, it is important to estimate the pressure drop and associated pump power. The mass flow rate m and pressure drop Δp of the LN_2 are the key parameters for choosing circulation pump. The mass flow can be determined by

$$m = \frac{Q_{tol}}{c(T_o - T_i)} \tag{3.20}$$

where Q_{tol} is the heat load of the cables system, and can be calculated from above in paper, c is specific heat of LN_2, T_{i}, T_{o} are the inlet and outlet temperature of the cable.

$$\Delta p = f\frac{\rho \upsilon^2 L}{2d} \tag{3.21}$$

where f is the friction factor, ρ is the density of LN_2, υ is the velocity of the LN_2, L is the length of the channel, d is the equivalent diameter.

A warm-dielectric type 10 kA/1.5 kV/360 m HTS DC power cable has been installed in Henan province, China, to supply a bus bar for an electrolytic aluminum workshop, and it has been in operation since 2014 [11]. The conductor consists of 5 layers of Bi-2223 HTS tapes and inter-layer insulation tapes. The inner and outer diameters of the cable conductor are 41.0 and 46.2 mm, respectively, representing two concentric corrugated stainless steel tubes. Testing shows that heat loss of the cryogenic envelope is about 1.0 W/m. The cryogenic envelope was fabricated by jointing 8 segments, with each joint between 2 segments constructed by means of a dual vacuum layer insertion, leading to a lower thermal loss of 3 W for each joint. This kind of jointing technique for cryogenic envelopes would be useful in the

development of long distance HTS cables in the future. The termination consists of a main body, a current lead, and a chamber, which are designed and manufactured separately, so that it is easy for transportation and integration. For the 10 kA current lead, the ratio of length to cross section is 318.5 m^{-1}, and the length is 2.9 m, this design can reduce the heat losses from the lead to 43 W/kA. Sub-cooled liquid nitrogen at about 70 K is used to cool the cable system. In order to maintain the temperature difference within 70–77 K, the system's pressure is in the range of 1–5 bar, and then the backward flow of liquid nitrogen is cooled down by a four-cylinder Stirling refrigerator with cooling power of 4 kW at 77 K and about 3.3 kW at 70 K.

After installation shown in Fig. 3.18, the cable was tested. At 77 K, the I_c by 1 μm/cm was up to 12.0 kA. The voltage drop in the cable was changed as the current was increased, and repeated tests showed the same result. 2 h of operation at 10 kA showed that the voltage drop in the cable is stable.

The loss in the 10 kA cable system is calculated by

$$P = C_p \times M \times (T_2 - T_1) \tag{3.22}$$

where C_p is the specific heat of liquid nitrogen, M is the flow rate of liquid nitrogen, and T_1 and T_2 are the inlet and the outlet temperature of the cable system

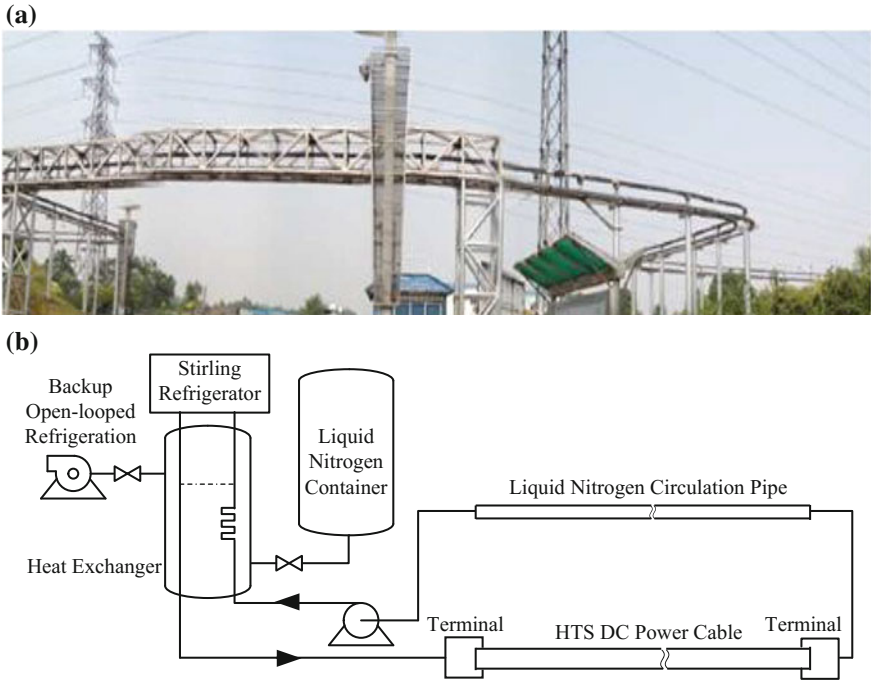

Fig. 3.18 10 kA HTS DC power cable system

respectively. So, through accurate measurement of the cable inlet and outlet temperatures, the cable system loss can be precisely calculated, for example, for T_1 = 66.21 K, T_2 = 69.01 K, and M = 24.24 kg min^{-1}, then P = 2262 W.

Summary of the advanced HTS DC transmission is made as follows. The HTS DC electrical power transmission, as analyzed both for its steady state and dynamic state characteristics, shows that it becomes a suitable technology with great advantages of energy saving, and possibly higher system stability by reducing voltage and therefore lower system cost. More superior features are possible to combine HTS fault current limiting and HTS switching concepts to the technology. Based on the HTS J_e values, which has over 100 times of the normal conductor's value, the high current capacity of HTS cables practically allows up to ten times of the power for the DC transmission systems to be delivered at equivalent voltages, or equivalent power to be delivered at reduced voltages. Losses in a HTS AC cable system can be divided mainly into the following components: HTS conductor AC loss, thermal leak through thermal insulation, induced losses in shield and in thermal insulation. However, for a HTS DC cable system, only the heat leak is left as the predominant loss source. Other losses in the HTS DC transmission systems do exist such as the loss from the power electronic devices. Reduction of energy consumption using this HTS DC cable in normal operation is substantial in networks. HTS cables ideally make $R_L I_d^2 = 0$. This significantly reduces the conventional cable resistive loss, for example, $\sim 8\%$ i.e. 96.4 MW resistive power loss in a system (500 kV/1200 MW/1080 km/0.0155 W/km) with normal cable. Not only the HTS DC cables have the high transport current density and high power delivery capability, but also more significantly is this delivery without resistive loss and could result in lower system voltages. To lower the system voltage levels, means the significant reduction of the network costs, avoiding very expensive costs from high voltage insulation and converter stations.

3.5 Smart Grids with HTS Transmission Systems

3.5.1 Principle of the Low-Voltage Rated DC Power Transmission Network

A sample analysis of a smart grid HTS DC power transmission system. An integrated low-voltage rated HTS DC power system has potential with multifunctions to suit smart grids. Due to the energy intermittency from renewable energy sources, various energy storage systems are utilized to allow increased power capacity and stability. As compared to other energy storage systems, superconducting magnetic energy storage (SMES) system is highlighted for fast speed response and high power density. The continuous SC and SMES developments make it convinced to introduce the SMES into a superconducting DC power transmission system. To have both the high-power high-efficiency power transmission and fast-response power compensation features integrated in one superconducting power system, a

novel low-voltage rated DC power transmission network integrated with DC SCs and SMES devices is proposed and studied. The system fault current limitation and power fluctuation compensation characteristics is then investigated.

The low-voltage rated DC power transmission network is presented in Fig. 3.19. The network is able to take advantage to implement the hybrid energy transfer of the hydrogen and electricity. As an alternative cooling method, the liquid hydrogen (LH_2) transferred can not only be used to provide hydrogen energy for the fuel cells (FCs) such as FC vehicles (FCVs), but also can be used as the refrigeration fluid for cooling the SCs and SMES devices.

For the SC system, a main DC cable is used to transfer the electric power from the utility grid and RESs to local residential and industrial areas, while N branch DC cables are used to distribute the electric power to various power loads. The RESs mainly consist of AC output type distributed generators (DGs) such as wind turbines and hydro turbines, and DC output type DGs such as photovoltaic (PV) cells and FCs. The two types of DGs are connected with the main DC cable through the operations of AC/DC and DC/DC power conversions, respectively.

For the SMES system implanted, it is in one of three types: (i) The first type connected with the utility grid and RESs is used to locally compensate the transient output power fluctuations from the utility grid and RES themselves; (ii) The second type connected with the AC loads, DC loads and electric vehicles (EVs) is used to

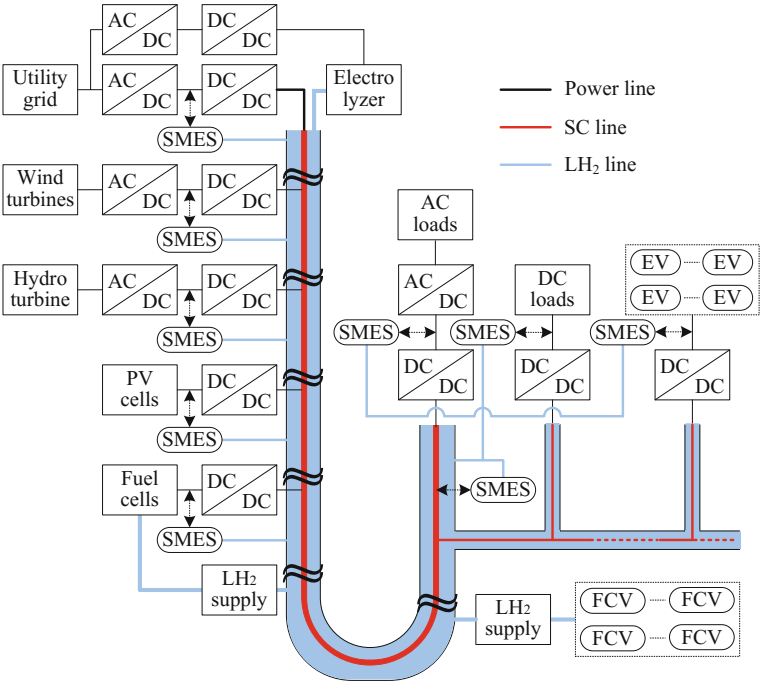

Fig. 3.19 Sketch of the low-voltage rated DC power transmission network

serve as fast-response uninterruptible power supplies (UPSs) for improving the output power quality; (iii) The third type connected with the bus line between the main cable and N branch cables is used to bridge the utility grid and RESs with various distributed loads, and thus to buffer the power fluctuations from the utility grid and RESs and to compensate the load fluctuations from the distributed loads.

To evaluate the performance of the integrated SC and SMES systems under short circuit and power fluctuation conditions, the SC model system includes one 200 V/100 kA/20 MW main cable and five 200 V/20 kA/4 MW branch cables. The third type SMES model system includes one 0.06 H/15.5 kA/7.2 MJ coil assembly and one bridge-type chopper assembly. The coil assembly has twenty 1.2 H/775 A/360 kJ solenoidal units in parallel. Each unit is connected to the bus line between the main cable and five branch cables through one bridge-type chopper unit. To suit such a high current capacity, a solenoidal coil with step-shaped cross-sectional shape can be introduced and designed.

3.5.2 System Circuit Modelling

The simulation model is built with the Matlab/Simulink software, as shown in Fig. 3.20. A controllable voltage source (CVS) is used to simulate the electric power generated by various ESSs. Six PI section line blocks and their series-connected lossy resistance modules are used to simulate one 200 V/100 kA/20 MW main cable and five 200 V/20 kA/4 MW branch cables. Four 200 V/20 kA/4 MW resistive loads from Load 1 to Load 4 are used to simulate the distributed loads located in the terminals from the branch cable 1 to branch cable 4. Three 200 V/10 kA/2 MW

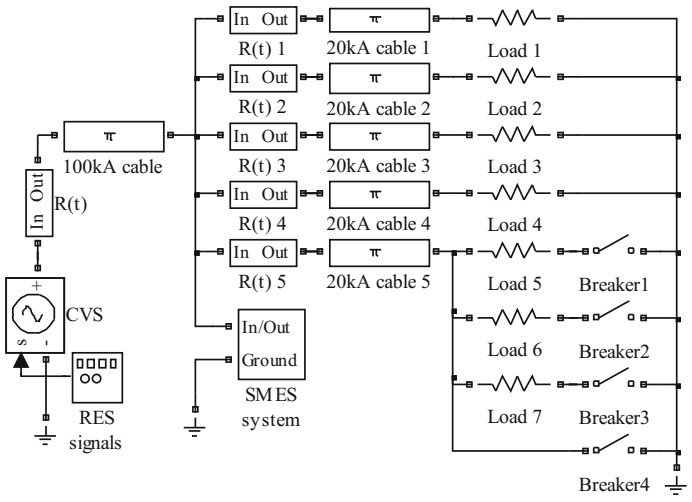

Fig. 3.20 Simulation model in the Matlab/Simulink

resistive loads from Load 5 to Load 7 are used to simulate the distributed loads located in the terminal of the branch cable 5. The SMES system is connected to the bus line between the main cable and branch cables to compensate the real-time power fluctuations.

3.5.3 Fault Current Limitation by SC

To evaluate the fault current limitation characteristic of the superconducting cable, an additional breaker 4 is used to simulate a short-circuit fault in the branch cable 5. In the simulations, the cable inductance and cable capacitance per unit length are set as 2 mH/km and 8.6 pF/km, respectively. The total lengths of the main cable and each branch cable are set as 10 and 3 km, respectively.

Figure 3.21 shows the simulated result of fault current $I_{fault}(t)$ through the branch cable 5. If the FCL function is not applied, $I_{fault}(t)$ increases rapidly to about 50 kA at 1.86 s and continues up to about 105 kA at 6 s. In the case of the FCL function is applied, the exponential growth in the superconducting resistance $R(t)$ can limit the fault current effectively. Figure 3.22 shows the load current $I_{load}(t)$ through the branch cable 1.

3.5.4 Power Fluctuation Compensations by SMES

Three 200 V/ 10 kA/2 MW resistive loads from Load 5 to Load 7 are connected or disconnected to the cable terminal by controlling the three series-connected breakers from Breaker 1 to Breaker 3. Three operation states of the connected resistive loads are consequently achieved: (i) When one of the three breakers closes, the connected resistive load is operated in a power swell state; (ii) When two of the three breakers close, the connected resistive loads are operated in a rated power state; (iii) When all the three breakers close, the connected resistive loads are operated in a power sag state.

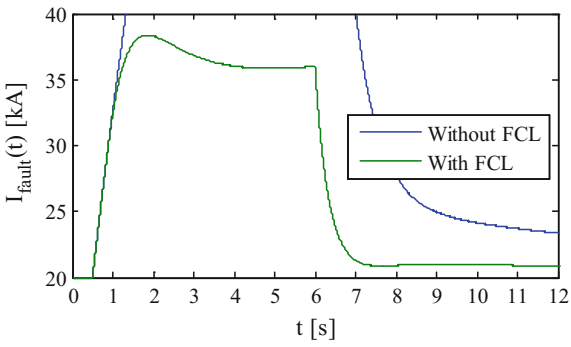

Fig. 3.21 Fault current $I_{fault}(t)$ during a short-circuit fault

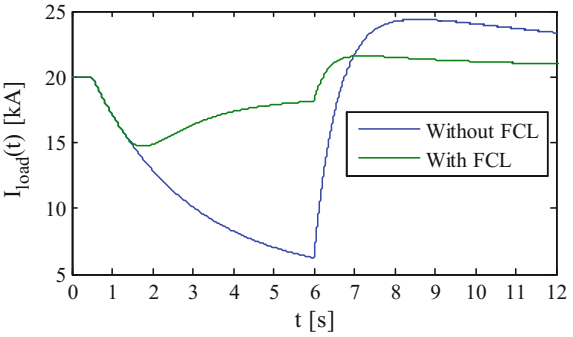

Fig. 3.22 Load current $I_{load}(t)$ during a short-circuit fault

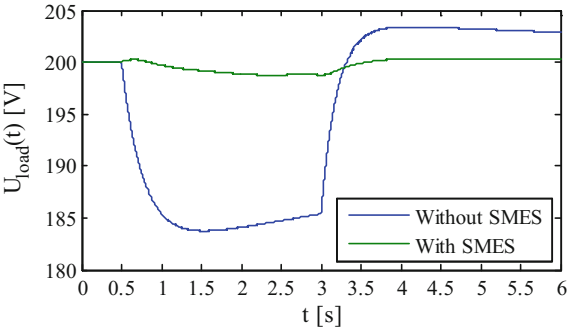

Fig. 3.23 Load voltage $U_{load}(t)$ during a power sag period

Figure 3.23 shows the simulated load voltage $U_{load}(t)$ during the power sag period from 0.5 to 3 s. If the SMES system is not applied, the load voltage $U_{load}(t)$ will decrease rapidly to about 183.8 V at 1.5 s and then increase gradually. At the time t = 3 s when two of the three breakers close, $U_{load}(t)$ increases exponentially to about 203.3 V at 3.8 s. In the case of the SMES system is applied, the twenty bridge-type chopper units are operated in the discharge-storage mode to compensate the shortfall power from the bus line. As a result, $U_{load}(t)$ is maintained around its rated voltage with a maximum voltage ripple of about 198.8 V at 3 s. Figure 3.24 shows the simulated load voltage $U_{load}(t)$ during the power swell period from 0.5 to 3 s. From the result, the SMES system can protect the load voltage effectively under both power sag and power swell conditions.

3.5.5 Fault Current Limitation by SC and SMES

From the simulation results and analyses under a short-circuit fault condition, the DC SC having the self-acting FCL characteristic can simultaneously protect the load voltage and current of the adjacent branch cables, but there are still unavoidable load voltage and current drops after the fault occurrence. This is

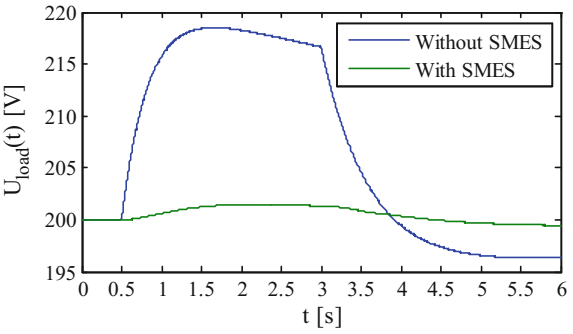

Fig. 3.24 Load voltage $U_{load}(t)$ during a power swell period

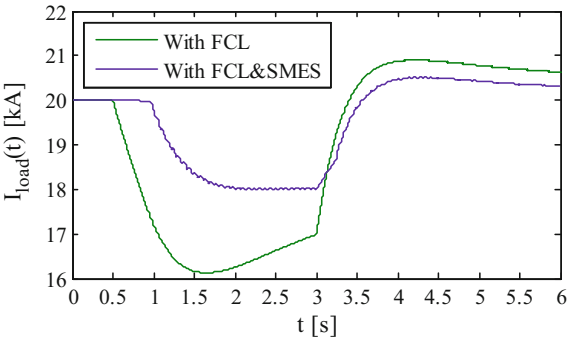

Fig. 3.25 Load current $I_{load}(t)$ with the FCL function only and with the cooperative FCL and SMES functions

because the quenching degree becomes increasingly serious as the fault current rises, and thus the resulting superconducting resistance increases exponentially from zero to a maximum value along with the quenching time.

To achieve a better protection effect, the SMES is applied to cooperate with the DC SC. The DC SC and SMES are equivalent to a fault-current-dependent increased voltage source U_{sc} and a decreased current source I_L, respectively. A load-voltage-dependent switch is closed to switch on the SMES when the bus voltage U_{bus} is lower than its rated value. Thus, the increased U_{sc} offsets the line voltage to limit the fault current, while the discharging current protects the voltage and current drops across the adjacent branch cables. As shown in Fig. 3.25, the load current $I_{load}(t)$ remains around 20 kA from 0.5 to 1 s. This means that the fault has virtually no impact on the adjacent branch cables if the fault time duration is less than 0.5 s. From 1 to 3 s, $I_{load}(t)$ drops gradually to a minimum load current of about 18 kA and then remains nearly unchanged. As compared to the load current curve with the FCL function only, the ratio between the minimum load current and rated load current increases from about 0.8–0.9. Moreover, the maximum load current after the fault disappearance drops from about 21.5–20.5 kA. Figure 3.26 shows the fault current $I_{fault}(t)$ with the FCL function only and with the cooperative FCL and SMES functions.

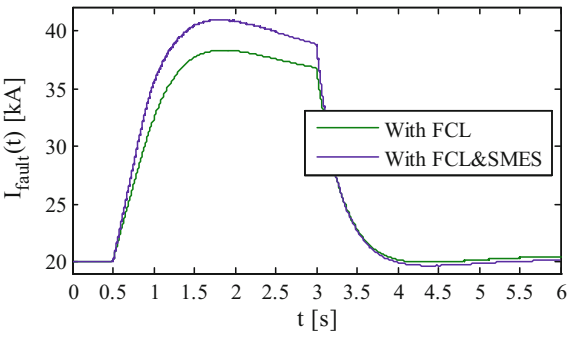

Fig. 3.26 Fault current $I_{fault}(t)$ with the FCL function only and with the cooperative FCL and SMES functions

It should be noted that the introduction of SMES also results some negative effects for the fault current limitation. The maximum fault current is about 41 kA, which is about 2.5 kA higher than that with the FCL function only. Due to the higher fault current and its resulting energy consumption, the dissipated LH_2 increase to about 0.062 L/m before 2 s and about 0.295 L/m after 2 s. When the fault is removed at t = 3 s, the fault recovery pathways are nearly the same.

3.5.6 System Performance Summary

A low-voltage rated DC power transmission network integrated with superconducting DC cables and SMES devices is a valid solution as analyzed. During a fault, the maximum fault current and minimum load current in the case presented are about 1.9 times and 0.8 times of the rated load current. The ratio between the minimum load current and rated load current can be increased from about 0.8–0.9 when the SMES is applied to cooperate with the superconducting DC cable. During a power fluctuation, the designed high-power SMES device enhances the power quality effectively. The minimum load voltage during a power sag period and maximum load voltage during a power swell period are about 0.9 times and 1.1 times of the rated load voltage.

3.6 Practical Development of HTS Cables and Their Power Transmissions

3.6.1 Impact of HTS Cables to Power Grids

For more than ten years, several HTS cables have been tested in real grid applications worldwide. The experience gathered in these tests shows that all technical requirements are fulfilled so far, and a high reliability can be assured. The HTS systems are on the verge of commercialization, which however will essentially

depend on the price of the HTS material as well as its cable technological developments. The large scale and wide application of HTS power cables will change the transmission concept and structures, and will significantly impact to the plan, design and operation of electric power grids.

The development of HTS cables is invoked by present requirements of increasing system voltage or/and current in the power systems, which losses can be largely reduced in a long distance with high current and voltage transmission. Concentric HTS cables for MV applications are very compact, exhibit a very good electromagnetic compatibility, and are thermally independent from the environment. For concentric HTS cable systems, the required right of way is much smaller and the installation is easier compared to conventional cable systems.

In some countries especially European countries, cities' power is supplied predominantly through high, medium and low voltage power cable systems. Many of these cables as well as associated substations are approaching the end of their lifetime. Employing HTS systems, which consist of cables and FCLs, as replacement for conventional cables could be an interesting option.

Various HTS cable application fields can be summarized as:

(a) Load centers in big cities: to meet the increase of power supply capacity requirement; to save the inability to expand the scope of cable laying.
(b) Large current buses: to simplify the power systems and increase reliability with low cost.
(c) Bottleneck sections of power transmissions: to replace unsuitable or unsurvivable overhead lines and special cases such as to cross river.
(d) DC power buses: huge current e.g. electric furnace to avoid high loss.
(e) Efficiency and safety enhancement: to incorporate with SMES and power transmission with AC or DC fault current limiting reactors.
(f) Novel concept: to design a HTS energy pipeline to combine electric power and liquefied natural gas or hydrogen transportation.

3.6.2 Impact of HTS Cables to Power Grids

3.6.2.1 Railway Application

There are various proposals to apply the HTS cables, for example, HTS DC cables for railway applications. Three different schemes of HTS power cables for railway applications:

(a) In a conventional feeding network with up and down train lines, the HTS DC cable using a single core type is placed parallel to the feeder and connected to the substation. In this case, the HTS DC cable is cooled by sub-cooled liquid nitrogen to ensure the HTS DC cable to be able carrying e.g. a current of 5 kA in a continuous power transmission line with a voltage class of 1.5 kV. In this scheme, a large quantity of HTS wires are needed, meanwhile radiation heat also occurs.

(b) A double core or a two-in-one type cable is used to connect the up and down tracks. Because separate cooling paths with the same coolant are needed, a large quantity of HTS wires and a larger cable diameter are required, which results a higher radiation thermal load.
(c) The third scheme is the same with the second one except for the type of HTS cable. A single-core HTS cable utilizing a counter flow cooling system is used to connect up and down tracks in the third example. In this case, the cost of the cryostat is minimized and the amount superconducting wire is reduced.
(d) From analysis, the third scheme is not only an effective solution for cooling the superconducting cables but it also brings a substantial reduction of the length of the expensive superconducting wire. In addition, the results also show that the prototype DC superconducting cable used in a feeder network is feasible.

3.6.2.2 Naval Applications

Large DC current bus bars and networks are required by large ships. Degaussing cable as another application is mainly used on naval ships to reduce their magnetic field, which forbids them from being detected by the magnetic sensors and magnetic mines. The HTS degaussing cable has the total length of 142 ft. It can deliver 4100 A current, and reached the general level of the ship degaussing conventional copper wires. At the same time the voltage of the cable was 0.5 V less than copper wires, or 1000 times lower than copper wires. And most importantly, the weight of the HTS degaussing cable was only 20% of the ordinary copper wires degaussing cable. Therefore, the HTS degaussing cable has definite advantages on low weight and small volume, which enables the cost of degaussing system reduce by 40%. Besides, benefit from the characteristics of zero resistance of the HTS wire, it only needs little energy to run the HTS degaussing system.

3.6.2.3 Spacecraft Charging Applications

Novel solar cell configurations and cover glass materials promise to make arcing, both of the primary electrostatic discharge (ESD) type and sustained arcing between cells or strings. Superconducting cables may obviate the high voltages that lead to arcing. If superconducting cables are used in spacecraft charging, there may be no need for high power system voltages, with the concomitant differential current collection that leads to differential charging. That is, the design goal of all parts of the spacecraft being at the same potential may become feasible. This may eliminate the root cause of ESD and sustained arcing.

Increasing power requirements may require longer transmission cables, which may increase the need for higher voltages to prevent efficiency losses. If superconducting cables become feasible and sufficient long cables the efficiency problem will not be presented.

However, if superconducting cables used in spacecraft charging, the only way that large amounts of power may be transmitted, is by transmitting large currents, which produces strong magnetic fields. For example, if the international space station power were transmitted at 5 V, instead of 160 V, the current would go up by 32 times. The increased magnetic field may then become more important for spacecraft control and stability.

3.6.2.4 Novel and Trend of HTS Power Transmissions

While looking into the prospect of HTS electric power transmissions, various concepts of the future HTS power transmission models are proposed, and form the development trend of the future HTS power grids.

For example, the concept of 'SuperCable' proposed by experts from USA, can simultaneously transport hydrogen and electricity. Each 'cable' delivers half the total hydrogen power. Furthermore, an idea about a 'SuperCity' connected with the 'SuperGrid' was also proposed, which is from only to transport electricity to simultaneously to transport electricity and hydrogen, from power transmission and distribution to power utilization.

In 'SuperCity' both hydrogen and electricity are produced centrally in a nuclear power plant, supplemented by roof-top solar photovoltaics and perhaps the combustion of waste biomass, and distributed throughout the community via a 'SuperCable' conveying cryogenic hydrogen and electricity using superconducting wires refrigerated by the former.

As another case, a low-voltage rated DC power transmission network integrated with superconducting DC cables and SMES devices is potentially an option as introduced above.

A kind of combined energy transmission concept can be developed; energy pipeline is also a promising application, which deliveries fuel energy with integration of HTS DC electric power transmission in the energy pipeline. Natural gas in this case is utilized as the coolant of the HTS cable.

3.6.3 Development Status of HTS Cables

What the HTS wires have brought to an advanced electric power cable? HTS cables can achieve larger power transmission capacity and lower power loss with a compact size in general. This is effective in reducing the costs of cable system construction and operation. As environmental features, HTS cables are able to reduce energy consumption because of lower transmission loss. In addition, because HTS cables are cooled with liquid nitrogen that is used as an insulating material, the HTS cables are non-flammable and non-explosive in nature. Moreover, superconducting shield layers lead to no leakage of the magnetic field at

the outside of the cable. Therefore, the HTS cable doesn't affect its outside with any electro-magnetic influence.

Reliability is one of the most important factors for the power cables which work for a long time as a component of the infrastructure. The primary factor of degradation in conventional cables is considered to repeated expansion and contraction of the cable itself due to temperature change caused by load fluctuation and ambient temperature change throughout a day or a year. On the other hand, HTS cables are operated at the almost constant temperature in liquid nitrogen so that they are not expected to have any damage due to thermo-mechanical motion during their operation.

There are a few countries which have initiated HTS cable development programs, the world's first applicable HTS cable 30 m/12.5 kV/1.25 kA with three single phases developed by the Southwire in USA, were constructed during the first two quarters of 1999, installed by the third quarter of 1999, energized on January 6, 2000, and inauguration on February 18, 2000. The second superconducting 30 m/30 kV/104 MW cable system designed with a room temperature dielectric has been developed, installed and operated in the public network of Copenhagen Energy in a two-year period between May 2001 and May 2003. The third HTS cable project for a 30 m/35 kV/2 kA, 3 phases, warm dielectric HTS cable system is operated in China, which has been installed in the China southern power grid at the Puji substation in Kunming, Yunan province, in 2004. Table 3.5 shows the parameters of the first three HTS cables running in practical power grids or networks. Other countries such as Japan, Germany, and Korea also ploughed into the investigation and development of HTS AC cables, their early object and hope is to realize short distance (<500 m), low loss, and high capacity power transmission. Other HTS AC cables developed include American Southwire/DOE-305 m, AMSC/DOE/Nexans-600 m, IGC/Sumitomo-350 m, and CRIEPI/Furukawa/METI-500 m reached in Japan.

In China, for example, the Chinese first and world's third HTS power cable project was started in the second half of 2002 and on site system installation was finished at Puji Substation of China Southern Power Grid in March 2004. This cable system consists of three 33.5 m, 35 kV 2 kA_{rms} cables, six terminations, and a closed cycle liquid nitrogen cooling station. The conductors of the cables were made of 4 layers of Bi-2223 HTS tapes. Off grid field testing and live grid trial operation have been carried out since the completion of the installation.

Table 3.5 The first three HTS cables running in networks

Nations	America	Denmark	China
Rating	12.5 kV/26 MW	36 kV/104 MW	35 kV/121 MW
Refrigeration structure	CD D-channel	WD S-channel	WD D-channel
Running temperature	70–80 K	76.5–79.5 K	70–76 K
Termination loss	230 W/ea.	150 W/ea.	108 W/ea.
HTS tape	Bi-2223	Bi-2223	Bi-2223

The 35 kV cable system had delivered more than 8×10^8 kWh of electricity to 4 industrial customers before its operation was suspended.

3-phase, 10.5 kV/1.5 kA/22 MVA/75 m HTS AC power cable prototype was developed by the IEE CAS, which was installed and demonstrated in a distribution grid of Changtong Power Cable Factory in Baiyin, China at the end of 2004. Each cable consists of 36 Bi-2223 tapes spirally reeled into two layers on the corrugated pipe and soldered to the copper terminals by low-melting-point alloy solder.

A 1.3 kV/10 kA/13 MVA/360 m HTS DC cable prototype was developed and tested by IEE CAS in 2012. The cable is used to connect the substation and the bus bar of an aluminum electrolyzing workshop in Henan Zhongfu Industrial Co. Ltd., as shown in Fig. 3.27. In addition to normal operation, testing analysis and demonstration have also been conducted. The HTS conductor consists of 5 layers of Bi-2223 tapes.

Another example is the most recent case. In Essen, Germany, the AmpaCity HTS system will be installed to connect substations of Dellbrügge and Herkules, and a 1 km cable system having capacity of 10 kV/40 MVA and consisting of a resistive type FCL has been tested in the end of 2013. In Essen, the connection of the substations is mostly realized with 110 kV underground cables (UGC), and a few overhead line (OHL) links. Through introducing medium voltage cables, especially HTS cables, for connecting 10 kV busses of different substations, a new grid concept becomes feasible. The intention of this measure is to simplify the grid in reducing the amount of 110 kV cable systems and the number of transformers. In the simplified system two substation types can be found, switching substations without any transformers and therefore transformer substations. In comparison to the grid concept with conventional 110 kV cables, in total 12.1 km of 110 kV cable system, five 40 MVA transformers as well as the associated 110 and 10 kV switchgear become dispensable. Instead, 23.4 km of 10 kV HTS cable system, the associated switchgear for the eight cable connections, and three 10 kV bus ties are required. The electric power supply with medium voltage superconductor cable systems in city centers offers technical and economical advantages compared to conventional high voltage technology.

Fig. 3.27 10 kA HTS DC power cable and system in Henan, China

Worldwide development of HTS cable systems are summarized in Table 3.6, while Table 3.7 shows the HTS wires and cable structures used in the projects shown in the Table 3.6.

Table 3.6 The main project of HTS power cable in the world

	Research institute	Length (m)	Rated voltage (kV)/ current (kA)
China	Innopower Superconductor Cable Co., Ltd.	33.5	35/2
	IEE CAS Baiyin	75	10.5/1.5
	IEE CAS Henan	362	1.3/10
American	Southwire/DOE/Oak Ridge NL	30	12.4/1.25
	Albany: SP/SEI/BOC/NGPC	350 (320 + 30)	34.5/0.8
	Columbus: Southwire/NKT/ AEP/ORNL/ Praxair/AMSC	200	13.2/3
	Long Island Power Authority LIPA SPI: DOE/AMSC	600	138/2.4
Denmark	NKT/TUD/RNL/DETA	30	30/2
Japan	Sumitomo Electric Industries/TEPC	100	66/1
	CRIEPI/CEPC/Furukawa	500	77/1
Korea	KEPCO	100	22.9/1.25
Russia	FGCUES/RDCPE	430 × 2	20/2.5
Germany	Nexans, KIT, German Federal Ministry of Economics and Technology	1000	10/2.3

Table 3.7 HTS wires and structures used in the main projects worldwide

	Material	Type	Year connected to grid
China	Bi-2223	3 phase AC WD	2004
	Bi-2223	3 phase AC WD	2004
	Bi-2223	DC WD	2012
American	Bi-2223	3 phase AC CD	2000
	Bi-2223 + Y-123	3 phase AC CD	2006
	Bi-2223	3 phase AC CD	2006
	Bi-2223	3 phase AC CD	2008
Denmark	Bi-2223	3 phase AC WD	2001
Japan	Bi-2223	3 phase AC CD	2001
	Bi-2223	1 phase AC CD	2004
Korea	Bi-2223	3 phase AC CD	2005
	Y-123	DC CD	2014
Russia	Bi-2223	3 phase AC CD	2013
Germany	Bi-2223	3 phase AC CD	2014

AC HTS cables and systems have been well developed but the DC HTS cables and systems are not practically developed yet. HTS DC cables are with the advantages of high transport current capability, no resistive loss and compact system, therefore high-power and high-efficiency transmissions for delivering the electric power directly from various renewable energy sources (RESs) to power consumers can be achieved. The continuous developments of the HTS BSCCO, YBCO, and medium temperature superconductor (MTS) MgB_2 have increased the potential of DC SCs to be industrialized. As for the low-voltage high-current power distribution and utilization, hundreds of kA can be delivered and technically verified in combination with LH_2 delivery, or conceptually designed for supplying commercial buildings such as internet data center. As models presented and analyzed, HTS techniques become available with substantial advantages, and will form a new generation system for DC electric power transmissions.

HTS technologies are available to build HTS cables, and a number of HTS cables have been practically built by some countries. Development of HTS power cables provides an effective solution for the electric power systems of megalopolises and various special applications. In the near future, the HTS cable applications are forecasted, where the demand for electricity is rising rapidly but the installation of added transmission lines is impossible or environmentally undesirable for many cases. In the long run, opportunities for HTS cable may also include long distance transmission and distribution of electrical power energy, particularly in a high capacity DC power grid and a smart grid.

3.7 HTS Power Transmissions with Energy Efficiency Improvement

The most important and unique property of superconductors is the zero-resistance. So, application of HTS devices has become an effective way to efficiency improvement. Like various HTS devices such as HTS cables, HTS transformers, HTS generators, and HTS SFCL, SMES can be used for efficiency improvement in power generation, transmission, distribution, and utilization systems. The higher energy efficiency brought about by HTS devices is mainly achieved by improvement in generation efficiency and power-network loss reduction. HTS generators and transformers have higher efficiency compared to conventional devices. About 50–60% of energy losses can be reduced by replacing conventional cables with HTS cables because of its zero-resistance characteristic. An active power loss comparison between HTS cable and conventional cable for 1000 kV ultra-high voltage (UHV) and ±660 kV high voltage DC (HVDC) transmission lines is presented in Fig. 3.28.

The power transmission efficiency is greatly improved by HTS cables. The more transmitted power there is in the HTS cables, the more the power losses are reduced. For typical transmitted power 4000 MW in a UHVAC transmission line, the power loss will be reduced by about 41.04 MW with HTS cables, and since the

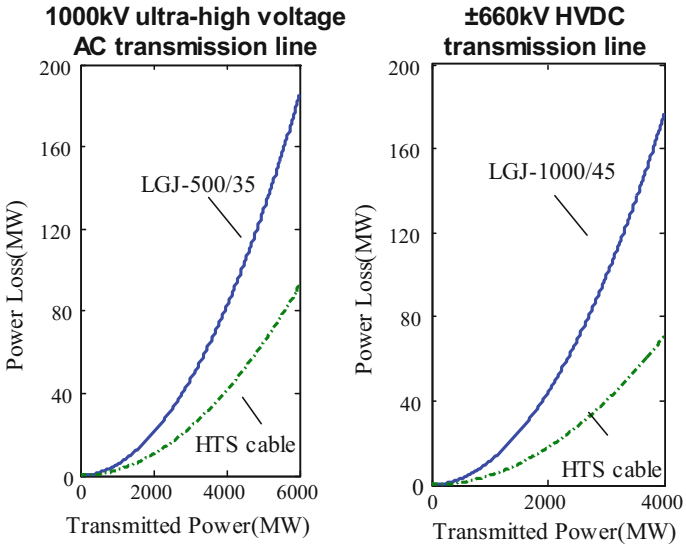

Fig. 3.28 Power loss comparison between conventional cable and HTS cable

annual operation time of transmission line is 5000 h, the total amounts of energy conservation will be 205,200 MWh. The potential of HTS devices to improve energy efficiency is significant, but there are also some challenges related to cost, reliability, and the coordination between HTS devices and power systems.

3.8 Energy Efficiency Case Analysis and Carbon Dioxide Reduction of a HTS Power Network

HTS power devices are favored to improve the energy utilization efficiency in modern power systems. For instance, high-capacity and high-efficiency HTS DC cables have significant potential to deliver electricity directly from distant renewable energy sources to local power consumers, whereas high-power and high-efficiency SMES devices have obvious advantages in both momentary and peak power compensation for achieving a high-quality power supply.

In the 10 kV/1.15 kA/20 MW conventional AC network case in Fig. 3.29a, the 20 MW of electric power that is delivered from one 20 MW/10 km main AC cable is firstly transformed to the 0.4 kV user-side voltage level through ten 10 kV/0.4 kV/2 MVA transformer units, and it is then distributed through ten 2 MVA branches to various distributed loads through ten 20 MW/1 km branch AC cables. According to the Chinese National Standard for conductors in insulated cables (GB-T3956-2008), the lossy resistances from the copper cores result in about 510 kW transmission loss in the main AC cable and about 1298 kW transmission

loss in the ten branch AC cables. The total electricity dissipation will be 15,838,080 kWh per year.

To reduce the conventional transmission and distribution loss, one 0.2 kV/100 kA/20 MW/10 km and ten 0.2 kV/10 kA/2 MW/1 km HTS DC cables can be applied to form a superconducting DC network with the same capacity, as shown in Fig. 3.29b. Considering the heat leakages from the long-distance cable pipelines and high-capacity current leads located at the main and branch cable terminals, the total lossy power value for the main DC cable and ten branch cables is about 20 kW at 77 K. The loss for corresponding realistic power in total is about 800 kW consumed by the practical refrigeration systems. Therefore, the total energy conservation can be summed up to 8,830,080 kWh per year compared to the conventional AC network. Table 3.8 shows the main specification comparisons between the conventional AC network and the superconducting DC network.

In addition, the ten 10 kV/0.4 kV/2 MVA conventional transformer units also cause relatively high electricity wastage. According to the Chinese National Standard for dry-type power transformers (GB-T10228-2008), the ten transformer

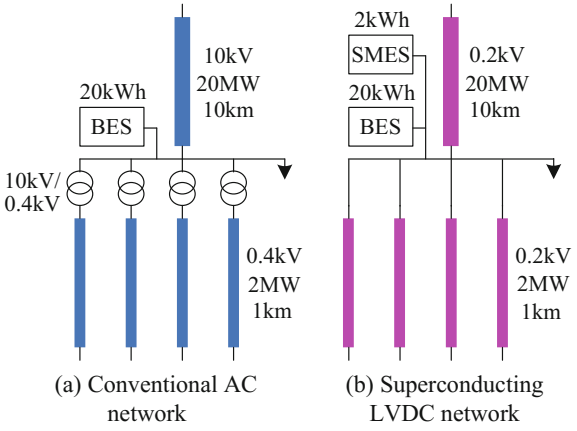

Fig. 3.29 Schematic diagrams of two sample power distribution networks

Table 3.8 Main specification comparisons between conventional AC network and superconducting DC network

Items		20 MW cable	2 MW cable
Conventional AC network	Rated voltage (kV)	10	0.4
	Rated current (A)	1155	2886
	Lossy power (kW)	510	1298
	Lossy energy per year (kWh)	4,467,600	11,370,480
Superconducting DC network	Rated voltage (kV)	0.2	0.2
	Rated current (A)	100,000	10,000
	Lossy power (kW)	400	400
	Lossy energy per year (kWh)	3,504,000	3,504,000

units with a full-load loss of 17.1 kW per unit will generate about 1,497,960 kWh per year. In comparison, such large electricity wastage can be removed completely in the superconducting DC network. Even when the ten conventional transformer units are replaced by superconducting units in a superconducting AC network with the same capacity, the operational loss from each 10 kV/0.4 kV/2 MVA superconducting transformer unit is only about 7.2 kW. This means that the total energy conservation can be summed up to 867,240 kWh per year compared to the ten conventional transformer units.

To carry out dynamic energy managements in the superconducting DC network, one 2 kWh SMES device and one 20 kWh battery energy storage (BES) device could be integrated to form an economical hybrid energy storage system. If this SMES device is upgraded to full-scale 20 kWh capacity, the capital cost will sharply rise from about 3.56 M$ to 16.95 M$. Moreover, the typical charge-discharge efficiencies of the SMES and BES are about 90 and 70%, respectively. Assume that the 2 kWh SMES device carries out 100 full charge-discharge operations per hour and thus, that the total energy consumption from the SMES per year is about 350,400 kWh. If a sole BES device is applied, however, its energy consumption will add up to an extra 700,800 kWh per year.

In sum, the total transmission losses (P_{sup}, P_{con}) in the superconducting LVDC network and the conventional AC network can be estimated by

$$P_{sup} = \eta_{sup} N_{cable} S_{cable} + \eta_{lead} N_{lead} P_{cable} + \eta_{smes} P_{ex} \tag{3.23}$$

$$P_{con} = \eta_{con} N_{cable} S_{cable} + \eta_{tran} N_{tran} P_{tran} + \eta_{bes} P_{ex} \tag{3.24}$$

where η_{sup} is the unit lossy power per km of superconducting DC cable; N_{cable}, the number of main or branch cables; S_{cable}, the length of the main or branch cables; η_{lead}, the unit lossy power per kA of current lead; N_{lead}, the number of main or branch cables; P_{cable}, the delivered power of the main or branch cables; η_{smes}, the unit lossy power per kW of SMES device; η_{con}, the unit lossy power per km of the conventional AC cables; η_{tran}, the unit lossy power per kW of the branch transformers; N_{tran}, the number of branch transformers; P_{tran}, the delivered power of the branch transformers; and η_{bes}, the unit lossy power per kW of the BES device. Considering the in-grid operations for a whole year, the total energy consumption comparisons between the conventional and HTS power devices are shown in Table 3.9. As compared to the conventional power devices with the same

Table 3.9 Energy consumption comparisons between conventional and superconducting power devices

Items	Conventional	Superconducting	Saved energy
20 MW cable	4,467,600 kWh	3,504,000 kWh	963,600 kWh
10 × 2 MW cable	11,370,480 kWh	3,504,000 kWh	7,866,480 kWh
10 × 2 MW trans.	1,497,960 kWh	630,720 kWh	867,240 kWh
20 kWh ESS	1,051,200 kWh	350,400 kWh	700,800 kWh

capacities, the superconducting cables, superconducting transformers, and SMES devices in the 20 MW power network can save about 8,830,080 kWh, 867,240 kWh, and 700,800 kWh respectively. Based on the rate of 1 kWh–1 kg CO_2 emission, this single 20 MW HTS cable system will reduce about 10,398,120 kg of CO_2 emissions per year. Therefore, conclusion can definitely be made that the applications of HTS power devices have significant effects on the system energy efficiency enhancement.

3.9 Summary and Conclusion

This work has gone through the HTS cable techniques from HTS material properties, HTS cable design, HTS AC transmission, HTS DC transmission, and then HTS smart grid. The achievement of HTS cables and transmissions to date has also briefly described with the focus on their practical grid applications.

HTS cable techniques have been both theoretically and practically verified to be viable for broad industrial applications. HTS wires have been identified for the HTS cable application with satisfied electrical properties at an economical operation temperature. HTS materials are technically available and have been applied for various model HTS cable design and operation.

Advantages of HTS AC transmissions have been practically verified with a number of trial lines in operation. On top of energy saving and high efficiency, the impact of the HTS AC transmissions to modern power grids also includes: to meet the increased power supply capacity requirement; to save the inability to expand the scope of cable laying in big cities; to replace the current un survivable lines; to solve bottleneck sections of power transmissions; to simplify the power systems and increase reliability with large current buses at low cost.

The HTS DC cable represents a very attractive alternative to HTS AC cables. The HTS conductor loss in a DC HTS cable is negligible when operated below its critical current. In a DC power transmission cable, there is no reactive power and no loss in the insulation, and there is also no HTS AC loss. The DC cable is also more compact. These make the design of a DC HTS cable much less complex than the AC case. HTS cables are consequently developed to build DC power transmission systems with the advantages of high transport current capability, no resistive loss and compact systems. The zero resistance of HTS materials is observed only to work with a DC current, while transmission loss is generated with an AC current. Moreover, it is necessary to take measures to solve the inherent problems of HTS AC cables, such as protection against short circuit currents and avoiding unbalanced AC current in each HTS conductor tape. A HTS DC cable, on the other hand, is a cable that utilizes the advantages of superconductivity most effectively without HTS AC cable's inherent problems. Also to lower the system voltage levels, means the significant reduction of the network costs, avoiding very expensive costs from high voltage insulation and converter stations. The application

field of DC HTS cables ranges from low-voltage and high-current to high-voltage and large-capacity applications, from back-to-back to interconnection applications, and other applications.

Besides the electric power distributions and transmissions, there are a number of novel HTS cable applications proposed, such as applications in railway, navy, spacecraft, energy pipeline, and a concept of supergrid. Unique HTS characteristics or functions can be best utilized, such as superconductor quench or persistent current. A sample case has been studied in detail and presented in which a low-voltage rated DC power transmission network integrated with HTS DC cables and SMES devices. As analyzed, it forms a smart HTS grid. Apart from high transport current capability, the HTS DC cable implanted has demonstrated to achieve the self-acting fault current limitation during its quench, and also to protect the voltage and current of adjacent cables under a short-circuit condition. During a power fluctuation, the designed high-power SMES device enhances the power quality effectively. Therefore, the cooperative operations of HTS DC cables and SMES devices are favored for retaining high-safety and high-stability electricity, and can be well expected to achieve smart DC power transmissions in future smart grids.

A number of HTS trial transmission lines are presented and analyzed which verify and identify that HTS cables and transmissions are not only scientifically and technically available, but also their practical application and manufacture are possible to achieve.

Acknowledgements The authors would like to deliver their appreciations to Z. H. Chen, X. Y. Chen, X. Y. Xiao, C. S. Li, Y. Q. Xing for their assistance to this work.

References

1. Jin JX, Tang YJ, Xiao XY, Du BX, Wang QL, Wang JH, Wang SH, Bi YF, Zhu JG (2016) HTS power devices and systems: principles, characteristics, performance, and efficiency. IEEE Trans Appl Supercond 26(7):3800526
2. Jin JX, Xin Y, Wang QL, He YS, Cai CB, Wang YS, Wang ZM (2014) Enabling high-temperature superconducting technologies toward practical applications. IEEE Trans Appl Supercond 24(5):5400712
3. Jin JX, Chen XY, Qu R, Fang HY, Xin Y (2015) An integrated low-voltage rated HTS DC power system with multifunctions to suit smart grids. Physica C (Amsterdam, Neth) 510:48–53
4. Jin JX (2007) High efficient dc power transmission using high-temperature superconductors. Physica C 460–462:1443–1444
5. Huang Q, Jin JX, Zhang JB (2006) Simulation study on performance of a long-distance superconducting DC power transmission system. Electr Power 39(3):45–49
6. Jin JX (2009) High temperature superconductors and their strong current applications. Metallurgical Industry Publishing House of China, Beijing
7. Xin Y, Hou B, Bi YF, Xi HX, Zhang Y, Ren AL, Yang XC, Han ZH, Wu ST, Ding HK (2005) Introduction of China's first live grid installed HTS power cable system. IEEE Trans Appl Supercond 12(2):1814–1817

8. Xin Y, Ren AL, Hong H, Li HH (2013) Superconducting power cable. China Electric Power Press, Beijing
9. Zong XH, Wei D, Han YW, Tang T (2016) Development of 35 kV 2000 A CD HTS cable demonstration project. IEEE Trans Appl Supercond 26(7):5403404
10. Grilli F et al (2014) Computation of losses in HTS under the action of varying magnetic fields and currents. IEEE Trans Appl Supercond 24(1):8200433
11. Dai S, Xiao L, Zhang H, Teng Y, Liang X, Song N, Cao Z, Zhu Z, Gao Z, Ma T, Zhang D, Zhang F, Zhang Z, Xu X, Lin L (2014) Testing and demonstration of a 10-kA HTS DC power cable. IEEE Trans Appl Supercond 24(2):5400104

Chapter 4
Advanced Electrical Machines for Oceanic Wave Energy Conversion

Omar Farrok and Md. Rabiul Islam

4.1 Introduction

The ocean is one of the biggest sources of the renewable energy sources (RESs) and a number of countries are surrounded by this ocean. The energy of the oceanic wave is harvested in different techniques [1]. The total wave power is estimated 10 TW in the ocean, which can contribute the total electrical power generation in the world [2]. It is available in most of the time with wave power of 20–30 kW/m in each year on average [3]. In the European Union, the wave power ranges from 20–60 kW/m on average in each year from the Atlantic Ocean. For this reason, the oceanic wave energy (OWE) can be considered a vital RES. The OWE has the energy of nearly 8000–80,000 TWh in each year [4]. According to the report of Electric Power Research Institute (EPRI), it is found that, there are tremendous potential of wave energy resource of the coastal areas of U.S.A. which is 2640 TWh/year. This energy is approximately two third of the electrical energy generation of 4125 TWh in U.S.A. in 2010. The amount of total extractable OWE is 1170 TWh/year, which is composed of 160 TWh/year for the East Coast, 250 TWh/year for the West Coast, 620 TWh/year for the Alaska, 60 TWh/year for the Gulf of Mexico, 80 TWh/year for Hawaii, and 20 TWh/year for the Puerto Rico [5]. OWE also demonstrates its great potential to feed the existing energy demands of electrical power.

O. Farrok (✉)
Department of Electrical and Electronic Engineering (EEE), Ahsanullah University of Science and Technology (AUST), 141–142 Love Road, Tejgaon I/A, Dhaka 1208, Bangladesh
e-mail: omarruet@gmail.com; omar.eee@aust.edu

M. R. Islam
Department of Electrical and Electronic Engineering, Rajshahi University of Engineering and Technology, Rajshahi 6204, Bangladesh
e-mail: rabiulbd@hotmail.com

M. R. Islam et al. (eds.), *Renewable Energy and the Environment*, Renewable Energy Sources & Energy Storage, https://doi.org/10.1007/978-981-10-7287-1_4

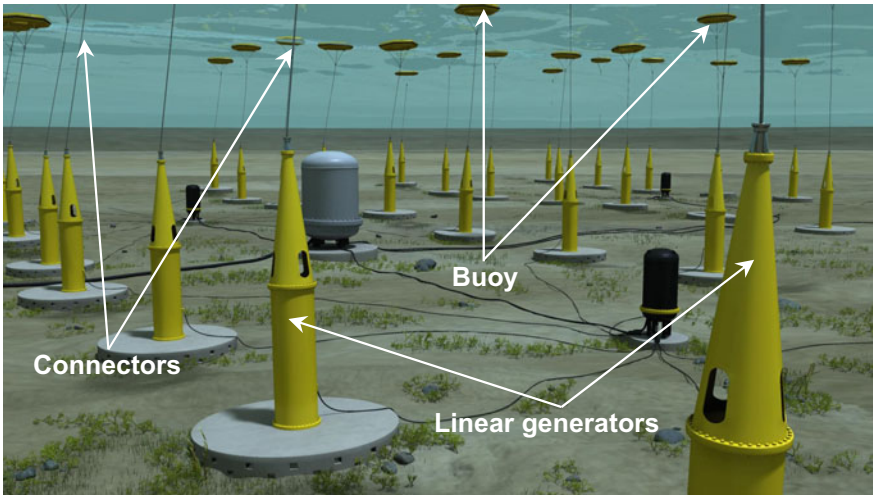

Fig. 4.1 LGs connected to the buoy [6]

At present, most of the electrical machines are connected to various types of hydro-electrical power plants. These conventional machines are of rotating type and need to drive with high angular velocity due to their design topology. For these reason additional mechanical gear arrangements are required to drive these generators because the velocity of water is low in nature. Moreover, the natural source of suitable hydropower is limited. Therefore, the continuously increasing demand of electricity inspired the researchers to find some alternatives. Such an alternative is the linear generators (LGs) which are shown in Fig. 4.1.

In this consequence, advanced electrical machineries have been invented, tested and applied such as different types of LGs. Figure 4.1 represents that, each of the LGs is connected to a buoy for the wave energy conversion (WEC) system. The Oscillating Water Column (OWC), Archimedes Wave Swing (AWS), Pelamis structure, Mighty Whale, Wave Dragon are some prominent wave energy devices for wave energy conversion (WEC) [7–9]. The AWS usually contains a hollow cylinder and a cap fixed on the sea-bottom filled with air, called a float as shown in Fig. 4.2. The float changes its position in vertical direction. When sea waves come,

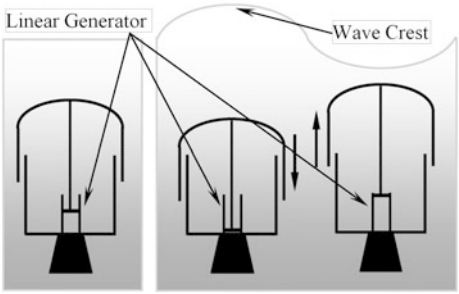

Fig. 4.2 LGs connected to the AWS type converter [12]

the float sinks because of increase of the weight of the water above, while the pressure of the air in the cylinder increases and vice versa. In the power buoy, the bobbing motion of the float is linearly moved; the wave energy is extracted which is further converted into electrical power. The point absorber is basically a floating body which vertically moves to each other relatively owing to the wave action using the change in the wave height at a single point for WEC. The relative up and down motion caused by passing waves is utilized to drive hydraulic or electromechanical energy converters for power generation [10, 11].

At present, the direct drive system (DDS) has been widely accepted owing to direct capture of sea wave energy because its efficiency is more compared to the traditional wave energy converters [13]. LGs are engaged for directly transformation of the low speed mechanical energy into electricity. DDS thus eliminates intermediate mechanical arrangements e.g. translators, a crank, a linkage or converters. The LGs have high power density than the rotating generators and they are highly efficient, therefore, the involvement of LGs is increasing [14]. The generated voltage from the PMLG can be further regulated as described in [15] where a fuzzy logic controller was incorporated.

4.2 Traditional Machines for Energy Conversion

The Oscillating Water Column (OWC) is a WEC which contain a hollow tunnel containing a turbine connected to the generator. With the incident of the oceanic wave, there is a lot of air pressure variation due to the hollow structure submerged in the ocean. This pressure variation makes the turbine to rotate which in turn generates electrical [16]. Such type of WEC using OWC is illustrated in Fig. 4.3.

The water column channel is horizontal which is facing out of the waves that imposing on the buoy and the motion of this device itself. The reason is the fluctuation of the hydrodynamic pressure to the opening of the water column due to wave action. This fluctuation of pressure induces the oscillating motion in vertical orientation in the chamber submerged in the ocean.

This partially submerged chamber filled with water where the water column rises and falls in response to the pressure from ocean waves. Both the upward and downward movements of the column generate force to drive air through a turbine, as a result the turbine drives a generator for electricity production [18]. Several strategies of turbine control have been explored in the field of PTO control for OWC devices. Most of these issues are needed to consider fixing OWC systems. An arrangement of Wells turbine combined with blow-off valve airflow control is discussed in [19] for speed control that uses hydrodynamic models of the Azores Pico plant. High moment of inertia is assumed for which the control of the generator torque is required. The optimum speed–torque control law is used in this control, considering the averaged torque of the turbine and the averaged torque of the generator are equal for some of the oceanic wave periods, with instantaneous variations which are absorbed by this high moment of inertia. Similar control

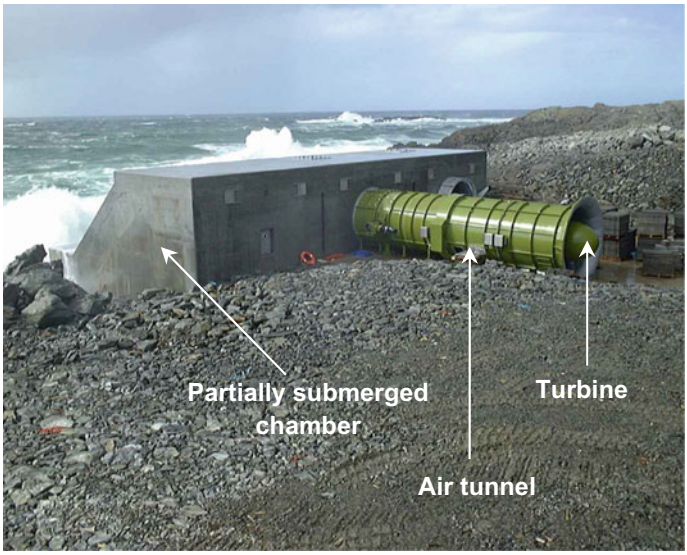

Fig. 4.3 A rotational type generator installed to a WEC system [17]

techniques are used in [19] for developing a model of an OWC which consists a series blow off valve to control the air flow and Wells turbine speed control.

Most of the conventional methods for WEC have some of the common demerits. The demerits are the complex and costly structure, difficult in maintenance, has the low conversion efficiency. As a result the electrical power production is ineffective for these methods [20].

4.3 Modeling of Wave Energy Sources

In most of the cases, constant speeds or Sinusoidal speeds are common approximations for simulating LGs. The typical range of vertical velocity of wave is 0–2 m/s with a time period of wave from 4–6 s [21]. The linear wave has been considered in the mathematical model of ocean wave. The vertical wave displacement of is similar to sinusoidal function, assuming linear wave the vertical position of wave and velocity can be expressed as given in the following.

$$p(t) = H_m \sin\left(\frac{2\pi}{T_w} t \pm \theta_i\right) \tag{4.1}$$

$$v(t) = H_m \frac{2\pi}{T_w} \cos\left(\frac{2\pi}{T_w} t \pm \theta_i\right) \tag{4.2}$$

Here, $p(t)$ and $v(t)$ represents position or displacement of wave and velocity respectively. H_m, θ_i and T_w represent height, initial phase angle and period of the oceanic wave respectively. If, the translator velocity is represented by v_t and the pole pitch of the PMLG is represented by P_τ the generated frequency, f_g of the PMLG is determined by:

$$f_g = \frac{v_t(t)}{2P_\tau} \tag{4.3}$$

The variation of magnetic flux, Φ with respect to time can be expressed as following:

$$\Phi(t) = \overline{\Phi} \sin\left(\frac{\pi}{P_\tau} p(t) \pm \theta_i\right) \tag{4.4}$$

If, k_w is the winding factor, N is the turn number, and Φ_{ag} (wb) is the air gap flux, the induced emf/phase, E_p can be found by:

$$E_p = \pi\sqrt{2} f_g N k_w \Phi_{ag} \tag{4.5}$$

Figure 4.4 represents the block diagram by MATLAB/Simulink software which was represented in [12]. All of the significant parameters were considered in this block diagram. These parameters are made variable before and during simulation time. As the frequency and amplitude of the oceanic wave vary on time, the function "Random" has the purpose of changing the wave parameters. This function has a closer interpretation of the real oceanic wave rather considering fixed wave parameters. A PMLG was also simulated in [12] using this block diagram. Different selector switches namely S1, S2, S3, and S4 were used for different mode selections. Such as, S1 selector switch sets the mode of either equal length of the stator and translator (Equal_S) or longer stator (Longer_S).

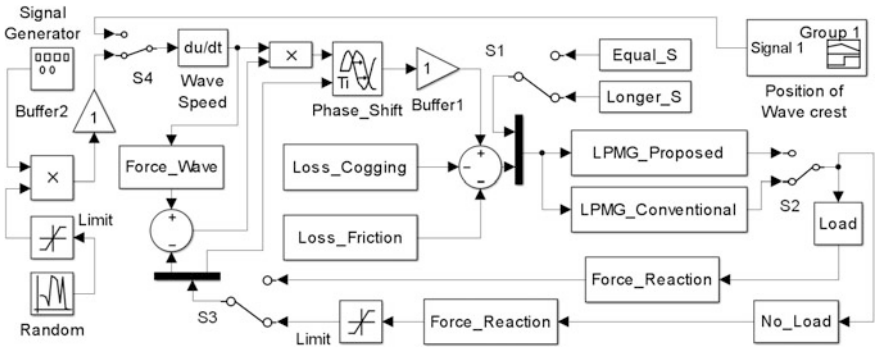

Fig. 4.4 Block diagram of the WEC and PMLG [12]

4.4 Research and Development in Designing New Machines

In recent years, researches have been carried out on the basis of direct driven method. By the extraction of OWE directly, the translator of an LG is connected directly to the slower motion of wave energy devices. This arrangement reduces intermediate mechanical connections and makes the system able to generate electrical power directly. A modern LG connected to a power buoy is shown in Fig. 4.5. The LG shown in Fig. 4.5 is known as DDS which has been considered very efficient [22].

A number of modern LGs contains permanent magnets (PMs) are used generally in the translator for magnetic field generation. For this reason, these LGs are called the PMLG. Most of the PMLG are of synchronous generator type. The PMs can be placed either in the translator or in the stator. If the PMs are placed in the translator, the armature is placed in the stator such as in [23]. On the other hand, as the translator is moving, the armature winding is placed in the stator rather than in the translator. Flux switching PMLG is such an example where both the PMs and the armature are placed in the stator. Electromagnetic LGs [24] are not being used commercially for WEC for much loss in the copper winding. However, most of the existing LG need a voltage regulator [25] to produce regulated electricity form irregular oceanic wave. The modern effective LGs are, Vernier hybrid machines [27], Flux switching PMLG, and switched reluctance generators [21]. Because of

Fig. 4.5 Upper portion of the power buoy [26]

the low and variable speed of wave energy devices, the conversion efficiency is low. The magnetic flux of a PM used in LGs is not adjustable which has bad effect on voltage regulation.

4.5 Superconductor Based Compact and Lightweight Machines

Very recently, the superconductor based generators for WEC are incorporated with DDS. The superconducting magnet (SM) has the property of very high magnetic flux density compared to the conventional PMs. Therefore, the generator consisting SMs can generate electricity more effectively. A tubular type linear generator has been proposed [28] where the laboratory made MgB_2 superconducting winding has been used due to the advantage of simple manufacturing, isotropic feature, and low cost. The bending radius of the MgB_2 is small, that is why it is suitable for the electric machine windings. The refractory glass fiber has been implemented to achieve inter-turn insulation of MgB_2. The current density of MgB_2 superconductor is greater than 10^4 A/cm^2 under the condition of 2 T of magnetic flux density. The resistance of MgB_2 becomes nearly to zero at 40 K or lower temperature. The ring superconductor windings structure has been used in the proposed generator. One phase construction of this LG with superconducting winding is shown in Fig. 4.6.

A flat type superconducting magnetic linear generator (SMLG) has been proposed in [29]. The SMLG is constructed with a translator and stator. The stator sets exists both of the left and right side of the translator. Second generation high temperature superconductor (HTS) has been used to create superconducting magnets (SMs). The field excitation using SMs have been placed inside the stator that has existed on both sides of the translator. Figure 4.7 shows the construction with dimension and magnetic flux density of the stator and translator of the proposed SMLG. The HTS tapes of relative permeability of 0.4 have been used for raping the steel core to form SMs which is excited by direct current. The SMLG has been constructed of ten windings and twenty coils. The winding contains a coil pair with 180° phase shifted to each other, where one coil is wounded in counterclockwise

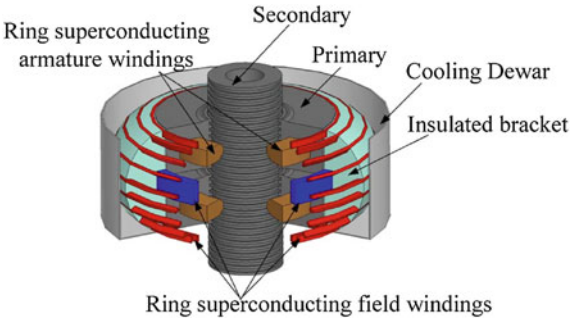

Fig. 4.6 A tubular LG containing superconductors [28]

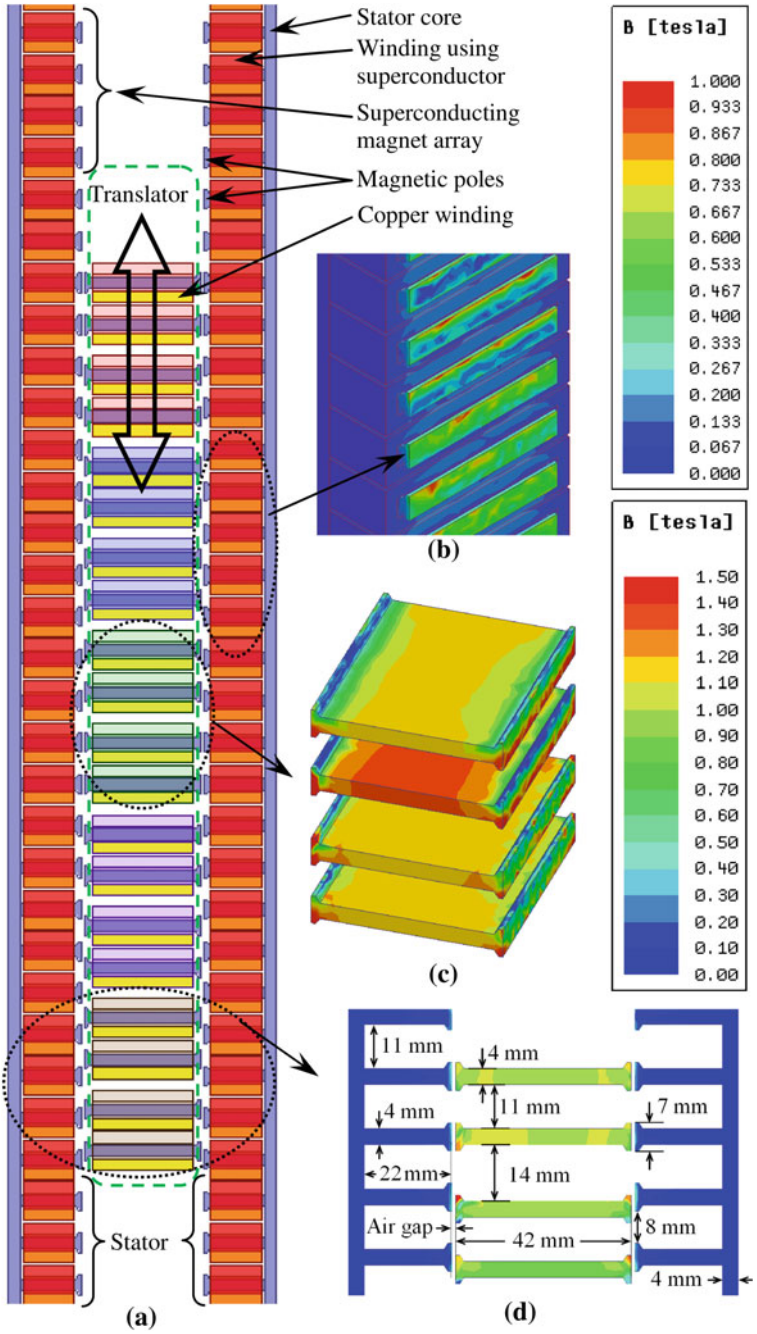

Fig. 4.7 Design of the proposed SMLG: **a** the construction, **b** stator core flux density, **c** translator core flux density and **d** dimensions [29]

direction and another coil is wounded in clockwise direction. The windings are slightly phase shifted by a specific value for reducing the cogging force and force ripples. The 3D Cartesian coordinate system has been considered to explain the direction of different forces. The applied force, Force_z is working vertically along z axis. Forces along x axis and y axis are symbolized by Force_x and Force_y, respectively. The cogging force and force ripples of the SMLG are very low, a vital criteria for preventing the damage of bearings and related moving accessories. The generated voltage, current and power of the SMLG are shown in 8–10 for the translator velocity of 1 m/s, air gap length of 1 mm and a resistive load of 3 Ω.

The superconductor (SC) can also improve the performance of a flux switching PMLG (FSPMLG). The FSPMLG design has been newly optimized and simulated both for copper conductor (CC) and SC. In the previously and newly optimized FSPMLG, ordinary CC has been used in the stator windings. Due to the internal resistance of the CC there are some voltage drops across the copper coils, which results loading effect power loss. Application of the SC can resolve these problems as CC has no internal resistance. The comparison of the terminal voltages, currents, and powers of the FSPMLG are shown in Figs. 4.8, 4.9 and 4.10, respectively.

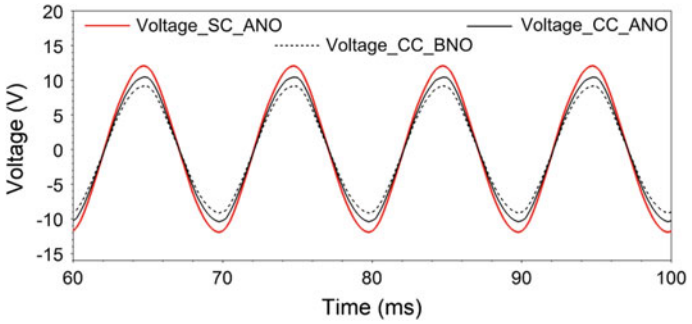

Fig. 4.8 Comparisons of the terminal voltages

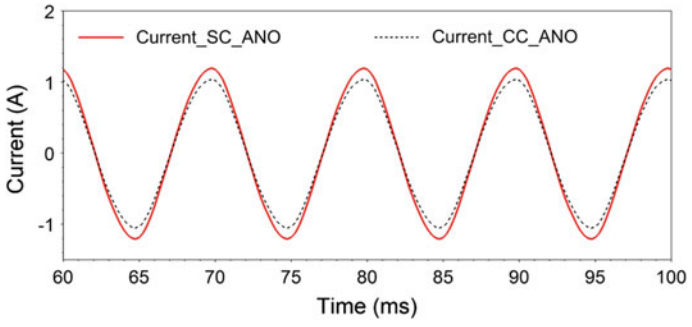

Fig. 4.9 Comparisons of the load currents

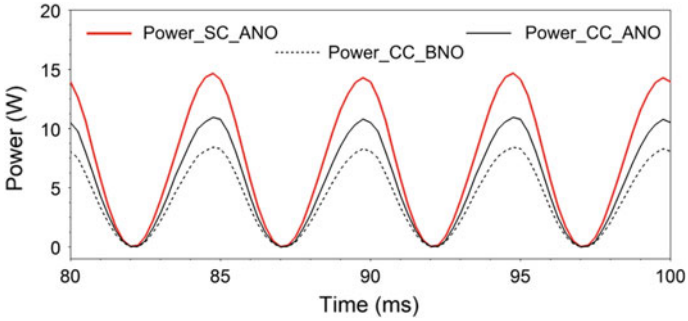

Fig. 4.10 Comparisons of the output powers

In Fig. 4.8, Voltage_SC_ANO represents the terminal voltage for using SC in the stator coil after newly optimization has been carried out. Voltage_CC_ANO represents the terminal voltage for using CC and new optimization. Voltage_CC_BNO stands for the terminal voltage for using CC and before new optimization.

In Fig. 4.9, Current_SC_ANO and Current_CC_ANO represent the load currents for using SC and CC, respectively in the stator coil after newly optimization has been carried out. In Fig. 4.10, Power_SC_ANO represents the output power for using SC in the stator coil after newly optimization has been accomplished. Power_CC_ANO and Power_CC_BNO represent the output powers of the FSPMLG before and after newly optimization have been done, respectively. Simulation results show that using of SC (second generation high temperature superconductor) instead of CC improves the performance of the newly optimized FSPMLG noticeably.

4.6 High Power Density LG

In the conventional LG, the existence of cogging force that requires structural mass and complicated design makes the generator to heavy, therefore, the weight is very large [30–32]. A number of linear generator technologies developed in small-scale rating are summarized in Table 4.1 that represents the weight per kW power generation of different LG.

Table 4.1 Power densities of some of the conventional LGs

Type of the LG	Power density (Kg/kW)
Columbia PT. iron cored LG [31]	1878.13
Spar and Float iron cored LG [33]	1446
Multi-phase air cored LG [34]	351.42
Novel topology air cored LG [31]	256.5

If, m is the mass of an object, ρ is the density of the object and h is the height then, the potential energy, $E_p = mgh = \rho Vgh$, but, for the ocean wave the volume of the water changes with time. The potential energy of the oceanic wave, E_{pw} depends on the volume and height of the sea water and the volume depends on. The wave energy flux or wave power per unit of wave-crest length, P_w can be calculated from:

$$p_w = \frac{\rho g^2}{64\pi} H_w^2 T \cong \left(0.5 \frac{kW}{m^3 s}\right) H_w^2 T = 0.5 H_w^2 T \frac{kW}{m} \tag{6}$$

The above formula states that, wave power is proportional to the wave energy period and to the square of the amplitude of the sea wave [35, 36]. When the significant wave height is given in meters, and the wave period in seconds, the result is the wave power in kilowatts (kW) per meter of wave-front length. The energy of a horizontal area depends mainly on the wave height for a particular location. In that case, ρ and g may be considered constant. For the horizontal surface of 1 m^2, the total energy per unit area (1 m^2) can be expressed as:

$$E_W = \frac{1}{8} \rho g H_w^2 = \frac{1}{2} \rho g A_w^2 \tag{7}$$

which indicates that, according to the linear wave theory, the average energy density per unit area of gravity waves on the water surface is proportional to the wave height squared. If, T is the wave energy period, then the wave power, P_w per unit horizontal area (1 m^2) can be calculated from $P_w = \frac{E_w}{T}$. Therefore, considering 1 m of wave height and 5 s of time period, the oceanic wave surface has the potential of approximately 1 kW/1 m^2 for the specific gravity of 1.025 of sea water. This high energy potential can be coped with the higher power density of LG mounted to a point absorber type PTO system.

4.6.1 Construction of the High Power Density LG

The proposed high power density PMLG (HPDPMLG) contains some PMs in the stator situated both sides of the translator as shown in Fig. 4.11. The North Pole (N) and the South Pole (S) of the PM are facing to the pole shoe of red and green colors, respectively. Copper coils are wounded on the steel cores. The dashed red, blue, and green rectangles represent phase-A, phase-B, and phase-C, respectively that are basically the translator part. The dimension and some parameters of the PMLG are given in Table 4.2.

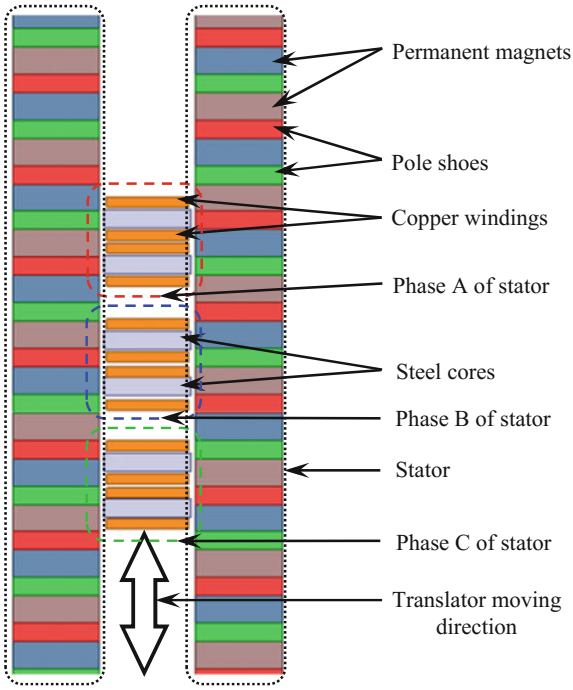

Fig. 4.11 Cross sectional view of the HPDPMLG

Table 4.2 Parameters of the HPDPMLG

Name of the item	Value
Translator and stator pitch (mm)	21
Width of the translator (mm)	40
Width of the stator (mm)	40
Pitch factor of pole shoe	0.381
Turn number of copper coil (turns)	50
Number of coils in a winding	2
Cross section of the conductor (mm^2)	2.5
Winding factor	0.6
Depth of the PMLG (m)	0.1
Width of the PMLG (mm)	124
Thickness of PM (mm)	13
Width of PM and Pole shoe (mm)	40
Thickness of pole shoe (mm)	8
Ratio of translator and stroke length	2
Velocity/speed of the translator (m/s)	0.5–2
Air gap length (mm)	1.5–3.5
Internal resistance of windings (Ω)	0.2
Load resistance (Ω)	2–5

4.6.2 Working Principle of the HPDPMLG

The PMs, pole shoes, air gaps, and the direction of induced current through the conductor are shown in Fig. 4.12. The working principle of the proposed generator can be realized from Figs. 4.12 and 4.13. As the translator is moving vertically with the oceanic wave, therefore the position of the translator varies and the direction of magnetic flux changes.

If the movement of the translator is considered upward direction, the position of the translator changes as in Fig. 4.13 from the position according to that shown in Fig. 4.12. Hence, the magnetic flux direction according to Fig. 4.12 is opposite for the translator position as in Fig. 4.13. Therefore, directions of the induced current through the conductor are opposite to each other and thus ac voltage is induced in this conductor.

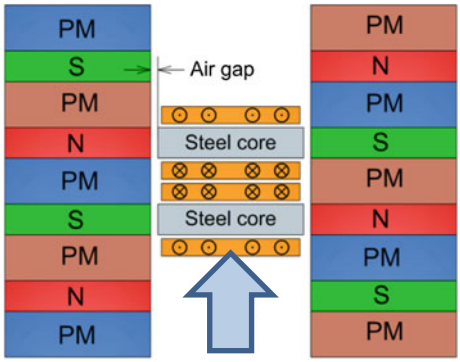

Fig. 4.12 Direction of current induced in the HPDPMLG's coil for a particular time

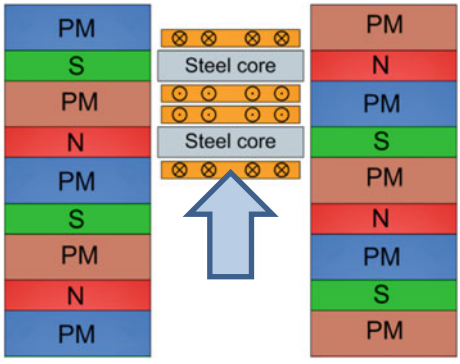

Fig. 4.13 Direction of current induced in the HPDPMLG's coil after some intervals

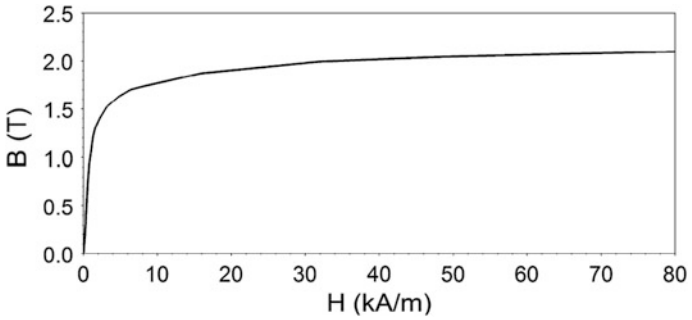

Fig. 4.14 Magnetization curve of the steel core

4.6.3 Selection of Materials for the HPDPMLG

NdFeB PMs with magnetic coercivity of 835 kA/m, remanence of 1.132 T, and relative permeability of $\mu_r = 1.044$ are used in the proposed PMLG, to produce magnetic flux and the winding coils are made of copper conductors. The commonly used steel core is selected for stator and translator which is of high magnetic saturation point, available, and low cost. The magnetization curve of the steel core used in the PMLG is given in Fig. 4.14.

4.6.4 Equivalent Circuit Diagram of the HPDPMLG

The equivalent circuit diagrams of the proposed HPDPMLG for Δ-connected and Y-connected loads are shown in Figs. 4.15 and 4.16, respectively.

The equivalent series resistance of each phase is considered equal and denoted by R_a. E_a, E_b, and E_c, represent the generated voltages of phase-A, phase-B,

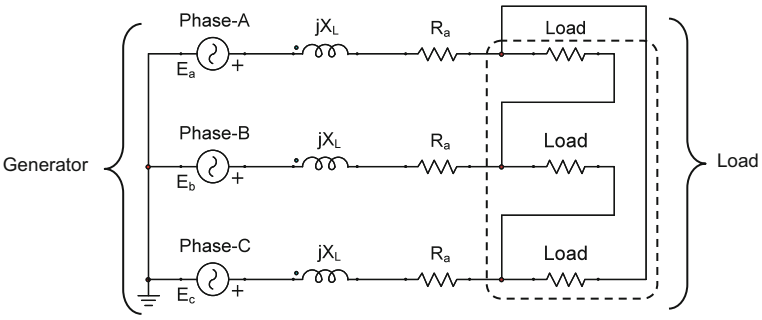

Fig. 4.15 Equivalent circuit diagram of the HPDPMLG for the Δ-connected load

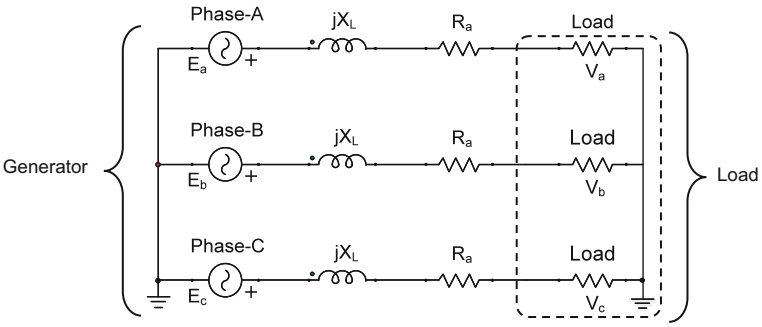

Fig. 4.16 Equivalent circuit diagram of the HPDPMLG for the Y-connected load

and phase-C, respectively. The magnetic excitation is fed from the PM array as shown in Fig. 4.16. Terminal voltages are measured across the load.

4.6.5 EMF Equations and Vector Diagram

According to Fig. 4.16 the emf equations may be represented as

$$E_a = R_a i_a + L_s \frac{di_a}{dt} + v_a \tag{8}$$

$$E_b = R_b i_b + L_s \frac{di_b}{dt} + v_b \tag{9}$$

$$E_c = R_c i_c + L_c \frac{di_c}{dt} + v_c \tag{10}$$

where v_a, v_b, and v_c are the terminal voltages, i_a, i_b, and i_c are line currents, L_s is synchronous reactance. On the other hand, the induced voltages depend on the translator velocity. Therefore, the voltage induced per phase winding, e_Φ may be expressed as:

$$e_\Phi = K_E \cos\left(\frac{\pi}{\tau} z\right) v(t) \tag{11}$$

where K_E, is the voltage constant depends on the number of turns per coil, the air gap flux density, common depth of the stator and translator and average velocity or speed of the translator; τ is the pole pitch, z is the vertical displacement, and $v(t)$ is the translator velocity. The vector diagram of the PMLG connected to a resistive load is shown in Fig. 4.17. The angle between the induced voltage and terminal

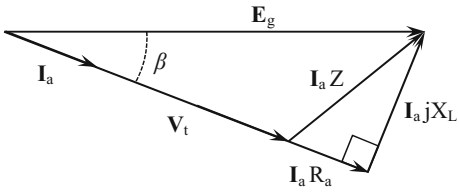

Fig. 4.17 Vector diagram of the HPDPMLG for a resistive load

voltage is denoted by β. The induced voltages per winding per phase of the proposed three phase generator may be written as follows.

$$E_a = e_\Phi = K_E \cos\left(\frac{\pi}{\tau} z\right) v(t) \tag{12}$$

$$E_c = K_E \cos\left(\frac{\pi}{\tau} z - \frac{2\pi}{3}\right) v(t) \tag{13}$$

$$E_c = K_E \cos\left(\frac{\pi}{\tau} z - \frac{2\pi}{3}\right) v(t) \tag{14}$$

4.6.6 Simulation Results of the HPDPMLG

The PMLG design is represented using 3-D Cartesian coordinate system in this simulation. The applied force is denoted by Force_z working along z-axis, so, the translator moves along z-axis as shown in Fig. 4.18.

The width and depth of this design are along y-axis and x-axis, respectively. Cogging forces are working along y-axis and is denoted by Force_y. To generate electricity it is needed to apply force along z-axis and during the operation Force_x and Force_y are generated which is of no use. Therefore, they are the force components and should be maintained to a possible lower value.

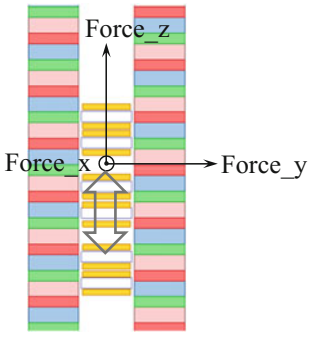

Fig. 4.18 Direction of different forces of the HPDPMLG

4.6.7 Variation of Load of the HPDPMLG

The induced voltage and current in a winding for a 4 Ω load, 2 mm air gap length, and 1 m/s translator speed are shown in Fig. 4.19. The induced voltage and currents are in opposite phases. The terminal voltage, load current, and power of the HPDPMLG for the same load and air gap length are shown in Fig. 4.20. The terminal voltage and current are in phases due to the resistive load. The applied force and magnetic flux linkage of the HPDPMLG for the same load and air gap length are shown in Fig. 4.21.

As the generated voltage is almost sinusoidal, the waveform of applied force and magnetic flux are also sinusoidal. The load currents and powers of the HPDPMLG for 2, 3, and 5 Ω loads are shown in Figs. 4.22 and 4.23, respectively. With the increase in load, the value of current and power are increased.

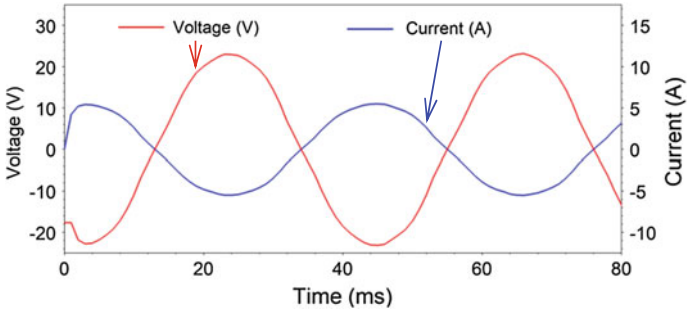

Fig. 4.19 Induced voltage and current waveforms of the HPDPMLG

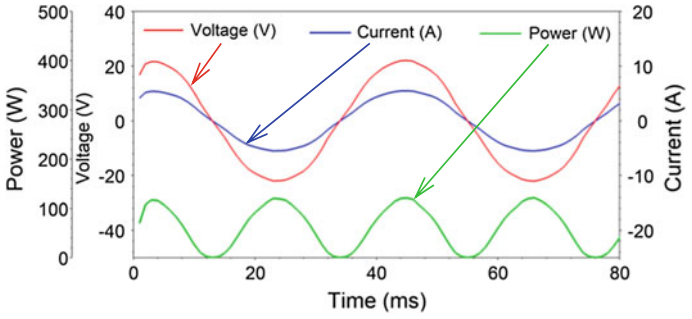

Fig. 4.20 Voltage, current, and instantaneous power of the HPDPMLG

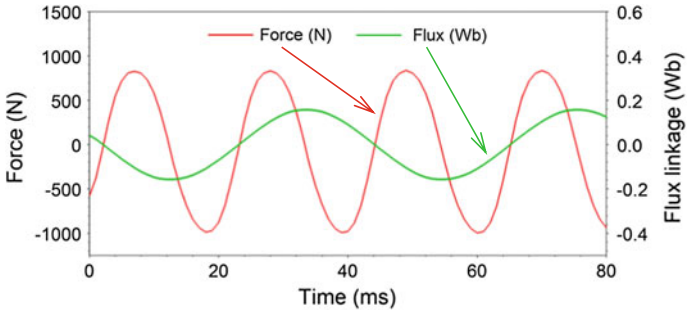

Fig. 4.21 Force and flux linkage of the HPDPMLG

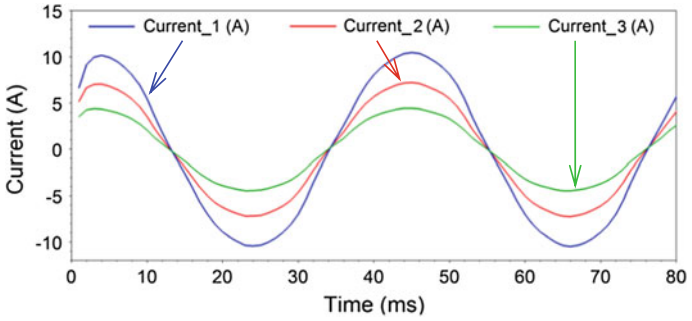

Fig. 4.22 Current waveforms of the HPDPMLG

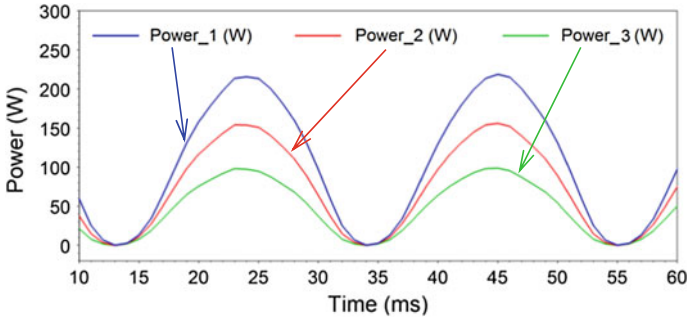

Fig. 4.23 Generated powers of the HPDPMLG

4.6.8 Variation of the Air Gap Length

The terminal voltage and current in a winding for a 3 Ω load, 3 mm air gap length and 1 m/s translator speed are shown in Fig. 4.24. The terminal voltage, current,

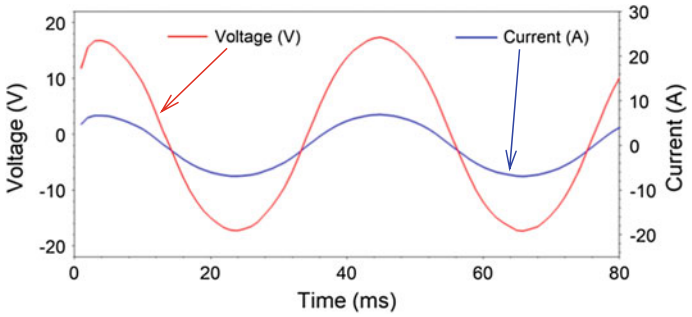

Fig. 4.24 Terminal voltage and load current of the HPDPMLG

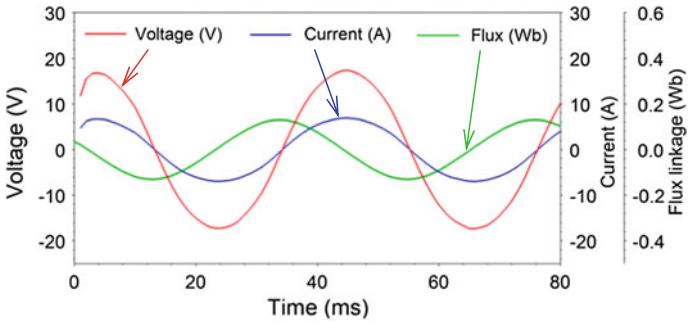

Fig. 4.25 Voltage, current, and flux linkage of the HPDPMLG

and flux for the same condition are shown in Fig. 4.25. The applied force and force components for the same condition are shown in Fig. 4.26. The terminal voltages, load currents and powers are tabulated in Tables 4.3, 4.4 and 4.5, respectively for different air gap lengths. These tables show numerical values of peak to peak, rms, and period of the voltage, current and power waveforms for different air gap

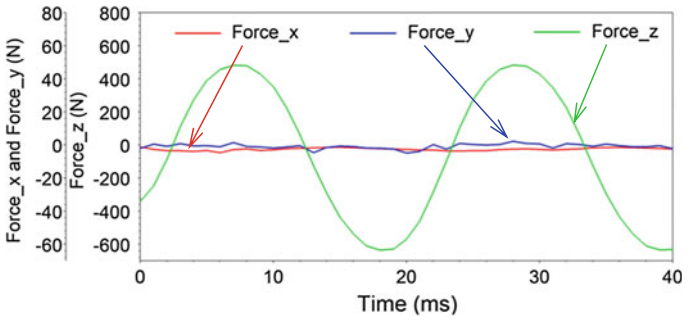

Fig. 4.26 Different forces of the HPDPMLG

Table 4.3 RMS voltages of the HPDPMLG for different air gaps

Legend name	Air gap (mm)	RMS value (V)	Peak to peak (V)	Period (ms)
Voltage_1	1.5	16.4634	46.151	42.0127
Voltage_2	2	17.7229	51.1591	41.9883
Voltage_3	2.5	14.9847	41.4976	41.9883
Voltage_4	3	13.4612	37.41	42.0127
Voltage_5	3.5	12.0443	33.7957	41.9883

Table 4.4 Numerical values of currents of the HPDPMLG for different air gaps

Legend name	Air gap (mm)	RMS value (A)	Peak to peak (A)	Period (ms)
Current_1	1.5	6.5487	18.9478	41.9355
Current_2	2	6.0838	17.0929	38.0557
Current_3	2.5	5.5376	15.3695	38.1045
Current_4	3	4.9746	13.8555	38.129
Current_5	3.5	4.4508	12.5169	38.129

Table 4.5 Generated powers of the HPDPMLG for different air gaps

Legend name	Air gap (mm)	RMS value (W)	Peak to peak (W)	Period (ms)
Power_1	1.5	134.5276	224.5864	21.0029
Power_2	2	113.4839	182.6241	20.9932
Power_3	2.5	92.8963	147.8794	21.0225
Power_4	3	74.8811	120.1866	21.0029
Power_5	3.5	60.2209	98.1558	21.0127

lengths. The terminal voltage, load current, and generated power decrease with increase in air gap length. The waveforms of the terminal voltages, load currents and powers quantified in Tables 4.3, 4.4 and 4.5 are illustrated in Figs. 4.27, 4.28 and 4.29, respectively.

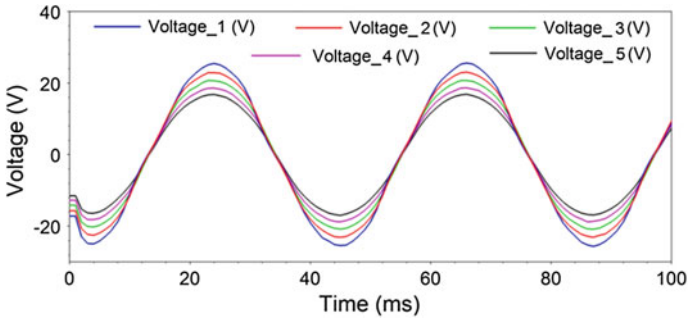

Fig. 4.27 Voltage waveforms of the HPDPMLG for different air gaps

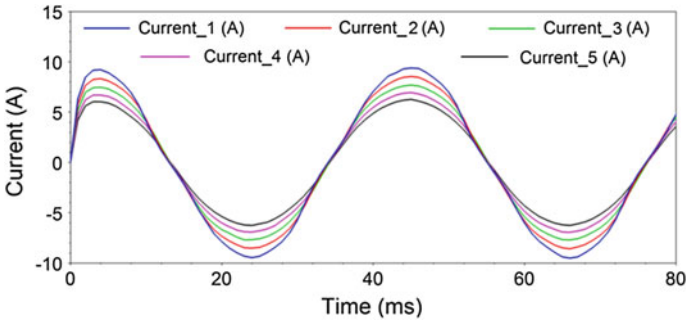

Fig. 4.28 Current waveforms of the HPDPMLG for different air gaps

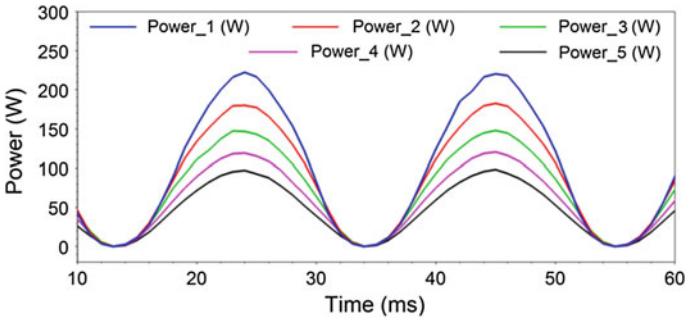

Fig. 4.29 Generated powers of the HPDPMLG for different air gaps

4.6.9 Variation of Translator Speed

The terminal voltage and load current in a winding for a 2.5 Ω load, 2 mm air gap length and 0.75 m/s translator speed are shown in Fig. 4.30 and the generated

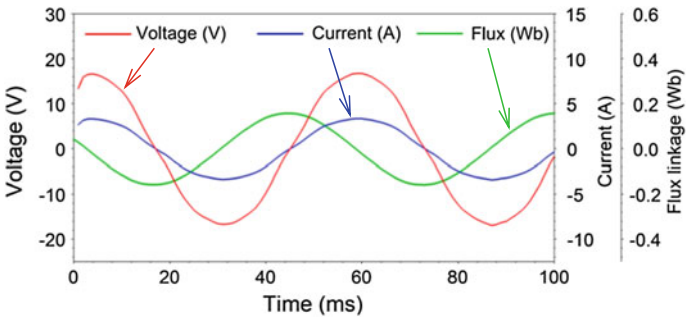

Fig. 4.30 Voltage, current, and flux linkage of the HPDPMLG for 0.75 m/s speed

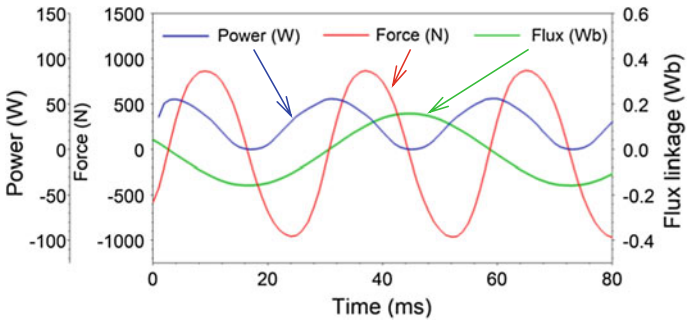

Fig. 4.31 Power, force, and flux linkage of the HPDPMLG for 0.75 m/s speed

Table 4.6 Terminal voltages of the HPDPMLG for different translator's speeds

Legend name	Speed (m/s)	RMS value (V)	Peak to peak (V)	Period (ms)
Voltage_1	0.5	8.2455	23.1818	84.0254
Voltage_2	0.75	11.8908	35.3018	56.0073
Voltage_3	1	16.7929	46.463	42.0147
Voltage_4	1.25	20.9472	57.7374	33.602
Voltage_5	1.5	25.089	69.3107	28.0079
Voltage_6	2	33.2258	91.3839	21.0012

Table 4.7 Load currents of the HPDPMLG for different translator's speeds

Legend name	Speed (m/s)	RMS value (A)	Peak to peak (A)	Period (ms)
Current_1	0.5	1.5807	4.458	76.3045
Current_2	0.75	2.284	6.7888	53.4895
Current_3	1	3.2243	8.9352	42.0059
Current_4	1.25	4.0202	11.1034	32.1449
Current_5	1.5	4.8134	13.329	27.9952
Current_6	1.75	5.5662	15.4615	23.0015
Current_7	2	6.3687	17.5738	20.1416

Table 4.8 Numerical value of powers for different translator's speeds

Legend name	Speed (m/s)	RMS value (W)	Peak to peak (W)	Period (ms)
Power_1	0.5	8.9438	24.8715	41.9941
Power_2	0.75	20.8328	57.7811	27.9982
Power_3	1	35.0388	100.2655	20.9969
Power_4	1.25	54.4378	154.5444	16.7959
Power_5	1.5	78.7741	226.5885	13.5302
Power_6	1.75	106.0557	303.2046	11.5974
Power_7	2	139.6225	393.0912	10.1399

Table 4.9 Magnetic flux linkages of the HPDPMLG for different translator's speeds

Legend name	Speed (m/s)	RMS value (Wb)	Peak to peak (Wb)	Period (ms)
Flux linkage_1	0.5	0.1112	0.3152	84.0665
Flux linkage_2	1	0.1104	0.3149	42.0024
Flux linkage_3	1.5	0.1092	0.3139	28.0079
Flux linkage_4	2	0.1093	0.3129	21.0012

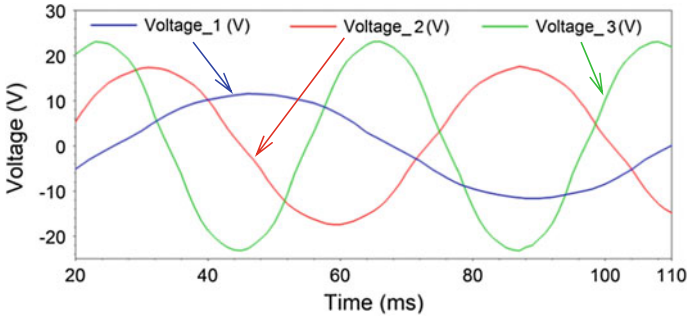

Fig. 4.32 Generated voltages of the HPDPMLG for 0.5, 0.75, and 1 m/s speeds

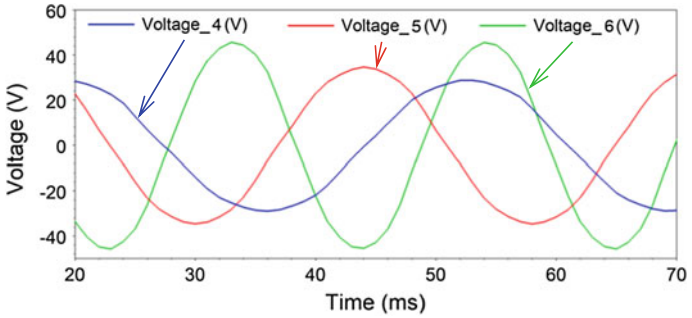

Fig. 4.33 Generated voltages of the HPDPMLG for 1.25, 1.5, and 2 m/s speeds

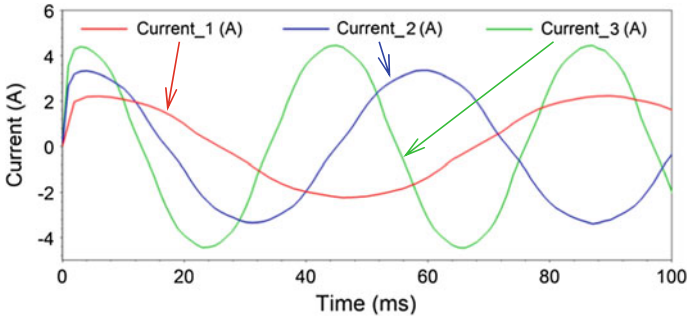

Fig. 4.34 Current waveforms of the HPDPMLG for 0.5, 0.75, and 1 m/s speeds

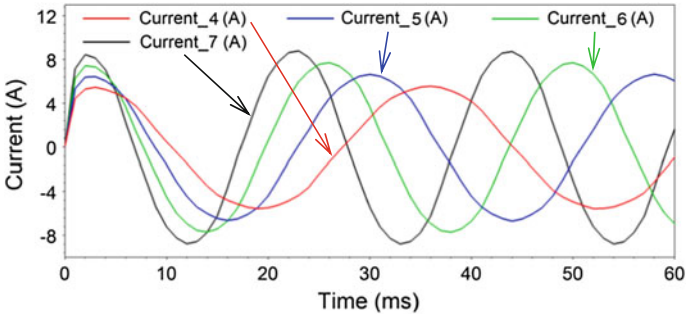

Fig. 4.35 HPDPMLG's current waveforms for 1.25, 1.5, 1.75, and 2 m/s speeds

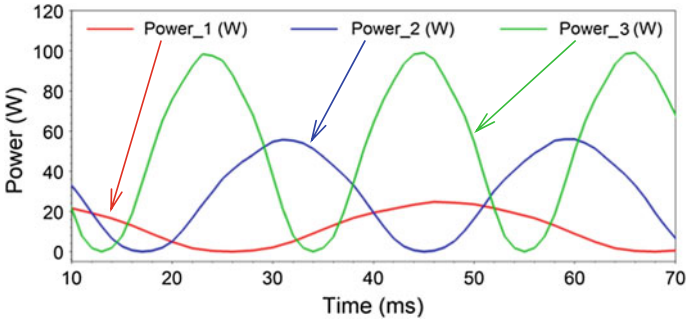

Fig. 4.36 Generated powers of the HPDPMLG for 0.5, 0.75, and 1 m/s speeds

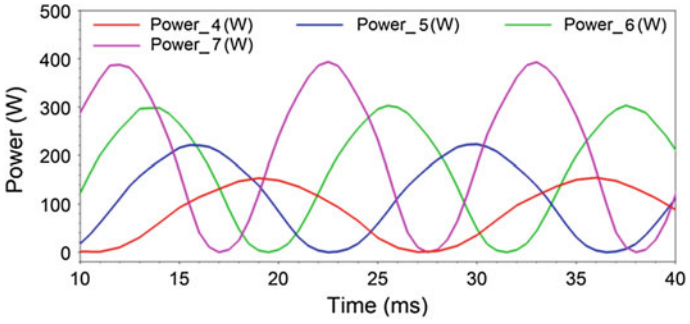

Fig. 4.37 Generated powers of the HPDPMLG for 1.25, 1.5, 1.75, and 2 m/s speeds

power, force, and flux for the same condition are shown in Fig. 4.31. Tables 4.6, 4.7, 4.8 and 4.9 represent simulated results of the voltage, current, power, and magnetic flux linkage, respectively, for different speeds/velocity of the translator. The induced voltage waveforms for different translator speeds are shown in

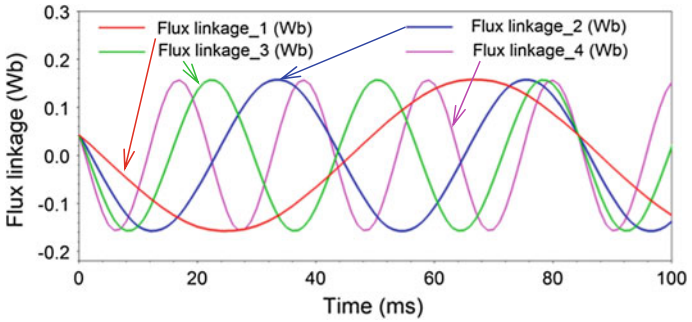

Fig. 4.38 Flux linkages of the HPDPMLG for 0.5, 1, 1.5, and 2 m/s speeds

Figs. 4.32 and 4.33. The currents for different translator speeds are shown in Figs. 4.34 and 4.35. The instantaneous powers for different translator speeds are shown in Figs. 4.36 and 4.37. The magnetic flux linkages for different speeds are shown in Fig. 4.38.

4.7 Summary

In order to improve the WEC system, there is no other alternative without chronological progress of the existing generators. Modern LGs play an important role in eliminating the additional mechanical gear arrangement. Thus the WEC systems incorporating LGs using DDS are advantageous and more feasible in economic aspect. Optimization methods are very important for generation of more electrical power for the same LG which were represented in [37, 38]. Simulation results show that, LGs can effectively generate electrical power even at lower velocity of rising and falling water surface. Moreover, new implementation of superconductor and SMs in the LG opens a new opportunity in developing WEC system. Use of SMs helps to make the LG compact and of high power density. Finally, using the HPDPMLG, more electrical power generation with less PMLG size is possible. Various characteristics of the HPDPMLG are shown in detail in the simulation results. The simulation results represented in this chapter is highly consistent with the ANSYS/Ansoft and MATLAB/Simulink software packages.

References

1. Vermaak R, Kamper MJ (2012) Design aspects of a novel topology air-cored permanent magnet linear generator for direct drive WECs. IEEE Trans Ind Electron 59(5):2104–2115
2. Wu F, Zhang XP, Ju P, Sterling MJH (2008) Modeling and control of AWS based wave energy conversion system integrated into power grid. IEEE Trans power Systems 23(3): 1196–1204

3. Cruz J (2008) Ocean wave energy: current status and future perspectives. Springer, Berlin, Heidelberg, Springer Series in Green Energy and Technology, ISBN 978-3-540-74894-6, ISSN 1865–3529
4. EPRI (2011) Mapping and assessment of the United States ocean wave energy resource. Palo Alto, CA
5. Chuankun W, Shi W (2008) The ocean resources and reserves evaluation in China. In: 1st National symposium on ocean energy, Hangzhou, China, pp 169–179
6. Seabased group [Online]. Available at: http://hornonline.com/seabased-group. Accessed on 24 July 2017
7. Henderson R (2006) Design, simulation, and testing of a novel hydraulic power take-off system for the Pelamis wave energy converter. Renew Energy 31(1):271–283
8. Kofoed JP, Frigaard P, Friis-Madsen E, Sorensen HC (2006) Prototype testing of the wave energy converter wave dragon. Renew Energy 31(2):181–189
9. O'Sullivan DL, Lewis AW (2011) Generator selection and comparative performance in offshore oscillating water column ocean wave energy converters. IEEE Trans Energy Convers 26(2):603–614
10. Polinder H, Damen MEC, Gardner F (2004) Linear PM generator system for wave energy conversion in the AWS. IEEE Trans Energy Convers 19(3):583–589
11. Nasiri A, Zabalawi SA, Jeutter DC (2011) A linear permanent magnet generator for powering implanted electronic devices. IEEE Trans Power Electron 26(1):192–199
12. Farrok O, Ali MM (2014) A new technique to improve the linear generator designed for oceanic wave energy conversion. In: International conference on electrical and computer engineering, Bangladesh, pp 714–717
13. Zhao SW, Cheung NC, Gan W, Yang J (2010) High-precision position control of a linear-switched reluctance motor using a self-tuning regulator. IEEE Trans Power Electron 25(11):2820–2827
14. Prudell J, Stoddard M, Amon E, Brekken TKA, Jouanne A (2010) A permanent-magnet tubular linear generator for ocean wave energy conversion. IEEE Trans Ind Appl 46(6):2392–2400
15. Farrok O, Islam MR, Sheikh MRI (2015) Fuzzy logic based an improved controller for wave energy conversion systems. In: International conference on electrical engineering and information communication technology, Bangladesh, pp 1–6
16. Ceballos S, Rea J, Lopez I, Pou J, Robles E, O'Sullivan DL (2013) Efficiency optimization in low inertia Wells turbine-oscillating water column devices. IEEE Trans Energy Convers 28 (3):553–564
17. Oscillating water column [Online]. Available at: http://owc-wec.weebly.com/oscillating-water-columns.html. Accessed on 24 July 2017
18. Sabzehgar R, Moallem M (2009) A review of ocean wave energy conversion systems. In: Electrical power and energy conference, pp 1–6
19. O'Sullivan DL, Lewis AW (2011) Generator selection and comparative performance in offshore oscillating water column ocean wave energy converters. IEEE Trans Energy Convers 26(2):603–614
20. Nasiri A, Zabalawi SA, Jeutter DC (2011) A linear permanent magnet generator for powering implanted electronic devices. IEEE Trans Power Electron 26(1):192–199
21. Pan JF, Zou Y, Cheung N, Cao G (2014) On the voltage ripple reduction control of the linear switched reluctance generator for wave energy utilization. IEEE Trans Power Electron 29(10): 5298–5307
22. Cheun C (2011) Supervisory interval type-2 TSK neural fuzzy network control for linear microstepping motor drives with uncertainty observer. IEEE Trans Power Electron 26(7): 2049–2064
23. Farrok O, Islam MR, Sheikh MRI (2016) Analysis of the oceanic wave dynamics for generation of electrical energy using a linear generator. J Energy 3437027:14. https://doi.org/10.1155/2016/3437027

24. Farrok O, Islam MR, Sheikh MRI, Guo YG, Zhu JG, Xu W (2015) Analysis and design of a novel linear generator for harvesting oceanic wave energy. In: IEEE international conference on applied superconductivity and electromagnetic devices, Shanghai, China, pp 272–273. https://doi.org/10.1109/ASEMD.2015.7453569
25. Farrok O, Sheikh MRI, Islam MR (2015) An advanced controller to improve the power quality of microgrid connected converter. In: International conference on electrical and electronic engineering, Rajshahi, Bangladesh, pp 185–188. https://doi.org/10.1109/CEEE.2015.7428251
26. Lockheed Backs World's Largest Wave Energy Project. Available at https://www.forbes.com/sites/williampentland/2014/02/11/lockheed-backs-worlds-largest-wave-energy-project/#36120f5849d1. Accessed on 24 July 2017
27. Brooking PRM, Mueller MA (2005) Power conditioning of the output from a linear vernier hybrid permanent magnet generator for use in direct drive wave energy converters. Proc Inst Elect Eng Gener Transm Distrib 152(5):673–681
28. Wang J, Qu R, Liu Y, He J, Zhu Z, Fang H (2015) Comparison study of superconducting wind generators with HTS and LTS field windings. IEEE Trans Appl Supercond. 25(3) (art. 5201806)
29. Farrok O, Islam MR, Islam Sheikh MR, Guo Y, Zhu J, Xu W (2016) A novel superconducting magnet excited linear generator for wave energy conversion system. IEEE Trans Appl. Supercond 26(7) (art. 5207105)
30. Mueller MA, McDonald AS, Macpherson DE (2005) Structural analysis of low-speed axial-flux permanent-magnet machines. Elect Power Appl IEEE Proc 152(6):1417–1426
31. Vermaak R, Kamper MJ (2012) Design aspects of a novel topology air-cored permanent magnet linear generator for direct drive wave energy converters. IEEE Trans Industr Electron 59:2104–2115
32. Nilsson K, Danielsson O, Leijon M (2006) Electromagnetic forces in the air gap of a permanent magnet linear generator at no load. J Appl Phys 99(3) (art. 034505)
33. Prudell Joseph et al (2010) A permanent-magnet tubular linear generator for ocean wave energy conversion. IEEE Trans Ind Appl 46(6):2392–2400
34. Gargov NP, Zobaa AF (2012) Multi-phase air-cored tubular permanent magnet linear generator for wave energy converters. Renew Power Gener IET 6:171–176
35. Li Ye, Yi-Hsiang Yu (2012) A synthesis of numerical methods for modeling wave energy converter-point absorbers. Renew Sustain Energy Rev 16:4352–4364
36. Wolfbrandt A (2006) Automated design of a linear generator for wave energy converters—a simplified model. IEEE Trans Magn 42(7):1812–1819
37. Farrok O, Islam MR, Zhu J (2017) Stator tooth shape optimization of a permanent magnet linear generator for harvesting oceanic wave energy. Presented: 21st International conference on the computation of electromagnetic fields, Daejeon, Korea
38. Farrok O, Islam MR, Sheikh MRI, Xu W (2016) A new optimization methodology of the linear generator for wave energy conversion systems. In: IEEE international conference on industrial technology, Taipei, Taiwan, pp 1412–1417. https://doi.org/10.1109/ICIT.2016.7474965

Chapter 5
Wind Energy System with Matrix Converter

Kotb B. Tawfiq, A. F. Abdou and E. E. EL-Kholy

5.1 Introduction

Nowadays, there are more and more concerns over fossil fuel exhaustion and the environmental problems caused by fossil fuel based conventional power generation. To solve those problems renewable energy is widely accepted as one of the appropriate alternatives, in particular, the wind and the solar energies. Some load centers like ships, islands and remote villages require their own electric power supply like stand-alone electric generators for the excitation required for their local loads. These requirements encourage researchers to search and develop a method for providing the required excitation by a simple technique for longest time like renewable sources of energy. The significant favorable advantage of utilizing renewable sources is the absence of harmful emissions. The Wind Energy Conversion System (WECS) is bit-by-bit gaining interest as a suitable source of renewable energy. There are two types of Wind Turbine (WT): horizontal axis configuration and vertical axis configuration. A Squirrel Cage Induction Generator (SCIG) is preferable in isolated load application as it is cost-effective. The SCIG also has the ability to self-protection against short circuits and does not require routine maintenance. So, it is used to convert the captured mechanical energy from the WT into electrical energy. Different types of AC-AC power converters will be introduced in this chapter. A Matrix Converter (MC) is used to control the rms value and frequency of the load voltage. An indirect space vector modulation

K. B. Tawfiq (✉) · A. F. Abdou · E. E. EL-Kholy
Electrical Engineering Department, Faculty of Engineering, Menoufia University, Shebeen El-Kom, Egypt
e-mail: Kotbbasem29@yahoo.com

A. F. Abdou
e-mail: afathi82@yahoo.com

E. E. EL-Kholy
e-mail: e.e.el-kholy@ieee.org

M. R. Islam et al. (eds.), *Renewable Energy and the Environment*, Renewable Energy Sources & Energy Storage, https://doi.org/10.1007/978-981-10-7287-1_5

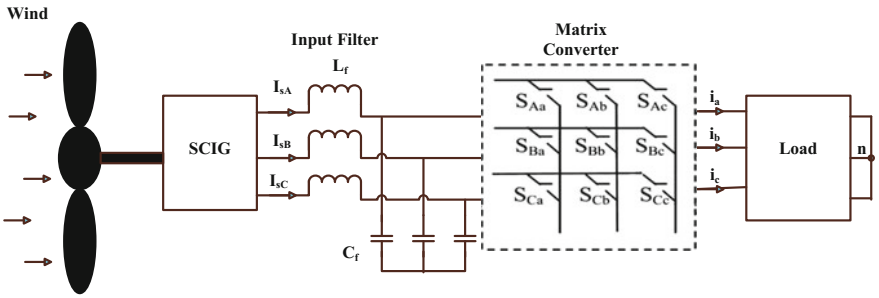

Fig. 5.1 Block diagram of matrix converter in wind energy system

(ISVM) technique will be introduced, in addition to showing how to transform from the indirect matrix converter to direct ones. Moreover, a modified algorithm for space vector modulation (SVM) will be introduced [1]. The advantage of the modified algorithm, as well as the ability of MC to give a wide range of output frequency, controlling the phase angle between the input current and voltage and achieving a unity input displacement factor will be discussed [2, 3]. A modified open loop controller for the SVM of MC provides output voltage and frequency with constant values even if the wind speed changes. Finally, experimental and simulation results are discussed for each part in this chapter (Fig. 5.1).

5.2 Wind Energy Conversion Systems

This part introduces a short description of WT types, WTs and SCIG's advantages, and disadvantages, characteristics and modeling.

5.2.1 Wind Turbine

The function of the wind turbine is transforming the wind kinetic energy into mechanical energy. A WT can spins about either a vertical or a horizontal axis. Therefore, there are two types of WT, the vertical axis and the horizontal-axis turbines.

5.2.1.1 Horizontal Axis–Wind Turbine

Figure 5.2a shows the construction of the horizontal-axis wind turbines (HAWTs). The electrical generator is at the top of the tower. To obtain a suitable speed to drive the electrical generator a gearbox must be used to turn the blades slower rotation

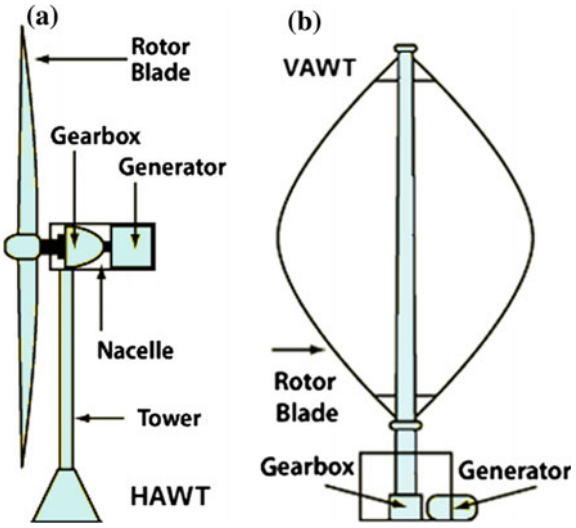

Fig. 5.2 **a** HAWT, **b** VAWT [1]

into quick rotation [2]. HAWTs have a tall tower base which enables to collect a large amount of energy compared to the short tower base. Every 10 meters up the ground, the wind speed increases by 20% and the output power increases by 34%. A HAWT has a variable blade pitch, which enable the blades of the turbine to have the optimum angle so that it can collect the maximum amount of wind energy. Moreover, it has a high efficiency, as the moving of the turbine blades is perpendicularly to the wind. The disadvantage of HAWT is the tower requires enormous construction so that it can hold the gearbox, generator and the heavy blades. Moreover, it has a high cost as it requires very tall and expensive cranes to carry the shaft of the turbine and the generator. HAWTs cause disrupting of the environmental landscapes due to their tall height. It affects radar installations and creating signal clutter due to the reflections from the tall tower. An additional control mechanism is required to turn the blades toward the wind [3, 4].

5.2.1.2 Vertical Axis–Wind Turbine

The rotor shaft of vertical-axis wind turbines (VAWTs) is arranged perpendicularly to the ground. The advantage of VAWT is it does not need an additional control mechanism to move the blades to the suitable side for the wind. The generator and gearbox are in the ground as shown in Fig. 5.2b. The advantage of that is making the maintenance process easy. The VAWT can install in different places such as highways and roofs. It has a low speed compared to HAWT and low speed means less noise. It does not kill wildlife and birds as it is more visible and has a low speed. The disadvantages of VAWTs are the lower efficiency compared to HAWTs, lower speed rotation because the turbine blades are near the ground and this does

not take the advantage of higher speed as in HAWT, so the output power in the VAWT is small compared to the HAWT [5–8].

5.2.1.3 Modelling of Wind Turbine

The produced mechanical power generated from the WT is calculated from Eq. (5.1).

$$P = \frac{1}{2}\rho C_p A_r v_w^3 \tag{5.1}$$

The power coefficient C_p depends on the rotor blade pitch angle β and the tip speed ratio λ according to Eq. (5.2)

$$C_p(\lambda, \beta) = 0.73\left(\frac{151}{\lambda_i} - 0.58\beta - 0.002\beta^{2.14} - 13.2\right) \tag{5.2}$$

$$\lambda_i = \frac{1}{\frac{1}{\lambda - 0.02\beta} - \frac{0.003}{\beta^3 + 1}} \tag{5.3}$$

$$\lambda = \frac{\omega_r R_r}{v_w} \tag{5.4}$$

where, P is the mechanical power, ρ is the density of air in g/m^3, A_r is the rotor area of WT in m^2, ($A_r = \pi R_r^2$, where R_r is the radius of rotor blade) and v_w is the wind speed in m/s. Figure 5.3 illustrates the calculated wind turbine power-speed characteristics at different wind speeds. Figure 5.4 shows the implementation of a wind turbine using MATLAB Simulink [3, 4].

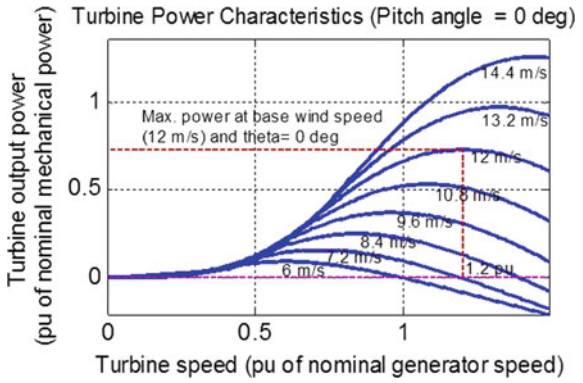

Fig. 5.3 Wind turbine power-speed characteristics

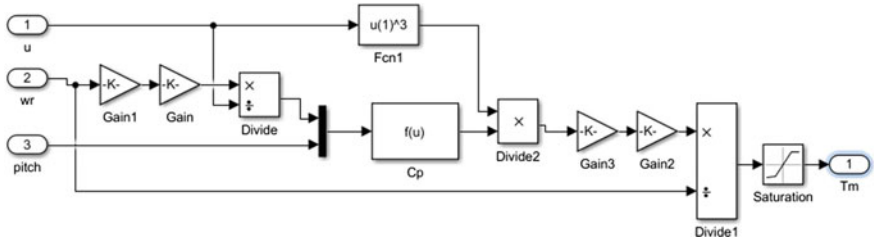

Fig. 5.4 Simulink model of wind turbine torque

5.2.1.4 Self-excited Induction Generator

The induction machine is a popular machine, which may be utilized as a motor or generator. An induction machine will generate electrical power if it is driven at a speed slightly above its synchronous speed while being connected to the supply. This part introduces principles of operation of the induction machine, equivalent circuit, torque-speed characteristics and torque equation. The value of the generated voltage is dependent on the value of the capacitance required to provide reactive power for the excitation [3, 5]. The SCIG is suitable for isolated operation due to its ruggedness, low cost of construction, less maintenance, and it is an inexpensive alternative to synchronous ones. For an isolated generation in remote areas, a variable capacitor is required to build up the voltage in a SCIG [3].

5.2.1.5 Excitation Method

Induction motors and generators require reactive power for their excitation. They can take the required reactive power for excitation from the grid if they are grid connected. An induction generator usually used to supply the remote loads that are not connected to the grid, and the generator can take the required reactive power for excitation from a capacitor bank. Due to the residual magnetism, when the rotor speed increases above synchronous speed, small voltage and current will be produced in the capacitors that are connected to the terminal of the stator. The function of the capacitor bank is to provide the reactive power required for excitation in addition to the reactive power needed for the load. The suitable value for the capacitor bank required for SCIG was calculated as described in [2] (Fig. 5.5).

5.2.1.6 Modeling of Induction Generator

All electrical machines can be expressed by the same equation sets regardless they operate as motors or generators. These equations can be divided in two groups;

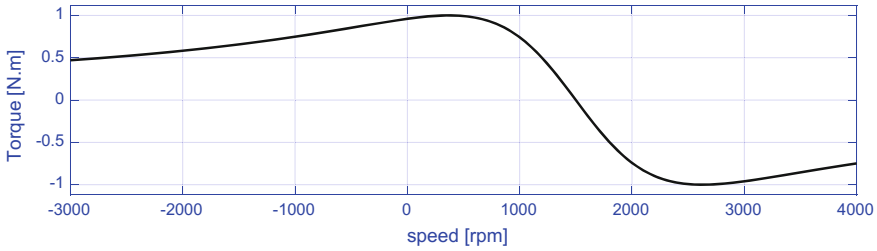

Fig. 5.5 Torque-speed characteristics for induction machine

torque equations and voltage equations. The following assumption is used to deal with the machine equations: neglecting the saturation of iron [6], the magnetic permeability of iron is assumed to be infinitely compared to the air gap permeability, which means that the magnetic flux is radial to the gap. Neglecting all iron losses, symmetric and balanced three-phase induction machine and constant air gap, stator and rotor windings represent distributed windings that always generate a sinusoidal magnetic field distribution in the gap.

All the explained hypotheses enable to use the following set of equations which describe the dynamic behavior of the induction machine [7, 8].

$$\begin{Bmatrix} V_s^{abc} \\ V_r^{abc} \end{Bmatrix} = \begin{bmatrix} r_s^{abc} & 0 \\ 0 & r_r^{abc} \end{bmatrix} \begin{Bmatrix} i_s^{abc} \\ i_r^{abc} \end{Bmatrix} + \frac{d}{dt} \begin{Bmatrix} \lambda_s^{abc} \\ \lambda_r^{abc} \end{Bmatrix} \tag{5.5}$$

where, V_s^{abc} is the voltage vector of stator's winding, V_r^{abc} is voltage vector of rotor's winding, i_s^{abc} is current vector of stator's winding, i_r^{abc} is current vector of rotor's winding, λ_s^{abc} is stator's winding flux linkage vector, λ_r^{abc} is rotor's winding flux linkage vector. r_s^{abc} and r_r^{abc} are the resistance vectors of stator's and rotor's windings. The flux linkage can be described as a function of stator and rotor currents as given in Eq. (5.6) (Fig. 5.6).

$$\begin{Bmatrix} \lambda_s^{abc} \\ \lambda_r^{abc} \end{Bmatrix} = \begin{bmatrix} L_{ss}^{abc} & L_{sr}^{abc} \\ L_{rs}^{abc} & L_{rr}^{abc} \end{bmatrix} \begin{Bmatrix} i_s^{abc} \\ i_r^{abc} \end{Bmatrix} \tag{5.6}$$

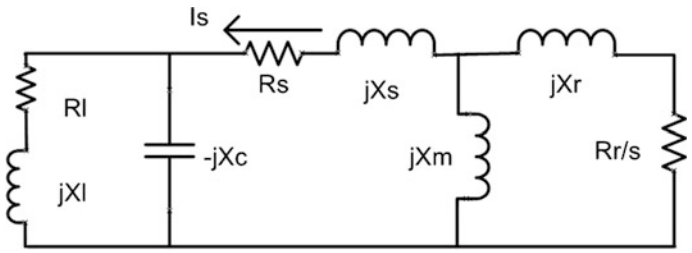

Fig. 5.6 One-phase equivalent circuit of induction generator

where, each term represents a 3-dimensional matrix or a three-dimensional vector. The vector can be described as:

$$
\begin{aligned}
V_s^{abc} &= \begin{bmatrix} v_{sa} \\ v_{sb} \\ v_{sc} \end{bmatrix}, \quad V_r^{abc} = \begin{bmatrix} v_{ra} \\ v_{rb} \\ v_{rc} \end{bmatrix}, \quad i_s^{abc} = \begin{bmatrix} i_{sa} \\ i_{sb} \\ i_{sc} \end{bmatrix}, \quad i_r^{abc} = \begin{bmatrix} i_{ra} \\ i_{rb} \\ i_{rc} \end{bmatrix} \\
L_{ss}^{abc} &= \begin{bmatrix} L_{ss}+L_{ls} & L_{sm} & L_{sm} \\ L_{sm} & L_{ss}+L_{ls} & L_{sm} \\ L_{sm} & L_{sm} & L_{ss}+L_{ls} \end{bmatrix}, \quad r_s^{abc} = \begin{bmatrix} r_s & 0 & 0 \\ 0 & r_s & 0 \\ 0 & 0 & r_s \end{bmatrix} \\
L_{rr}^{abc} &= \begin{bmatrix} L_{rr}+L_{lr} & L_{rm} & L_{rm} \\ L_{rm} & L_{rr}+L_{lr} & L_{rm} \\ L_{rm} & L_{rm} & L_{rr}+L_{lr} \end{bmatrix}, \quad r_r^{abc} = \begin{bmatrix} r_r & 0 & 0 \\ 0 & r_r & 0 \\ 0 & 0 & r_r \end{bmatrix} \\
L_{sr}^{abc} &= \left\{L_{rs}^{abc}\right\}^t = L_{sr} \begin{bmatrix} \cos\theta_r & \cos\left(\theta_r + \frac{2\pi}{3}\right) & \cos\left(\theta_r - \frac{2\pi}{3}\right) \\ \cos\left(\theta_r - \frac{2\pi}{3}\right) & \cos\theta_r & \cos\left(\theta_r + \frac{2\pi}{3}\right) \\ \cos\left(\theta_r + \frac{2\pi}{3}\right) & \cos\left(\theta_r - \frac{2\pi}{3}\right) & \cos\theta_r \end{bmatrix}
\end{aligned}
\tag{5.7}
$$

where, L_{ss}: the stator winding self-inductance, L_{sm}: stator winding mutual inductance, L_{rr}: the rotor winding self-inductance, L_{rm}: rotor winding mutual inductance, L_{sr}: mutual inductance between stator and rotor winding maximum value, L_{ls}: stator winding leakage inductance, L_{lr}: rotor winding leakage inductance.

5.2.2 AC-AC Converter

An AC-AC converter can be classified into two groups as depicted in Fig. 5.7. The first group is an AC Voltage regulator which can control the rms value of voltage at a constant frequency. The second one is the frequency converter which can control the voltage rms in addition to control the frequency. The frequency converter can be

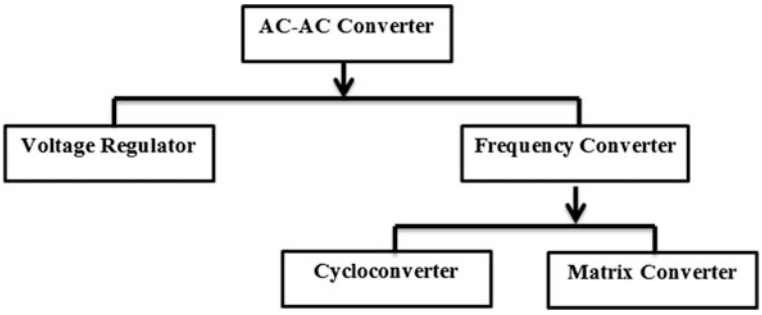

Fig. 5.7 AC-AC Converters

classified in two groups, firstly a cycloconverter which is a converter that has naturally commutation with the ability of bidirectional power flow and it does not have a limitation on its size like in SCR inverter with commutation elements. The cycloconverter main limitations are:

1. The range of frequency for sub harmonic-free with efficient operation is limited; and
2. Input displacement factor at low output voltages is poor.

The second one is the MC by which the output frequency can be controlled with values that may be equal, greater or less than the input frequency, in addition to, can control the rms value of the load voltage and. the phase angle between the input current and voltage as well as the value of the input displacement factor with a unity value could be achieved [9].

5.3 Matrix Converter

The MC is a set of a nine-bidirectional switches which help to connect the load directly with the three-phase input voltage with no need for any dc link. Therefore, it can be designed in a compact and simple form. The MC provides the advantage of power flow in both direction and the displacement factor at its input with a unity value can be provided. Also, it has minimal energy storage requirement, which permits to dispose of massive and lifetime-constrained capacitor, but the MC does not take its suitable place in the industry due to the disadvantages of the limited input output voltage transfer ratio which is 0.866 [10]. Because of the bi-directional switch, some MC types need more number of switches compared to the conventional rectifier inverter type [11]. Input filters are required to reduce the high frequency harmonics and clamping circuits are needed to protect switches from over voltages due to energy stored in inductive loads. The main structure of MC as shown in Fig. 5.8 consists of:

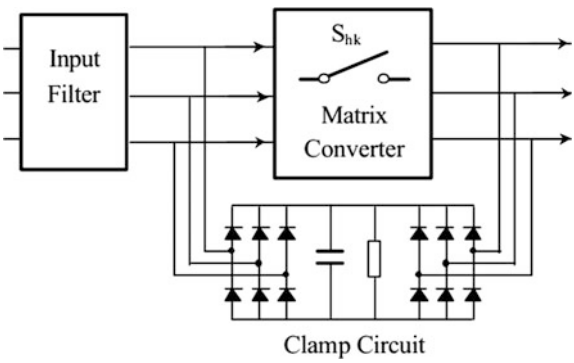

Fig. 5.8 The main structure of MC

1. Matrix switches.
2. Input filter.
3. Clamping circuit.

5.3.1 Matrix Switches

A bi-directional switch is required for MC. It has the ability to connect the current in both directions, but these switches are not available in our markets so far. Thus, conventional unidirectional can be used to obtain bi-directional switches as presented in Fig. 5.9. The bi-direction switch used in this prototype is shown in Fig. 5.9a [12].

5.3.1.1 Diode Bridge with a Single Switch

This switch consists of four ultra-fast diodes with a controllable unidirectional switch as described in Fig. 5.5a. The advantage of this switch is that it has a simple construction and requires only insulated-gate bipolar transistor (IGBT). The disadvantage of this switch is it requires 36 ultra-fast diodes and nine isolated power supply as shown in Table 5.1 [2].

5.3.1.2 Common Emitter Bi-directional Switch

This switch consists of two ultra-fast diodes with two controllable unidirectional switches as presented in Fig. 5.9b. The advantage of this switch is that it can control

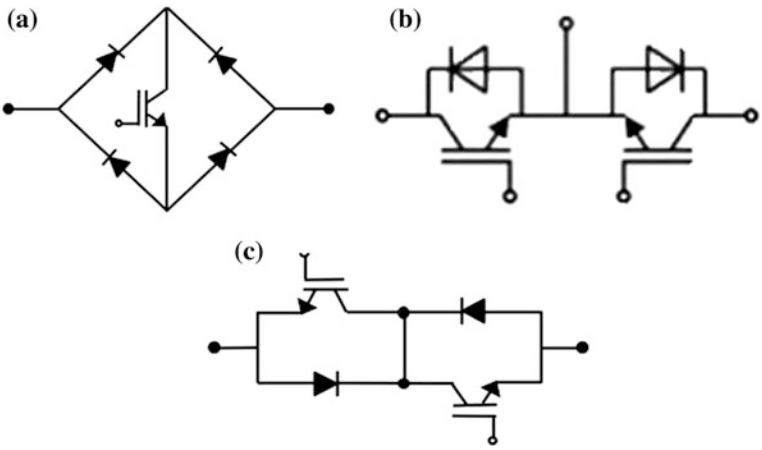

Fig. 5.9 **a** Bridge of diodes with single IGBT, **b** Common emitter bi-directional switch, **c** Common collector bi-directional Switch

Table 5.1 The difference between bi-directional switches

AC-Switch	MOSFET	Diode	Isolated gate supplies	Gate signal
Bridge of diodes with single Switch	9	36	9	9
Common emitter bi-directional switch	18	18	9	18
Common collector bi-directional switch	18	18	6	18

the current through switch. The disadvantage of this switch is it requires more gate drives power supplies and more IGBTs as shown in Table 5.1 [3].

5.3.1.3 Common Collector Bi-directional Switch

This switch consists of a two ultra-fast diode with two controllable unidirectional switches (IGBT) as shown in Fig. 5.9c. This switch has the same advantage of the common emitter one, but it requires only six isolated gate power supplies. The disadvantage of this switch, compared to diode bridge with a single switch, is it requires more IGBTs.

5.3.2 Input Filter

As all power electronic-based converters, the MC injects harmonics into the grid, which affects other equipment connected to the same system. The power converter must meet the requirements given in IEEE 519. This standard refers to the allowable injected harmonic contents into the electrical network. Therefore, the MC requires a suitable input filter to reduce these harmonic components. To reduce the current harmonics in the supply, an LC low-pass filter can be included, as shown in Fig. 5.10. The input filter has to meet the following main requirements: high efficiency, small size and low cost and very small voltage drop across the filter inductance [13].

5.3.3 Clamp Circuit

The clamp circuit protects matrix switches from over voltages. Figure 5.10b shows the clamp circuit used to protect matrix switches. When all switches of the MC are turned off, the inductive load has to discharge the energy stored in it without

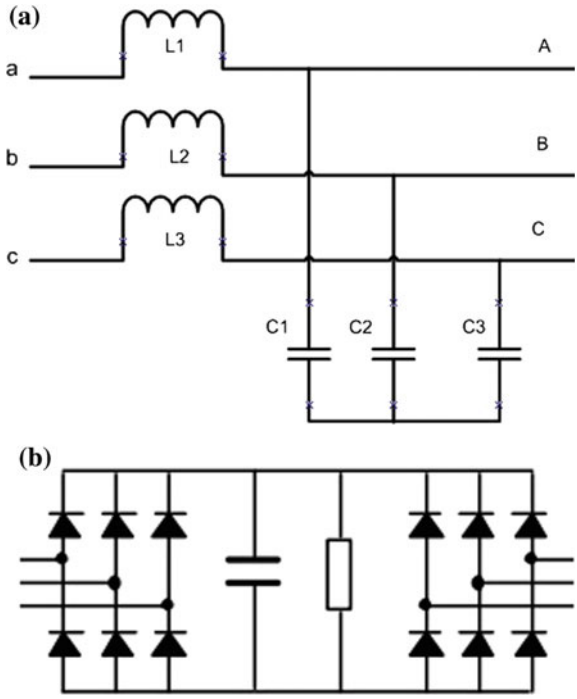

Fig. 5.10 **a** Input filter, **b** Clamp circuit

making any dangerous over voltages. Therefore, the energy stored in the inductive loads can be discharged through the clamp circuit [6].

5.3.4 Control of the Matrix Converter

The MC comprises of nine-bi-directional switches which allow connecting all input lines to connect with all output lines. If the switches of MC are arranged as shown on Fig. 5.11a, the MC power at its input must be the same output power as there is no any energy storage element. An ISVM technique is the control method used with the MC [10, 14].

5.3.4.1 Transformation from Indirect to Direct MC

Figure 5.12b shows that the ISVM technique deals with the MC as a rectifier-inverter converter with a virtual dc link. The indirect MC consists of two stages, the first stage is a current source rectifier based on switches S1–S6, second stage is voltage source inverter, which has a standard three phase voltage source topology based on six switches S7–S12 [15, 16].

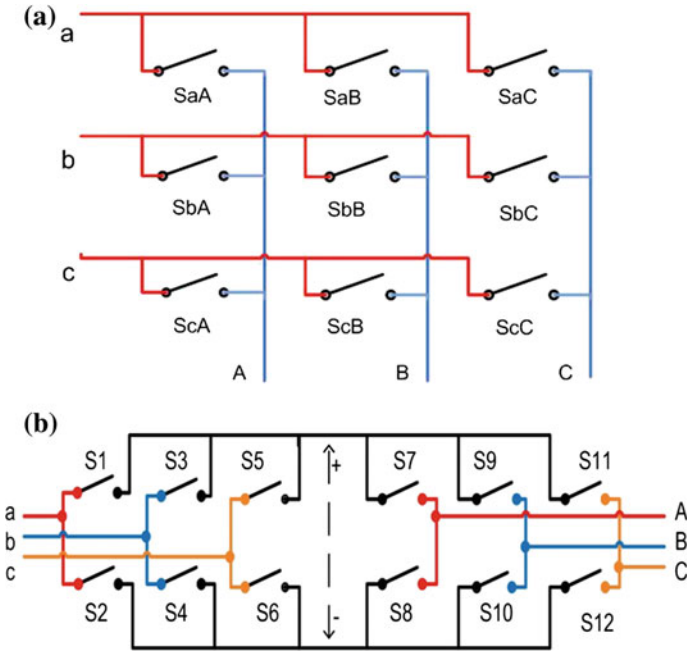

Fig. 5.11 **a** Direct topology of MC, **b** Indirect topology of IMC

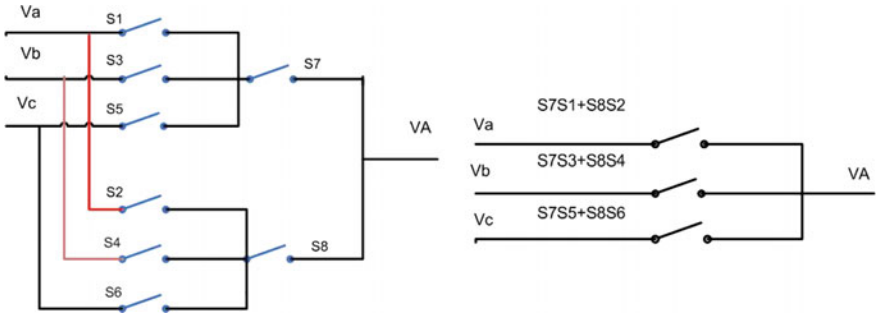

Fig. 5.12 Transformation from Indirect MC to Direct MC in phase A

$$V_{DC} = E{*}V_{abc}, \quad V_{ABC} = N{*}V_{DC}\ V_{ABC} = \mathrm{N} * \mathrm{E} * V_{abc}, \quad \mathrm{K} = \mathrm{N} * \mathrm{E} \tag{5.8}$$

$$E = \begin{bmatrix} S_1 & S_3 & S_5 \\ S_2 & S_4 & S_6 \end{bmatrix}, \; N = \begin{bmatrix} S_7 & S_8 \\ S_9 & S_{10} \\ S_{11} & S_{12} \end{bmatrix}, \; K = \begin{bmatrix} S_{aA} & S_{bA} & S_{cA} \\ S_{aB} & S_{bB} & S_{cB} \\ S_{aC} & S_{bC} & S_{cC} \end{bmatrix} \tag{5.9}$$

$$\begin{bmatrix} S_{aA} & S_{bA} & S_{cA} \\ S_{aB} & S_{bB} & S_{cB} \\ S_{aC} & S_{bC} & S_{cC} \end{bmatrix} = \begin{bmatrix} S_7 & S_8 \\ S_9 & S_{10} \\ S_{11} & S_{12} \end{bmatrix} \begin{bmatrix} S_1 & S_3 & S_5 \\ S_2 & S_4 & S_6 \end{bmatrix} \tag{5.10}$$

where, the matrix N represent the transfer function of the inverter, matrix E represent the transfer function of the rectifier and K represent transfer function of MC. This method deals with MC as a rectifier-inverter converter. Therefore, the space vector of the inverter output voltage and space vector of the rectifier input current can be decoupled to control the direct MC. As shown in Eq. (5.11), the output phases can be compounded by the product and sum of input phases through rectifier and inverter switches $S_1 - S_6$ and $S_7 - S_{12}$, respectively. The output phase A can be obtained from the input phases a, b and c for direct MC as shown in the first row of the matrix in (5.12) using the ISVM and this can be illustrated again in graphical viewpoint as shown in Fig. 5.12 [17, 18].

$$\begin{bmatrix} V_A \\ V_B \\ V_C \end{bmatrix} = \begin{bmatrix} S_7 & S_8 \\ S_9 & S_{10} \\ S_{11} & S_{12} \end{bmatrix} \begin{bmatrix} S_1 & S_3 & S_5 \\ S_2 & S_4 & S_6 \end{bmatrix} \begin{bmatrix} v_a \\ v_b \\ v_c \end{bmatrix} \tag{5.11}$$

$$\begin{bmatrix} V_A \\ V_B \\ V_C \end{bmatrix} = \begin{bmatrix} S_7S_1 + S_8S_2 & S_7S_3 + S_8S_4 & S_7S_5 + S_8S_6 \\ S_9S_1 + S_{10}S_2 & S_9S_3 + S_{10}S_4 & S_9S_5 + S_{10}S_6 \\ S_{11}S_1 + S_{12}S_2 & S_{11}S_3 + S_{12}S_4 & S_{11}S_5 + S_{12}S_6 \end{bmatrix} * \begin{bmatrix} v_a \\ v_b \\ v_c \end{bmatrix} \tag{5.12}$$

5.3.4.2 Indirect Space Vector Modulation

The main idea of the ISVM is to decouple the controlled output voltage of the inverter and the input current for the source rectifier. In this section, SVMs for current sources rectifier and voltage source inverter are introduced, then the two modulations can be decoupled to control the direct MC [19, 20].

Space Vector of the Current Source Rectifier

The current source rectifier consists of six switches S1–S6, as shown in Fig. 5.13. The rectifier has to generate constant dc voltage from three phase input voltage. The virtual dc link voltage and input currents can be calculated from the rectifier transfer function as follows [21, 22].

$$\begin{bmatrix} V_{DC}^{+} \\ V_{DC}^{-} \end{bmatrix} = \begin{bmatrix} S_1 & S_3 & S_5 \\ S_2 & S_4 & S_6 \end{bmatrix} \begin{bmatrix} V_a \\ V_b \\ V_c \end{bmatrix} \tag{5.13}$$

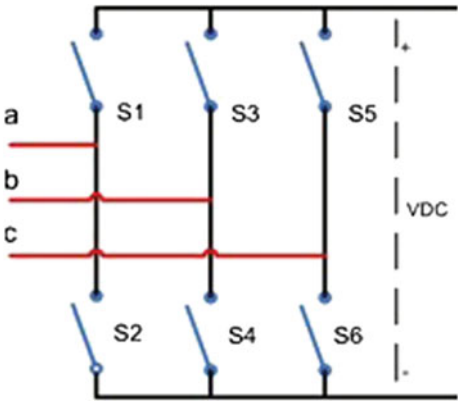

Fig. 5.13 Current source rectifier

$$\begin{bmatrix} I_a \\ I_b \\ I_c \end{bmatrix} = \begin{bmatrix} S_1 & S_2 \\ S_3 & S_4 \\ S_5 & S_6 \end{bmatrix}^T \begin{bmatrix} I_p \\ I_n \end{bmatrix} \tag{5.14}$$

The input current space vector I_{IN} can be expressed as:

$$I_{IN} = \frac{2}{3}\left(I_a + a.I_b + a^2.I_c\right) \tag{5.15}$$

There are only allowed nine switching states for the virtual rectifier so that an open circuit can be avoided in rectifier dc link. These nine switching states can be classified into three zero input current vectors I_0 and six active input current vectors $I_1 - I_6$ as described in Fig. 5.14a. The current space vector state I_1 (a b) means that input phase a is connected to the positive terminal of the virtual dc link (V_{DC+}) and input phase b is connected to the negative terminal (V_{DC-}). Table 5.2 lists the possible switching states and relevant switching vectors. In addition, amplitude and angle of the input current space vector are evaluated for six active vectors and three zero vectors [3, 23]. Figure 5.14a shows the configuration of the discrete seven space vectors of the input current in a hexagon complex plane and the reference input current vector I^*_{IN} within a sector of the input current hexagon. The I^*_{IN} can be obtained by impressing the adjacent active vectors I_γ and I_δ with the duty cycles d_γ and d_δ, respectively, as shown in Fig. 5.14b. By using the current–time product sum of the adjacent active vectors, the reference input vector can be expressed as follows [2, 24].

$$I^*_{IN} = d_\gamma I_\gamma + d_\delta I_\delta + d_{oc} I_0 \tag{5.16}$$

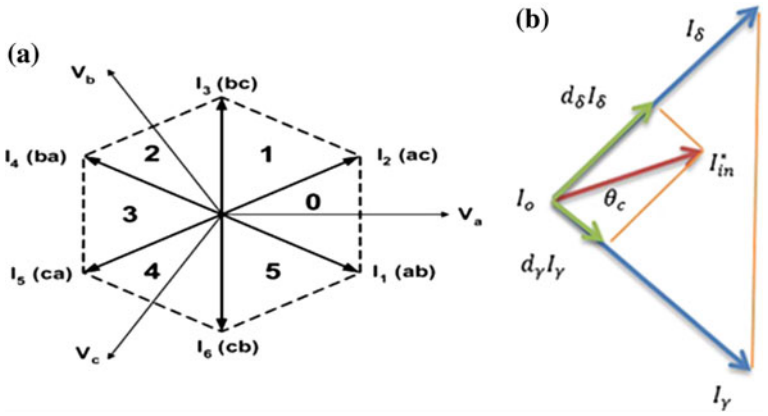

Fig. 5.14 **a** Space vector of current source rectifier, **b** Composition of the reference input current

Table 5.2 Switching states and vectors for current source rectifier

Type	On switch	Vectors	$\begin{bmatrix} S_1 & S_3 & S_5 \\ S_2 & S_4 & S_6 \end{bmatrix}$	I_a	I_b	I_c	I_{IN}	$\angle I_{IN}$
Active	S_1S_4	I_1	$\begin{bmatrix} 1 & 0 & 0 \\ 0 & 1 & 0 \end{bmatrix}$	I_p	$-I_p$	0	$\frac{2}{\sqrt{3}}I_p$	$\frac{-\pi}{6}$
	S_1S_6	I_2	$\begin{bmatrix} 1 & 0 & 0 \\ 0 & 0 & 1 \end{bmatrix}$	I_p	0	$-I_p$	$\frac{2}{\sqrt{3}}I_p$	$\frac{\pi}{6}$
	S_3S_6	I_3	$\begin{bmatrix} 0 & 1 & 0 \\ 0 & 0 & 1 \end{bmatrix}$	0	I_p	-I_p	$\frac{2}{\sqrt{3}}I_p$	$\frac{\pi}{2}$
	S_2S_3	I_4	$\begin{bmatrix} 0 & 1 & 0 \\ 1 & 0 & 0 \end{bmatrix}$	$-I_p$	I_p	0	$\frac{2}{\sqrt{3}}I_p$	$\frac{5\pi}{6}$
	S_2S_5	I_5	$\begin{bmatrix} 0 & 0 & 1 \\ 1 & 0 & 0 \end{bmatrix}$	$-I_p$	0	I_p	$\frac{2}{\sqrt{3}}I_p$	$\frac{-5\pi}{6}$
	S_4S_5	I_6	$\begin{bmatrix} 0 & 0 & 1 \\ 0 & 1 & 0 \end{bmatrix}$	0	$-I_p$	I_p	$\frac{2}{\sqrt{3}}I_p$	$\frac{-\pi}{2}$
Zero	S_1S_2	I_0	$\begin{bmatrix} 1 & 0 & 0 \\ 1 & 0 & 0 \end{bmatrix}$	0	0	0	0	0
	S_3S_4	I_0	$\begin{bmatrix} 0 & 1 & 0 \\ 0 & 1 & 0 \end{bmatrix}$	0	0	0	0	0
	S_5S_6	I_0	$\begin{bmatrix} 0 & 0 & 1 \\ 0 & 0 & 1 \end{bmatrix}$	0	0	0	0	0

The duty cycle of the active vectors can be described as in [2]:

$$d_\gamma = m_c.\sin\left(\frac{\pi}{3} - \theta_c\right) \tag{5.17}$$

$$d_\delta = m_c . \sin(\theta_c) \tag{5.18}$$

$$d_{0c} = 1 - \left(d_\gamma + d_\delta\right) \tag{5.19}$$

where, the angle of the reference vector for input current can be represented by θ_c. The m_c represent the modulation index of the required input current vector and define such as;

$$m_c = \frac{I_{IN}^*}{I_{DC}} \tag{5.20}$$

Space Vector of the Voltage Source Inverter

The Voltage Source Inverter (VSI) consists of six switches $S_7 - S_{12}$ as shown in Fig. 5.15. This VSI has to give three-phase output voltages from constant virtual DC input voltage [25, 26]. The output voltage can be represented as a function of DC input voltage and transfer function of the inverter as given in Eq. (5.21). The dc link current can be derived by using the transposed of the transfer function of the inverter as in Eq. (5.22)

$$\begin{bmatrix} V_A \\ V_B \\ V_C \end{bmatrix} = \begin{bmatrix} S_7 & S_8 \\ S_9 & S_{10} \\ S_{11} & S_{12} \end{bmatrix} \begin{bmatrix} \frac{V_{DC}}{2} \\ \frac{-V_{DC}}{2} \end{bmatrix} \tag{5.21}$$

$$\begin{bmatrix} I_p \\ I_n \end{bmatrix} = \begin{bmatrix} S_7 & S_8 \\ S_9 & S_{10} \\ S_{11} & S_{12} \end{bmatrix}^T \begin{bmatrix} I_A \\ I_B \\ I_C \end{bmatrix} \tag{5.22}$$

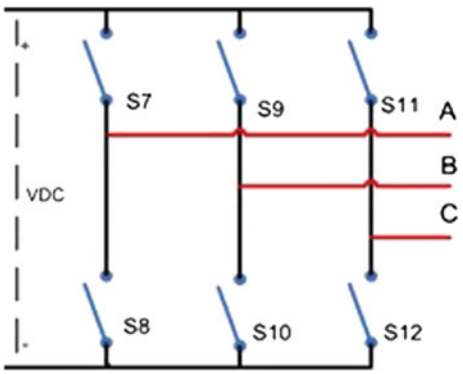

Fig. 5.15 Voltage source inverter

The output voltage space vector V_{out} can be expressed as follows:

$$V_{out} = \frac{2}{3}\left(V_A + a.V_B + a^2.V_C\right), \quad a = 1 * e^{j120} \tag{5.23}$$

There are only eight switching states allowed for the inverter switches, so the output must not be short and the load must not be opened at any instant [27, 28]. These eight permitted combinations can be classified into six active nonzero output voltage vectors $V_1 - V_6$ and two zero output voltage vectors V_z. The voltage space vector V_1 (100) means that the output phase V_A is connected to the positive terminal of the virtual dc link (V_{DC+}) and the phases V_B, V_C are connected to the negative terminal (V_{DC-}). Table 5.3 lists the possible switching states and relevant switching vectors. In addition, the amplitude and angle of the output voltage space vector are evaluated for six active vectors and two zero vectors [24, 29].

Figure 5.16a describes the configuration of the hexagon of the discrete seven space vectors of the inverter in a complex plane. The vector of the reference output voltage V_O^* can be generated from the vector sum out of the seven discrete vectors,$V_1 - V_6$ and V_z. This hexagon can be classified into six sectors. The duty cycles d_α and d_β for active vectors V_α and V_β, respectively. The reference voltage vector V_O^* within a sector of the voltage hexagon can be derived from Fig. 5.16b.

$$V_o^* = d_\alpha V_\alpha + d_\beta V_\beta + d_z V_z \tag{5.24}$$

$$d_\alpha = \frac{T_\alpha}{T_s} = m_v \,.\, \sin\left(\frac{\pi}{3} - \theta_v\right) \tag{5.25}$$

Table 5.3 Switching states and vectors for voltage source inverter

Type	On Switch	Vectors	$\begin{bmatrix} S_7 & S_9 & S_{11} \\ S_8 & S_{10} & S_{12} \end{bmatrix}$	V_A	V_B	V_C	V_{out}	$\angle V_{out}$
Active	$S_7S_{10}S_{12}$	$V_1(100)$	$\begin{bmatrix} 1 & 0 & 0 \\ 0 & 1 & 1 \end{bmatrix}$	$\frac{V_{DC}}{2}$	$\frac{-V_{DC}}{2}$	$\frac{-V_{DC}}{2}$	$\frac{2}{3}V_{DC}$	0
	$S_7S_9S_{12}$	$V_2(110)$	$\begin{bmatrix} 1 & 1 & 0 \\ 0 & 0 & 1 \end{bmatrix}$	$\frac{V_{DC}}{2}$	$\frac{V_{DC}}{2}$	$\frac{-V_{DC}}{2}$	$\frac{2}{3}V_{DC}$	$\frac{\pi}{3}$
	$S_8S_9S_{12}$	$V_3(010)$	$\begin{bmatrix} 0 & 1 & 0 \\ 1 & 0 & 1 \end{bmatrix}$	$\frac{-V_{DC}}{2}$	$\frac{V_{DC}}{2}$	$\frac{-V_{DC}}{2}$	$\frac{2}{3}V_{DC}$	$\frac{2\pi}{3}$
	$S_8S_9S_{11}$	$V_4(011)$	$\begin{bmatrix} 0 & 1 & 1 \\ 1 & 0 & 0 \end{bmatrix}$	$\frac{-V_{DC}}{2}$	$\frac{V_{DC}}{2}$	$\frac{V_{DC}}{2}$	$\frac{2}{3}V_{DC}$	$\frac{\pi}{1}$
	$S_8S_{10}S_{11}$	$V_5(001)$	$\begin{bmatrix} 0 & 0 & 1 \\ 1 & 1 & 0 \end{bmatrix}$	$\frac{-V_{DC}}{2}$	$\frac{-V_{DC}}{2}$	$\frac{V_{DC}}{2}$	$\frac{2}{3}V_{DC}$	$\frac{-2\pi}{3}$
	$S_7S_{10}S_{11}$	$V_6(101)$	$\begin{bmatrix} 1 & 0 & 1 \\ 0 & 1 & 0 \end{bmatrix}$	$\frac{V_{DC}}{2}$	$\frac{-V_{DC}}{2}$	$\frac{V_{DC}}{2}$	$\frac{2}{3}V_{DC}$	$\frac{-\pi}{3}$
Zero	$S_8S_{10}S_{12}$	$V_z(000)$	$\begin{bmatrix} 0 & 0 & 0 \\ 1 & 1 & 1 \end{bmatrix}$	$\frac{-V_{DC}}{2}$	$\frac{-V_{DC}}{2}$	$\frac{-V_{DC}}{2}$	0	0
	$S_7S_9S_{11}$	$V_z(111)$	$\begin{bmatrix} 1 & 1 & 1 \\ 0 & 0 & 0 \end{bmatrix}$	$\frac{V_{DC}}{2}$	$\frac{V_{DC}}{2}$	$\frac{V_{DC}}{2}$	0	0

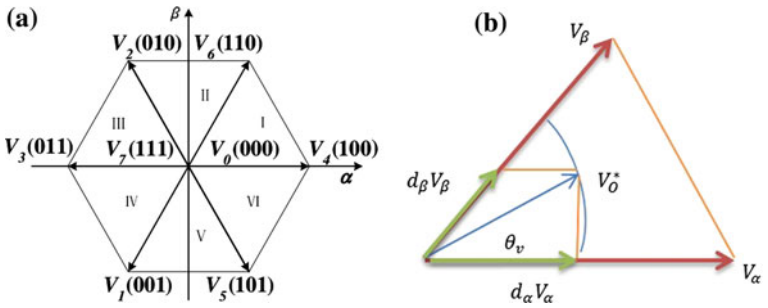

Fig. 5.16 **a** Inverter voltage hexagon, **b** Reference output voltage vector composition

$$d_\beta = \frac{T_\beta}{T_s} = m_v \,.\, \sin(\theta_v) \tag{5.26}$$

$$d_z = \frac{T_z}{T_s} = 1 - \left(d_\alpha + d_\beta\right) \tag{5.27}$$

where, T_α, T_β and T_z are the total duration times of the vectors V_α, V_β and V_z, respectively, and θ_v indicates the angle of the reference output voltage vector within the sector of the hexagon. The m_v represents the modulation index of the vector of the output voltage and it is defined such as [30];

$$m_v = \frac{\sqrt{3} v_{o,max}}{V_{DC}} \tag{5.28}$$

where, V_o is the desired output line voltage, $T_0 = \frac{T_z}{2}$

5.4 Modified Symmetric Sequence Algorithm

This section proposes a modified symmetric sequence algorithm for SVM. The proposed algorithm reduces THD of the output voltage. When the required reference vector for the output voltage of the inverter lies in sector 1 as shown in Fig. 5.16b, the inverter switches $S_7 - S_{12}$ does not have a state that represents this position, so this position can be represented by adjacent vectors V_α, V_β and V_z with duty cycles d_α, d_β and d_z. The main distinction between PWM algorithms that utilize adjacent vectors is zero vector selection, sequence in which the adjacent vectors are applied and splitting of the duty cycle of each adjacent vector.

5.4.1 Conventional Symmetric Sequence Algorithm

One of SVM algorithms is symmetric sequence algorithm that has a low THD as shown in Fig. 5.17a. The duty cycles of each vector V_α, V_β and V_z (d_α, d_β and d_z) is calculated during each switching time T_s. In the conventional symmetric sequence algorithm, the duty cycle of vector V_α (d_α) is divided to two equal periods, d_β also and d_z is divided to three periods $\frac{d_z}{2}, \frac{d_z}{4}$ and $\frac{d_z}{4}$. The sequence in this method is $V_z - V_\alpha - V_\beta - V_z - V_\beta - V_\alpha$ [2].

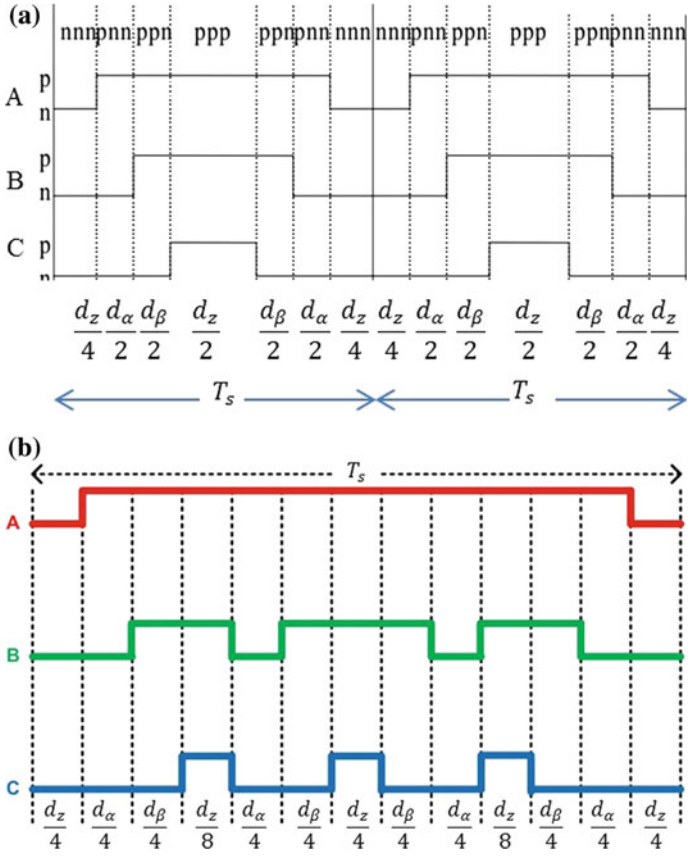

Fig. 5.17 **a** Conventional symmetric sequence algorithm, **b** Modified symmetric sequence algorithm

5.4.2 Modified Symmetric Sequence Algorithm

In this section, a modified symmetric sequence algorithm will be proposed, the sequence in which the vectors are applied. The modification in this algorithm will be the number of divisions of each duty cycle for each vector. In the modified algorithm the duty cycle of V_α (d_α) is divided to four equal periods, d_β also and d_z is divided to five periods $\frac{d_z}{4}, \frac{d_z}{4}, \frac{d_z}{4}, \frac{d_z}{8}$ and $\frac{d_z}{8}$. The sequence in the proposed algorithm is as follow $V_z - V_\alpha - V_\beta - V_z - V_\alpha - V_\beta - V_z - V_\beta - V_\alpha - V_z - V_\beta - V_\alpha - V_z$ as shown in Fig. 5.17b.

5.4.3 Implementation of Modified Symmetric Sequence Algorithm

This part introduces how to implement the SVM for VSI with modified symmetric sequence algorithm by using MATLAB Simulink. Figure 5.18a shows how to transform the reference output voltage into vector angle and vector amplitude. By using the angle of the reference output voltage, we can know number of sector in which the reference output voltage is located. If the required reference vector for the output voltage of the inverter lies in sector 1 as shown in Fig. 5.18a the inverter switches $S_7 - S_{12}$ does not have a state that represents this position, so this position can be represented by adjacent vectors V_α, V_β and V_z with duty cycles d_α, d_β and d_z. After calculating the duty cycles of each adjacent vectors, the modified symmetric sequence algorithm will be used. Figure 5.18b shows the trend of implementation modified symmetric sequence algorithm in MATLAB Simulink. The first step after calculating duty cycles for each adjacent vector in the modified symmetric sequence algorithm is to apply the zero vectors for a time equal to one-fourth of its period. This can be achieved by comparing the one-fourth of zero vectors duty cycle with a ramp signal with a switching time equal to 2 μs as shown in Fig. 5.18b. The second step is to apply the first vectors for a time equal to one-fourth of its period. This can be achieved by comparing the ramp signal with two signals as shown in Fig. 5.18b. The third step is to apply the second vectors for a time equal to one-fourth of its period. This can be achieved by comparing the ramp signal with two signals as shown in Fig. 5.18b and so on.

5.4.4 Simulation Results for Symmetric Sequence Algorithm

Simulations were done using the MATLAB/Simulink software package. The simulation results for a MC interfaced 50 Hz three-phase supply with an isolated R-L load (R = 144 Ω, L = 0.25 H) will be presented. The modified symmetric

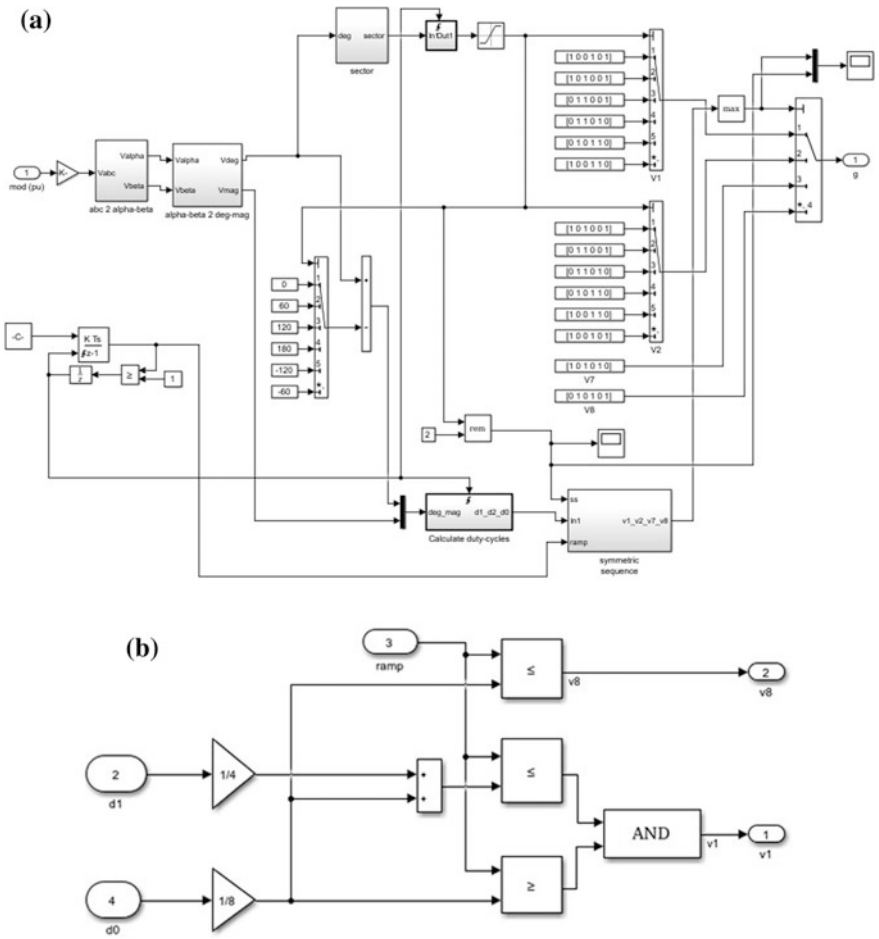

Fig. 5.18 Implementation of the modified symmetric sequence algorithm

sequence algorithm is used with indirect space vector to control the MC. The modified algorithm reduces the THD for the output voltage as shown in Fig. 5.20, also THD for output voltage with conventional symmetric sequence is shown in Fig. 5.19. The simulation results showed that the THD of output voltage is reduced with the proposed algorithm. The proposed method decreases the THD of the output voltage, so decreases cost and size of the required filter. The THD of the output voltage is shown in Table 5.4.

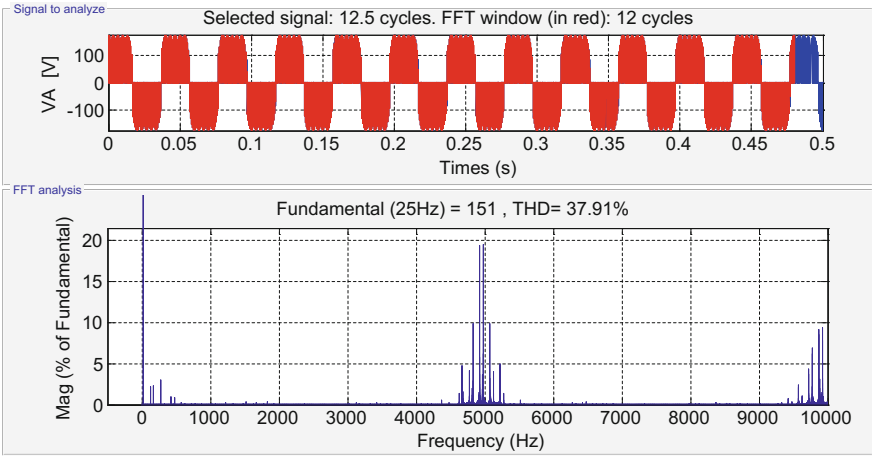

Fig. 5.19 THD for 25 Hz output voltage for conventional symmetric sequence algorithm

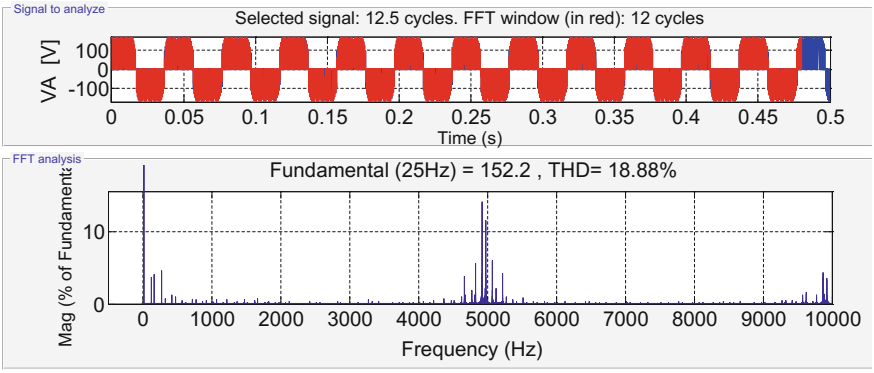

Fig. 5.20 THD for 25 Hz output voltage for modified symmetric sequence algorithm

Table 5.4 THD for conventional and modified symmetric sequence algorithm

Method	THD of output voltage (%)
Conventional symmetric sequence	37.91
Modified symmetric sequence	18.88

5.5 Modified Open Loop Control of MC

The MC can control the rms value of output voltage and frequency, but the output voltage of it in case of open loop control is a percent of the input voltage. If q (the ratio between output voltage and input voltage) = 0.4 in the open loop control,

input voltage = 100 V, the output voltage will be 40 V but with the required frequency. If the input voltage changes from 100 to 50 V, the output voltage will be 20 V. If we need to obtain constant output voltage, the q ratio must be changed from 0.4 to 0.8, so the q ratio must depend on the input voltage and this can be achieved by modified open loop control. The modified open loop control takes a signal from three-phase input voltage and q ratio can be calculated from Eq. (5.29).

$$q = \frac{V_{out}^{*}}{V_{IN}} \tag{5.29}$$

From Table 5.5 and Eq. (5.29), the q ratio in case of modified open loop control depends on the input voltage where if the input voltage decreases, the q ratio increases so that a constant output voltage is obtained. Figure 5.21 shows the proposed modified open loop control of ISVM. Figure 5.21a shows the block diagram of the ISVM with the modification and Fig. 5.21b shows the modification in the MATLAB Simulink model.

5.5.1 Simulation Results for Modified Open Loop Control

Simulations were done using MATLAB/Simulink software package where the MC interfaced wind energy conversion system is used to feed an isolated R-L load (R = 2 Ω, L = 1 mH). The used output LC filter has a value of L = 2.3 mH, C = 100 μf [3]. To obtain the desired output voltage and frequency, the MC is controlled using ISVM with a modified open loop control. Figures 5.22 and 5.23 show the simulation results at different wind speeds with the open loop control. In the modified open loop control, the output voltage and frequency remains constant to 220 V, 50 Hz even if the wind speed changed. In case of the open loop control, the output voltage is a ratio of input voltage and therefore, the output voltage changed with speed as shown Fig. 5.22c. Table 5.6 gives the magnitude of voltages and frequency with the variation of wind speeds. Figures 5.22a and 5.23a show the wind velocity with time, where the speed of wind changed from 7 to 12 m/s at t = 0.3 s, from 12 to 9 m/s at t = 0.6 s, from 9 to 6 m/s at t = 1 s. Figure 5.22b shows the input voltage to MC (generated voltage), Fig. 5.22c shows the simulation results of output voltage of 50 Hz with the open loop control. It is clear from Fig. 5.22c that the magnitude of the output voltage is not constant.

Table 5.5 Modified open loop control and open loop control

V_{IN}	Open loop control		Modified open loop control	
	q	V_{out}	q	V_{out}
100	0.4	40	0.4	40
50	0.4	20	0.8	40

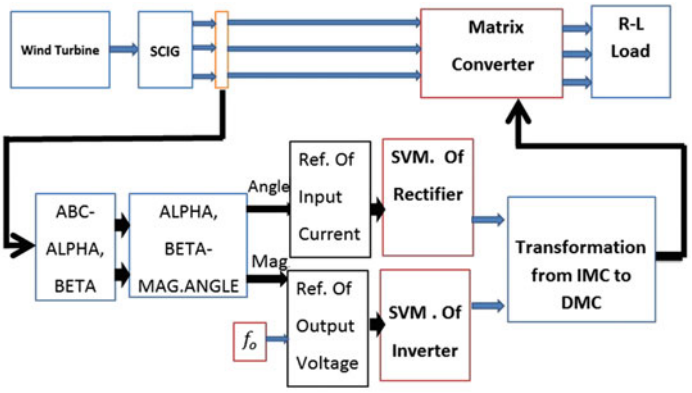

(a) Block diagram of model

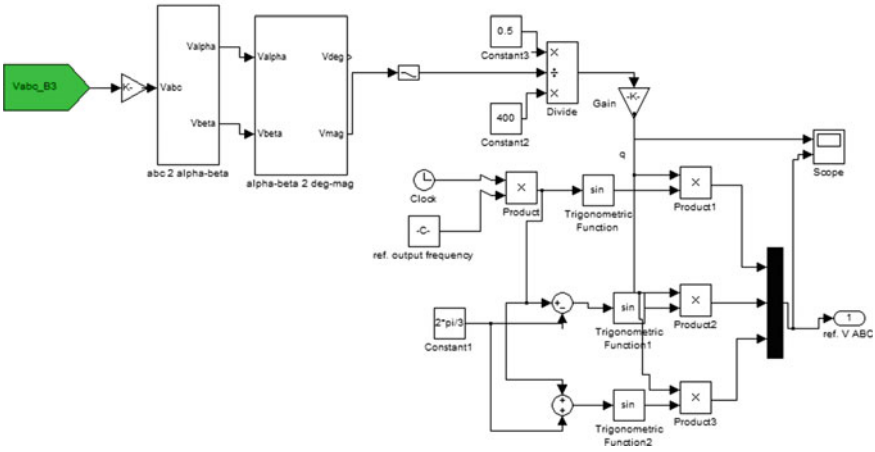

(b) Simulink of modification in the Model

Fig. 5.21 Modified open loop control of ISVM

Figure 5.22d shows the simulation results of the output current at 50 Hz with the open loop control. Figure 5.23b shows the input voltage to MC (generated voltage), where for t = 0:0.3 s the generated voltage is 320 V, 25 Hz, at t = 0.3:0.6 s the generated voltage is 460 V, 46 Hz, at t = 0.6:1 s the generated voltage is 380 V, 34 Hz, at t = 1:1.5 s the generated voltage is 280 V, 21 Hz. Figure 5.23c shows the simulation results for the desired output voltage of 220 V, 50 Hz with the modified open loop control. It is clear from Fig. 5.23c that the magnitude of the output voltage is constant and equal to 220 V. Figure 5.23d shows the simulation results of output current at 50 Hz with the modified open loop control.

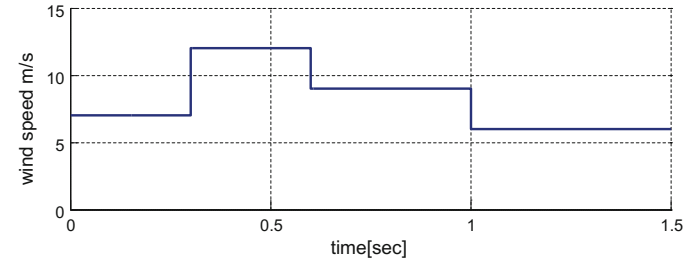

a- Dynamic response of wind speed

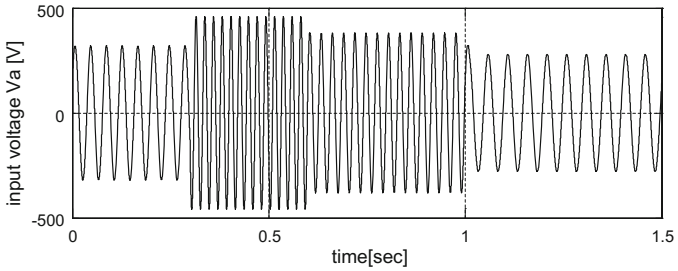

b- Input voltage V_a at different wind speeds

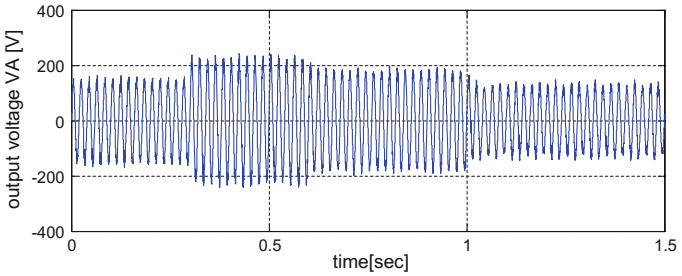

c- Output voltage V_A at 50 Hz

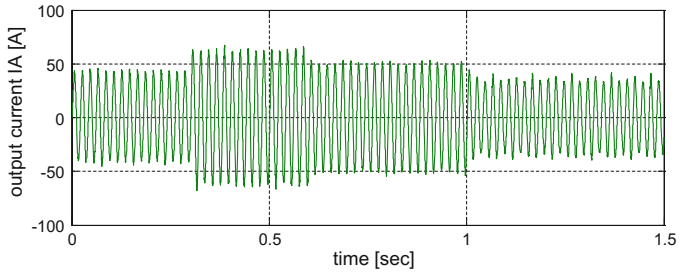

d- Output current $\boldsymbol{I_A}$ at 50 Hz

Fig. 5.22 Simulation results for open loop control of a matrix converter

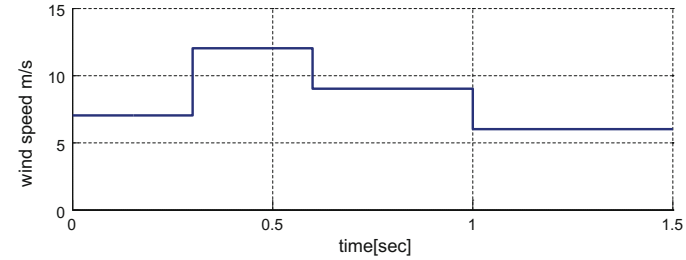

a- Dynamic response of wind speed

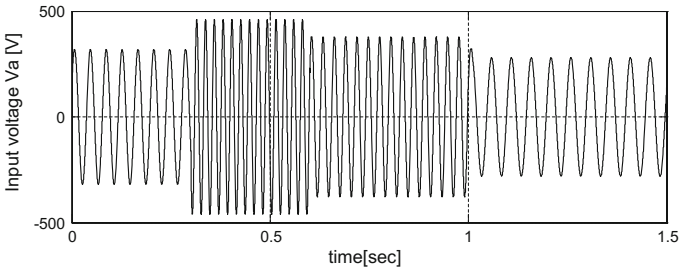

b- Input voltage V_a at different wind speeds

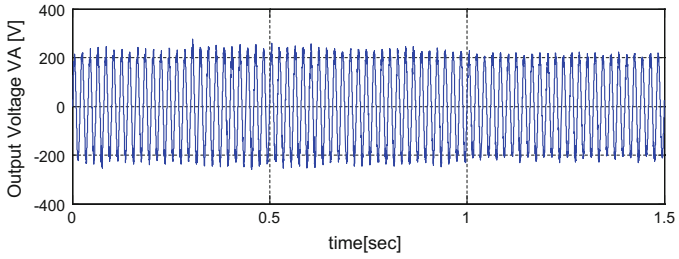

c- Output voltage V_A at 50 Hz

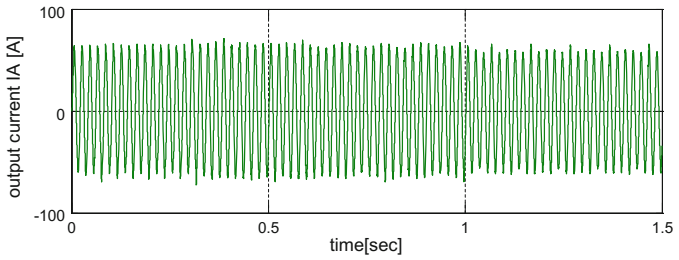

d- Output current I_A at 50 Hz

Fig. 5.23 Simulation results for modified open loop control of a matrix converter

Table 5.6 Variation of generated voltage and frequency with wind velocity

Wind velocity (m/s)	Voltage (V)	Frequency (Hz)
6	280	21
7	320	25
9	380	34
12	460	46

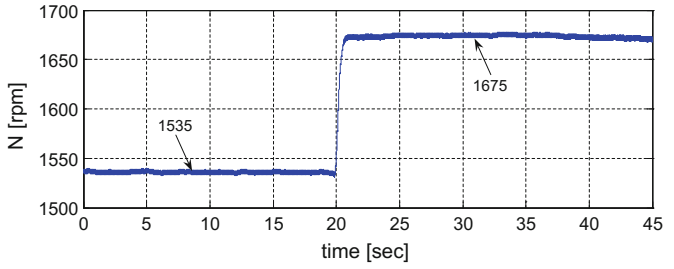

a- Speed response

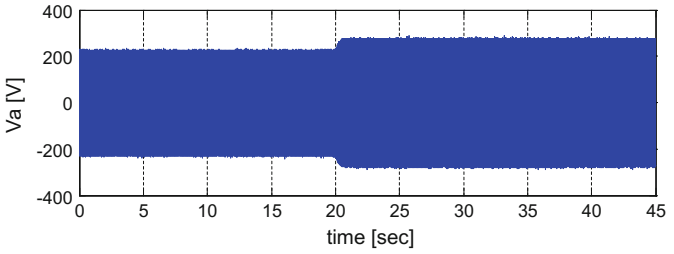

b- Input voltage V_a

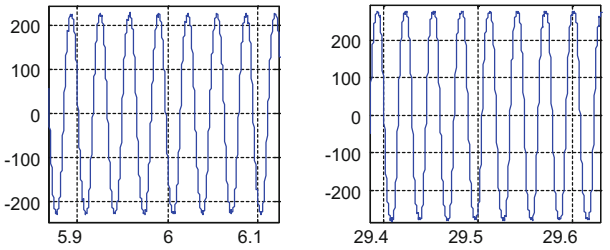

c- Zoomed view of input voltage V_a

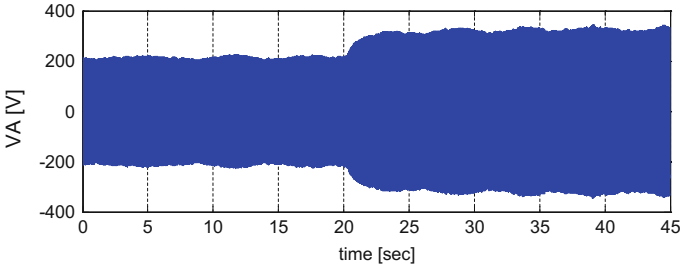

d- Output voltage V_A

Fig. 5.24 Experimental results with open loop control with output frequency 50 Hz

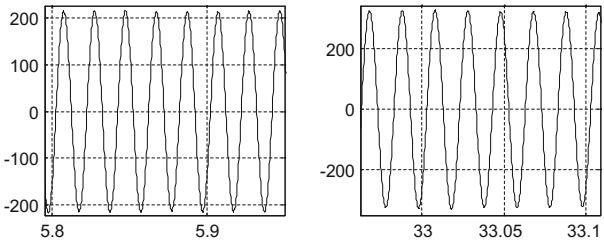

e- Zoomed view of output voltage V_A

Fig. 5.24 (continued)

5.5.2 *Experimental Results for Modified Open Loop Control*

Experimental results were performed using DSP1104, with an isolated, static load of (R = 20 Ω, L = 40 mH). The field and the armature voltage of dc motor is controlled to control its speed to simulate the wind turbine. Figure 5.24 shows the experimental results for change in speed at a time 20 s in case of the open loop control with 50 Hz output frequency, where Fig. 5.24a shows the change in speed where it from 1535 to 1675 rpm by increasing the armature voltage. Figure 5.24b shows the input voltage, where the rms value and the frequency of the input voltage increase with the increase in speed and the input frequency increases from 30 to 35 Hz as shown in the zoomed view of the input voltage in Fig. 5.24c. Figure 5.24d shows the output voltage for the open loop control and Fig. 5.24e shows the zoomed view of output voltage which has 50 Hz frequency. The output frequency does not change even if the input frequency changes. The rms value of the output voltage is a percent of the input voltage, so the rms value of the output voltage changes with a change in input voltage as shown in Fig. 5.24e.

Figure 5.25 shows the experimental results for a change in speed at t = 18.5 s in case of the modified open loop control with a 50 Hz output frequency, where Fig. 5.25a shows the change in speed where the speed changes from 1528 to 1653 rpm by increasing the armature voltage. Figure 5.25b shows the input voltage where the rms value and frequency of the input voltage increase with the increase in the speed. The input frequency increases from 29.3 to 33.5 Hz approximately as shown in the zoomed view of the input voltage in Fig. 5.25c. Figure 5.25d shows the output voltage in case of the modified open loop control. Figure 5.25e shows the zoomed view of output voltage which has frequency of 50 Hz. The output frequency does not change even if the input frequency changes. The rms value of the output voltage is a percent of the input voltage, so to obtain a constant rms value of the output voltage with the change in input voltage as shown in Fig. 5.25e; the reference output voltage must be inversely changed with change in input voltage.

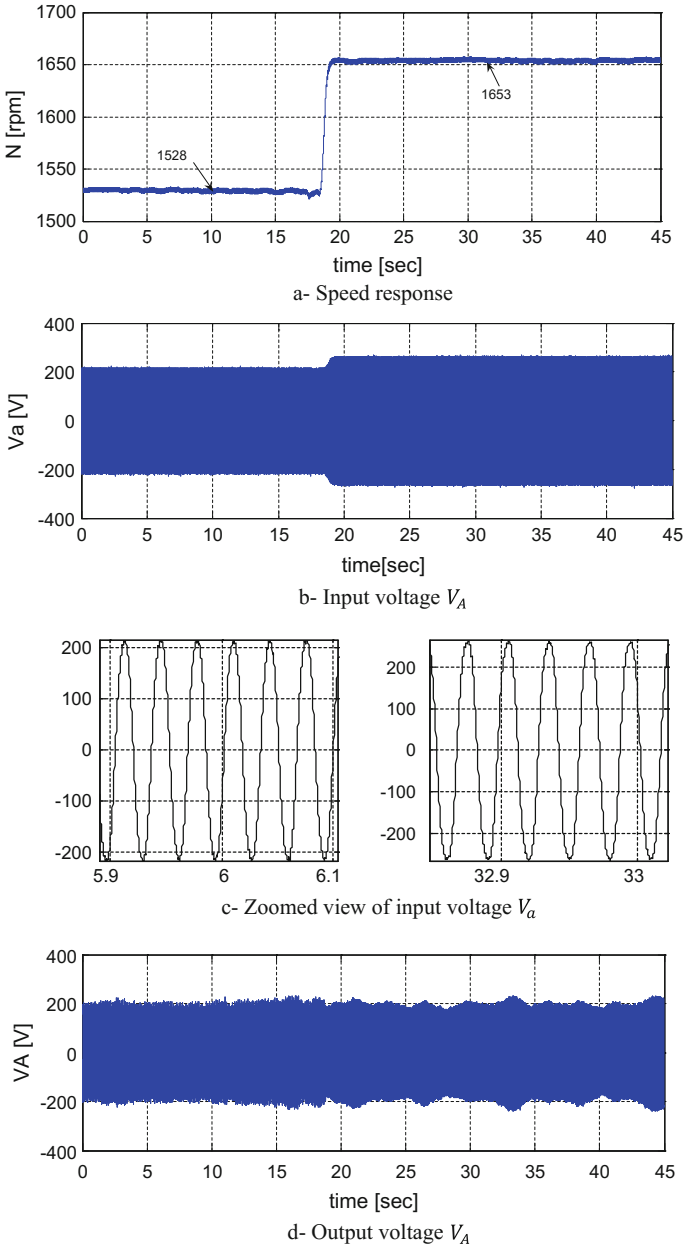

Fig. 5.25 Experimental results with modified open loop control with output frequency 50 Hz

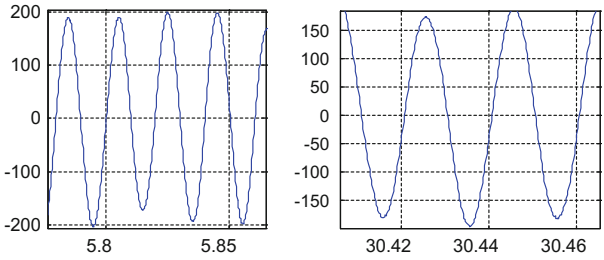

e- Zoomed view of output voltage V_A

Fig. 5.25 (continued)

5.6 Conclusion

This chapter introduces performance improvement of the MC fed from a wind energy system. A theoretical analysis is carried out supported by numerical analysis. The results have been carried out using a designed complete prototype setup. According to the initiating problems and aims mentioned in the introduction, the following are the achieved four scenarios. The first analysis has been done for using the MC to control the voltage and frequency of a static R-L load fed from WECS. The angle between the input voltage and current of MC is controlled and the input displacement factor with a unity value is achieved. The model produces a very good waveform on the output side with a wide range of frequency changes. Secondly, the analysis of transforming from the indirect to direct MC is introduced; in addition to introducing analysis for the ISVM. Thirdly, a modified symmetric sequence algorithm for SVM is proposed. The proposed method is compared with the conventional algorithm and it has a lower output voltage THD. Fourthly, a modified open loop control of the ISVM is proposed which improved the performance of the MC with a variable speed operation of the wind turbine. Finally, all measured results showed good correspondence with those obtained by simulation.

References

1. Bharanikumar R, Kumar AN (2012) Performance analysis of a wind turbine-driven by permanent magnet generator with matrix converter. Turk J Electr Eng Comp Sci 20(3):299–317
2. Tawfiq KB, Abdou AF, EL-Kholy EE, Shokrall SS (2016) Application of matrix converter connected to wind energy system. In: 2016 Eighteenth international middle east power systems conference (MEPCON), pp 604–609
3. Tawfiq KB, Abdou AF, EL-Kholy EE, Shokralla SS (2016) Performance analysis of a matrix converter interfaced wind energy conversion system for static load application. In: 1st Future university international conference on new energy & environmental engineering (ICNEEE), Cairo, Egypt, vol 1, 11–14 Apr 2016

4. Bhatia SC (2014) Advanced renewable energy systems, in part-I. Woodhead publishing india Pvt Ltd, New Delhi, Cambridge, Oxford, Philadelphia
5. Singh GK (2002) Multi-phase induction machine drive research—a survey. Electr Power Syst Res 61:139–147
6. Halder S, Saha TK (2016) Modeling and performance analysis of digital control drive of induction machine in synchronous reference frame. In: 2016 International conference on electrical power and energy systems (ICEPES), pp 333–338
7. Eltamaly AM (2002) New formula to determine the minimum capacitance required for self-excited induction generator. In: 33rd IEEE power electronics specialists conference, Cairns Convention Centre, Queensland, Australia, 23–27 June 2002
8. Liu Y, Bazzi A (2017) Improved maximum torque-per-ampere control of induction machines by considering iron loss. In: 2017 IEEE international electric machines and drives conference (IEMDC), pp 1–6
9. Kharitonov SA, Balagurov MV, Geist AV (2016) Mathematical model of AC-AC converter. In: 17th international conference of young specialists on micro/nanotechnologies and electron devices (EDM), pp 417–420
10. Ward EE, Härer H (1969) Preliminary investigation of an inverter fed five-phase induction motor. Proc Inst Electr Eng 116(6):980–984
11. Diaz M, Cardenas R, Espinoza M, Rojas F, Mora A, Clare JC et al (2017) Control of wind energy conversion systems based on the modular multilevel matrix converter. IEEE Trans Ind Electron 64(11):8799–8810
12. Dabour SM, Allam SM, Rashad EM (2015) Indirect space-vector PWM technique for three to nine phase matrix converters. In: IEEE 8th GCC conference & exhibition, pp 1–6
13. Dabour SM, Rashad EM (2012) Analysis and implementation of space-vector-modulated three-phase matrix converter. IET Power Electron 5:1374–1378
14. Yang M, Shanshan W, Xiaoguang Z (2016) A model predictive torque control method for dual induction motor drive system fed by indirect matrix converter. In: IEEE 8th international power electronics and motion control conference (IPEMC-ECCE Asia), pp 2837–2841
15. Halder S, Agrawal A, Agarwal P, Srivastava SP, Das S (2016) Matrix converter fed PMSM drive with maximum torque per ampere control. In: IEEE 1st international conference on power electronics, intelligent control and energy systems (ICPEICES), pp 1–4
16. Athulya MT, Subramanian S (2016) SVPWM based control of matrix converter for gearless operation of wind energy power conversion system. In: Biennial international conference on power and energy systems: towards sustainable energy (PESTSE), pp 1–6
17. Miura Y, Yoshida T, Fujikawa T, Miura T, Ise T (2016) Operation of modular matrix converter with hieralchical control system under cell failure condition. In: IEEE energy conversion congress and exposition (ECCE), pp 1–8
18. Bessegato L, Norrga S, Ilves K, Harnefors L (2016) Control of modular multilevel matrix converters based on capacitor voltage estimation. In: IEEE 8th international power electronics and motion control conference (IPEMC-ECCE Asia), pp 3447–3452
19. Sandeep J, Ashok S, Ramchand R (2016) Carrier based space vector modulation for matrix converters. In: IEEE 1st international conference on power electronics, intelligent control and energy systems (ICPEICES), pp 1–6
20. Zhang JW, Dorrell DG, Li L (2016) Applications of the direct space vector modulation controlled matrix converter as the unified power flow controller. In: 8th IET international conference on power electronics, machines and drives (PEMD 2016), pp 1–6
21. Li X, Sun Y, Zhang J, Su M, Huang S (2017) Modulation methods for indirect matrix converter extending the input reactive power range. IEEE Trans Power Electron 32:4852–4863
22. Huisman H, Roes M, Lomonova E (2016) Continuous control set space vector modulation for the 3*3 direct matrix converter. In: 18th european conference on power electronics and applications (EPE'16 ECCE Europe), pp 1–10

23. Morisaki S, Abe T, Higuchi T (2015) Experimental loss estimate for matrix converter using ARCP soft switching technique. In: 18th international conference on electrical machines and systems (ICEMS), pp 1898–1902
24. Han H, Li Z, Mao Y, Wang H, Dan H, Wen M (2015) A simple current control strategy for four-leg direct Matrix converter. In: Chinese automation congress (CAC), pp 2174–2179
25. Tran QH, Nguyen TD, Hong-Hee L (2016) Three-vector modulation scheme to improve output performance for five-leg indirect matrix converter fed open-end load. In: IEEE 8th international power electronics and motion control conference (IPEMC-ECCE Asia), pp 2133–2138
26. Pittermann M, Drabek P, Bednar B (2015) Single phase high-voltage matrix converter for traction drive with medium frequency transformer. In: IECON 2015—41st annual conference of the IEEE industrial electronics society, pp 005101–005106
27. Aoki K, Yamamura N, Ishida M (2015) Improvement of the switching system in the power distribution for three-phase to single-phase matrix converter system with neutral line. In: 18th international conference on electrical machines and systems (ICEMS), pp 442–447
28. Sebtahmadi SS, Borhan AH, Mekhilef S (2015) An industrial optimum current control scheme for IM drive fed by ultra sparse Z-source matrix converter under abnormal input voltage. In: IEEE 2nd international future energy electronics conference (IFEEC), pp 1–6
29. Shi B, Zhou B, Han N, Qin X, Zhou X, Zhang J (2016) Open-circuit fault diagnosis for rectifier stage in indirect matrix converter. In: IECON 2016—42nd annual conference of the IEEE industrial electronics society, pp 6273–6277
30. Arioni AD, Oliveira SVG (2016) A generalized mathematical analysis for matrix converters. In: IECON 2016—42nd annual conference of the IEEE industrial electronics society, pp 6231–6236

Chapter 6
Matrix Converter Switching and Commutation Strategies for Grid Integration of Distributed Generation

Md Sawkat Ali, M. Mejbaul Haque and Peter Wolfs

6.1 Introduction

For the practical implementation of MCs, one of the challenges is the commutation process. In this chapter, solutions for the commutation process are developed. Two switching topologies are available. These are classified as the one degree of freedom topology (with one active device) and the two degrees of freedom topology with two active devices.

Different types of commutation processes are explored in this chapter as shown in Fig. 6.1. Initially, the discussion focusses on the overlap and dead-band commutations and then, based on their limitations, examines two-, three- and four-step commutation processes.

However, as these existing procedures still have limitations, an improved four-step current sensing-based commutation process is proposed. The commutation process is extended on the 'n'-time switching arrangement. For a clear demonstration of the proposed improved commutation methods, the state machines and switching tables are shown in two- to 'N'-leg commutations, with a set of logical agreements developed for safe switching commutation [1]. The industrial success of the MC will depend not only on the commutation but also be contingent on the connection between them and the switches.

M. S. Ali · M. Mejbaul Haque (✉) · P. Wolfs
Central Queensland University, Rockhampton, QLD 4702, Australia
e-mail: m.haque@cqu.edu.au

M. S. Ali
e-mail: sawkat.aust@gmail.com

P. Wolfs
e-mail: p.wolfs@cqu.edu.au

M. R. Islam et al. (eds.), *Renewable Energy and the Environment*, Renewable Energy Sources & Energy Storage, https://doi.org/10.1007/978-981-10-7287-1_6

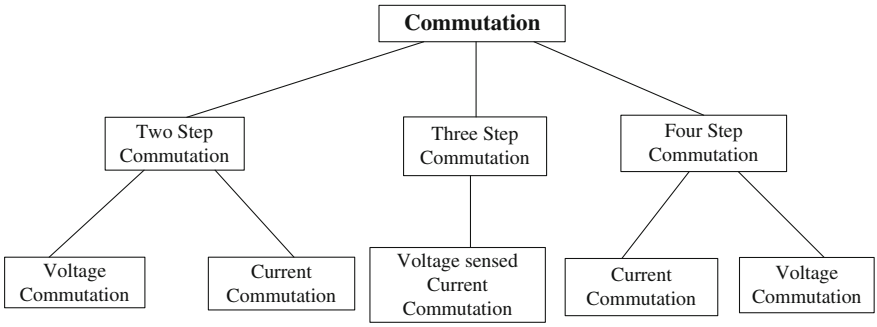

Fig. 6.1 Tree diagram of MC commutation

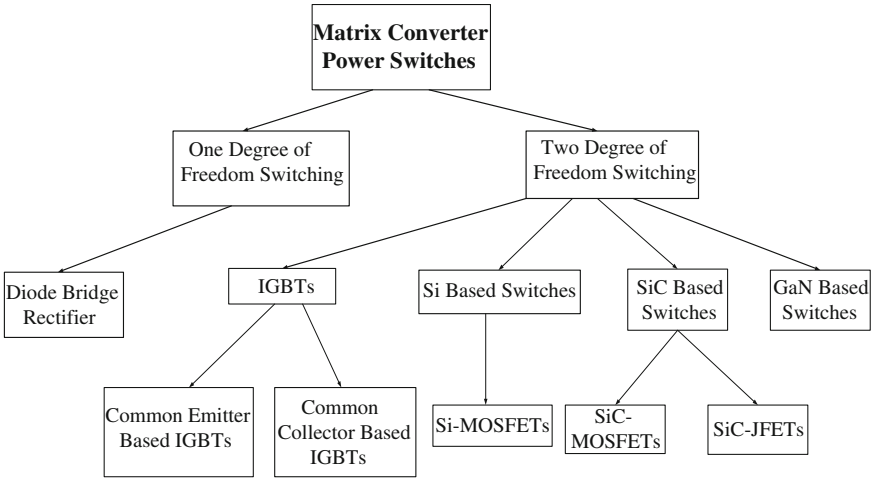

Fig. 6.2 Tree diagram of MC switches

This chapter also discusses switching categories on the basis of their switching degrees of freedom. To explain the changes in MC switching, a chart is presented in Fig. 6.2. This chart illustrates the first and second degrees of switching freedom, with the tree span introducing their different semiconductor-based switches.

6.1.1 Commutation Strategies

A MC is normally operated with voltage stiff sources at its input terminals and current stiff loads connected to its output terminals. This causes a dilemma. The continuity of the output current sequences requires that at least one switch connected to each output terminal is closed at all times. This implies switches must

overlap during commutation. However, a short circuit must not appear across the input terminals. This implies switches must not overlap during commutation. This dilemma can be resolved and this is the focus of this chapter.

6.1.1.1 Overlap Commutation

An overlap commutation process is introduced in [1] in which the concept is to make switches overlap. A two-leg switching process is presented in Fig. 6.3. The switching sequence is shown in the state machine diagram in Fig. 6.4 and in Table 6.1. In the overlap commutation switching sequence, the output leg is always connected via the SW_1 and SW_2 switches and, as a result, a short circuit current is produced. If the short circuit current exceeds the switching tolerable limit, then some form of current restricting is needed. Inductor can play the current controlling obligatory role but, an extra input voltage clamping circuit is required for the MC. Therefore, this process is not a preferred way for the MC's commutation.

6.1.1.2 Dead-Band Commutation

Dead-band commutation is the inverse process of overlap commutation which is discussed in [1] and illustrated in Fig. 6.3. Commutation is based on the idea of breaking switch SW2 before switch SW1. Figure 6.5 and Table 6.2 clearly demonstrate how the commutation process follows the switching path. In this process, no overlap switching is established but, at a certain time, the output phase turns into a non-conducting mode, and a clamping process will be needed. To

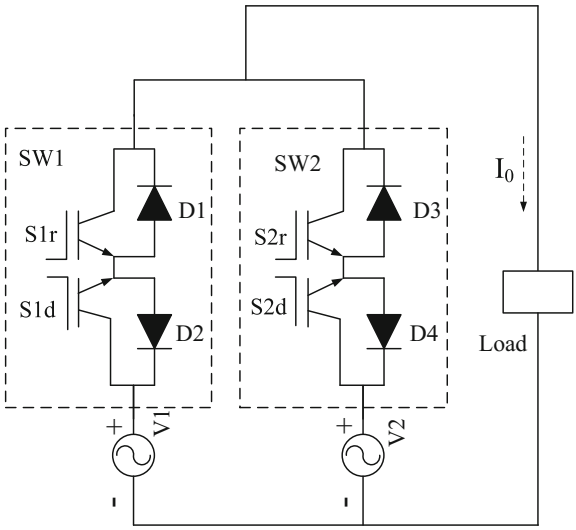

Fig. 6.3 Basic two-leg switching diagram

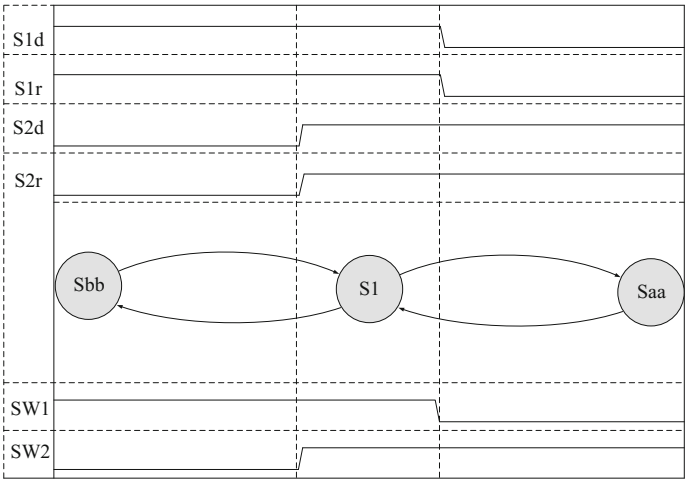

Fig. 6.4 Diagram of overlap commutation process with timing

Table 6.1 State and switches for overlap commutation

State/switches	Sd1	S1r	S2d	S2r
Saa	1	1	0	0
S1	1	1	1	1
Sbb	0	0	1	1

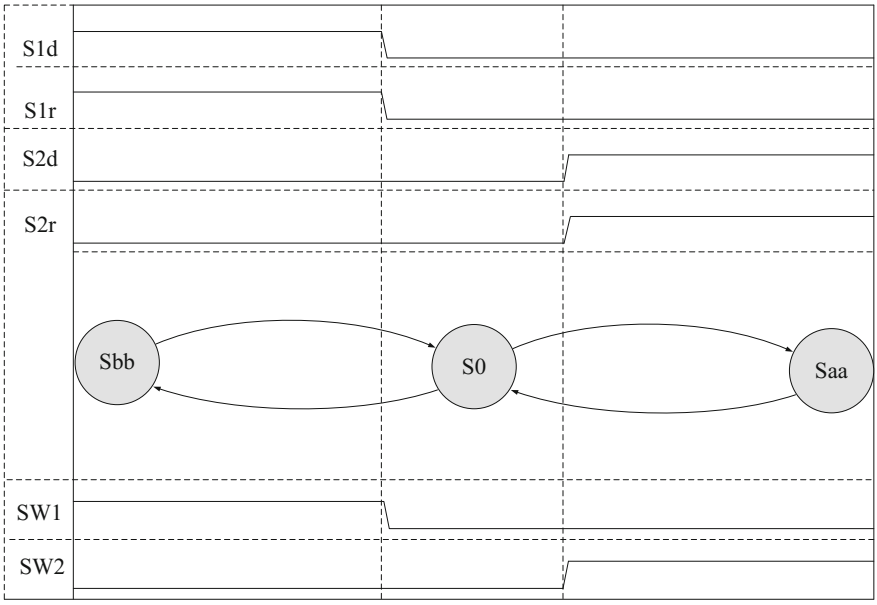

Fig. 6.5 Diagram of dead-band commutation with timing

Table 6.2 State and switches for dead-band commutation

State/switches	Sd1	S1r	S2d	S2r
Saa	1	1	0	0
S0	0	0	0	0
Sbb	0	0	1	1

overcome the limitation that this commutation switching does not follow the MC's basic rules, a snubber circuit can be introduced on every switch. Nevertheless, this proposed explanation is not a viable solution for the experimental setup on a MC as it will introduce a great deal of power loss on the system.

6.1.1.3 Two-Step Commutation

Based on the above limitations, a two-step commutation technique has been introduced in [2, 3]. In the two-leg switching combination shown in Fig. 6.8, the switching sequence follows the output load current approach. In bidirectional switching, it is necessary to know the current direction which leads to determining the switching that will operate at a particular given time.

In the experimental setup, the current measuring transducers [Hall Effect (HE)] are positioned at the output terminals. At high currents, the current direction is clear [4]. A transducer always has a zero offset error. At low currents, the direction will be uncertain. For positive current, switches S1d and/or S2d conduct and, at the same time, switches S1r and S2r are in the off mode. Similarly, for a negative current, switches S1r and S2r are gated on and the IGBTs turned on to allow the current to flow in the reverse direction. If the current is very small, and less than the accuracy of the measurement transducers to clearly determine the current direction, dead band commutation must be used. In this case, a small, low power, output voltage clamp is applied. A two-step current commutation switching pattern with positive, negative and zero current flows and switch state vectors are presented in Figs. 6.6 and 6.7 respectively.

However, there are the following limitations to two-step commutation:

- In the presence of internal switch commutation, dead-band and overlap commutation are created in the two-step method;
- Reducing the commutation step will decrease the time required for the whole switching process but increase the logical computational load [5]; and
- Determining the current sign is a vital challenge for the current reference-based two-step commutation process for which a short circuit may be considered.

6.1.1.4 Three-Step Commutation

The results obtained from the above commutation strategies, being controlled by the direction of the output current, are not sufficiently robust for reliable MC operation.

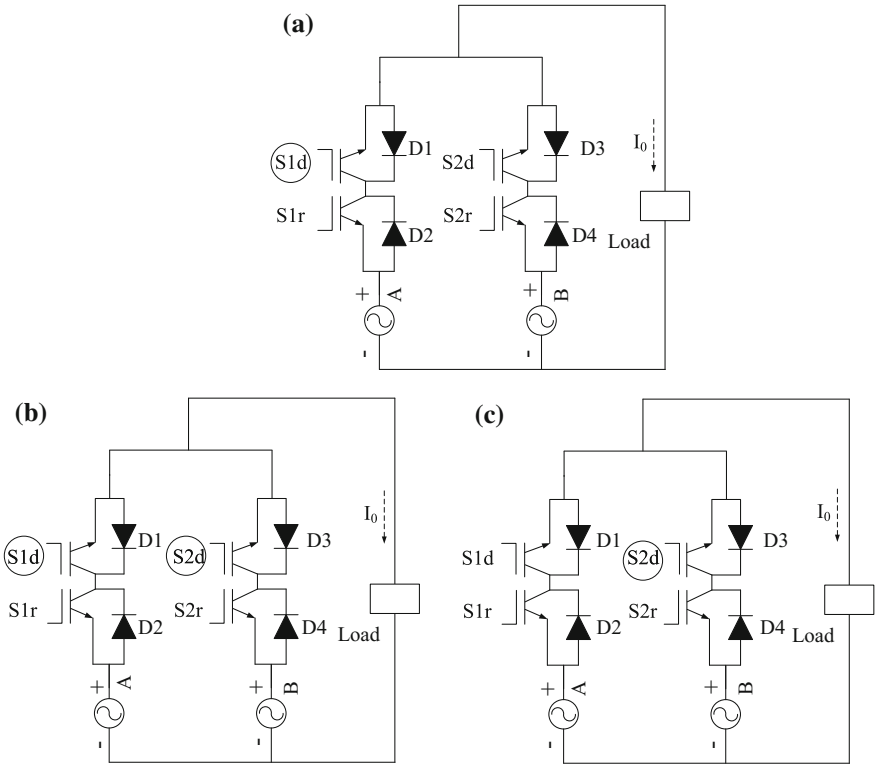

Fig. 6.6 Switching sequence for two-step current commutation: **a** initial step; **b** 1st step; and **c** 2nd step

For the non-hazard switching sequences, a new three-step input voltage and output current reference based commutation technique is introduced. This three-step commutation process takes less commutation time than the four-step one.

It is flexible in terms of the step-time settings whereby different steps follow different time intervals. The sum of the total time for the switching sequence is reduced. Diagrams of a three-step voltage-sensed current commutation and state switching sequences are presented in Figs. 6.8, 6.9 and 6.10. The three-step commutation indicates how the commutation steps occur based on the directions of output current and input voltage.

For $I_0 > 0$ and $V_{12} > 0$ conditions in Fig. 6.10, the switching steps are organised as follows:

- Initial step [Saa (1100)]: switches S1r and S1d are turned on.
- Step 1 [S1 (1100)]: switch S1r, which does not carry the output current, is turned off.

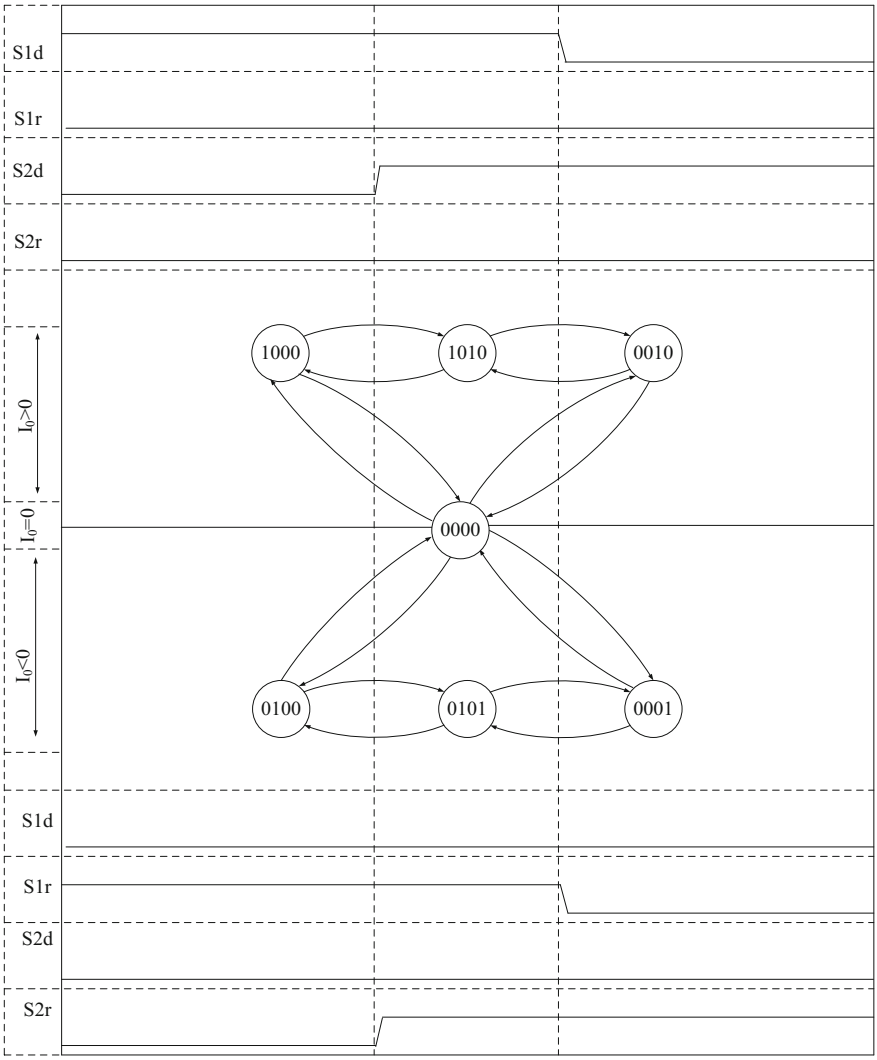

Fig. 6.7 Diagram of two-step two-leg current commutation switching state

- Step 2 [S5 (1100)]: switch S2d, which carries the output current, is turned on.
- Step 3 [Sbb (1100)]: switch S1d is turned off and switch S2d takes its place by being switched on, with both processes activated at the same time.

This switching sequence shown in Fig. 6.9 for three-step commutation can be similarly performed for other voltage and current reference combinations.

The advantage of this method is that it has one less step than four-step commutation.

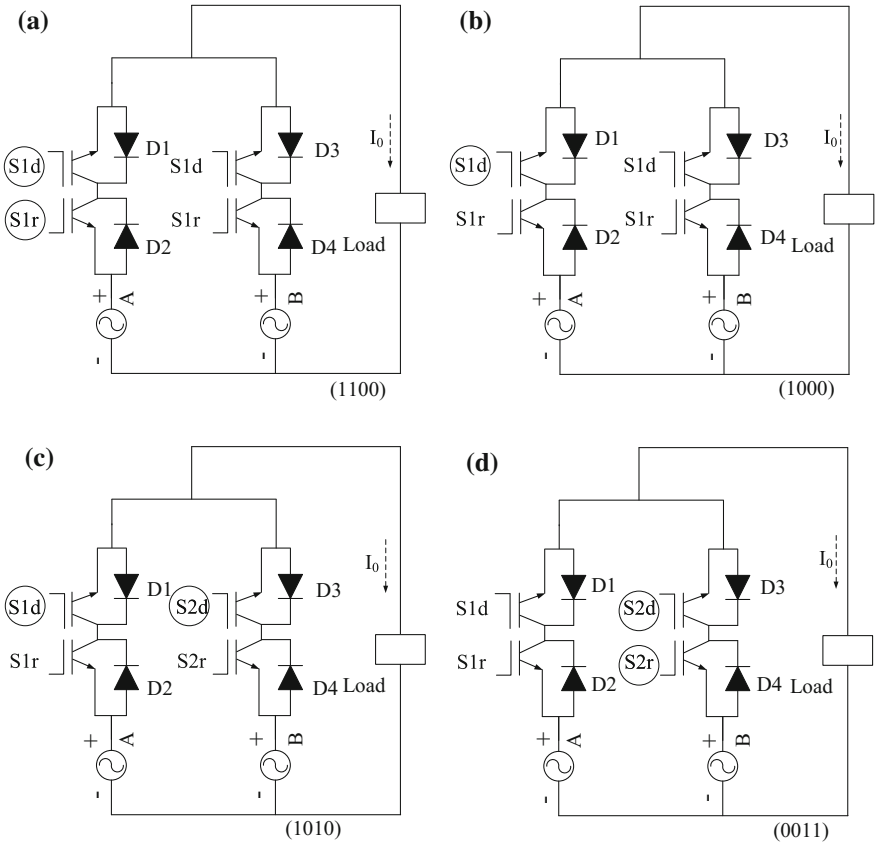

Fig. 6.8 Three-step two-leg switching sequence when $I_0 > 0$, $V_{AB} > 0$: **a** initial step; **b** 1st step; **c** 2nd step; and **d** 3rd step

The three-step commutation process discussed above can achieve a non-hazard proper switching by the use of dual reference signals. However, it still has the drawbacks that:

- Its sequence is complex as two controlling variables influence the sequence of switching states; and
- It is more likely that a short circuit pathway may take place if the measured voltage changes its direction at the time of commutation.

6.1.1.5 Four-Step Commutation

Discussions are continued on the commutation process and, based on this, a developed four step commutation is illustrated in Fig. 6.11. Two by two degrees of freedom SiC-MOSFET switches are used to control the forward and reverse

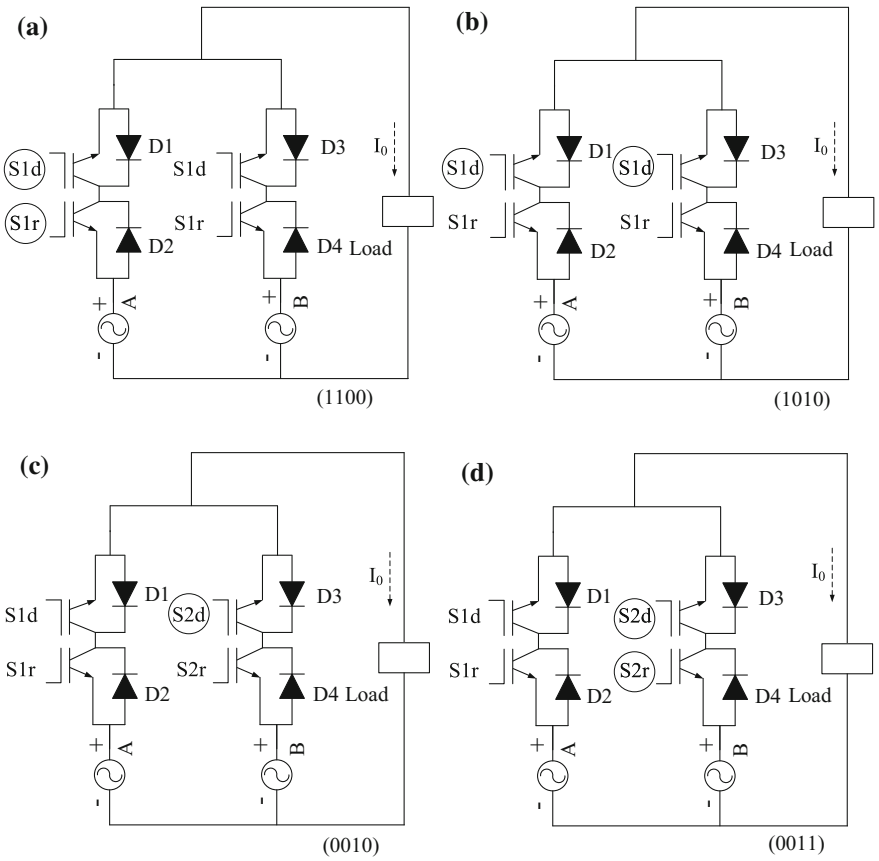

Fig. 6.9 Three-step two-leg switching sequence when $I_0 > 0$, $V_{AB} < 0$: **a** initial step; **b** 1st step; **c** 2nd step; and **d** 3rd step

conduction within the switching system. In the two-leg commutation in Fig. 6.12a, the switches turn on and turn off to follow the load current polarity. For the proper switching, safe switching combinations as shown in Table 6.3 are needed. Two states are observed in this table, i.e. one being main states that are unconditional and the other being intermediate ones that rely on the current flow direction. It is assumed that there would be a positive current sign when $I_0 > 0$ and a negative when $I_0 < 0$ and, if the current is indeterminate, the switching sequence will adopt a dead band commutation. For the abnormal condition of current measurement, each switch is linked with a zero state for the extra safety of the switching commutation. This developed state machine graph is illustrated in Fig. 6.11 in which the switching trail can be clearly understood for each current path and the dead band situation.

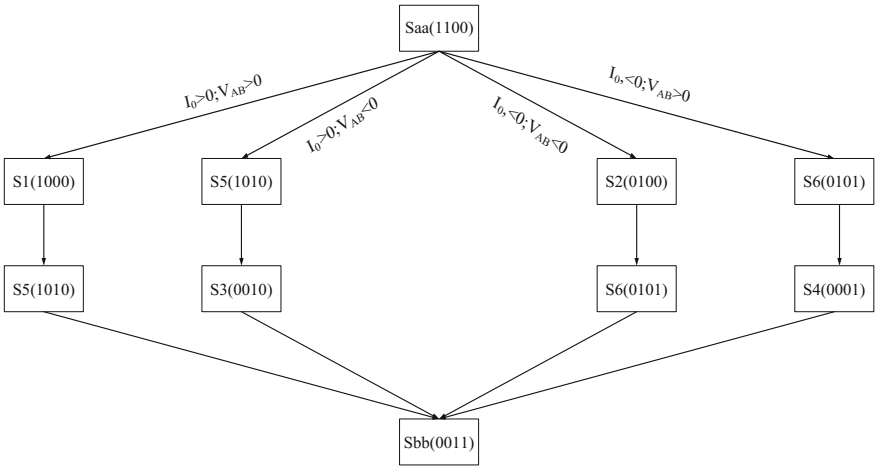

Fig. 6.10 Diagram of three-step two-leg switching

For four-step commutation with the condition of $I_0 > 0$, the following switching steps are conducted:

- Initial step: the SiC-MOSFET's switches S1d and S1r are in the on position. In Fig. 6.12a, the dotted line indicates the current flow path. The switching arrangement of this initial step is '1100'.
- Step 1: Fig. 6.12b, follows the '1000' switching sequence. In this step, the SiC-MOSFET's switch (S1r) is deactivated because the switching sequence is independent of reverse load current. To visualise the effect of this step, a dotted line showing the conduction path is provided in the switching diagram (Fig. 6.12b).
- Step 2: Fig. 6.12c represents the '1010' switching sequence. In this step, switch S2r is activated where the current flows from source to load side. For more visualisation, the dotted lines show the conduction paths.
- Step 3: Fig. 6.12d illustrates the '0010' switching sequence. In this step, switch S1d is in the off position and conducts the output current flow inside the off going bidirectional switch. The active switching path is also marked by the dotted lines in Fig. 6.12d.
- Step 4: Fig. 6.12e shown the '0011' switching path. In this switching sequence, switch S1r is turned on and active switch does not take part in the flow of the current on the incoming switch. The active switch '0011' is marked by a dotted line in Fig. 6.12e.

Similarly, for the $I_0 < 0$ current condition, another four step current commutation can be developed.

For more visualisation of the switching arrangements, a combined state and switching diagram is provided in Fig. 6.13. Where the explanation is continued based on the different current polarity.

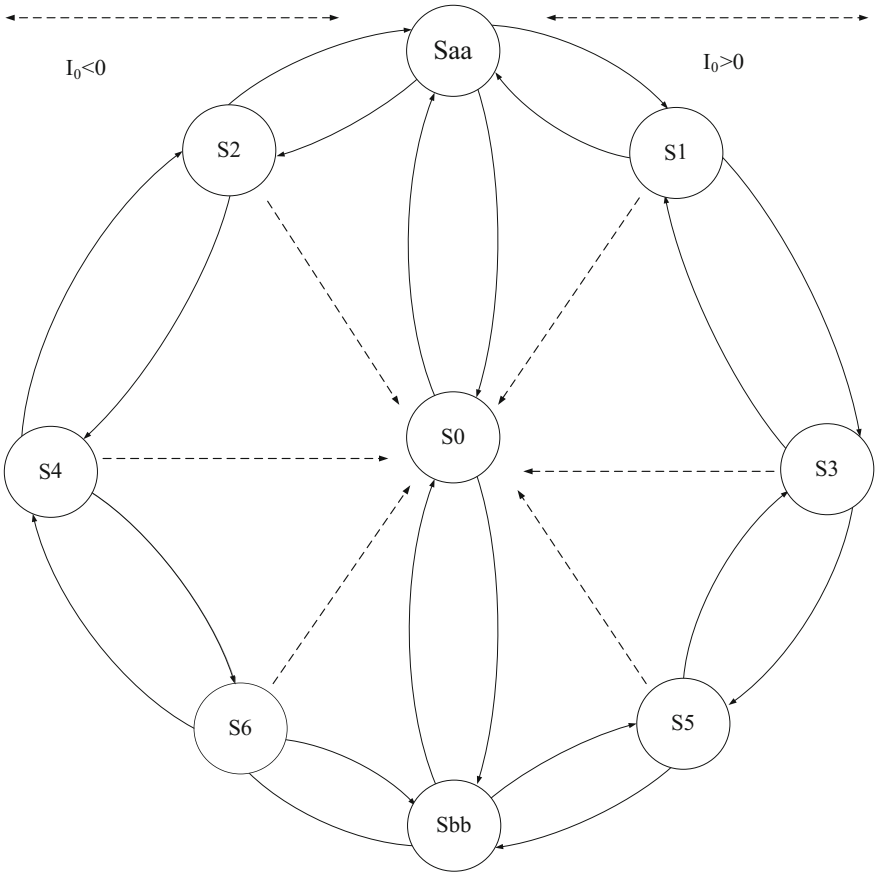

Fig. 6.11 Four-step two-leg state diagram

In a similar way, four step three- and four leg commutations are explained. The explored three- and four leg commutations are depicted in Figs. 6.14 and 6.15 respectively and no hazard in main and intermediate switching states is found in all cases in Tables 6.4 and 6.5 respectively.

Based on technological developments, a CAS series LEM was used for measuring the output currents [4]. However, if errors cause the current direction to be inaccurately assessed, the wrong sequence may be followed. To better protect against this unexpected condition, a dead-time commutation is used at low currents. Another limitation of four-step commutation is for any commutation outside between the inputs phases; gate drives have the capability to ensure that the correct devices turn on during the bidirectional switching operation for a normal current flow. This is resolved by setting a proper threshold level.

For N-leg four-step commutation, the switching sequences are shown in Table 6.6, where the main and intermediate states are introduced. The state diagram

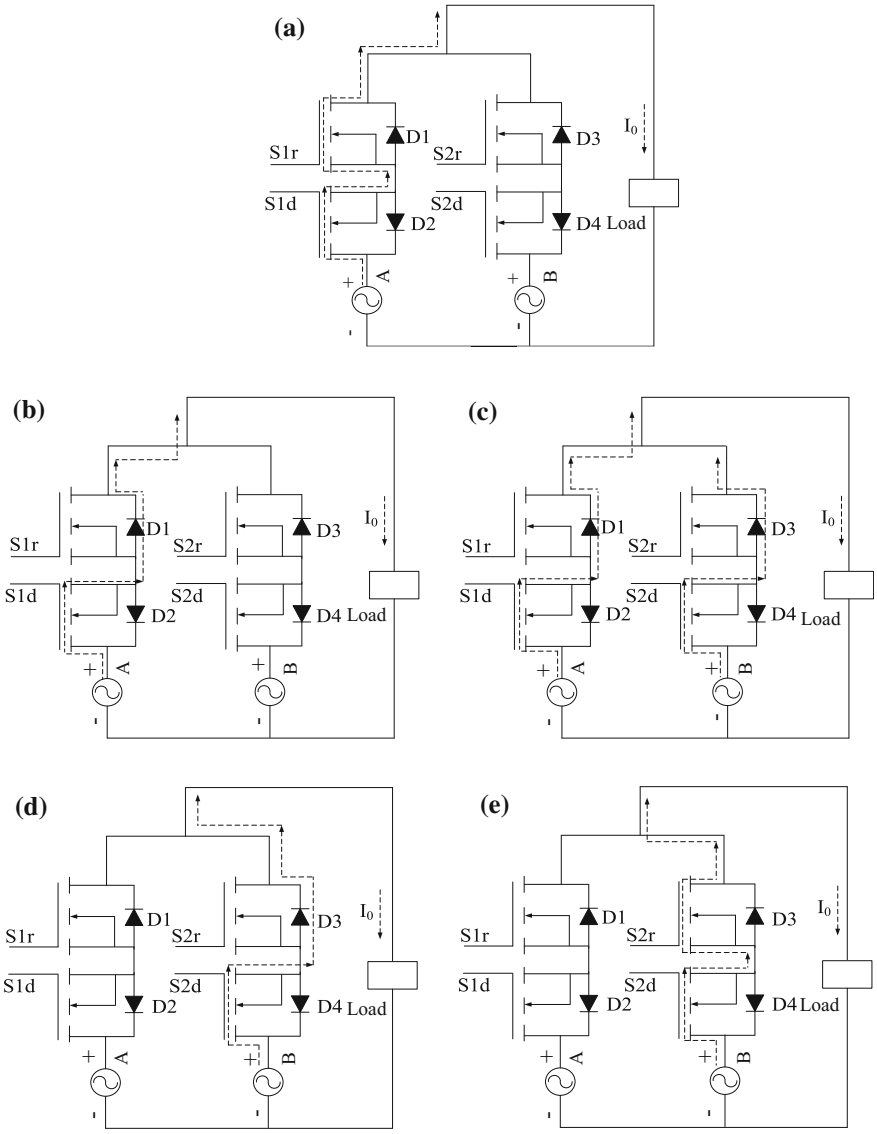

Fig. 6.12 Switching diagram for four-step two-leg current commutation: **a** initial step; **b** 1st step; **c** 2nd step; **d** 3rd step; and **e** 4th step

in Fig. 6.16 shows the different current direction conditions. For the positive current direction, from the A to B phases, the state transition follows the Saa-S1-S9-S3-Sbb pathway and, similarly for the B to C and N phases, the transition path is as shown in Fig. 6.16. In a comparable way, the negative current direction takes a different state pathway which is also shown in Fig. 6.16. Additionally, an antiparallel

Table 6.3 Switching sequence for two-leg four-step commutation

State/switches/current sign	S1d	S1r	S2d	S2r	I_0
Saa	1	1	0	0	±
Sbb	0	0	1	1	±
S1	1	0	0	0	+
S3	1	0	1	0	+
S5	0	0	1	0	+
S2	0	1	0	0	−
S4	0	1	0	1	−
S6	0	0	0	1	−
S0	0	0	0	0	±

arrangement for bi-directional switching of the N phases MC scheme has also been shown in Fig. 6.17.

From the discussion of different types of commutation, it can be summarised that the improved four-step commutation should be a good option for a MC. In the next section, different switch implementations are discussed.

6.1.2 Switching Topologies

6.1.2.1 One Degree of Freedom Switch

For the design of a forced commutated cyclo-converter, four diodes and a gate turn-off switching device were considered in [6], where the switch operates with one degree of freedom. The arrangement developed in [7] consists of a bridge rectifier with a controllable device. The bi-directional diode bridge with one device is proposed in [8]. In Fig. 6.18, the IGBT is active all the time that the switch is in the on state [9].

This structural diode bridge-switching arrangement has the advantage of providing one active device that is needed to complete bilateral switching [10], but this also has drawbacks [10, 11]. The drawbacks are:

- As current will flow the IGBT and two diodes (D1, D4 forward and D3, D2 reverse direction current flow respectively), these three devices are active at the same time with greater associated conduction loss; and
- As the IGBT diode bridge-switching module continuously provides the current flow path, the direction of the current flow cannot be controlled. Therefore, when the direction of the current changes, the switch current direction does not change due to the associated diodes.

For more flexible operation, the zero switch loss IGBT-based bi-directional switch proposed in [12] has a bi-directional blocking capability and less switching loss.

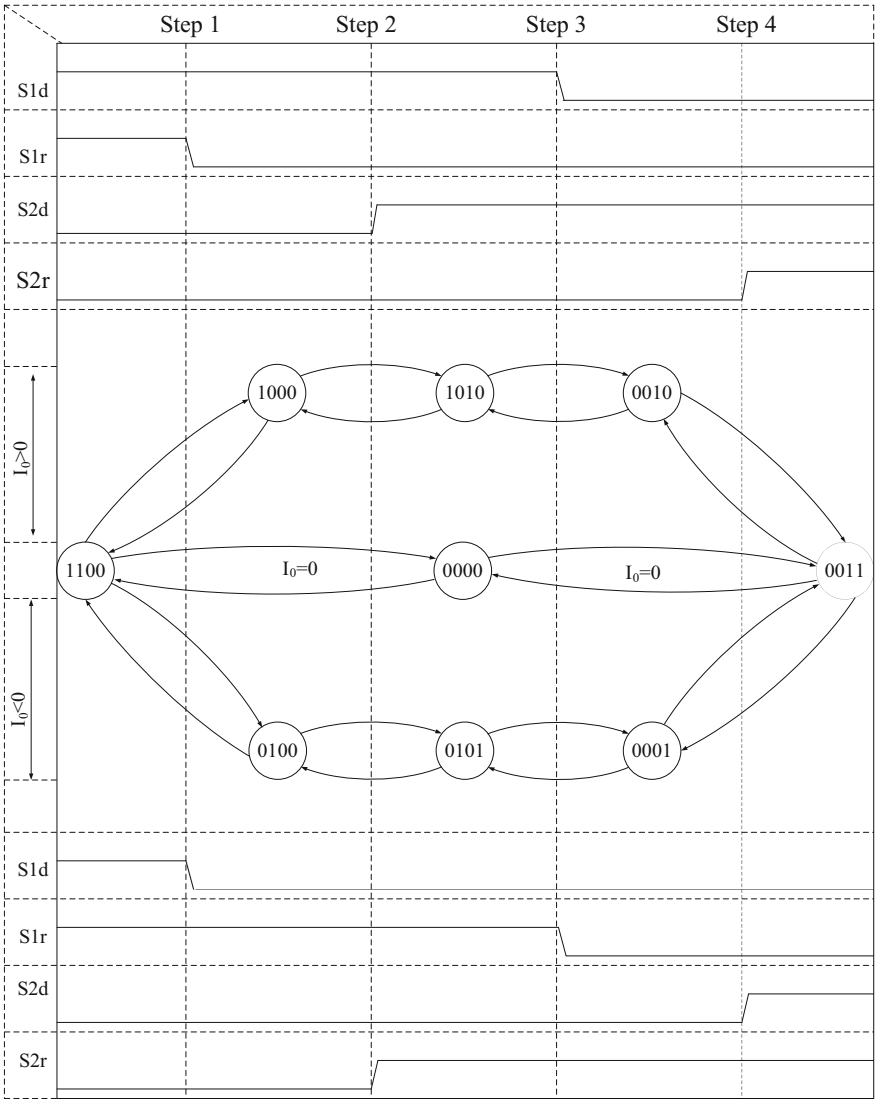

Fig. 6.13 Diagram of four-step two-leg state and switching

A resonant turn off allows zero switch loss [13] using some passive elements, as shown in Fig. 6.19. The proposed switches are turned on at zero current and turned off at the zero voltage at the same time.

The advantage of this system is that there is zero turn on current due to 'L1' and zero turn off voltage due to capacitor 'C'.

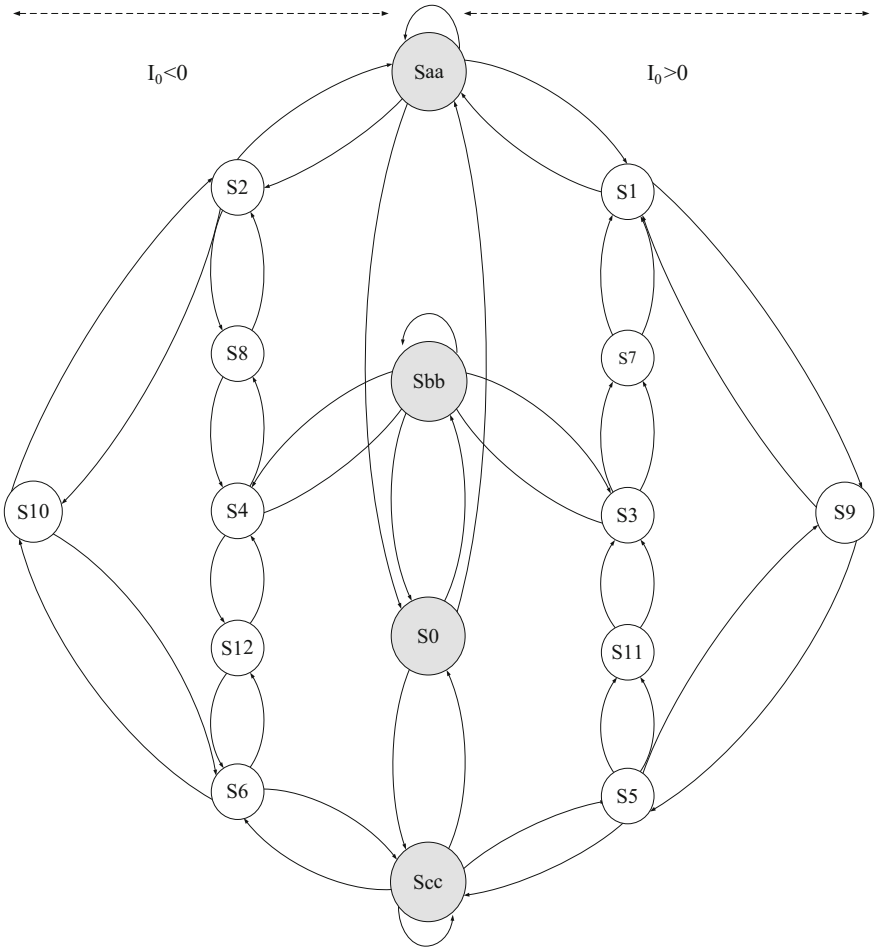

Fig. 6.14 Four-step three-leg state diagram

6.1.2.2 Two Degree of Freedom Switch

Si IGBT Switches

To overcome the limitation of the one degree of freedom diode bridge-switching process, a common emitter (CE) and common collector -based two degrees of freedom IGBT switch with an antiparallel of diodes was proposed in [10]. In Fig. 6.20, CE- and common collector-based switching cells are shown, the diodes of each of which have a reverse voltage-blocking capability. The benefit of CE systems is that they have the same gate driver ground point, that is, two IGBTs are driven at the same point [9]. Two IGBTs allow independent control of switching for each current direction. These anti-parallel arrangements fulfil the basic criteria for a safe

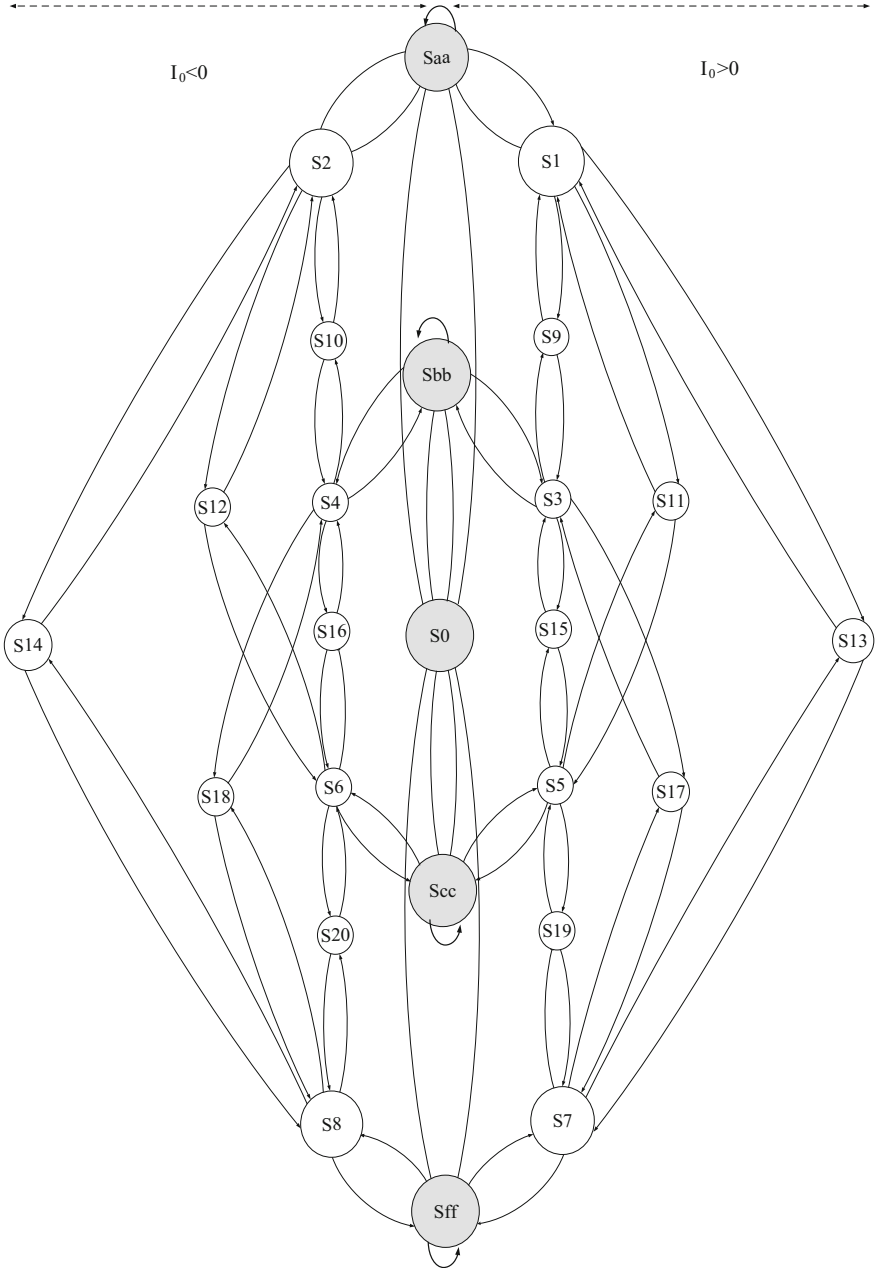

Fig. 6.15 Four-step four-leg state diagram

Table 6.4 Switching sequence for four-step three-leg commutation (positive, negative and zero current conditions)

State/ switches/ current sign	S1d	S1r	S2d	S2r	S3d	S3r	I_0
Saa	1	1	0	0	0	0	±
Sbb	0	0	1	1	0	0	±
Scc	0	0	0	0	1	1	±
S1	1	0	0	0	0	0	+
S2	0	1	0	0	0	0	−
S3	0	0	1	0	0	0	+
S4	0	0	0	1	0	0	−
S5	0	0	0	0	1	0	+
S6	0	0	0	0	0	1	−
S7	1	0	1	0	0	0	+
S8	0	1	0	1	0	0	−
S9	1	0	0	0	1	0	+
S10	0	1	0	0	0	0	−
S11	0	0	1	0	0	0	+
S12	0	0	0	1	0	0	−
S0	0	0	0	0	0	0	±

commutation process by eliminating local snubber circuits and reducing the switching loss [14]. Furthermore, two degrees of freedom switching incurs less conduction loss, that is, only one diode and one switch will conduct at a particular given time.

Furthermore, in the complex six-pack CE IGBT-based switching module building process discussed in [10], the system provides a lower stray inductance effect on the commutation path. A more detailed discussion of CE and common collector is provided in [15], where the proposed switching occurs without a central common connection. However while, for the CE arrangement, only a six-pack isolated power supply is required to run the gate drivers.

The following are possible disadvantages of the common collector:

- To make a three by three MC, nine bi-directional common collector switches are needed which require a switching arrangement with 18 isolated power supplies; and
- For antiparallel common collector bi-directional IGBT switches, an external body diode is needed; for a compact circuit arrangement, this switching concept is not viable.

Si-MOSFETs and Si-GaN Switches

Silicon-MOSFETs and IGBTs have been the workhorses of power electronics. However, they have limitations on speed, forward drop and reverse recovery.

Table 6.5 Switching sequence for four-step four-leg commutation (positive, negative and zero current conditions)

State\Switches\ Current sign	S1d	S1r	S2d	S2r	S3d	S3r	S4d	S4r	I_0
Saa	1	1	0	0	0	0	0	0	
Sbb	0	0	1	1	0	0	0	0	
Scc	0	0	0	0	1	1	0	0	
Sdd	0	0	0	0	0	0	1	1	
S2	1	0	0	0	0	0	0	0	
S4	0	0	1	0	0	0	0	0	
S6	0	0	0	0	1	0	0	0	
S8	0	0	0	0	0	0	1	0	I>0
S10	1	0	1	0	0	0	0	0	
S12	1	0	0	0	1	0	0	0	
S14	1	0	0	0	0	0	1	0	
S16	0	0	1	0	1	0	0	0	
S18	0	0	1	0	0	0	1	0	
S20	0	0	0	0	1	0	1	0	
S0	0	0	0	0	0	0	0	0	I=0
Saa	1	1	0	0	0	0	0	0	
Sbb	0	0	1	1	0	0	0	0	
Scc	0	0	0	0	1	1	0	0	
Sdd	0	0	0	0	0	0	1	1	
S1	0	1	0	0	0	0	0	0	
S3	0	0	0	1	0	0	0	0	
S5	0	0	0	0	0	1	0	0	
S7	0	0	0	0	0	0	0	1	I<0
S9	0	1	0	1	0	0	0	0	
S11	0	1	0	0	0	1	0	0	
S13	0	1	0	0	0	0	0	1	
S15	0	0	0	1	0	1	0	0	
S17	0	0	0	1	0	0	0	1	
S19	0	0	0	0	0	1	0	1	

New wide band gap (WBG) materials offer improvements. A new cascaded GaN and the Si-based semiconductor switching for achieving zero voltage switching that has the advantage of a WBG high-speed switching frequency is provided in [14], with a low-voltage Si-based MOSFET connected in series to control the GaN on/off

Table 6.6 Switching sequence for 'N'-leg four-step commutation (positive, negative and zero current conditions) switching sequences for positive, negative and zero current conditions

State/switches/current sign	S1d	S1r	S2d	S2r	S3d	S3r	S4d	S4r		Snd	Snr	I_0
Saa	1	1	0	0	0	0	0	0	—	0	0	±
Sbb	0	0	1	1	0	0	0	0	—	0	0	±
Scc	0	0	0	0	1	1	0	0	—	0	0	±
Sdd	0	0	0	0	0	0	1	1	—	0	0	±
⋮	⋮	⋮	⋮	⋮	⋮	⋮	⋮	⋮		⋮	⋮	⋮
Snn	0	0	0	0	0	0	0	0	—	1	1	±
S1	1	0	0	0	0	0	0	0	—	0	0	+
S2	0	1	0	0	0	0	0	0	—	0	0	–
S3	0	0	1	0	0	0	0	0	—	0	0	+
S4	0	0	0	1	0	0	0	0	—	0	0	–
S5	0	0	0	0	1	0	0	0	—	0	0	+
S6	0	0	0	0	0	1	0	0	—	0	0	–
S7	0	0	0	0	0	0	1	0	—	0	0	+
S8	0	0	0	0	0	0	0	1	—	0	0	–
⋮	⋮	⋮	⋮	⋮	⋮	⋮	⋮	⋮	—	⋮	⋮	±
Sn1	0	0	0	0	0	0	0	0	—	1	0	+
Sn2	0	0	0	0	0	0	0	0	—	0	1	–
S9	1	0	1	0	0	0	0	0	—	0	0	+
S10	0	1	0	1	0	0	0	0	—	0	0	–
S11	1	0	0	0	1	0	0	0	—	0	0	+
S12	0	1	0	0	0	1	0	0	—	0	0	–
S13	1	0	0	0	0	0	1	0	—	0	0	+
S14	0	1	0	0	0	0	0	1	—	0	0	–
⋮	⋮	⋮	⋮	⋮	⋮	⋮	⋮	⋮	—	⋮	⋮	±
Sn3	1	0	0	0	0	0	0	0	—	1	0	+
Sn4	0	1	0	0	0	0	0	0	—	0	1	–
S15	0	0	1	0	1	0	0	0	—	0	0	+
S16	0	0	0	1	0	1	0	0	—	0	0	–
S17	0	0	1	0	0	0	1	0	—	0	0	+
S18	0	0	0	1	0	0	0	1	—	0	0	–
⋮	⋮	⋮	⋮	⋮	⋮	⋮	⋮	⋮	—	⋮	⋮	
Sn5	0	0	1	0	0	0	0	0	—	1	0	+
Sn6	0	0	0	1	0	0	0	0	—	0	1	–
S19	0	0	0	0	1	0	1	0	—	0	0	+
S20	0	0	0	0	0	1	0	1	—	0	0	–
⋮	⋮	⋮	⋮	⋮	⋮	⋮	⋮	⋮	—	⋮	⋮	±
Sn7	0	0	0	0	1	0	0	0	—	1	0	+
Sn8	0	0	0	0	0	1	0	0	—	0	1	–
⋮	⋮	⋮	⋮	⋮	⋮	⋮	⋮	⋮	—	⋮	⋮	
Sn9	0	0	0	0	0	0	1	0	—	1	0	+
Sn10	0	0	0	0	0	0	0	1	—	0	1	–

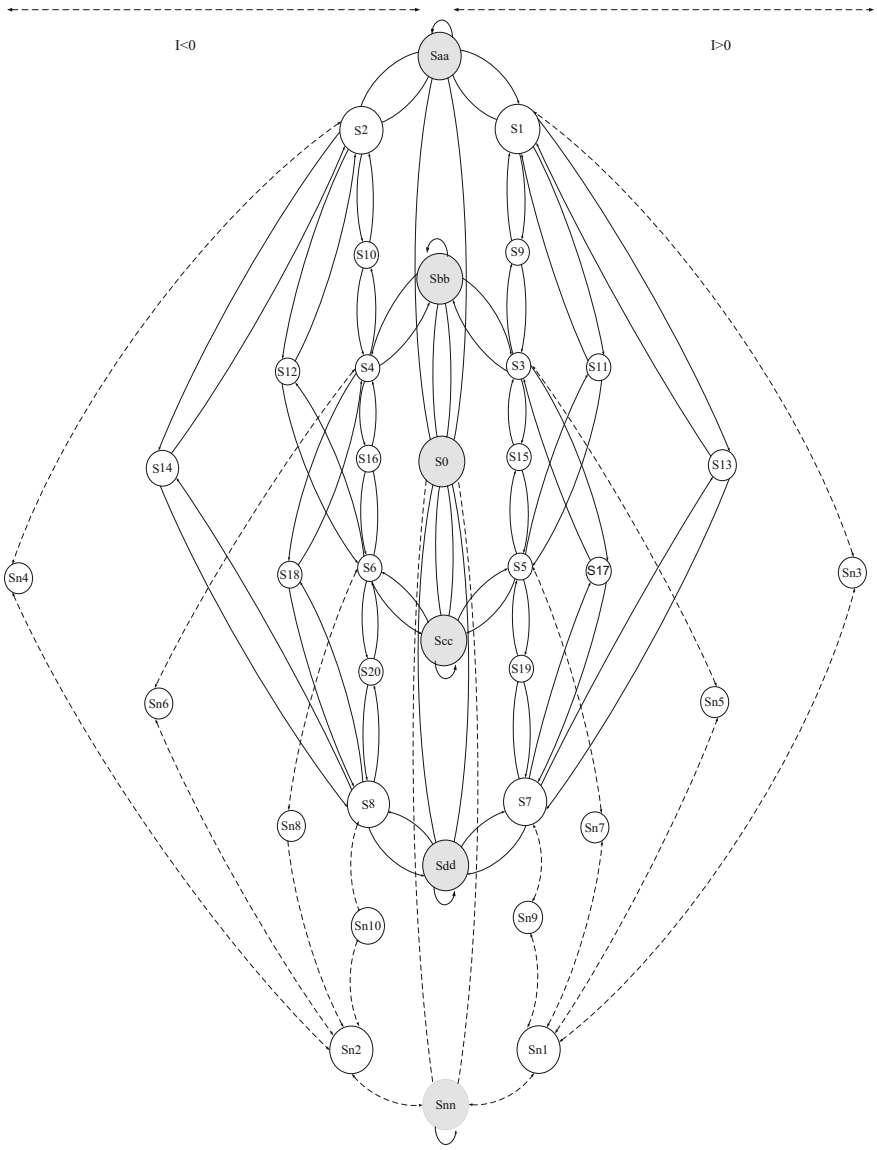

Fig. 6.16 'N'-leg four-step commutation process

switching state (Fig. 6.21). However, a problem can occur between the interactions of the two switching devices as a large parasitic effect is created and the switching system becomes more unstable [14]. To minimise these effects, a chip-on-chip technique is explored in [14].

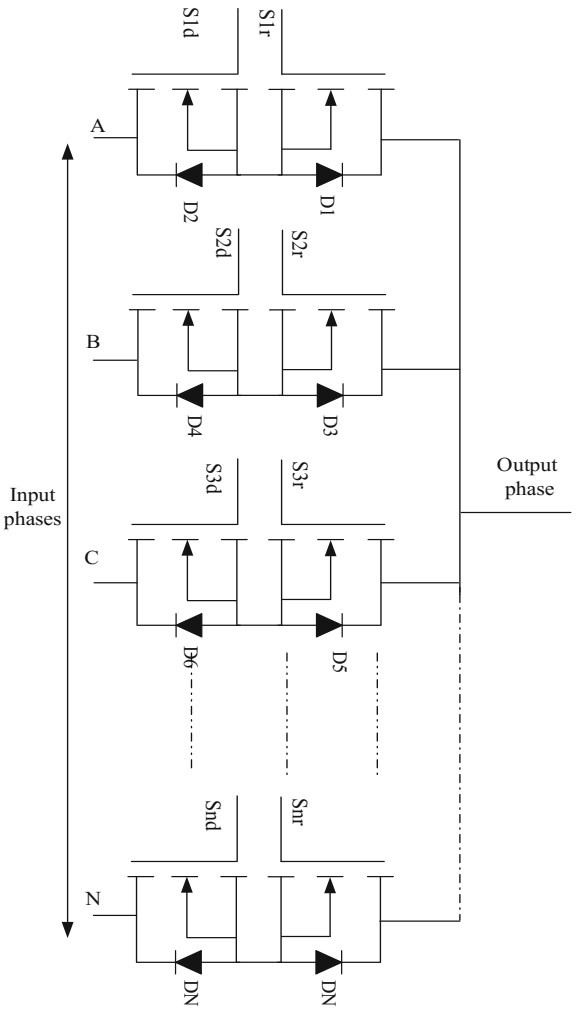

Fig. 6.17 'N'-leg MC switching scheme

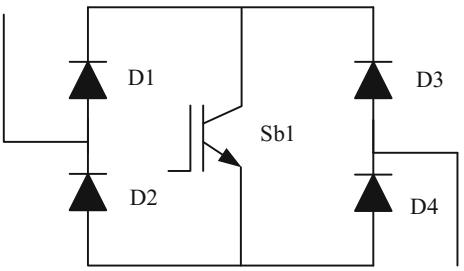

Fig. 6.18 Bridge-rectifier bi-directional switch

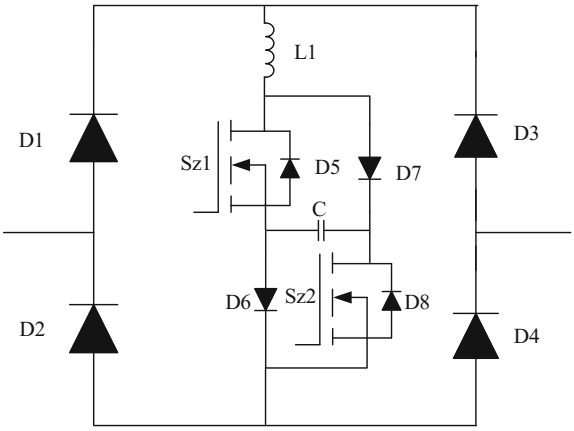

Fig. 6.19 Basic zero switching loss bi-directional switches

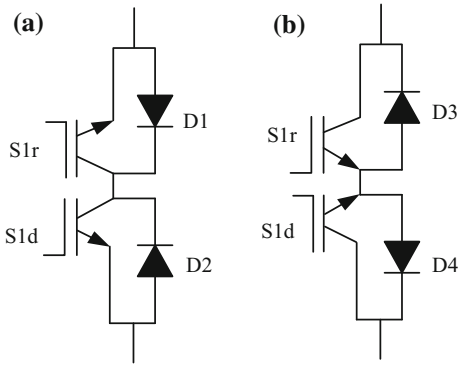

Fig. 6.20 **a** IGBT-based common-collector bi-directional switch and **b** IGBT-based common-emitter bi-directional switch

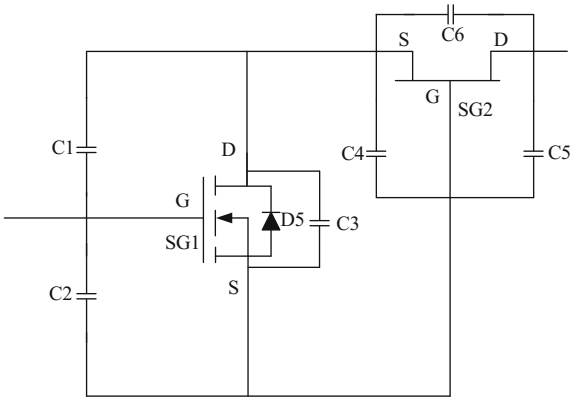

Fig. 6.21 Cascaded GaN devices

SiC-JFETs Switch

The SiC-based power switching devices provide a much faster switching rate than Si-based semiconductor ones. A SiC Schottky diode switch eliminates the reverse recovery effect in many applications. Replacing a traditional diode with a SiC Schottky diode may reduce the switching loss by approximately 30–50% which follows the hard switching condition [16–19]. Although the hybrid (Si-IGBT–SiC Schottky) Si-SiC reduces the switching loss, its limitation is that its power density and efficiency are not transferable to those of a traditional Si-based IGBT. A SiC-JFET has been introduced in [11]. Basically, it was developed based on the WBG semiconductors in which the dielectric breakdown field's strength and thermal conductivity are higher than those of Si-based switching devices [20, 21]. Due to its faster-switching speed, it has gained greater attention as a suitable switching device. However, its much faster-switching speed creates increased Miller currents within the switching circuit [22]. To eliminate this, a layer-optimised single-switch double-pulse tester technique and vertical channel SiC-JFETs have been introduced in [23–25]. Nevertheless, it has still lagged regarding reverse recovery characteristics [26]. An enhanced reverse characteristic SiC-JFET model is explored in [27]. However, it does not completely satisfy the high-temperature issue. To overcome that, normally-off SiC-JFETs are proposed in [28]. The proposed switching device follows an arrangement of no external anti-parallel diodes [29, 30]. The switching arrangement is shown in Fig. 6.22. This device has the potentiality to block the voltage and handle the current-carrying capability in both directions. However, the SiC JFETs still has some limitations.

The limitations are [20, 31]:

- Their switching devices are not economically viable as they require power modules which are more expensive than those of other switching devices;
- The switching performances of SiC power devices are often a trade-off between the complexity of the gate driver and the desired performance which is especially true for SiC-BJTs and -JFETs; and
- Another challenge is starting them properly, that is, ensuring that a control supply is available before the grid is connected since they are normally on the state which can be resolved using a battery backup cell.

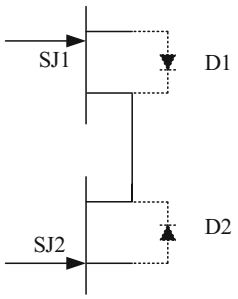

Fig. 6.22 SiC-JFETs switch

SiC MOSFETs Switch

The SiC-MOSFET has been identified as a potential device in a power electronic converter [32]. A great deal of research has recently been conducted on aspects of SiC-based MOSFET devices, such as higher switching efficiency and also high power density [33–38]. The switching performance of the SiC is improved in [39] in which the development of minimum gate-drive complexity is explored [30]. An evaluation taking into account SiC-MOSFET MC switching [40] shows that it has the capability to operate over a wide temperature range [41]. Structurally, a SiC-MOSFET's has the advantages of lower on state resistance, a much lower switching loss, higher switching speed and higher temperature operating range [42, 43]. Basically, it has much lower drift resistance and minor tail current gain [11] which enables a higher switching frequency and also maintains a very low body diode's recovery loss. The more specific advantages of a SiC-MOSFET are:

- Increased switching efficiency because of its reduced switching loss; and
- A reduction in the size of passive components, such as inductors and capacitors, due to its increased switching frequency.

6.1.3 Experimental Set-Up for Switching and Commutation Strategies

An experimental set-up was built to test the behaviour of the switching device and its commutation strategies. In this experiment, dc voltages were applied to the input terminals of the MC to operate the system operating as a dc-dc buck converter at fixed duty cycles type operation. Figure 6.23 shows a two-leg switch and load which would be used for Si-MOSFETs and SiC-MOSFETs with three state switching [44].

6.1.3.1 Si-MOSFETs Switching Strategies

Period 1: The switch S2r and the body diode of switch S2d conducts while switch S1r remains open.
Period 2: In this period, the body diode of switch S1r and S1d conduct. As the Si-MOSFET's reverse recovery response is slow, a high current flows from switch S1r to S2r via the body diode of the switch S1d and S2d.
Period 3: In this period, reverse recovery of switch S2d is completed. The current flows through switch S1r to the load via the body diode of switch S1d.

For the better visualisation of period 1, period 2 and period 3 conduction paths, dotted lines are provided on Fig. 6.23.

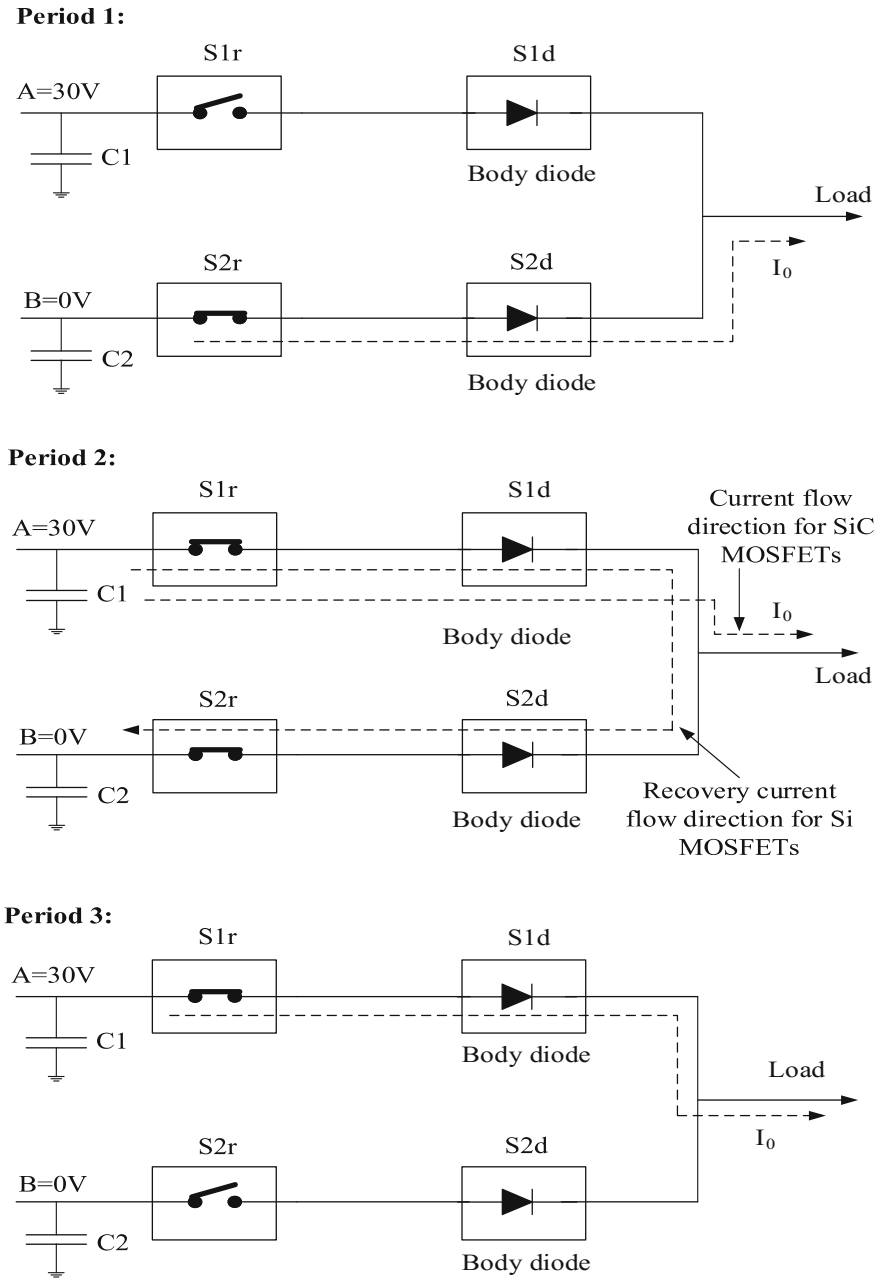

Fig. 6.23 Experimental setup for different switching arrangements

6.1.3.2 SiC-MOSFETs Switching

Period 1: In this switching process, switch S2r and the body diode of switch S2d is convoying, at that moment switch S1r is not in conduction mode. For the better visualisation of this period, a current conduction path is provided which marked by a dotted line.
Period 2: In this case, the body diode of the switch S1r and S1d conducts. However, due to the SiC MOSFET's faster reverse recovery capability, no current will flow from the switch S1r to S2r via the body diode of the switches S1d and S2d. The dotted line shows the direction of current flow in this case.
Period 3: The current flows from switch S1r to the load through the body diode of switch S1d, which is shown by a dotted line.

To test the viability of the switching device performance, the MC is first implemented and tested with Si-MOSFETs switches. Figure 6.24 shows the switching responses where the top, middle and bottom traces represent the gate to source voltage, the drain to source voltage and the drain to source current respectively.

Based on the switching combinations, the response of the switches are divided into three periods. In period-1, no current drifts through the active switch S1r and the body diode. In Period-2, a tremendous amount of current flows from the switch S1r to S2r via the S2d switch's body diode. In continuation, for the huge generated current, switch S1r gained higher turn off voltages. The current overshoot is illustrated in the bottom trace in Fig. 6.24, which is around 15 A. To minimise the reverse recovery issue, a switch modification is done by the SiC MOSFETs. The modified switches have the faster response capability of the body diodes and the reverse recovery is much lower. Figure 6.25 shows the switching modification impact. The figure illustrates that there is no ringing on the switching rising edge.

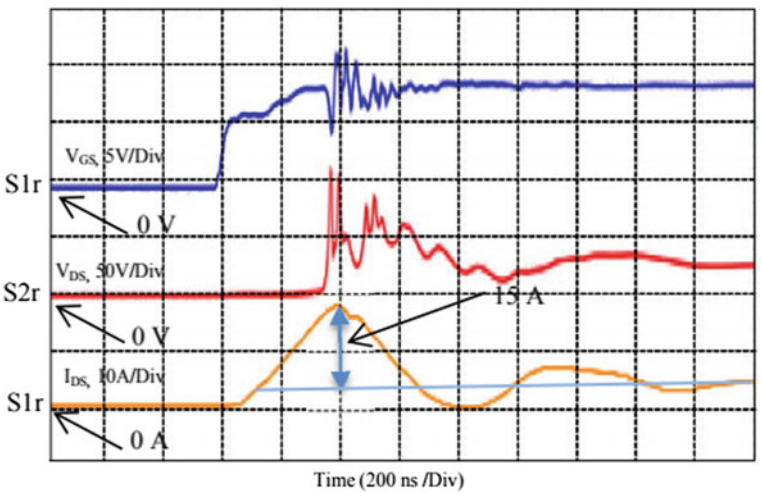

Fig. 6.24 Switching responses using Si MOSFETs

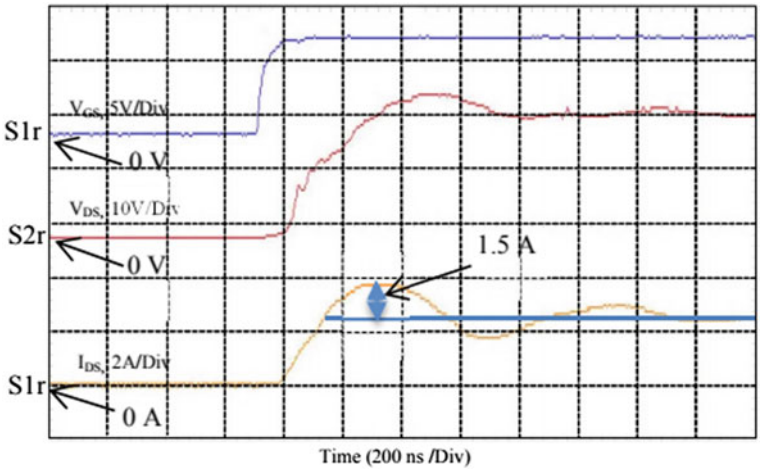

Fig. 6.25 Switching responses using SiC MOSFETs

On that figure, the switching current overshoot is 1.5 A which is 10 times less than the Si-MOSFET based switching.

Another experiment is conducted to test the MC for proper commutation as shown in Fig. 6.26. The experimental setup is designed to supply DC inputs of 15, 10 and 5 V on the A, B and C phases respectively with the SiC-MOSFETs device. The results are presented in Fig. 6.27 and demonstrate that the commutation process follows the proper staircase arrangement. This means that it follows the proper switching sequence.

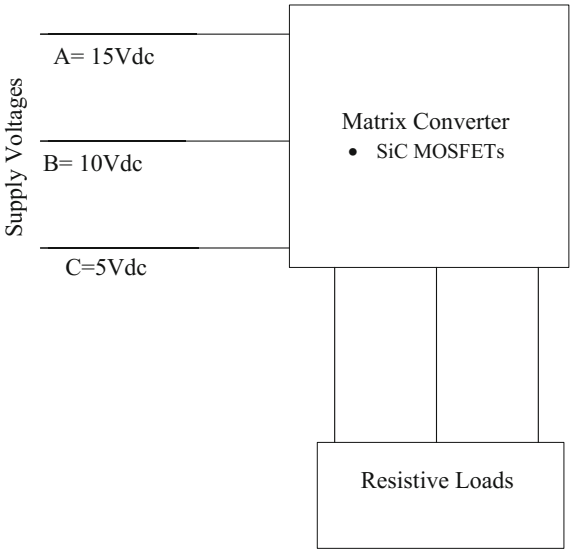

Fig. 6.26 Experimental setup for checking proper commutation steps

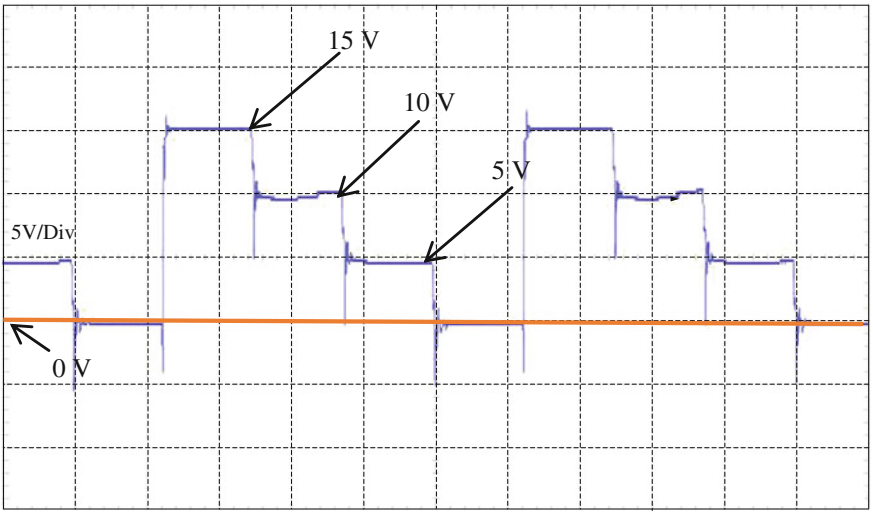

Fig. 6.27 Proper commutation steps

For the experimental validation of the improved four-step commutation process, an experimental setup is developed and the experimental results show that the line to line output voltages for a matrix converter operating with AC input voltages produces the three phase output AC waveform shown in Fig. 6.29. The physical converter is shown in Fig. 6.28, which is a four by four matrix for LV voltage

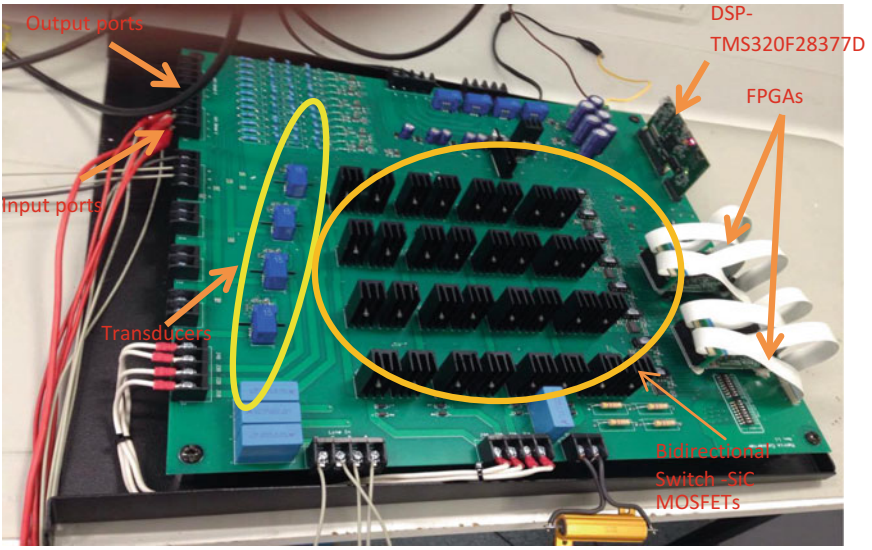

Fig. 6.28 MC prototype

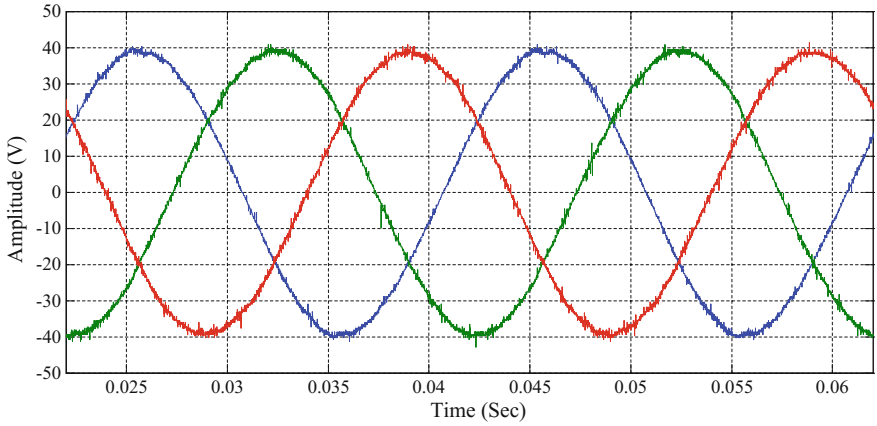

Fig. 6.29 Experiment response of output voltage with AC supply and balanced load

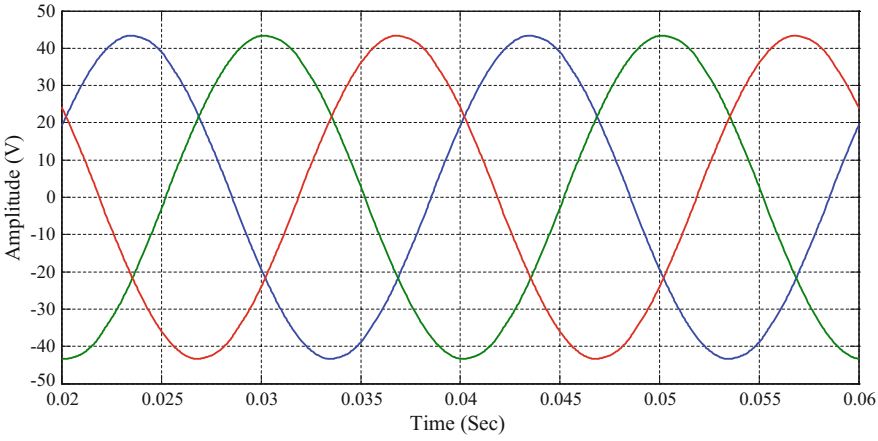

Fig. 6.30 Simulation response of output voltage with AC supply and balanced load

regulation operations. The MC is controlled by a Texas Instruments Delfino TMS320F28377D processor and FPGAs (FS609) are used to implement the commutation state machines. The simulation model was also developed and analysed. Figure 6.30 shows the simulation response of the line to line AC output voltage which closely follows the experimental response.

6.2 Summary

In this chapter, various two-, three- and four-step commutation strategies were investigated for proper switching of the MC. After considering their limitations, a four-leg four-step commutation strategy was selected. Both the advantages and limitations of each switching process were presented which led to a new switching process being followed in the application of the MC. Finally, it was determined that four step commutation based SiC-MOSFETs were the best choice for MC application. The prototype's responses from the commutation process with different current conditions, positive, negative and zero, were examined in the FPGA platform. An experimental setup with different types of switching combinations was also built in the MC application, with the experimental results showing that the reverse recovery time of a SiC-based MOSFET was much faster than the Si-based MOSFETs. The responses clearly demonstrated that there was no distortion on the rising edge of the step transition. However, there was a parasitic effect which led to slight ringing. To minimise this, an RC damper was introduced in the experimental hardware. The simulation and experimental results reveal that the SiC- MOSFET based MC can be applicable for the mitigation of power quality issues in LV and MV networks with distributed generation.

References

1. Burany N (1989) Safe control of four-quadrant switches. Conference Records of IEEE-Industry Applications Society Annual Meeting (IAS), 1-5 Oct 1989, San Diego, California, USA, pp 1190–1194
2. Empringham L, Wheeler PW, Clare JC (1998) Intelligent commutation of matrix converter Bi-directional switch cells using novel gate drive techniques. Proceedings of power electronics specialists conference (PESC),18–21 May 1998, Fukuoka, Japan, pp 707–713
3. Empringham L, Wheeler PW, Clare JC (2000) A matrix converter induction motor drive using intelligent gate drive level current commutation techniques. Proceedings of industry applications conference (IAC), pp 1936–1941
4. Iseghem PV (2008) CAS/CASR/CKSR series current transducers insulated highly accurate measurements from 1.5 to 50 ARMS. Available https://www.digikey.com.au/Web%20Export/Supplier%20Content/LEM_398/PDF/LEM_CAS_CASR_CKSR.pdf?redirected=1
5. Lettl J, Linhart L, Bauer L (2011) Matrix converter commutation time reduction. PIERS proceedings
6. Ziogas PD, Khan SI, Rashid MH (1986) Analysis and design of forced commutated cycloconverter Structures with improved transfer characteristics. IEEE Trans Ind Appl 33 (3):271–280
7. Neft CL, Schauder CD (1992) Theory and design of a 30-Hp matrix converter. IEEE Trans Ind Appl 28(3):546–551
8. Beasant RR, Beattie WC, Refsum A (1990) An approach to the realisation of a high power Venturini converter. 21st Annual IEEE Conference on Power Electronics Specialists (PESC), San Antonio, TX, USA, 1990, pp 291–297
9. Wheeler PW, Grant DA (1993) A low loss matrix converter for AC variable-speed drives. Fifth European conference on power electronics and applications, 1993, Brighton, UK, pp 27–32

10. Wheeler PW, Rodriguez J, Clare JC, Empringham L, Weinstein A (2002) Matrix converters: a technology review. IEEE Trans Ind Electron 49(2):276–288
11. Scott MJ, Fu L, Yao C, Zhang X, Xu L, Wang J, Zamora RD (2014) Design considerations for wide band gap based motor drive systems. IEEE international electric vehicle conference (IEVC), 17–19 Dec 2014, Michele Ceccucci, Italy, pp 1–6
12. Bernet S, Matsuo T, Lipo TA (1996) A matrix converter using reverse blocking NPTIGBT's and optimised pulse patterns. IEEE power electronics specialists conference (PESC), June 1996, Baveno, Italy, pp 107–113
13. Pan CT, Chen TC, Shieh JJ (1993) A zero switching loss matrix converter. 24th annual IEEE power electronics specialists conference (PESC), 20–24 June 1993, Seattle, WA, USA, pp 545–550
14. Huang X, Du W, Lee FC, Li Q, Liu Z (2016) Avoiding Si MOSFET Avalanche and achieving zero-voltage switching for cascade GaN devices. IEEE Trans Power Electron 31(1):593–600
15. Klumpner C, Nielsen P, Boldea I, Blaabjerg F (2000) New steps towards a low-cost power electronic building block for matrix converters. Proceedings of industry applications society annual meeting (IAS), 08–12 Oct 2000, Rome, Italy, pp 1964–1971
16. Richmond J (2003) Hard-switched silicon IGBTs, cut switching losses in half with silicon carbide Schottky diodes. Available http://www.cree.com
17. Nakazawa M, Miyanagi T, Iwamoto S (2012) Hybrid Si-IGBT and SiC-SBD modules. Available http://www.fujielectric.com
18. Ozpineci B, Chinthavali M, Tolbert L, Kashyap A, Mantooth H (2009) A 55-kW three-phase inverter with Si IGBTs and SiC Schottky diodes. IEEE Trans Ind Electron 45(1):278–285
19. Veereddy D, Lieser E, Gangi MD (2011) 1200 V/100 A Si IGBT/SiC diode co-pack cuts switching losses. Available http://powerelectronics.com
20. Empringham L, De Lillo L, Schulz M (2014) Design challenges in the use of silicon carbide JFETs in matrix converter applications. IEEE Trans Power Electron 29(5):2563–2573
21. ROHM (2014) Application note-SiC power devices and modules. Available http://pdf.directindustry.com/pdf/rohm-semiconductor/application-note-sic-power-devices-modules/13683–594485.html
22. Josifovic I, Gerber JP, Ferreira JA (2012) Improving SiC JFET switching behavior under influence of circuit parasitic. IEEE Trans Power Electron 27(8):3843–3854
23. Sheridan DC, Ritenour A, Kelley R, Bondarenko V, Casady JB (2010) Advances in SiC VJFETs for renewable and high-efficiency power electronics applications. In: proceedings international power electronic conference (ECCE), 21–24 June 2010, Sapporo, Japan, pp 3254–3258
24. Li Y, Alexandrov P, Zhao JH (2008) 1.88-mΩ cm^2 1650-V normally on 4H-SiC TI-VJFET. IEEE Trans on Electron Dev 55(8):1880–1886
25. Veliadis V, Chen LS, Stewart EE, McCoy M, McNutt T, Van Campen S, Clarke C, De Salvo G (2005) 2.1 mΩ cm^2, 1.6 kV 4H-silicon carbide VJFET for power applications. In: proceedings semiconductor device research symposium, 07–09 Dec 2005, Bethesda, MD, USA, pp 166–167
26. Lai JS, Yu H, Zhang J, Alexandrov P, Li Y, Zhao JH, Sheng K, Hefner A, Young M (2005) Characterization of normally-off SiC vertical JFET devices and inverter circuits. In: proceedings industry applications conference (IAC), 02–06 Oct 2005, Kowloon, Hong Kong, China, pp 404–409
27. Shillington R, Gaynor M, Harrison M, Heffernan B (2010) Applications of silicon carbide JFETs in power converters. In proceedings Australasian universities power engineering conference (AUPEC), 05–08 Dec 2010, Christchurch, New Zealand, pp 1–6
28. Peftitsis D, Tolstoy G, Antonopoulos A, Rabkowski J, Jang-Kwon L, Bakowski M, Angquist L, Nee HP (2010) High-power modular multilevel converters with SiC JFETs. IEEE energy conversion congress and exposition, pp 2148–2155
29. Cai C, Zhou W, Sheng K (2013) Characteristics and application of normally-Off SiC-JFETs in converters without antiparallel diodes. IEEE Trans Power Electron 28(10):4850–4860

30. De Lillo L, Empringham L, Schulz M, Wheeler P (2011) A high power density SiC-JFET-based matrix converter. Proceedings of the 14th European conference on power electronics and applications (EPE), 30 Aug–01 Sept 2011, Birmingham, United Kingdom, pp 1–8
31. Pittini R, Zhang Z, Andersen MAE (2013) Switching performance evaluation of commercial SiC power devices (SiC JFET and SiC MOSFET) in relation to the gate driver complexity. IEEE annual international energy conversion congress and exhibition (ECCE) Asia, 03–06 June 2013, Melbourne, Australia, pp 233–239
32. ROHM (2017) SCT2120AF, N-channel SiC power MOSFET. Available http://www.rohm.com/web/global/products/-/product/SCT2120AF
33. Bellone S, Corte FGD, Albanese LF, Pezzimenti F (2011) An analytical model of the forward I-V characteristics of 4 H-SiC p-i-n diodes valid for a wide range of temperature and current. IEEE Trans Power Electron 26(10):2835–2843
34. Gachovska T, Hudgins JL, Bryant A, Santi E, Mantooth HA, Agarwal AK (2012) Modeling, simulation, and validation of a power SiC BJT. IEEE Trans Power Electron 27(10): 4338–4346
35. Sun K, Wu H, Lu J, Xing Y, Huang L (2014) Improved modeling of medium Voltage SiC MOSFET within wide temperature range. IEEE Trans Power Electron 29(5):2229–2237
36. Wood RA, Salem TE (2011) Evaluation of a 1200 V, 800 A all-SiC dual module. IEEE Trans Power Electron 26(9):2504–2511
37. Ning P, Wang F, Ngo KD (2011) High-temperature SiC power module electrical evaluation procedure. IEEE Trans Power Electron 26(11):3079–3083
38. Xu Han TJ, Jiang D, Tolbert LM, Wang F, Nagashima J, Kim SJ, Kulkarni S, Barlow F (2013) Development of a SiC JFET-based six-pack power module for a fully integrated inverter. IEEE Trans Power Electron 28(3):1464–1478
39. Safari S, Castellazzi A, Wheeler PW (2013) Performance evaluation of bidirectional SiC switch devices within matrix converter. 15th European conference on power electronics and applications (PEA), 02–06 Sept 2013, Lille, France, pp 1–9
40. Safari S, Castellazzi A, Wheeler P (2012) Evaluation of SiC power devices for a high power density matrix converter. In: IEEE energy conversion congress and exposition (ECCE), 15–20 Sept 2012, Raleigh, NC, USA pp 3934–3941
41. Funaki T, Balda JC, Junghans J, Kashyap AS, Mantooth HA, Barlow F, Kimoto T, Hikihara T (2007) Power conversion with SiC devices at extremely high ambient temperatures. IEEE Trans Power Electron 22(4):1321–1329
42. Duong TH, Berning DW, Hefner AR, Smedley KM (2007) Longterm stability test system for high-voltage, high-frequency SiC power devices. IEEE Appl Power Electron Conf 2007:1240–1246
43. Agarwal A, Das M, Hull B, Krishnaswami S, Palmour J, Richmond J, Ryu SH, Zhang J (2006) Progress in silicon carbide power devices. In Proceedings 64th device research conference (DRC), 26–28 June 2006, Pennsylvania, USA, pp 155–158
44. Ali S, Wolfs P (2016) An improved four step commutation process for silicon carbide based matrix converters. 2016 Australasian universities power engineering conference (AUPEC), 25–28 Sept 2016 Brisbane, Australia, pp 1–5

Chapter 7
Control of Renewable Energy Systems

Nasif Mahmud, Ahmad Zahedi and Md. Shamiur Rahman

7.1 Introduction

The storage of conventional energy sources is getting depleted rapidly and the consumer demand is gradually increasing. The only thing that can mitigate this imbalance is the utilization of renewable energy system (RES). The interconnection of renewable energy sources is becoming a popular tradition nowadays to satisfy the ever increasing energy demand and to ensure green energy consumption. However, because of the stochastic nature of the renewable energy sources (such as, solar energy, wind energy etc.), a large-scale accommodation of RES introduces some critical dynamics in the traditional three-phase distribution network which have adverse impact on the operation and protection of the system [1–3].

The integration of large-scale RES in the power electric networks has stronger impact on low voltage distribution networks comparing to transmission networks. The reasons are [4]:

- When the low-voltage distribution networks were built, they were designed in such a way that power would always flow unidirectionally from the generation side towards the consumer side. However, when we integrate large-scale RES in the distribution network, the surplus power after satisfying the consumer demand, flows back to traditional grid. As a result, the power flow does not remain unidirectional anymore; rather it becomes bidirectional that has adverse impact on the operation and protection of the system.

N. Mahmud (✉) · A. Zahedi
College of Science and Engineering, James Cook University, Townsville, Australia
e-mail: nasif.mahmud@my.jcu.edu.au

Md. Shamiur Rahman
Department of Engineering, Macquarie University, Sydney, NSW, Australia

M. R. Islam et al. (eds.), *Renewable Energy and the Environment*, Renewable Energy Sources & Energy Storage, https://doi.org/10.1007/978-981-10-7287-1_7

- Distribution networks work in radial topology.
- The resistance to reactance ratio of low-voltage distribution network is relatively higher than the transmission network. As a result, the active power flow has more impact on the network comparing to the reactive power.

Besides, as RESs are connected close to consumer loads, they have significant effects on the distribution network's operation, stability and economy [5–7].

7.2 Issues that Arise Due to Increased Penetration of Renewable Energy Systems

An increased accommodation of RES arises several issues in the system. These issues can be classified into three categories, which are [3]:

(1) Technical issues.
(2) Commercial issues.
(3) Regulatory issues.

The technical issues are discussed in brief below:

The technical issues can be classified into four major categories, which are:

(1) Power quality issue.
(2) Protection issue.
(3) Voltage regulation issue.
(4) Stability issue.

These technical issues are discussed in brief below:

7.2.1 Power Quality Issue

Renewable distributed generators (DG) are connected very close to the consumer loads. If a significant portion of the consumer load is satisfied by the renewable DGs, the drawn power from traditional grids will be significantly reduced. As a result, the power loss through the distribution system will also be proportionally decreased which enhances the power delivery efficiency [8].

7.2.2 Protection Issue

A large-scale integration of RES has impact on the magnitude and direction of fault current which may cause wrong actions of protections relays and fuses. The bi-directional power flow caused by the interconnection of renewable energy systems affects both fault location and service restoration functionality. Fault current

generated by the renewable energy systems triggers fault indicators between the fault and the renewable energy system locations which leads to wrong fault location diagnosis.

7.2.3 Voltage Regulation Issue

The integration of RES into the traditional distribution network is not yet problem free. The voltage regulation issue is the most significant issue that actually limits the penetration of renewable energy system into the grid. Due to the reverse excess power flow during high renewable DG generation, there is a voltage rise along the feeder. The voltage rise generally gradually increases from the substation transformer towards the feeder length depending on the DG locations and percentage of penetrations.

The voltage regulation challenge that arises when increased amount of renewable DGs are interconnected depends on several parameters, which are [9]:

1. Topology of the distribution network system.
2. Voltage level varies along with the length of the distribution feeder: Usually, the voltage gradually increases along the feeder length during high generation period and decreases during high load period. The effect of the interconnection depends on the feeder voltage level where the renewable energy source is connected.
3. Percentage of penetration of RES: Previously, the interconnection of renewable energy systems was not any significant concern as the percentage of penetration was not significant and the impact of penetration was small. However, nowadays a significant amount of RES is being interconnected which is posing huge impact on the operation of the low voltage distribution system.
4. Amount of customer load demand at any given time: If the power that is generated by the RES is consumed by the load totally, there is no voltage rise issue taking place. However, there is always an unbalance between power generated by RES and load demand.

7.2.4 Stability Issue

The stability of the distribution network is a significant concern nowadays due to the rapid increase of RES integration. The stability issues can be categorized as:

(1) **Voltage stability**: Voltage stability of the low-voltage distribution system can be affected by high DG penetrations. Considering the stochastic characteristics of RESs and grid regulations and depending on the penetration of RESs, the system can experience both advantageous and harmful effects from the view of steady state stability.

(2) **Frequency stability**: High penetration of RESs with zero inertia and higher ramp rate can affect the frequency stability of distribution system. If large-scale PVs are integrated into the system, a consequential amount of synchronous generators are replaced which result in reduced system inertia. In that case, the conventional generators existing in the system will provide torque and inertia to prevent any instability events. This can arise the frequency instability issue.

Many researchers are working on the optimized limit of RES penetration percentage. However, this limits the amount of penetration and is not welcome by the DG manufacturers [10].

7.3 Voltage Regulation Challenge of Distribution Network

Voltage regulation issue is the most noteworthy issue that arises while integrating large amount of RESs into low and medium voltage distribution network [11–13]. The voltage through the low-voltage distribution feeder needs to be within an allowable zone for the stable operation of the system. Usually, the allowable voltage variation along the system is ±6% [14]. However, this range may vary from utility to utility. Let's consider a conventional two bus distribution system.

Figure 7.1a shows a 2-bus conventional distribution feeder. Where,

V_G Grid side voltage,
V_{PCC} Voltage at point of common coupling (PCC),
R Resistance of the distribution feeder,
X Reactance of the distribution feeder,
OLTC On-load tap changer,
P_L Active power consumed by the load,
Q_L Reactive power consumed by the load.

In Fig. 7.1b, renewable distributed generator (DG) has been connected with the consumer bus which causes voltage rise at PCC. Let's consider that,

P_{DG} Active power generated by renewable DG,
Q_{DG} Reactive power generated by renewable DG.

The voltage at PCC in Fig. 7.1b is,

$$\hat{V}_{PCC} = \hat{V}_G + \hat{I}(R + jX) \tag{7.1}$$

where,

$\hat{V}_{PCC}$ Phasor quantity of DG bus voltage (PCC voltage),
$\hat{V}_G$ Phasor quantity of grid voltage,
$\hat{I}$ Phasor quantity of current.

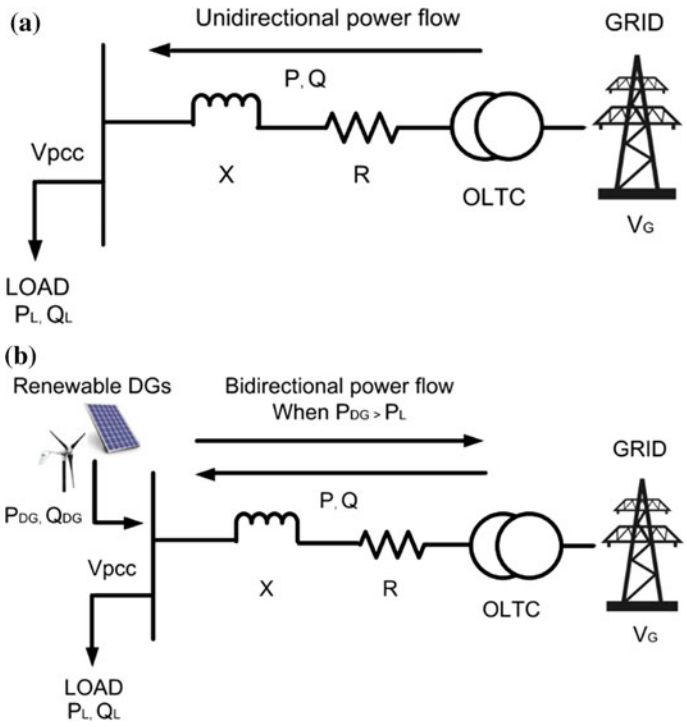

Fig. 7.1 A 2-bus distribution feeder, **a** conventional, **b** with DG

The power flow through the feeder can be written as,

$$P + jQ = \hat{V}_{PCC} \tag{7.2}$$

So, the current flow through the feeder,

$$\hat{I} = \frac{P - jQ}{\hat{V}^*_{PCC}} \tag{7.3}$$

So, Eq. (7.1) can be expressed as,

$$\hat{V}_{PCC} = \hat{V}_G + \frac{P - jQ}{\hat{V}^*_{PCC}}(R + jX) \tag{7.4}$$

$$= \hat{V}_G + \frac{RP + XQ}{\hat{V}^*_{PCC}} + j\frac{XP - RQ}{\hat{V}^*_{PCC}} \tag{7.5}$$

The angle between DG bus voltage and grid voltage is very small. Therefore, the voltage drop along the feeder is approximately equal to the real part of the voltage

drop. If we consider the DG bus voltage as reference bus, the angle of DG bus voltage is 0. As a result, Eq. (7.3) can be approximated as,

$$\Delta V \approx V_{PCC} - V_G \approx \frac{RP + XQ}{V_{PCC}} \tag{7.6}$$

where, ΔV Voltage drop across the distribution feeder.
V_{PCC} can be assumed as unity, if we consider it as base voltage. So, Eq. (7.6) can be written as follows,

$$\Delta V \approx V_{PCC} - V_G \approx RP + XQ \tag{7.7}$$

where,

$$P = (P_{DG} - P_L),$$
$$Q = (\pm Q_{DG} - Q_L)$$

So, Eq. (7.7) can be written as,

$$V_{PCC} \approx V_G + R(P_{DG} - P_L) + X(\pm Q_{DG} + Q_L) \tag{7.8}$$

We can calculate the allowable maximum percentage of penetration of DGs without affecting the feeder voltage. Two worst case scenarios need to be considered to calculate it, which are:

(1) Maximum generation minimum load ($P_{DG} = P_{DGmax}$, $P_L = 0$, $Q_L = 0$)
(2) Maximum load minimum generation ($P_{DG} = 0$, $Q_{DG} = 0$, $P_L = P_{Lmax}$).

For the first worst case scenario, (7.8) becomes,

$$V_{PCC} \approx V_G + RP_{DGmax} \tag{7.9}$$

$$\text{Or,} \quad P_{DGmax} \approx \frac{V_{PCC} - V_G}{R} \tag{7.10}$$

Let's consider, V_{PCCmax} is the allowable maximum voltage at DG bus. Therefore, to retain the feeder voltage within allowable zone, P_{DGmax} needs to be,

$$P_{DGmax} \leq \frac{V_{PCCmax} - V_G}{R} \tag{7.11}$$

For the second worst case scenario, (7.8) becomes,

$$V_{PCC} \approx V_G - RP_{Lmax} \tag{7.12}$$

$$\text{Or,} \quad P_{L\max} \approx \frac{V_G - V_{PCC}}{R} \tag{7.13}$$

Let's consider, V_{PCCmin} is the minimum allowable voltage across the feeder. So, to retain the bus voltage within allowable zone, P_{Lmax} needs to be,

$$P_{L\max} \leq \frac{V_G - V_{PCC\min}}{R} \tag{7.14}$$

Distribution network operators prefer to connect the RES at higher voltage level in the feeder where the effect is weaker. On the other hand, the DG developers prefer to connect the renewable DGs at the lower voltage level where connection expense is lesser [15, 16].

7.4 Voltage Control Strategies

There are many strategies to control the feeder voltage. They are discussed briefly as below.

7.4.1 Traditional Voltage Regulators

Voltage regulation through the low-voltage distribution feeder is usually done by some traditional voltage regulators, which are:

(1) On-load tap changer (OLTC)
(2) Switched capacitors (SC)
(3) Step voltage regulator (SVR).

A brief description of each is given below:

(1) **On-load tap changing transformer (OLTC)**: OLTCs adjust their taps to regulate the voltage through distribution system by measuring current through feeder and estimating the voltage drop. When large-scale RES are interconnected with the network, the overall situation through the feeder is unpredictable and uncontrollable by OLTCs [10]. Besides, due to RES's stochastic output and dynamic behavior of loads, the voltage variations along the feeder occur so rapidly that traditional OLTCs cannot regulate as fast as they require. New solid states OLTCs provide coordinated control capability with communication with lesser maintenance cost [17].
(2) **Step voltage regulator (SVR)**: Step voltage regulators (SVR) are located along the feeder and they regulate the feeder voltage by changing taps like OLTCs. SVRs have the similar limitations of slow operation comparing with the fast

system dynamics when intermittent renewable DGs are connected. Moreover, the increased frequent mechanical contacts those are needed for the tap changes reduce the device lifetime significantly.

(3) **Switched capacitors (SC)**: A switched capacitor (SC) is an electronic circuit element that works by moving charges into and out of capacitors when switches are opened and closed.

7.4.2 Voltage Regulation Strategies

Several strategies with different controllable components have been discussed to mitigate the feeder voltage deviation issue. They are discussed briefly below:

(a) **Generation curtailment**: This is the simplest method to resolve the voltage deviation issue. A voltage rise across the system basically occurs because of the reverse power flow through the distribution feeder when generated power is more that the consumers' loads. The excess power, after satisfying the consumers' demand, flows back to the grid. If that excess power is curtailed, the voltage rise problem is mitigated. However, this strategy causes wastage of generated power.

(b) **Reactive power control**: This is another efficient strategy to regulate the distribution feeder voltage. The DG interfacing inverters inject/absorb reactive power for voltage control during the time of voltage deviations. However, the reactive power capacity of DG interfacing inverters is restricted and the injected/absorbed reactive power causes power loss through the system [18].

(c) **Area based OLTC coordination**: The Voltage along the distribution feeder is regulated using the coordinated operation of the OLTCs. However, they are not efficient enough for voltage control when large-scale RESs are connected into the system.

(d) **Consumption shifting and curtailing**: Consumption shifting or curtailing by RESs can be another approach for voltage deviation mitigation.

(e) **Energy storage**: The utilization of battery energy storage system (BESS) is another efficient strategy for voltage control. Voltage across the distribution feeder can be regulated by controlling the charge/discharge of the BESS. However, charging/discharging of BESSs frequently decreases the life-span and regulating voltage with BESS require big investment [19].

These control solutions can be implemented in different structures. They are as follows:

(i) Centralized control structure.
(ii) Decentralized control structure.
(iii) Distributed control structure.

They are discussed briefly as follows:

7.4.2.1 Centralized Control Structure

In this control strategy, control actions are performed by the central control body. Information from different network locations is sent to the centralized controller. The centralized controller analyzes the information and initiates control action if there are any deviations from reference. To implement the appropriate control action, the centralized controller needs to know information from all the network locations which is hardly available in distribution systems. In that case, estimated measurements compensate the absence of real time measurements. Transmission systems utilize state-estimation algorithm in an efficient way for unavailable data [20]. However, the state-estimation algorithm for transmission systems cannot be used for distribution systems straightaway.

Centralized control strategy is the most efficient control strategy for small size networks with unidirectional power flow. However, this strategy is losing its popularity for some causes. They are mentioned below:

- Centralized control strategy needs large investments in communication infrastructure as information from all over the network needs to be conveyed towards the centralized control body. This strategy is not economically feasible for large-interconnected systems.
- A huge number of variables need to be controlled by a single control body which causes increased computational burden.
- Power flow solution is requires in this strategy at each time step.
- This control strategy does not support '*plug and play*' property.

7.4.2.2 Decentralized Control Structure

A decentralized control strategy is applied based on local information implemented by local controllers. Corresponding voltage controllers take information from their surroundings, analyse the data and take control action on local variables in cases of deviations from the reference value [21]. A decentralized control strategy does not need to ensure large communication network to operate. However, this control strategy has some drawbacks as well. They are as follows:

- Control capabilities of the decentralized controllers may not be fully utilized.
- Decentralized controllers have no understanding among one another and start to compete in controlling the voltage.

Decentralized controllers experience high stress.

7.4.2.3 Distributed Control Structure

In distributed control structure, the voltage controllers communicate with only the neighbouring controllers and implement a coordinated control action to mitigate the

voltage deviation. This structure does not require large communication infrastructure to operate and the controllers do not operate only considering local measurements. Therefore, this structure has the benefits of both centralized control structure and decentralized control structure which makes it popular nowadays. Some basic definitions of MAS concept, which has been introduced recently as a potential technology for coordinated voltage regulation, along with its application in power system have been discussed in [22].

7.5 Islanding Operation

7.5.1 Microgrid Control

The integration of multiple numbers of intermittent renewable sources and emerging loads like electric vehicles (EVs) into microgrid, introduce new technical and economical challenges. Appropriate control and proper coordination of microgrids are extremely important in order to address these challenges [23]. As a result, this section and other following sections of this chapter will try to explore related literatures on various microgrid control strategies.

7.5.1.1 Expected Features of Microgrid Controllers

Control challenges mentioned in the previous section needs to be handled by the designed microgrid controller. Expected features of the control system to ensure reliable, consistent and efficient operation of the microgrid involve:

Output control: Output refers to the voltage and current generated by various DG units in a microgrid. Desired microgrid controller should have the capability to control these outputs. A microgrid's control should control the output voltage and current so that all associated DG units track their predefined or generated set points/reference values and oscillation is accurately damped.
Power balance: Associated RES units in a microgrid should be capable of meeting load requirements even under extreme conditions like faults. It is expected that microgrid controller will control both active and reactive power and initiate necessary steps of power sharing and storage commands to balance overall power profile and simultaneously keeping voltage/frequency deviations within allowable levels.
Demand side management (DSM): Demand side management (DSM) is the mechanism to modify the consumer demand for energy by means of financial incentive and education. Generally, the objective of DSM is to motivate consumers to use less energy during peak hours, or to shift the time of energy consumption to off-peak hours for instance night time and weekends. Economical DSM strategies should be integrated within microgrid controller in order to ensure load frequency

control and active participation of prosumers. This will increase controllability over a portion of load [24, 25].

Economic dispatch: A proper and economical way to dispatch DG units particularly in islanded mode can contribute immensely in reduction of the operational costs and maximization of the profit by taking reliability into consideration.

Durable operational mode transient: An intelligent and reliable microgrid should operate in grid-tied, islanded and transition between these two modes. Various control techniques are applicable for grid-tied and islanded operation. To achieve seamless operation during transition between these two modes require fast islanding detection and proper transient performance. As a result a microgrid's controller should be properly responsive to the islanding detection signal and have robust transient handling capability [26].

7.5.1.2 Controlled Variables

Controllable variables for microgrid controllers are rather straight forward, which are: voltage (V), frequency (f), active (P) and reactive power (Q). In the grid-tied operation, the frequency and the voltage are determined and controlled by grid itself. During this mode, microgrid's controller handles and shares active and reactive power generated by RESs and supplies loads. Reactive power generated by individual DGs (i.e. wind turbine, diesel generators, etc.) or by interfacing voltage source converters (VSC) for solar modules, fuel cells, etc. can be injected to meet reactive power demand, voltage control and for power factor correction purpose. As it is mentioned in IEEE standard 1547 for interconnecting RESs with distribution systems, RES units are not allowed to regulate or control the PCC voltage during grid-tied operation to avoid interaction with conventional controllers [27].

In islanded mode of operation, the microgrid functions as a self-governing entity. Since system voltage and frequency are no longer controled by the grid, thus separate voltage and frequency controller need to be activated. An active power is balanced either by central controller or by local controller. Local controllers of DG units use local measurements to generated reference, on the other hand, central controllers generate reference values centrally and communicate these set points to DG associated local controllers. The main reason of such scheme is to ensure the contribution of all units to supplying the load by tracking pre-specified set points.

7.6 Hierarchical Microgrid Control Structure

Microgrid can operate in both grid connected mode and islanded mode. Microgrid control is a complicated topic to be addressed as it is desired that it will operate seamlessly during the transition between grid-tied to islanded mode or vice versa. The main objectives of microgrid controllers are [28]:

(1) Voltage and frequency regulation (in both operating mode)
(2) Proper load sharing and DER coordination (in both operating mode)
(3) Resynchronization of the system with main grid (transient mode)
(4) Power flow control between the microgrid and the main grid (grid connected mode)
(5) Optimizing the microgrid operational cost.

It is important to standardize microgrid control structure to correlate with new grid codes. In order to do so the standardized structure for automated interface between multiple enterprise and control systems given in ISA-95 is adopted [29]. According to [30, 31] the microgrid control structure shown in Fig. 7.2 would be as follows:

(1) **Level 3 (Tertiary Control)**: Tertiary control level is responsible for import and export power to/from the grid.
(2) **Level 2 (Secondary Control)**: Secondary control level is responsible for the restoration or synchronization of microgrid with grid. It is also responsible for maintaining all electrical levels within acceptable region.
(3) **Level 3 (Primary Control)**: Primary control level is responsible for parallel power sharing between multiple distributed generators (DGs) and stabilizing voltage and frequency using a droop or similar methods.
(4) **Level 0 (Inner Control Loops)**: This level is responsible for handling voltage or current regulation issues associated with each module.

In following sections, a brief review on existing literatures regarding these control structures is presented.

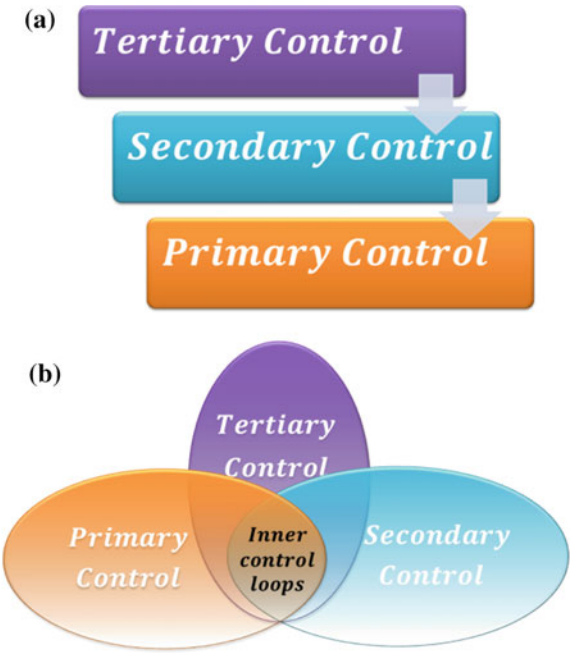

Fig. 7.2 Hierarchical microgrid control structure, **a** Primary, secondary and tertiary microgrid control, **b** Hierarchical microgrid control with inner control loops

7.6.1 Primary Control

The objectives of primary controls are:

(1) Stabilizing voltage and frequency. During islanded mode, voltage and frequency instability may appear due to the mismatch of power generation and power consumption.
(2) Ensuring plug-and-play property for RES and sharing the active and reactive power appropriately among them preferably without communication.
(3) Mitigating circulating currents that can cause over-current phenomenon in the power electronic devices and damage the DC-link capacitor.

There are an extensive amount of research work has been going on the optimum primary microgrid control due to unpredictable, non-linear and even sometimes identical dynamics of connected DERs. Some state-of-the-art primary microgrid controller structure and their features have been explored below.

7.6.1.1 Droop Based Method

Droop control is a commonly utilized local/primary control technique for microgrid application. These controllers are simple in structure and easy to practically implement. Droop control is preferred mostly because of its autonomous control and wireless structure without communication links between converters. Conventionally active power is controlled via frequency droop characteristics and reactive power is controlled via voltage droop characteristics. A brief overview of different droop characteristics adopted in literatures are given below.

An inverter based DG can be considered as an AC source itself if we neglect switching ripples and high frequency harmonics drawn in Fig. 7.3. Now let us consider if the converter output voltage is $E\angle\delta$ and the common AC bus voltage is $V_{com}\angle 0$ and the line impedance is $Z\angle\theta$ then the complex power S delivered from inverter based DGs to the common AC bus/grid would be,

$$S = V_{com}I^* = \frac{V_{com}E\angle\theta - \delta}{Z} - \frac{V_{com}^2\angle\theta}{Z} \tag{7.15}$$

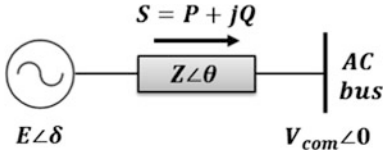

Fig. 7.3 Simplified diagram of a converter connected to the microgird

From Eq. (7.1), the real and reactive powers can be acquired using Euler's identity theorem i.e. $e^{i\theta} = \cos\theta + i\sin\theta$ as

$$\begin{cases} P = \frac{V_{com}E}{Z}\cos(\theta - \delta) - \frac{V_{com}^2}{Z}\cos\theta \\ Q = \frac{V_{com}E}{Z}\sin(\theta - \delta) - \frac{V_{com}^2}{Z}\sin\theta \end{cases} \tag{7.16}$$

Considering the line impedance to be purely inductive i.e. $\theta = 90°$ so Eq. (7.16) becomes

$$\begin{cases} P = \frac{V_{com}E}{Z}\sin\delta \\ Q = \frac{V_{com}E\cos\delta - V_{com}^2}{Z} \end{cases} \tag{7.17}$$

Considering the phase difference between converter output voltage and common AC bus voltage (i.e. δ) to be very small then we can assume that $\sin\delta \approx \delta$ and $\cos\delta \approx 1$ then Eq. (7.17) becomes

$$\begin{cases} P = \frac{V_{com}E}{Z}(\delta) \\ Q = \frac{V_{com}E - V_{com}^2}{Z} \end{cases} \tag{7.18}$$

From Eq. (7.18) we can conclude that active power is dependent on the phase difference between the converter output voltage and the common AC bus voltage (i.e. δ) and reactive power is dependent upon converter output voltage (i.e. E). As angular frequency, $\omega = \frac{d\delta}{dt}$, the conventional droop equations become [30, 32–37]

$$\begin{cases} \omega = \omega^* - D_P P \\ E = E^* - D_Q Q \end{cases} \tag{7.19}$$

where D_P and D_Q are droop coefficient, ω^* and E^* are angular frequency and RMS value of DER output voltage respectively at no load condition which will be considered as reference values later on this literature. Now the value D_P and D_Q are set considering two factors, they are maximum allowable deviation in voltage or frequency magnitude and converter power rating. So for a microgrid with N number of DGs in it the relation between active power, reactive power and their corresponding droop coefficients have to follow following relations [38, 39].

$$\begin{cases} D_{P1}P_1 = D_{P2}P_2 = \cdots = D_{PN}P_N = \Delta\omega_{\max} \\ D_{Q1}Q_1 = D_{Q2}Q_2 = \cdots = D_{QN}Q_N = \Delta E_{\max} \end{cases} \tag{7.20}$$

where $P_1, P_2, \ldots, P_N$ nominal active power rating of N DGs

$Q_1, Q_2, \ldots, Q_N$ nominal reactive power rating of N DGs

$D_{P1}, D_{P2}, \ldots, D_{PN}$ and $D_{Q1}, D_{Q2}, \ldots, D_{QN}$ are corresponding active and reactive power droop coefficient respectively.

ΔE_{max} and $\Delta\omega_{max}$ are maximum allowable voltage and angular frequency deviation. Primarily Eq. (7.14) is used to calculate corresponding droop coefficient in a microgrid.

During grid connected operation, angular frequency ω and output voltage E of associated DGs in microgrid are imposed by the grid. Therefore, active power reference P^{ref} and reactive power reference Q^{ref} are adjusted through ω^* and E^* respectively [40] as Eq. (7.21) (Fig. 7.4)

$$\begin{cases} P^{ref} = \frac{\omega^* - \omega}{D_P} \\ Q^{ref} = \frac{E^* - E}{D_Q} \end{cases} \tag{7.21}$$

For analysing the dynamic response and transient performance of the primary controller the system in Fig. 7.5 can be linearised with respect to angular frequency (ω) or phase deviation (δ) to get the linearised transfer function of the active power controller and with respect to VSC output voltage (E) to get the linearised transfer function of reactive controller. For example, the linearised active power controller equations derived from Eqs. (7.17) and (7.19) are

$$\begin{cases} \Delta P = G_P \Delta\delta \\ \Delta\omega = \Delta\omega^* - D_P \Delta P \end{cases} \tag{7.22}$$

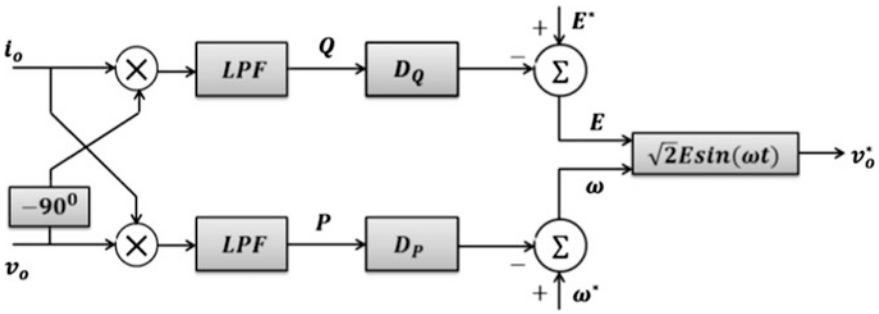

Fig. 7.4 Conventional droop control method

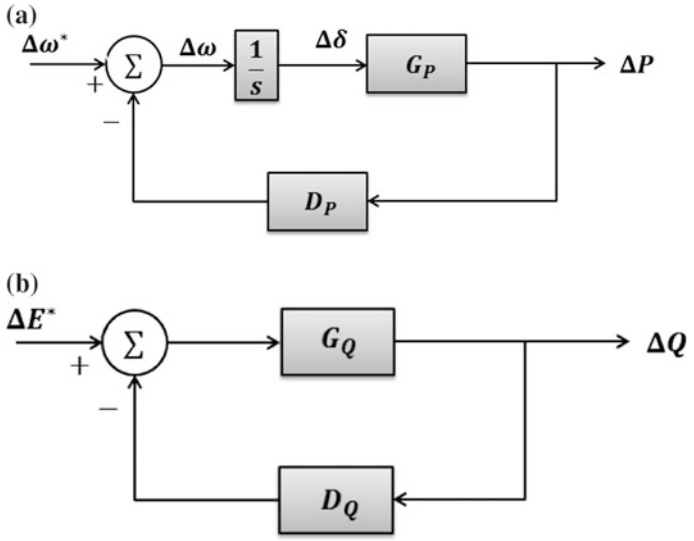

Fig. 7.5 Conventional droop based power control of microgrid

where,

$$\begin{aligned} G_P &= \frac{V_{com0}E_0}{Z}\cos\delta_0 \\ \Delta\delta &= \int \Delta\omega dt \end{aligned} \tag{7.23}$$

In Eq. (7.23) E_0, V_{com0} and δ_0 are initial operating points. As a result the small signal transfer function for the active power controller can be obtained by perturbing Eq. (7.22) and Eq. (7.23)

$$\Delta P(s) = \frac{G_P}{s + D_P G_P}\Delta\omega^*(s) \tag{7.24}$$

Similarly by linearising the second portion of Eqs. (7.11) and (7.13) with respect to inverter output voltage E we can get reactive power controller equations like below,

$$\begin{cases} \Delta Q = G_Q \Delta E \\ \Delta E = \Delta E^* - D_Q \Delta Q \end{cases} \tag{7.25}$$

where,

$$G_Q = \frac{V_{com0}}{Z}\cos\delta_0 \tag{7.26}$$

Thus from Eq. (7.25) we can derive transfer function of the reactive power controller as below,

$$\begin{aligned} \Delta Q &= G_Q(\underbrace{\Delta E^* - D_Q \Delta Q}_{\Delta E}) \\ \Rightarrow \Delta Q(s) &= \frac{G_Q}{1 + D_Q G_Q}\Delta E^*(s) \end{aligned} \tag{7.27}$$

The small signal models of both active and reactive power control using droop method are illustrated in Fig. 7.5. Advantages and disadvantages of conventional droop control method are pointed out below [41–48]:

Advantages:

(1) Simple structure.
(2) Ease in practical implementation.
(3) No communication links required.

Disadvantages:

(1) As there is only one controlled variable which is either D_P or D_Q for active or reactive droop control, multiple control objectives cannot be achieved.
(2) Only applicable for networks with high X/R ratio (i.e. highly inductive networks) thus not suitable for mostly resistive low voltage distribution networks.
(3) Reactive power may affect voltage regulation for critical loads as there is no global set point for voltage as opposed to frequency which may be 50 or 60 Hz throughout the network.
(4) It is not suitable for nonlinear loads. It cannot detect current harmonics generated by nonlinear loads which adversely affect DGs' output voltage.
(5) It utilizes average active and reactive power over a cycle which may show poor transient performance or instability
(6) Susceptible to large and fast load variance as load dynamics are not considered in controller design
(7) Unable to black start-up after major system collapse, system restoration requires additional endowment
(8) Due to uncertain output impedance across DERs local power sharing among different DGs are not ensured.
(9) Various loading condition affects its capability to impose a fixed global system frequency.

7.6.1.2 Non-droop Based Method

Active load sharing or communication based centralized methods have been used as primary controller as an alternative to droop based methods. Current or active/reactive power reference point is determined via different approaches. For example,

(a) **Centralized control**: In this method the average load current is evenly distributed among different DGs by providing same current set points for their corresponding converters [49, 50].
(b) **Master-slave control**: In this method one converter is considered as a master and works as a VSC to regulate the output voltage on the other hand the slave converters act as individual current source converters that actually follow the current pattern of the master converter [40, 50].
(c) **Average load sharing control**: In this method, the current reference for individual converters is continuously updated without considering the load current. [51, 52].
(d) **Circular chain control (3*C*)**: In this method all the modules are interconnected like links in chains and current references are determined by the reference of the previous converter [53].

Advantages and disadvantages of non-droop based control method are pointed out below:

Advantages

(1) It results in fast transient mitigation (centralized control).
(2) It features plug and play facility for DGs providing that generation and load is balanced and the dominant DG is present (Master-slave control).
(3) It offers appropriate current sharing.
(4) High power quality can be achieved.

Disadvantages:

(1) It requires communication links.
(2) Associated control loops require high bandwidth.

7.6.2 Secondary Control

Secondary control of a microgrid is also considered as the energy management system (EMS). The main task of microgrid secondary control is to ensure power quality, mitigate voltage and frequency deviation and coordinate DG units. These functionalities can be achieved by centralized operation or by decentralized coordination. A centralized operation relies on a central control body. The central control body enables the implementation of online optimization routines. It should

be noted that for successful operation of this approach requires simultaneous accumulation of all the relevant information at a single node. Conversely, the decentralized coordination allows interaction among various DG units within a particular microgrid in order to expedite a distributed decision making process. Apart from the difficulty in high level coordination among various DG units, the decentralize approach actually facilitates plug-and-play feature without making further change in controller setting. Usually, centralized control structure is more appropriate for isolated microgrid that has critical demand-supply balancing with a fixed infrastructure. On the other hand, a decentralized coordination is more appropriate for grid-tied microgrids with multiple owners. A detail review on existing literatures based on secondary microgrid controller is presented below [45].

7.6.2.1 Centralized Operation

A centralized secondary control structure consists of a central control body and multiple agents associated with it. For proper functionality, it requires simultaneous accumulation of all the relevant information regarding DG units, load and network related information. This information includes cost functions, technical characteristics/limitations, network parameters and operational modes. Information related to forecasting such as load demand, wind speed, solar irradiance etc. can also be considered as relevant information which helps determining an appropriate unit commitment (UC) and dispatch of the DG resources targeting selected objectives to ensure reliable microgrid operation. The central control body can operate based on either online calculations of the optimal (or near optimal) operation or pre-built and continuously-updated databases with information of suitable operating conditions. Hajimiragha and Zadeh [54] illustrates a practical example of this approach. A generalized architecture of secondary controller using centralized approach is shown in figure where the inputs fed to the central controller are,

(1) Forecasted power output of non-dispatchable DG units for N consecutive periods
(2) Forecasted local load for the N consecutive periods
(3) State of charge (SOC) of the energy storage system (ESS)
(4) Operational limits of dispatchable generators and ESS
(5) Security and reliability constraints of the microgrid
(6) Utility grid interconnection status based on various islanding detection method
(7) Forecasting of the grid energy prices

The outputs of the secondary controller by analysing and controlling fed inputs are

(1) Command to controllable loads (DSM) On/Off/Shift
(2) Reference point for dispatchable DG units for next period.

7.6.2.2 Decentralized Operation

A decentralized secondary control of a microgrid provides maximum possible autonomy for different DGs and loads while solving the energy management problem. Even though the control variable decisions are taken by local controller, decentralized secondary microgrid controller can use hierarchical structure to exchange information among multiple clusters of local controllers. The hierarchical structure of a secondary microgrid controller is composed of three levels namely Distribution Network Operator (DNO), Microgrid Central Controller (MGCC) and Local Controllers (LCs) [55, 56]. The DNO is a part of the tertiary control. It manages the interaction between microgrid and distribution network/utility grid. It also manages the communication among multiple microgrids. The MGCC is responsible for the coordination of the combined operation of DG units and their associated loads. It is also in charge of the economical and reliable operation and maintains continuous communication with the grid. The main tasks of LCs are to control DG units within single or multiple microgrids. The LCs also maintain communication with higher level controllers to achieve local and global objectives. Under decentralized structure, an LC has the liberty to communicate with MGCC and other LCs. Through this interaction LCs can share knowledge, request/offer a service, communicate expectations and exchange any relevant information that is required for microgrid operation. Primarily decentralized secondary controllers have been designed using the multi-agent system (MAS) concept in literatures. MAS concept can be narrated as a system that consists of multiple intelligent agents that communicate local information among one other in order to achieve a global or local objectives. The connectivity, functionalities, responsibilities of each agent and the characteristics of sharable information play a vital role in system performance. Agents are entities that have the ability to act on environment, possess communication ability, certain level of autonomy and limited knowledge of the environment and the global objective. An intelligent agent is expected to be reactive to the change in environment, proactive in seeking opportunities and social by depending on communication. These characteristics differentiate intelligent agents from conventional power system elements like relay, transformer etc. In order to address limited knowledge of agents, state estimation theory has been employed in power system. In spite of being communication capable, most of the control parts are done locally in smart agents.

7.6.2.3 Distributed Operation

A distributed cooperative control method is actually an extended version of multi-agent control scheme. This method is inspired by natural phenomena like swarming in insects, thermodynamics law, flocking in birds and synchronization in a physical system. In this system each agent communicates with other agent by exchanging limited information through restricted communication protocols and cooperates with each other to achieve a global or local objective. This control and

coordination can be achieved in various ways like using uni-directed graph, by solving average consensus problem or rendezvous problem or by flocking.

7.6.3 Tertiary Control

Tertiary control is the last control level of the hierarchical microgrid control structure. Tertiary microgrid control ensures economical and optimal operation and contributes in power flow management between microgrid and the host grid. Power flow between the main grid and microgrid during grid connected operation of microgrid can be achieved by adjusting and regulating amplitudes and frequency of the voltages of DG units. Initially microgrid active and reactive power (P_G & Q_G) are measured. Later these measured values are compared with their corresponding references (P_G^{ref} & Q_G^{ref}) to obtain references for the voltage and frequency (ω^{ref} & E^{ref}) respectively. The equations to achieve these objectives are,

$$\begin{cases} \omega^{ref} = K_{PP}^{Tertiary}(P_G^{ref} - P_G) + K_{IP}^{Tertiary}\int (P_G^{ref} - P_G)dt \\ E^{ref} = K_{PQ}^{Tertiary}(Q_G^{ref} - Q_G) + K_{IQ}^{Tertiary}\int (Q_G^{ref} - Q_G)dt \end{cases} \tag{7.28}$$

where $K_{PP}^{Tertiary}$, $K_{IP}^{Tertiary}$, $K_{PQ}^{Tertiary}$ and $K_{IQ}^{Tertiary}$ are proportional and integral gains. Generated references are fed to the secondary controller. Another task of the tertiary microgrid control is to ensure economical and optimal operation. For example, an optimal economic operation can be achieved if all DGs operate at equal marginal costs, C_{opt}, where marginal cost is defined as the ratio of the variation of total cost to variation of generated power. This objective can be achieved by gossiping algorithm. In this method, a random output power reference, P_i^0 and P_j^0, are considered for the ith DG unit and its random gossiping partner, jth DG unit, respectively. Later, based on the marginal cost curve the optimal output power is determined for associated DG units. Each of the associated DGs changes their output power to reach optimal point. The same technique is followed for other pairs of DGs until all DGs operate optimally.

7.7 Applications of Distributed Controller in Microgrid

7.7.1 Application in Voltage Regulation

The main objective of the microgrid voltage controller is to provide a flat voltage profile in the microgrid by maintaining the voltage level in different nodes within an acceptable range. Insignificant line impedance in transmission and distribution lines causes large current flow even under minuscule voltage differences across busses.

To prevent this, proper voltage regulation strategy is mandatory. Voltage controller can be designed either centrally or locally. Local voltage controller performs voltage regulation directly utilizing droop method through inner control loop (i.e. PI, PR, LQG etc.). A centralized or distributed clustered controller will update reactive power set point and communicate these references with local controllers of DGs. For low voltage (LV) and medium voltage (MV) grids, voltage control requires determination of active power set points in addition to reactive power set points due to their resistive network behaviours.

7.7.2 Application in Economic Power Coordination

Economical power coordination and optimal power flow (OPF) are important operational concerns. Conventional distributed optimization schemes usually do not take into consideration issues like time variability of communication links as they may lead to high computational burden. This may hamper OPF for microgrid application.

7.7.3 Application in Frequency Regulation

The main objective of microgrid frequency control is to have all associated DG units converge to a global frequency set point. Frequency control is applicable when DG units are electronically interfaced and have independent controllability on frequency and the microgrid is in an islanded mode. During frequency control operation at least one unit has to act as master unit with fixed frequency set point and other DG units should follow that unit as slave units. Every unit may have its own minimum and maximum allowable power and terminal voltage values. In conventional power system, there exists precise coupling between rotor angular speed and electrical frequency to aid frequency regulation. As previously mentioned in microgrid control challenges majority of renewable energy sources do not have inertia, as a result emulating a virtual inertia for these DG units are required to imitate the operation of synchronous generators.

7.8 Summary

Increased penetration of RES into traditional distribution system raises several crucial concerns in the operation and protection of the system and these concerns are being more significant rapidly. In this chapter, we presented the impacts of large-scale RES penetration and the control strategies to mitigate the issues. The implementation of advanced control strategies is the fundamental key of

accommodating large amount of intermittent RES without violating the steady state operation of the system. Different control strategies and methods along with their advantages and disadvantages for grid interconnected RES and islanded micro grid have been discussed.

References

1. Mahmud N, Zahedi A (2016) Review of control strategies for voltage regulation of the smart distribution network with high penetration of renewable distributed generation. Renew Sustain Energy Rev 64:582–595
2. Quezada VM, Abbad JR, Roman TGS (2006) Assessment of energy distribution losses for increasing penetration of distributed generation. IEEE Trans Power Syst 21(2):533–540
3. Lopes JP, Hatziargyriou N, Mutale J, Djapic P, Jenkins N (2007) Integrating distributed generation into electric power systems: a review of drivers, challenges and opportunities. Electr Power Syst Res 77(9):1189–1203
4. Zhu Y, Tomsovic K (2002) Adaptive power flow method for distribution systems with dispersed generation. IEEE Trans Power Deliv 17(3):822–827
5. Chiradeja P, Ramakumar R (2004) An approach to quantify the technical benefits of distributed generation. IEEE Trans Energy Convers 19(4):764–773
6. Tsikalakis AG, Hatziargyriou ND (2007) Environmental benefits of distributed generation with and without emissions trading. Energy Policy 35(6):3395–3409
7. Gil HA, Joos G (2008) Models for quantifying the economic benefits of distributed generation. IEEE Trans Power Syst 23(2):327–335
8. El-Khattam W, Salama MMA (2002) Impact of distributed generation on voltage profile in deregulated distribution system. In Proceedings of the power systems 2002 conference, impact of distributed generation, Clemson, SC, USA, pp 13–15
9. Ruiz-Romero S, Colmenar-Santos A, Mur-Pérez F, López-Rey Á (2014) Integration of distributed generation in the power distribution network: the need for smart grid control systems, communication and equipment for a smart city—use cases. Renew Sustain Energy Rev 38:223–234
10. Elmarkabi IM (2004) Control and protection of distribution networks with distributed generators. A dissertation submitted to the Graduate Faculty of North Carolina State University
11. Voltage control in distribution grids with distributed generation(I). Annals of mechanics and electricity. ICAI Engineers Association (Catholic Institute of Arts and Industries) 13th ICAI April 2012. (Revista Anales de la asociación de ingenierosdelICAI). http://www.revista-anales.es/web/n_13/seccion_3.html; 13 Apr 2012. Accessed 16 Feb 13
12. Zahedi A (2011) A review of drivers, benefits, and challenges in integrating renewable energy sources into electricity grid. Renew Sustain Energy Rev 15(9):4775–4779
13. Dugan RC, McGranaghan MF, Beaty HW (1996) Electrical power systems quality. McGraw-Hill, New York, NY, p c1996
14. Chen Z, Kong W (2007) Protection coordination based on a multi-agent for distribution power system with distribution generation units. In: International workshop on next generation regional energy system development
15. Liew SN, Strbac G (2002) Maximising penetration of wind generation in existing distribution networks. IEE Proc-Gener, Transm Distrib 149(3):256–262
16. Hird CM, Leite H, Jenkins N, Li H (2004) Network voltage controller for distributed generation. IEE Proc-Gener, Transm Distrib 151(2):150–156
17. Echavarría R, Claudio A, Cotorogea M (2007) Analysis, design, and implementation of a fast on-load tap changing regulator. IEEE Trans Power Electron 22(2):527–534

18. Mahmud N, Zahedi A, Mahmud A (2017) A cooperative operation of novel PV inverter control scheme and storage energy management system based on ANFIS for voltage regulation of grid-tied PV system. IEEE Trans Indus Inform
19. Mahmud N, Zahedi A, Mahmud A (2016) Dynamic voltage regulation of grid-tied renewable energy system with ANFIS. In: Australasian universities power engineering conference (AUPEC), 2016, pp 1–6. IEEE
20. Wood AJ, Wollenberg BF (2012) Power generation, operation, and control. Wiley, USA
21. Mahmud N, Zahedi A, Mahmud A (2016) ANFISPID-based voltage regulation strategy for grid-tied renewable DG system with ESS. In: Innovative smart grid technologies-Asia (ISGT-Asia), 2016 IEEE, pp 81–86. IEEE
22. McArthur SD, Davidson EM (2005) Concepts and approaches in multi-agent systems for power applications. In: Proceedings of the 13th international conference on intelligent systems application to power systems, 2005, pp 5-pp. IEEE
23. Rahman MS, Hossain MJ, Rafi FHM, Lu J (2016) A multi-purpose interlinking converter control for multiple hybrid AC/DC microgrid operations. In: Innovative smart grid technologies-Asia (ISGT-Asia), 2016 IEEE, pp 221–226. IEEE
24. Wang C, Nehrir MH (2008) Power management of a stand-alone wind/photovoltaic/fuel cell energy system. IEEE Trans Energy Convers 23(3):957–967
25. Alvial-Palavicino C, Garrido-Echeverría N, Jiménez-Estévez G, Reyes L, Palma-Behnke R (2011) A methodology for community engagement in the introduction of renewable based smart microgrid. Energy Sustain Dev 15(3):314–323
26. Bahrani B (2008) Islanding detection and control of islanded single and two-parallel distributed generation units (Doctoral dissertation)
27. Ieee, IEEE standard conformance test procedure for equipment interconnecting distributed resources with electric power systems, July 2005, ISBN 0738147362
28. Bidram A, Davoudi A (2012) Hierarchical structure of microgrids control system. IEEE Trans Smart Grid 3(4):1963–1976
29. Ambrosio R, Widergren S (2007) A framework for addressing interoperability issues. In: Power engineering society general meeting, 2007. IEEE, pp. 1–5. IEEE
30. Guerrero JM, Vasquez JC, Matas J, Castilla M, de Vicuna LG (2009) Control strategy for flexible microgrid based on parallel line-interactive UPS systems. IEEE Trans Industr Electron 56(3):726–736
31. Guerrero JM, Vasquez JC, Matas J, De Vicuña LG, Castilla M (2011) Hierarchical control of droop-controlled AC and DC microgrids—a general approach toward standardization. IEEE Trans Industr Electron 58(1):158–172
32. Rahman MS, Hossain MJ, Lu J (2016) Coordinated control of three-phase AC and DC type EV–ESSs for efficient hybrid microgrid operations. Energy Convers Manag 122:488–503
33. Guerrero JM, Matas J, De Vicuna LGDV, Castilla M, Miret J (2006) Wireless-control strategy for parallel operation of distributed-generation inverters. IEEE Trans Industr Electron 53 (5):1461–1470
34. Guerrero JM, Matas J, de Vicuna LG, Castilla M, Miret J (2007) Decentralized control for parallel operation of distributed generation inverters using resistive output impedance. IEEE Trans Industr Electron 54(2):994–1004
35. Guerrero JM, De Vicuna LG, Matas J, Castilla M, Miret J (2005) Output impedance design of parallel-connected UPS inverters with wireless load-sharing control. IEEE Trans Industr Electron 52(4):1126–1135
36. Guerrero JM, De Vicuña LG, Miret J, Matas J, Cruz J (2004) Output impedance performance for parallel operation of UPS inverters using wireless and average current-sharing controllers. In: Power electronics specialists conference, 2004. PESC 04. 2004 IEEE 35th annual, vol 4, pp 2482–2488. IEEE
37. Katiraei F, Iravani MR (2006) Power management strategies for a microgrid with multiple distributed generation units. IEEE Trans Power Syst 21(4):1821–1831

38. Rahman MS, Hossain MJ, Rafi FHM, Lu J (2016) EV charging in a commercial hybrid AC/DC microgrid: Configuration, control and impact analysis. In: Australasian Universities power engineering conference (AUPEC), 2016, pp 1–6. IEEE
39. Diaz G, Gonzalez-Moran C, Gomez-Aleixandre J, Diez A (2010) Scheduling of droop coefficients for frequency and voltage regulation in isolated microgrids. IEEE Trans Power Syst 25(1):489–496
40. Lopes JP, Moreira CL, Madureira AG (2006) Defining control strategies for microgrids islanded operation. IEEE Trans Power Syst 21(2):916–924
41. Yu X, Khambadkone AM, Wang H, Terence STS (2010) Control of parallel-connected power converters for low-voltage microgrid—part I: a hybrid control architecture. IEEE Trans Power Electron 25(12):2962–2970
42. Delghavi MB, Yazdani A (2011) An adaptive feedforward compensation for stability enhancement in droop-controlled inverter-based microgrids. IEEE Trans Power Delivery 26 (3):1764–1773
43. Kim J, Guerrero JM, Rodriguez P, Teodorescu R, Nam K (2011) Mode adaptive droop control with virtual output impedances for an inverter-based flexible AC microgrid. IEEE Trans Power Electron 26(3):689–701
44. Zhong QC (2013) Harmonic droop controller to reduce the voltage harmonics of inverters. IEEE Trans Industr Electron 60(3):936–945
45. Marwali MN, Jung JW, Keyhani A (2004) Control of distributed generation systems-Part II: Load sharing control. IEEE Trans Power Electron 19(6):1551–1561
46. Lee TL, Cheng PT (2007) Design of a new cooperative harmonic filtering strategy for distributed generation interface converters in an islanding network. IEEE Trans Power Electron 22(5):1919–1927
47. Sao CK, Lehn PW (2005) Autonomous load sharing of voltage source converters. IEEE Trans Power Delivery 20(2):1009–1016
48. Sao CK, Lehn PW (2008) Control and power management of converter fed microgrids. IEEE Trans Power Syst 23(3):1088–1098
49. Pogaku N, Prodanovic M, Green TC (2007) Modeling, analysis and testing of autonomous operation of an inverter-based microgrid. IEEE Trans Power Electron 22(2):613–625
50. Cheng YJ, Sng EKK (2006) A novel communication strategy for decentralized control of paralleled multi-inverter systems. IEEE Trans Power Electron 21(1):148–156
51. Sun X, Lee YS, Xu D (2003) Modeling, analysis, and implementation of parallel multi-inverter systems with instantaneous average-current-sharing scheme. IEEE Trans Power Electron 18(3):844–856
52. Sun X, Wong LK, Lee YS, Xu D (2006) Design and analysis of an optimal controller for parallel multi-inverter systems. IEEE Trans Circuits Syst II Express Briefs 53(1):56–61
53. Wu TF, Chen YK, Huang YH (2000) 3C strategy for inverters in parallel operation achieving an equal current distribution. IEEE Trans Industr Electron 47(2):273–281
54. Hajimiragha AH, Zadeh MR (2013) Research and development of a microgrid control and monitoring system for the remote community of Bella Coola: challenges, solutions, achievements and lessons learned. In: International conference on smart energy grid engineering (SEGE), 2013 IEEE, pp 1–6. IEEE
55. Katiraei F, Iravani R, Hatziargyriou N, Dimeas A (2008) Microgrids management. IEEE Power Energy Mag 6(3)
56. Rahman MS, Rafi F, Hossain M, Lu J (2015) Power control and monitoring of the smart grid with evs. Veh Grid: Linking Electric Veh Smart Grid 79:107